Studies of Catalytic Asymmetric Transfer Hydrogenation in Batch and Continuous Reactors

University College London
Department of Chemical Engineering

Xiuyan Sun

A thesis submitted for the degree of Doctor of Philosophy of the
University of London

UMI Number: U593532

UMI

Dissertation Publishing

ProQuest

TO MY BELOVED PARENTS

Abstract

The aim of this work was to design novel reactors to increase the reaction conversion and enantioselectivity for the asymmetric transfer hydrogenation (ATH) of acetophenone. The reactor designs should also be amenable to scale-out for increase of productivity. Asymmetric transfer hydrogenation of acetophenone with isopropanol is a reversible reaction and backwards reaction limits the reaction conversion and enantioslectivity. Novel reactor design aims to efficient acetone removal, which is a byproduct in the reaction system. By gas stripping, reaction equilibrium can be shifted and hence conversion and enantioselectivity improved.

Reaction conditions optimization was initially conducted in a laboratory batch reactor and a simple kinetic model was built. The catalyst deactivation, the effect of the temperature, substrate concentration, substrate/catalyst concentration ratio and acetone concentration on the ATH were investigated. The metal-ligand bifunctional mechanism was considered for the kinetic model. The gPROMS/gEST commercial software was used for kinetic parameters estimation.

Three continuous reactors (tubular reactor, rotating disc reactor and micromesh reactor) were designed and fabricated, each one encompassing a different gas/liquid contacting method. In the tubular reactor, gas/liquid contact is achieved through slugs. In the rotating disc reactor, gas/liquid contact is achieved through a thin film formed on the disc which rotates. In the micromesh reactor, a micromesh forms and stabilizes the gas/liquid interface. Acetone removal and asymmetric transfer hydrogenation studies were carried out under different conditions in these reactors and the performance of the different reactors were compared. The tubular reactor showed similar performance as the batch reactor. The rotating disc reactor enhanced acetone removal, thus improved the conversion and enantioselectivity. Acetone was removed most efficiently in the micromesh reactor. Therefore, the highest conversion and enantioslectivity were also obtained in this reactor. By simplified calculations, it was established that in order to increase the acetone removal efficiency, the ratio of gas to liquid flowrate and the gas-liquid interfacial area has to be increased.

The scale out/up concept was also demonstrated with the micromesh reactor. Scale out/up was achieved by increasing the number of meshes in parallel and enlarging the single mesh reactor. The conversion and enantioselectivity was slightly lower in the scaled out version reactor which is probably due to the fact that the flow distribution inside the reactor was not uniform.

Acknowledgements

First, I would like to thank my family, my parents, my brothers and sister. It is their love and support that gave me the courage and patience to finish my PhD.

Contents

List of Figures

List of Tables

18

Nomenclature

a	Gas-liquid interfacial area	m^{-1}
$[Ap]_0$	Initial acetophenone concentration	mol/l
$[Ap]$	Acetophenone concentration	mol/l
d	Hydraulic diameter	m
D	Diffusion coefficient	m^2/s
e.e.	Enantioselectivity	-
E.E.	Instantaneous enantioselectivity	-
$E.E._{initial}$	Initial Instantaneous enantioselectivity	-
E	Activation energy	J/mole
F_g	Nitrogen flowrate in mesh reactor	ml/min
F_L	Liquid flowrate in the mesh reactor	ml/min
Fo	Fourier number	-
g	Acceleration due to gravity	m/sec^2
G	Gas flowrate	ml/min
H	Module length	m
Hl	Thickness of the liquid channel	m
HTU	Height of transfer unit	m
k_m	Mass transfer coefficient in the membrane	m/s
k_0	Pre-exponential factor	
k_g	Mass transfer coefficient for the gas phase	m/s
k_L	Mass transfer coefficient for the liquid phase	m/s
K	Reaction rate constant	
K_{eq}	Equilibrium constant	
K_L^{Film}	Mass transfer coefficient in the liquid film	m/s
K_T	Total mass transfer coefficient in the membrane reactor	m/s
K_x	Overall mass transfer coefficient based on liquid side driving force	m/s
K_y	Overall mass transfer coefficient based on gas side driving force	m/s
L	Liquid flowrate	ml/min
L_m	Mixing length	m
m	Vapour liquid equilibrium ratio	

$n_{product}$ Number of moles of the product ((S)-1-phenylethanol and (R)-1-phenylethanol)

$n_{catalyst}$ Number of moles of the catalyst

N   Total number of measurements taken during all the experiments

NE   Number of experiments performed

NM_{ij} Number of measurements of the jth variable in the ith experiment

NTU   Number of transfer units

NV_i Number of variables measured in the ith experiment

P	Pressure	Pa
Pe	Peclet number	
r	Pore radius	m
R	Radius of the disc	m
[R]	(R)-1-phenylethanol concentration	mol/l
Re	Reynolds number	
[S]	(S)-1-phenylethanol concentration	mol/l
time	Reaction time	min
t_r	Average residence time	sec
t_m	Diffusive mixing time	sec
T	Temperature	^oC
TOF	Turnover frequency	
U	Average velocity	m/s
V_g	Mesh reactor gas chamber volume	ml
V_l	Mesh reactor liquid chamber volume	ml
v	Kinematics viscosity	
x	Acetone mole fraction in liquid phase	
y	Acetone mole fraction in gas phase	

$\overline{z}_{ijk}$:   kth measured value of variable j in experiment i

z_{ijk} :   kth (model-)predicted value of variable j in experiment I

Greek Symbols

$\Delta P_{C,W}$ Critical filling pressure of the wetting phase

$\Delta P_{C,NW}$ Critical filling pressure of the non-wetting phase

$\Delta P_{B,W}$ Breakthrough pressure of the wetting phase

$\Delta P_{B,NW}$ Breakthrough pressure of the non-wetting phase

Δy Average driving force in the membrane reactor

δm Thickness of membrane

ε Membrane porosity

ε_L Liquid hold up

ε_G Gas hold up

δ Thickness

θ :   Contact angle

σ_{ijk}^2 :   Variance of the kth measurement of variable j in experiment i

η Dynamic viscosity of the liquid

ω Speed of rotation

ρ Density

γ Surface tension

θ_A Advancing contact angle

θ_R Receding contact angle

θ_{APP} Apparent contact angle

τ Residence time

τ_g Average nitrogen residence time

τ_l Average liquid residence time

Chapter 1
Introduction

1.1 Motivation and objections

Asymmetric transfer hydrogenation with isopropanol as hydrogen donor has been extensively investigated (de Bellefon and Tanchoux 1998, Saluzzo and Lemaire 2002, Everaere et al 2003, Rautenstrauch et al 2003). The use of hydrogen donor has some advantages over the use of molecular hydrogen since it avoids the risks and the constraints associated with this reagent as well as the necessity for pressure vessels.

Batch operations, routinely used in the pharmaceutical and fine chemicals industries, can lead to problems with scale-up. One may appreciate potential limitations of batch operations by considering common round-bottomed flasks. In a 25-ml flask rapid top-to-bottom mixing is possible, but such mixing is slower in a 22-L vessel, in part due to the taller reactor height. Clearly micromixing is more of concern in the large vessel. Loss of selectivity when scaling up the processing of multifunctional molecules often indicates that rapid mixing is an important control element. Heat control in a large vessel is difficult when the mixing is ineffective. Concerns about micromixing and heat transfer are exacerbated with further scale up of batch operations in larger flasks and reactors, and small continuous reactor afford the best opportunities to control reaction conditions (Anderson 2000).

Many reactions can not be scaled up by simply increasing the reactor size without adverse consequence. Generating large amounts of materials by repeatedly running batch operations in a small reactor is a tedious approach that allows room for many errors. An alternative approach has been to continuously pass process streams through small reactors where the process conditions are tightly controlled. Operations in small reactors run in parallel can produce larger amounts of material by a "numbering up" or "scale out" approach. Benefits of continuous processing include control of product yields and quality, improved productivity, decreased safety concerns and others (Anderson 2001).

Overall, continuous processing, long established as cost-effective in the commodity chemicals sector, has been shown to be useful in the laboratory and pilot-plant scale-

up of pharmaceuticals and fine chemicals. The benefits of continuous processing include greater process control, enhanced margins of safety, increased productivity, and improved quality and yields. Many processes that can not be scaled up using batch operations can be readily scaled up in the laboratory and pilot plant through continuous operation. Continuous processing will be more commonly used in the future for scale up in the lab and pilot plant.

The aim of this work is to design novel reactors to increase the conversion and enantioselectivity for the Asymmetric Transfer Hydrogenation (ATH) of acetophenone. The reactor design should also be amenable to scale-out for productivity increase. In order to achieve this objective, comprehensive parametric studies were conducted in the batch reactor to investigate which is the limiting factor for the ATH reaction conversion and enantioselectivity. Kinetics were also investigated in the batch reactor which provided fundamental data for the reactor design. The results showed that acetone stripping was the limiting factor for the ATH. In order to remove acetone efficiently from the system and scale out easily, three gas-liquid reactors were designed: tubular reactor, rotating disc reactor and mesh reactor. The importance of the present work lies on the novelty of scale-out concept which provides a new method to improve the productivity fast and reliably.

1.2 Thesis Structure

In Chapter 1, the novel concept of scale out is introduced, together with its advantages compared to the conventional scale up process. The objectives of the present work are also given.

Chapter 2 summarizes the literature about the current progress of the ATH and gas-liquid contactors. The progress on the investigation of the mechanism and reaction condition optimization of the ATH is reviewed in this chapter. Traditional gas-liquid contactors, membrane contactors and micro gas-liquid contactors are also reviewed.

Chapter 3 describes batch reactor experiments carried out to investigate parameters which affect the ATH reaction conversion and enatioselectivity. The catalyst

deactivation, effect of temperature, substrate concentration, substrate/catalyst concentration ratio and acetone concentration on the ATH are studied and the reaction conditions are optimized.

Reaction kinetics is a key aspect of reactor design. Therefore, Chapter 4 describes formulation and evaluation of kinetic models. The metal-ligand bifunctional mechanism is applied and kinetic models are built. gPROMS/gEST commercial software is used for kinetic parameter estimation.

Chapter 5 describes the design of a tubular reactor and the associated experimental investigations. Tubular reactors are relatively inexpensive continuous reactors and easy to make. Moreover, the high surface area to volume ratio allows for rapid heat transfer and control of the reaction temperature. Therefore, a tubular reactor was chosen as tool to study the asymmetric transfer hydrogenation. The effect of premixing method, ultrasonic agitation, residence time, sodium isopropoxide (co-catalyst) amount, catalyst and substrate age, flowrate and mixing with micromixer and union tee are studied.

Chapter 6 describes the design of a rotating disc reactor (RDR) and associated experimental study. The liquid forms a thin film on the disc which provides a large gas-liquid contact area, thus enhances volatile compounds (acetone) removal from the system. Efficient acetone removal improves reaction conversion and enantioselectivity. The effect of different nitrogen flowrate, nitrogen introducing method, disc rotating speed and initial liquid volume on the acetone removal are studied. ATH with different substrate concentration, substrate/catalyst ratio and disc rotating speed are also studied.

Chapter 7 describes the design of a mesh reactor and associated experimental study. The mesh reactor provides a relatively large interfacial area between two phases. The interfacial area is constant which allows performance to be predicted easily. Scale out is more straightforward because its operation usually scales linearly. The effect of different types of membranes/meshes, nitrogen flowrate, liquid flowrate, acetone initial concentrations, and nitrogen saturation with isopropanol on the acetone removal are studied. Different temperature, substrate concentration, substrate/catalyst

ratio have been investigated for the ATH reaction. Scale out/up designs are also evaluated for productivity increase.

Chapter 8 summarizes the results from the different reactors. Comparisons of their performance are carried out and guidelines for further improvement are provided.

Chapter 2

Literature survey

2.1 Introduction

As a consequence of the importance of the synthesis of pharmacologically relevant substances, catalytic asymmetric hydrogenations are a field of considerable interest (Halpern 1982, Landis and Halpern 1987, Ashby and Halpern 1991, Noyori and Hashiguchi 1997, Palmer et al 1997, Palmer and Wills 1999, Blackmond 2000, Fache et al 2000, Noyori 2002, Crépy and Imamoto 2003, Fonseca and König 2003). Asymmetric transfer hydrogenation with isopropanol as hydrogen donor has been extensively investigated (de Bellefon and Tanchoux 1998, Saluzzo and Lemaire 2002, Everaere et al 2003, Rautenstrauch et al 2003). The use of hydrogen donor has some advantages over the use of molecular hydrogen since it avoids the risks and the constraints associated with this reagent as well as the necessity for pressure vessels.

Various metals have been used in asymmetric catalysis. In 1968 Knowles (2002) discovered that rhodium could be used in a chiral molecule to catalyse asymmetric hydrogenations. Crabtree et al (1977) showed that the cationic Ir catalyst, $[Ir(cod)(Pcy_3)(Py)]^+$ (Cod=cyclooctadiene, Py=pyridine, cy_3=tricyclohexylphosphine), was also active. Noyori (2002) developed a Ru-BINAP catalyst, which is widely used for the synthesis of fine chemicals and pharmaceutical products.

The batch reactor has dominated the reaction studies due to its flexibility of application. However, there are still other reactor designs that can potentially provide improved performance. de Bellefon et al (1998) used a centrifugal partition chromatograph (CPC) as a chromatographic catalytic reactor for the asymmetric transfer hydrogenation of acetophenone by isopropanol catalysed by Rh/chiral diamine system. The CPC allowed minimisation of the amount of catalyst required for testing new catalytic reaction, kinetics determination and/or catalyst selection. Smet et al (2004) applied a membrane reactor to the hydrogenation of dimethyl itaconate with Ru-BINAP and of an amino acid precursor with Rh-DUPHOS. The system kept its high activity and constant selectivity, while the membrane retained the expensive and toxic homogeneous transition metal complexes and thus created a possibility to re-use the catalyst. Moreover, the reaction could be run in a continuous way. Laue et al (2001) operated the asymmetric transfer hydrogenation process in a continuous membrane reactor. The ruthenium-based transfer hydrogenation catalysts were bonded to homogeneously soluble polymers (polystyrenes, methacrylates). The

resulting soluble polymer-bound catalyst (chemzymes) could be retained by ultrafiltation membranes and therefore applied for the asymmetric transfer hydrogenation of acetophenone in a chemzyme membrane reactor. High space-time yields up to $578 gL^{-1}d^{-1}$ and enantioselectvities up to 94% were achieved. Sandee et al (2001) used silica to support the catalyst (ruthenium complex of NH-benzyl-(1R,2S)-(-)-norephedrine complex) in a continuous flow reactor. A constant catalytic activity was observed and no catalyst deactivation occurred over a period of one week.

It is well known that the asymmetric transfer hydrogenation of acetophenone is reversible and the backwards reaction leads to erosion in the product enantioselectivity with conversion (Noyori and Hashiguchi 1997). Therefore, efficient acetone removal can shift the reaction equilibrium and increase the enantioselectivity. Various topics relevant to this investigation (kinetic modelling, traditional gas-liquid contactors, tubular reactors, rotating disc reactors, membrane contactors and micro gas-liquid contactor) are reviewed in this chapter.

2.2 Kinetic modelling

Reaction kinetics are the translation of the understanding of the chemical process into a mathematical rate expression that can be used in reactor design. Because of the importance of correct and safe design of chemical reactors, chemical reaction kinetics is a key aspect of research and development in chemical industries, in research institutions, and academic centres, as well as in industrial laboratories. When a series of experiments has been carried out, it is then necessary to develop a kinetic model, and try to adjust the kinetic parameters by fitting the mathematical expressions to the experimental data. In order to improve the efficiency and accuracy of kinetic modelling, a series of recommendations have been given (Berger et al 2001):

1. Strive for intrinsic kinetics rather than apparent kinetics where the transport effects and intrinsic kinetics are lumped.

2. Search for information on comparable chemical systems.

3. Use more theoretically-based models if reliability of the kinetics is required for extrapolation.

4. Avoid estimating a large number of different kinetic parameters from a small experimental data set.

5. Define several different kinetic models that may describe the system and model selection criteria to allow making a choice between these models.

6. Design additional experiments with two goals: (i) to facilitate the selection of the best model, and (ii) to improve the accuracy of the kinetic parameters.

7. Apply proportional weighting in order to achieve an equally good description of small experimental response values as for large experimental response values.

8. Choose a suitable software package to perform the parameter estimation.

Even a relatively simple mechanism of two or three steps can lead to a rate expression complicated enough to make analysis of observed concentration-time data difficult. Sometimes complex rate expressions can be made more tractable by using steady-state or equilibrium approximations, or by adjusting experimental conditions (Moore and Pearson 1981). Computer simulation provides an alternative means of calculating the concentration-time profiles predicted by an assumed mechanism. Most commonly this is done in the following way. For each elementary step in a complex mechanism, assume that the law of mass action correctly describes the dependence of rate on concentrations and that the rate constant at a given temperature is independent of the composition of the reaction mixture. Write differential equations that relate the rate of change of concentration of each chemical species to appropriate rate constants and concentrations. Finally, solve this set of ordinary differential equations to obtain the concentration of each species as function of time.

gPROMS® (general PROcess Modelling System) is an advanced general purpose process modelling, simulation and optimisation software available to the process industries today. gPROMS is used for model-based decision support in process and product design and process operations. It contains powerful, state-of-the art parameter estimation capabilities that have been applied successfully to a wide range of problems. Key features are:

- Multiple parameters occurring in dynamic or steady-state models may be estimated simultaneously. Nonlinear models of arbitrary size and complexity - including multi-unit flowsheets - may be used.

- Data from both dynamic and steady-state experiments may be used.
- The results of the estimation are subjected to extensive statistical analysis.

gPROMS estimation techniques include Least Squares and the Maximum Likelihood formulation. The latter provides simultaneous estimation of parameters in both:
- the physical model of the process
- the variance model of the measuring instruments, which can be:
  - constant variance
  - constant relative variance
  - heteroscedastic variance

The objective function to be minimised in the estimation of kinetic parameters can be written as:

$$\Phi = \frac{N}{2}\ln(2\pi) + \frac{1}{2}\min_{\theta}\{\sum_{i=1}^{NE} \sum_{j=1}^{NV_i} \sum_{k=1}^{NM_{ij}} [\ln(\sigma_{ijk}^2) + \frac{(\overline{z}_{ijk} - z_{ijk})^2}{\sigma_{ijk}^2}]\} \qquad (2-1)$$

where the symbols have the following definitions:

N: Total number of measurements taken during all the experiments

θ :   Set of model parameters to be estimated

       The acceptable values may be subject to given lower and upper bounds,

       i.e. $\theta^L \leq \theta \leq \theta^U$

NE: Number of experiments performed

NV_i: Number of variables measured in the ith experiment

NM_{ij}:   Number of measurements of the jth variable in the ith experiment

σ_{ijk}^2 :   Variance of the kth measurement of variable j in experiment i

$\overline{z}_{ijk}$: kth measured value of variable j in experiment i

z_{ijk} : kth (model-)predicted value of variable j in experiment I

Detailed statistical analysis of results includes residual and overlay plots, confidence ellipsoids, correlation matrix and model adequacy tests.

Parameter estimation is performed in gPROMS to determine reaction kinetic constants according to the following steps:

- Step 1, Construct a model of the process for which the measurements are being taken. Typically for reaction kinetics, this is a laboratory system which is small enough to ensure that extraneous effects - such as mixing phenomena - do not obscure the measurements.

- Step 2, Define the parameters to be estimated and the variance model to be used for each measuring instrument.

- Step 3, Enter the experimental data sets. As many experiments as required maybe included, and these may contain steady-state or dynamic data sets.

- Step 4, Execute the estimation run.

- Step 5, Check the results

2.3 Mechanisms of asymmetric transfer hydrogenation

The mechanistic aspects of homogeneous catalytic reactions have been addressed by a number of authors and some impressive developments have emerged over the years; nevertheless, this remains an area of constant evolution, as the understanding of many active systems is far from complete. In the transition-metal catalysis, two general reaction paths are well accepted: a stepwise process called the "hydridic route" shown in Figure 2-1 and a concerted process called the "direct hydrogen transfer" shown in Figure 2-2 (Bernard et al 1998).

In the hydridic route, the hydrogen donor interacts with the catalyst first. Then the hydrogen transfers from the hydrogen donor to the catalyst metal center. Finally the hydrogen transfer from the catalyst metal center to the hydrogen acceptor.
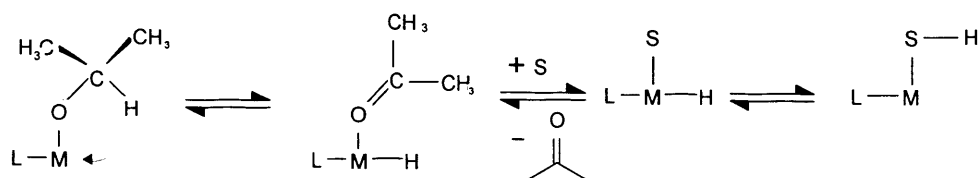
Figure 2-1 Representation of the hydridic route (L=ligand, M=metal, S=substrate)

In the direct hydrogen transfer route, both the hydrogen donor and the hydrogen acceptor are held by the catalyst metal center. The hydrogen transfers from the hydrogen donor to the hydrogen acceptor directly.
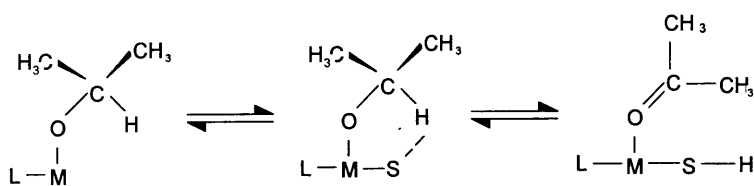
Figure 2-2 Representation of the direct hydrogen transfer (L=ligand, M=metal, S=substrate)

2.3.1 Catalyst cycle proposed by Gladiali et al (1990)

In the catalyst cycle proposed by Gladiali et al (1990) as shown in Figure 2-3, first, through interacting with sodium 2-proxide, transition metal 2-proxide is formed by catalyst 1 dropping off Cl. Then, the elimination of acetone from 2 by way of 3 forms the transition metal hydride 4. The metal hydride 4 reacts with substrate via 5 to form the secondary alkoxide 6. Finally, ligand exchange between 6 and 2-propanol via six-membered cyclic intermediate (Pamies et al, 2001) as shown in Figure 2-4 gives the product and species 2. The catalyst cycle is restored. This catalyst cycle is accepted by other researchers in this area (Touchard et al 1998, Danielle et al 2000).
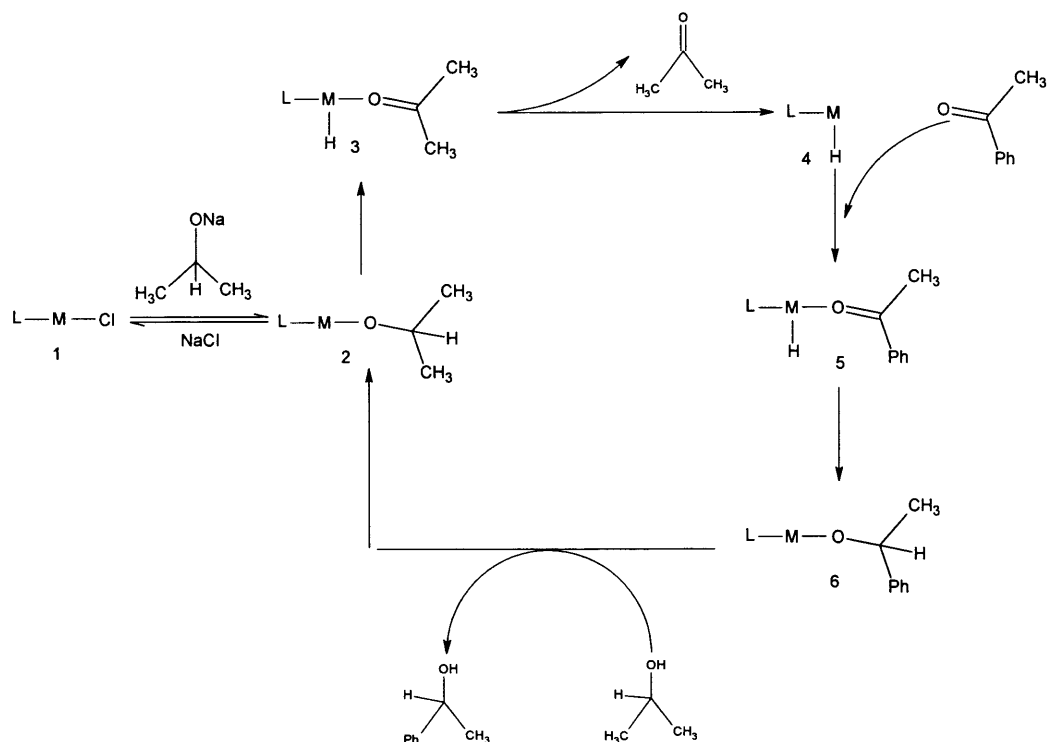
Figure 2-3 Catalyst cycle proposed by Gladiali et al (1990) (L=ligand, M=Metal complex)

33
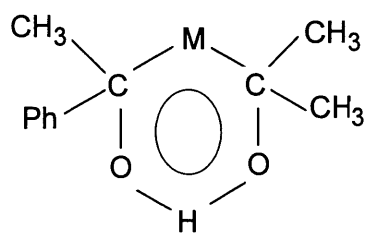
Figure 2-4 Six-membered cyclic intermediate

2.3.2 The metal-ligand bifunctional catalysis mechanism

Recently, through experimental findings (Hashiguchi et al 1995, Hacck et al 1997, Murata et al 1999) and theoretical calculations (Yamakawa et al 2000, Noyori et al 2000, 2001), Noyori proposed the metal-ligand bifunctional mechanism for hydrogen transfer as shown in Figure 2-5.
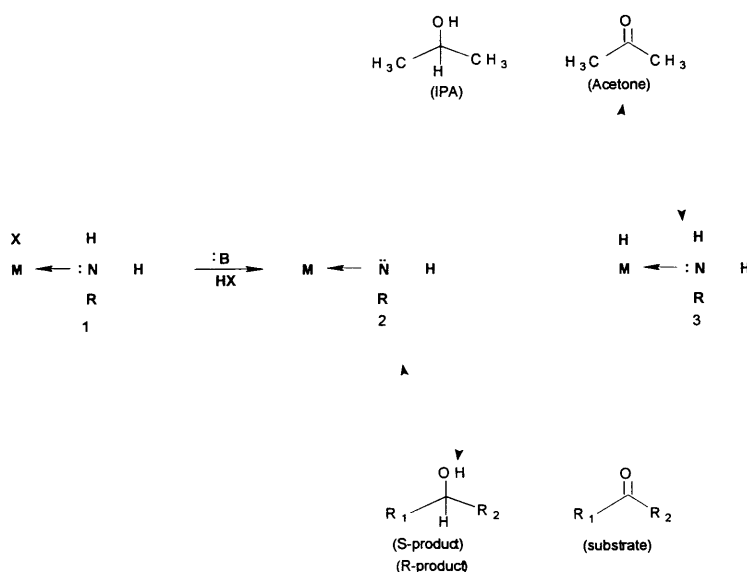
Figure 2-5 Metal-ligand bifunctional mechanism (X=chloride, M=metal, B=base)

In Figure 2-5, with the existence of base, the true catalyst 2 is formed by dropping off HX from the pre-catalyst 1. Then complex 3 is generated by the dehydrogenation of 2-propanol. In this step, Noyori et al studied the kinetics of the steady-state 2-propanol/acetone catalyst cycle (Haack and Noyori 1997). They found that the exchange between 2 and 3 with interaction of 2-propanol or acetone took place either directly or via a very short-lived intermediate. No other

34

complexes limiting the catalytic turnover were involved. The catalytic cycle is restored by the reduction of ketones with intermediate 3. The intermediate 2 and 3 in Figure 2-5 were detected of trace level. There are two possible transition states during the reduction of ketones: 6-membered transition state and 4-membered transition state in Figure 2-6.
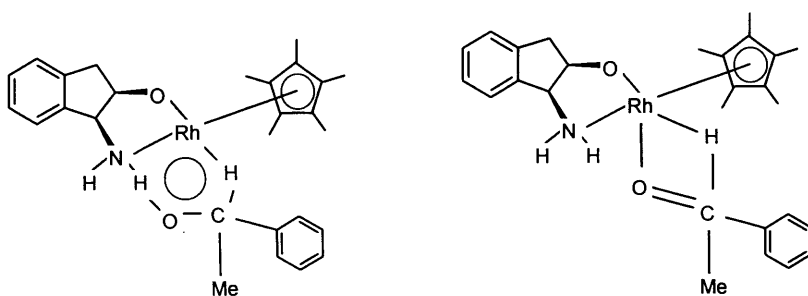
Figure 2-6 Possible transition states

2.4 General principles of reactor design

A general statement of the basic objectives in designing a reactor is to produce a specified product at a given rate from known reactants (Richardson and Peacock 1994). The two most important questions for the reactor design to be settled are:

a) The type of reactor to be used and its method of operation. Will the reaction be carried out as a batch process, a continuous flow process, or possibly as a hybrid of the two? Will the reactor operate isothermally or adiabatically?

b) The physical conditions of the reactants at the inlet to the reactor. Thus, the basic processing conditions in terms of pressure, temperature and compositions of the reactants on entry to the reactor have to be decided, if not already specified as part of the original process design.

Subsequently, the aim is to reach logical conclusions concerning the following principle features of the reactor:

1) The overall size of the reactor, its general configuration and the more important dimensions of any internal structures.

2) The exact composition and physical condition of the products emerging from the reactor. The composition of the products must of course lie within any

limits set in the original specification of the process.

3) The temperatures prevailing within the reactor and any provision which must be made of heat transfer.

4) The operating pressure within the reactor and any pressure drop associated with the flow of the reaction mixture.

The reactor design involves basic principles of chemical engineering with addition of chemical kinetics. Mass transfer, heat transfer, and fluid flow are all important and complications arise when interaction between these transfer processes and the reaction itself. In designing a reactor it is essential to weigh up all the factors involved and to consider them in order of importance.

2.4.1 Traditional gas-liquid contactors

The types of traditional equipment used for gas –liquid contact are shown in Figure 2-7 (Richardson and Peacock 1994).
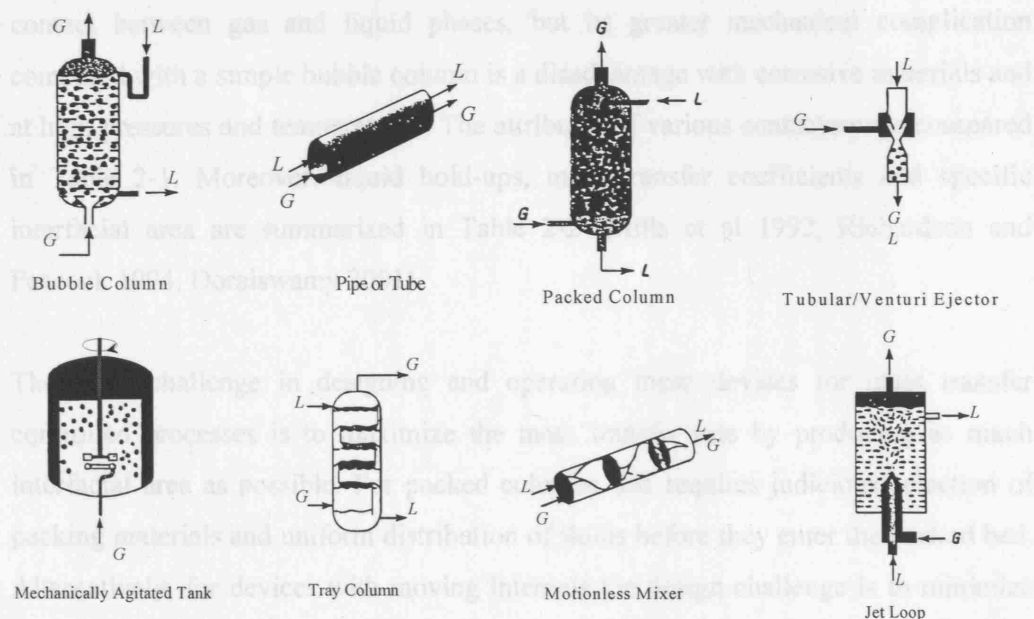
Figure 2-7 Traditional gas-liquid contactors

The packed column is often used when the purpose is to absorb a constituent from a gas. The liquid is distributed in the form of films over the packing, and the gas forms the continuous phase. The pressure drop for the gas is relatively low and packed

column is therefore very suitable for treating large volume flows of gas mixtures. In spray columns gas is the continuous phase and liquid hold-up is comparatively low. In the tray column, gas is dispersed in the liquid passing over the tray. Because the tray is relatively shallow, the pressure drop in the gas phase is fairly low, and the liquid hold-up, although a little larger than for a packed column, is still relatively small.

When a high liquid hold-up is required in the reactor, bubble column, packed bubble column and agitated tank may be used. The bubble column is simply a vessel filled with liquid, with a sparger ring at the base for dispersing the gas. One of the disadvantages of the simple bubble column is that coalescence of the bubbles tends to occur with formation of large slugs whose upper surfaces are in the form of spherical caps. In packed bubble column, the formation of very large bubbles is avoided by packing the vessel with rasching rings. The reactor thus becomes an ordinary packed column operated in a flood condition and with a sparger to disperse the gas. Naturally the maximum superficial gas velocity is much less than in an unflooded packed column. An agitated tank provides small bubbles and thus a high interfacial area of contact between gas and liquid phases, but its greater mechanical complication compared with a simple bubble column is a disadvantage with corrosive materials and at high pressures and temperatures. The attributes of various contactors are compared in Table 2-1. Moreover, liquid hold-ups, mass transfer coefficients and specific interfacial area are summarized in Table 2-2 (Mills et al 1992, Richardson and Peacock 1994, Doraiswamy 2001).

The main challenge in designing and operating these devices for mass transfer controlled processes is to maximize the mass transfer rate by producing as much interfacial area as possible. For packed columns this requires judicious selection of packing materials and uniform distribution of fluids before they enter the packed bed. Alternatively, for devices with moving internals the design challenge is to minimize the bubble or droplet size of the dispersed phase and maximize the number of bubbles and droplets. An important disadvantage is the interdependence of the two fluid phases to be contacted, which sometimes leads to difficulties such as emulsions, foaming, unloading and flooding. An alternative technology that overcomes these disadvantages and also offers substantially more interfacial area that conventional approach is non-dispersive contact via a thin film.

Table 2-1. Reactor types for gas-liquid systems and their main features.

Reactor Type	Mechanically agitated	Empty/Tray bubble column	Packed bubble column	Spray column	Wetted wall column/Falling film	Plunging jet/Venturi scrubber
Operation	▪ batch ▪ semibatch ▪ continuous	▪ batch ▪ continuous	continuous	continuous	continuous	continuous
Continuous phase	liquid	liquid	depends on flow arrangement	gas	gas liquid	depends on the operating conditions
Disperse phase	gas	gas	depends on flow arrangement	liquid (mist/spray/droplets)	-	depends on the operating conditions
Flow arrangements	-	▪ co-current ▪ counter-current	co-current-upwards/downwards counter-current	co-current	▪ co-current ▪ counter-current	co-current
How mixing is promoted	▪ mechanical stirring ▪ gas bubble rise	momentum transfer between gas bubbles and liquid	momentum transfer between gas and liquid	-	-	-
Other remarks	▪ superior heat and mass transfer coefficients	internal elements are use to modify residence time and mixing features		▪ pumping cost can be high ▪ drop coalescence difficult to control	liquid film thickness requires careful control	high gas-liquid mass transfer rates
Recommended use	▪ slow/moderate reactions ▪ large heat effects ▪ heating/cooling or both requirements	▪ slow reactions that require long residence time ▪ economic at high pressure ▪ moderate heat effects	▪ liquids are treated with small amount of gas ▪ large residence time for liquid is required ▪ low pressure drop required ▪ better for foaming liquids than plate column	▪ high corrosion ▪ selective absorption ▪ gas-phase pressure drop must be minimised ▪ high exothermically ▪ solid can be in solid phase	▪ high exothermicity ▪ reactant/produ cts thermally unstable ▪ large interfacial area is not necessary ▪ fast reactions	▪ adsorption ▪ desorption ▪ fast reactions

Table 2-2 Liquid hold-ups, mass transfer coefficients and specific interfacial area for various types of gas-liquid reactors.

Type of Reactor	$100\varepsilon_L/(\varepsilon_L + \varepsilon_G)$	k_g (gmol/cm^2 s atm)	k_L (cm/s)	a cm^2/cm^3 reactor	$k_L a$ (s^{-1})
Mechanically agitated bubble reactor	20-29	-	$(0.3\text{-}4) \times 10^{-2}$	1-20	$(0.3\text{-}80) \times 10^{-2}$
Bubble columns	60-98	$(0.5\text{-}2) \times 10^{-4}$	$(1\text{-}4) \times 10^{-2}$	0.5-6	$(0.5\text{-}24) \times 10^{-2}$
Packed bubble columns	60-98	$(0.5\text{-}2) \times 10^{-4}$	$(1\text{-}4) \times 10^{-2}$	0.5-3	$(0.5\text{-}12) \times 10^{-2}$
Packed columns					
• counter-current	2-24	$(0.03\text{-}2) \times 10^{-4}$	$(0.4\text{-}2) \times 10^{-2}$	0.1-3.5	$(0.04\text{-}7) \times 10^{-2}$
• co-current	2-95	$(0.01\text{-}3) \times 10^{-4}$	$(0.4\text{-}6) \times 10^{-2}$	0.1-17	$(0.04\text{-}102 \times 10^{-2})$
Plate columns					
• bubble caps	10-95	$(0.5\text{-}2) \times 10^{-4}$	1.5×10^{-2}	1-4	$(1\text{-}20) \times 10^{-2}$
• sieve plates	10-95	$(0.5\text{-}6) \times 10^{-4}$	$(1\text{-}20) \times 10^{-2}$	1-2	$(1\text{-}40) \times 10^{-2}$
Spray columns	2-20	$(0.5\text{-}2) \times 10^{-4}$	$(0.7\text{-}1.5) \times 10^{-2}$	0.1-1	$(0.07\text{-}1.5) \times 10^{-2}$
Tubular reactors					
• horizontal	5-95	$(0.5\text{-}4) \times 10^{-4}$	$(1\text{-}10) \times 10^{-2}$	0.5-7	$(0.5\text{-}70) \times 10^{-2}$
• colloid-vertical	5-95	$(0.5\text{-}8) \times 10^{-4}$	$(2\text{-}5) \times 10^{-2}$	1-10	$(2\text{-}100) \times 10^{-2}$
• Submerged and plunging jet	94-99		$(0.15\text{-}0.5) \times 10^{-2}$	0.2-1.2	$(0.03\text{-}0.06) \times 10^{-2}$
• Hydrocyclone	70-93		$(10\text{-}30) \times 10^{-2}$	0.2-0.5	$(2\text{-}15) \times 10^{-2}$
• Ejector reactor	-	$(2\text{-}10) \times 10^{-4}$	-	1-20	-
• Venturi	5-30		$(5\text{-}10) \times 10^{-2}$	1.6-25	$(8\text{-}25) \times 10^{-2}$

2.4.2 Two-phase tubular reactor

2.4.2.1 Mixing

Before reactants flow into the tubular reactor, they have to be premixed. Mixing in minute spaces can basically rely only on two principles which are diffusion and convection. Diffusion between short distances, establishing high concentration gradients, was initially the most frequently applied principle by simply making the channels themselves smaller and smaller. Soon, the limits of that strategy, also in terms robustness (fouling) and cost (complex microfabrication), became obvious. In recent years, various methods were developed to overcome the limits by diffusion mixing, all of them based on the induction of secondary-flow (convective) patterns which are superimposed on the main flow, often in the vertical direction to the flow axis. This includes recirculation patterns, chaotic advection and swirling flows. Convection is effective for mixing, since it serves to enlarge mixing interfaces. Convection of 'gross' mass portions can be used at a much larger scale to stir complete chamber volumes, e.g. by ultrasound, by electrokinetic instability or acoustic means. At high Reynolds numbers, turbulent mixing can be utilized; however, this is often not practicable, as this implies achievement of unrealistic large flow velocities. The few speciality equipment types known to use turbulence rely either on free-guided flows or guide through meso-scale channels (Hessel et al 2005).

Besides the Reynolds number ($Re = U \cdot d / v$), the Peclét number ($Pe = U \cdot d / D$) and the Fourier number ($Fo = t_r/t_m$) are commonly used as dimensionless groups to characterise convective/diffusive problems. Here U, d, v denote the average velocity, the hydraulic and the kinematic viscosity. t_r and t_m denote the average residence time and the diffusive mixing time, defined as $t_r = L/U$ and $t_m = d^2/D$, where L denotes the longitudinal length. The Reynolds number (Re) characterises the ratio of inertial to viscous forces. The Peclet number (Pe) describes the ratio of mass transport by convection to that by diffusion. The Fourier number (Fo) originating from transient diffusive heat and mass transfer, relates to the progress of diffusive transport processes to various geometries and has been commonly employed for determine mixing time. For laminar uniaxial flows the mixing length L_m is found to be proportional to Pe times the channel width (Hessel et al 2005).

For the flow range of 10-100000m^3/h, static mixers are standard equipment in the process industries. Micromixers have flows in the sub-ml/h to 10m^3/h ranges which covers the whole flow range up to the conventional static mixers (Figure 2-8) (Thakur et al 2003, Hessel et al 2005).
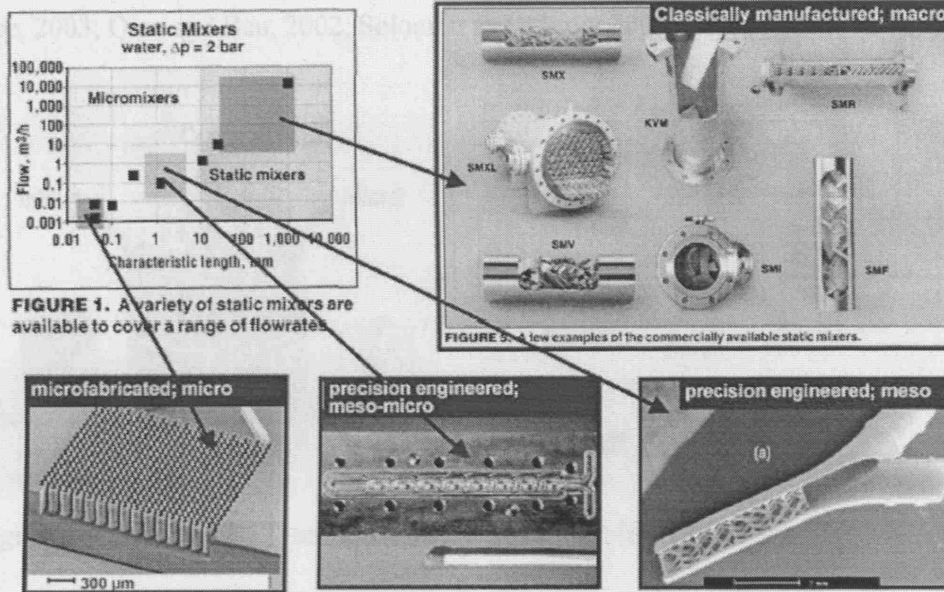
Figure 2-8 Micromixers (laboratory-scale) and microstructured mixers (pilot-scale) close the gap to static mixers, yielding apparatus for a multi-scale concept (Hessel et al 2005)

Two basic principles are followed to induce mixing at the microscale. First, energy input from the exterior can be used, termed *active mixing*. These external energy sources are ultrasound (Yang et al., 2001), acoustic, bubble-induced vibrations (Liu et al., 2003, 2002), electrokinetic instabilities (Oddy et al., 2001), periodic variation of flow rate (Glasgow and Aubry, 2003; Niu and Lee, 2003; Qian and Bau, 2002), electrowetting-induced merging of droplets (Palk et al., 2003), magneto-hydrodynamic action (West et al., 2002).

As a second means, the flow energy, e.g. due to pumping action or hydrostatic potential, is used to restructure a flow in a way which results in faster mixing. This is known as *passive mixing*. Thin lamellae are created in special feed arrangements,

termed interdigital (Bessoth et al., 1999; Drese, 2003; Ehlers et al., 2000; Ehrfeld et al., 1999; Hardt and Schönfeld, 2003; Hessel et al., 2003; Löb et al., 2004). A serial way of creating multi-lamellae can be achieved by Split-and-Recombine (SAR) flow guidance (Schönfeld et al., 2004; Schwesinger et al., 1996). Chaotic mixing creates eddy-based flow patterns which provide high specific interfaces, albeit bearing the danger of being spatially inhomogeneous (Jen et al., 2003; Jiang et al., 2004; Niu and Lee, 2003; Qian and Bau, 2002; Solomon and Mezic, 2003; Stroock et al., 2002).
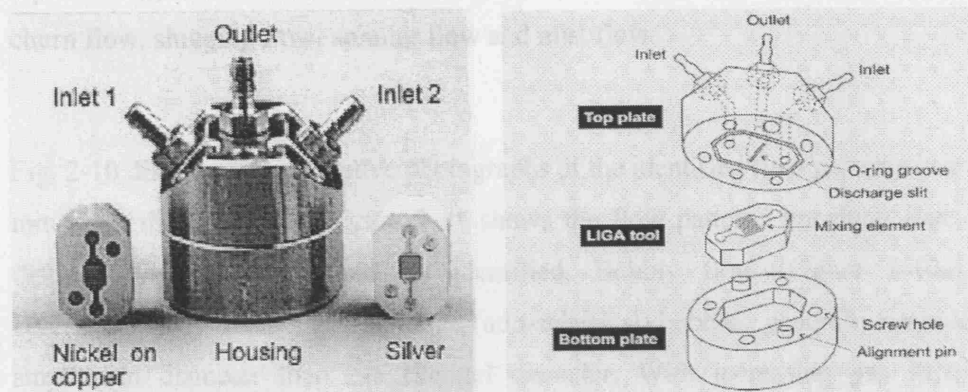
Figure 2-9 Standard Slit Interdigital Micro Mixer (Ehrfeld et al 1999)

In this work, a Standard Slit Interdigital Micro Mixer (SSIMM) was used. The mixer is an assembly of three components, namely a LIGA device containing the mixing element which is embedded in a two-piece housing. The LIGA devices are made of nickel on copper (i.e. a nickel layer with micro-channels on a copper base plate) or of silver. The stainless steel housing is built of two pieces, the top and bottom plate connected to inlets and outlets (see Figure 2-9). The design of the mixing element is based on a layer containing 15 fluid channels for each fluid with a width of 40 μm, respectively, and a depth of 300 μm supported by a base plate. The divided sub-streams in the micro-channels penetrate each other but do not contact due to separating walls. To achieve a deep penetration of both fluids (well-defined multi-lamination) for micro-channels of variable depth and width, the pressure loss in this part of the mixer has to be individually adapted. This is performed by restricting the contact area (mixing zone) by a slit on top of the mixing element. The slit is connected to the outlet by a drilled hole of 500 μm diameter which does not break through to the surface facing the micro-channels.

2.4.2.2 Two-phase slug flow reactor

In two-phase slug flow reactor, gas and liquid are usually introduced into the reactor through T or Y shape mixer. Two-phase flow patterns in microchannels, including channels with diameters close to 1 mm, have been recently studied by several investigators (Elperin and Fominykh 1995, Triplett et al 1999, Cheng and Li 2001, Shemer 2003, Taha and Cui 2004). Triplett et al (1999) could identify bubbly, slug, churn, slug-annular and annular flow patterns (Figure 2-10). Heiszwolf et al (2001) reported dispersed bubble flow, bubble flow, elongated bubble flow, Taylor flow, churn flow, slugging flow, annular flow and mist flow.

Fig. 2-10 displays representative photographs of the identified flow patterns in a 1.097 mm-inner diameter tube. Figure 2-11 shows the flow patterns transition lines. Five distinct flow patterns could be identified. Bubbly flow (Figure 2-10a) was characterized by distinct and distorted (non-spherical) bubbles, generally considerably smaller in diameter than the channel diameter. With increasing gas superficial velocity (which leads to increasing void fraction) the bubbles crowded near the channel top and eventually led to the development of the slug flow (Figure 2-10b), characterized by elongated cylindrical bubbles. Parameter changes leading to higher void fraction (e.g. increasing gas superficial velocity and/or decreasing liquid superficial velocity) lead to longer bubbles and shorter liquid slugs. The bubbles, however, appear to effectively occupy most of the channel cross-section.

(a) (b)

(c) (d)

(e)
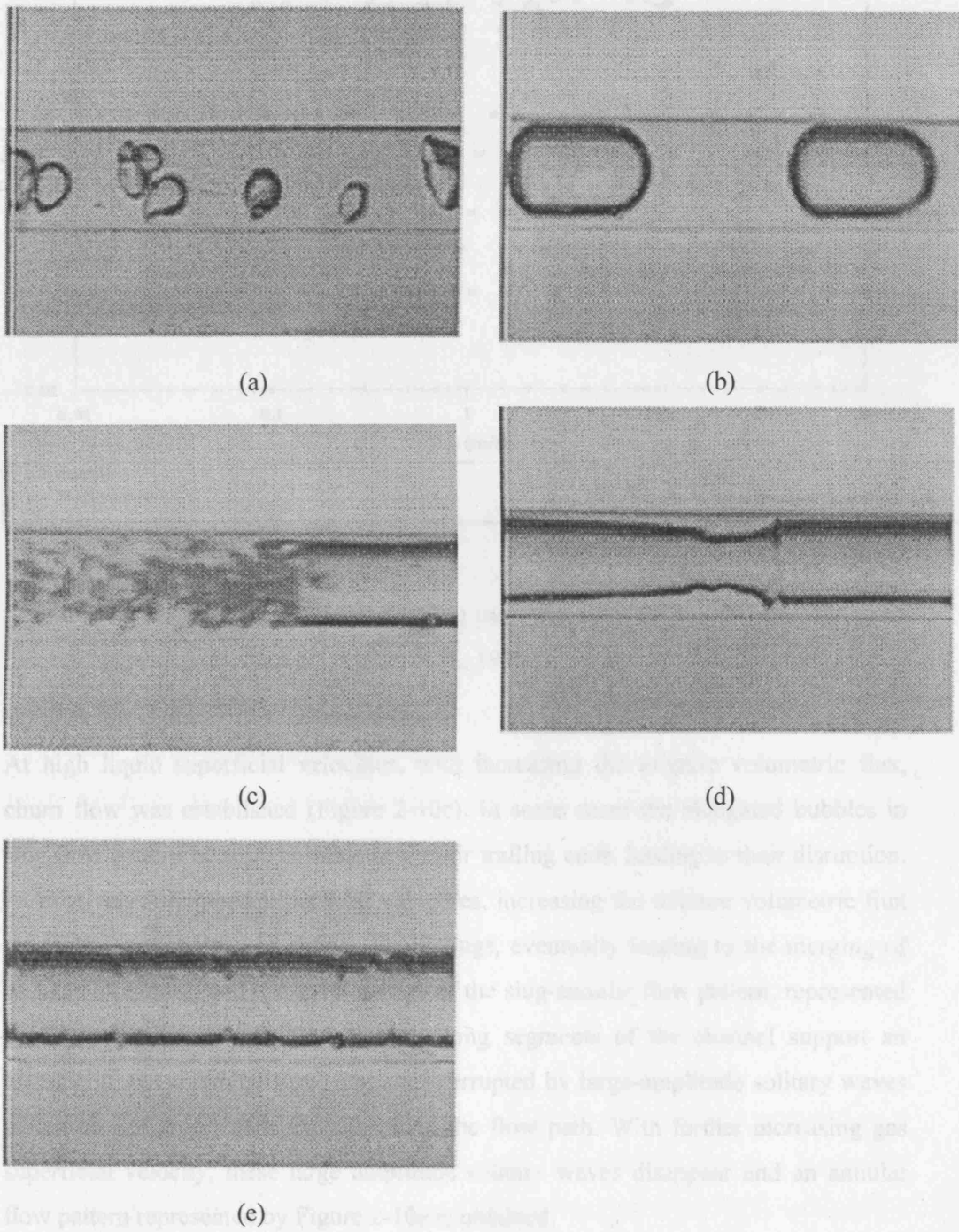
Figure 2-10 Photographs of flow patterns in a 1.097 mm diameter tube (a) bubbly; (b) slug; (c) churn; (d) slug-annular; (e) annular. (Triplett et al 1999)
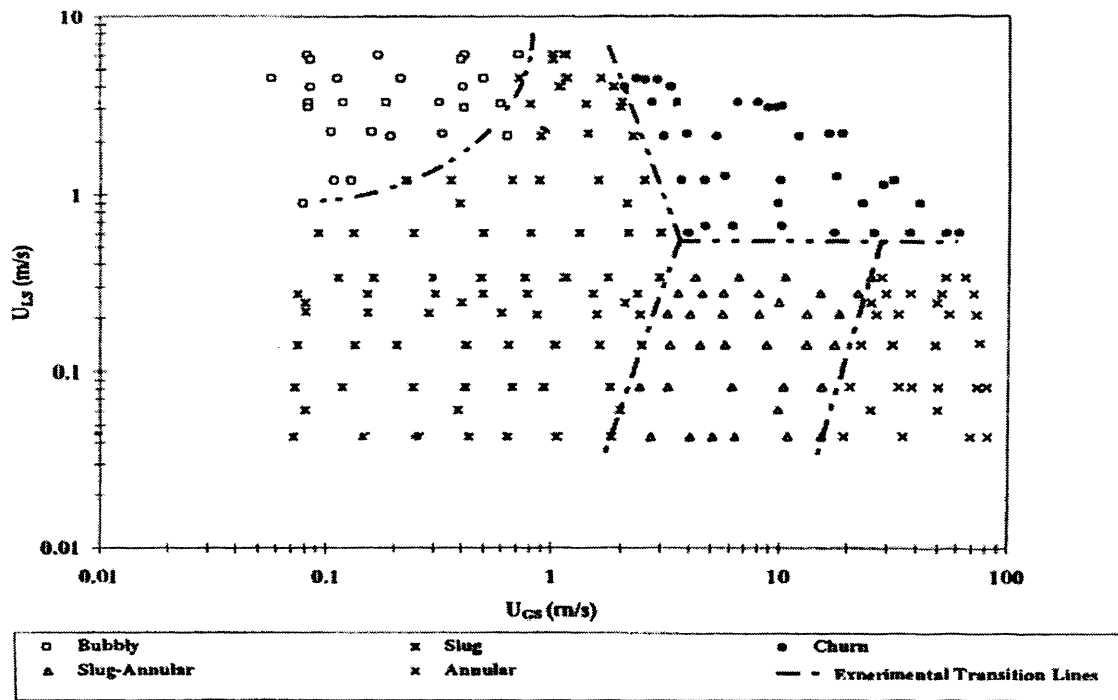
Figure 2-11 Flow patterns and flow pattern transition lines for a 1.097-mm diameter circular cross section channel (Triplett et al., 1999).

At high liquid superficial velocities, with increasing the mixture volumetric flux, churn flow was established (Figure 2-10c). In some cases the elongated bubbles in slug flow pattern became unstable near their trailing ends, leading to their disruption. At relatively low liquid superficial velocities, increasing the mixture volumetric flux led to longer bubbles and shorter liquid slugs, eventually leading to the merging of elongated bubbles, and the development of the slug-annular flow pattern, represented by Figure 2-10d. In this flow pattern, long segments of the channel support an essentially wavy-annular flow, and are interrupted by large-amplitude solitary waves which do not grow sufficiently to block the flow path. With further increasing gas superficial velocity, these large amplitude solitary waves disappear and an annular flow pattern represented by Figure 2-10e is obtained.

In slug flow, the gas bubbles have a diameter nearly equal to that of the channel leaving only a thin liquid film between the bubble and the wall. Because the gas bubbles almost block the channels, the liquid flow between two consecutive liquid

45

slugs may be neglected. Due to the stationary wall, a circulating flow is induced in a moving liquid slug. This circulation flow refreshes the gas-liquid interface of the gas bubble continuously, leading to a high gas-liquid mass transfer rate (Heiszwolf et al 2001).

Slug flow provides a useful and convenient method of augmenting radial heat and mass transfer. Slug flow has been demonstrated to augment significantly radial mass transfer in reactors with catalytically active walls (Horvath et al 1973). Radial mixing was found to increase with Reynolds number, and rapidly increased with decreasing slug length. Enhancement of radial increase in heat transfer by slug flow has been demonstrated by Oliver and Wright (1964) and Oliver and Young Hoon (1968). It is demonstrated that injecting gas bubbles is a cheap and effective way of reducing concentration polarisation and thus enhancing the permeate flux in hollow fibre membrane modules (Bellara et al 1997, Ghosh and Cui 1999, Smith and Cui 2004). Slug flow can be obtained in a monolith over a wide range of operating conditions (Berčič and Pintar 1997, Heiszwolf et al 2001). Slug flow also occurs in physiological systems during blood flow through the pulmonary and peripheral capillaries of the body where slugs of plasma are trapped between red blood cells (Prothero and Burton 1961, Lighthill 1968). Red blood cells separated by blood plasma, are easily deformable under stress and, in the smaller blood vessels, behave like bubbles. Prothero and Burton (1961) pointed out that strong circulation ahead of the red cells was found very effective on nutrient distribution.

2.4.3 Rotating disc reactor
2.4.3.1 General characteristics
A rotating disc contactor is considered as a disc or a number of discs mounted on a central, horizontal shaft which is placed in a liquid-filled trough. The disc is partially immersed in the liquid, and its upper part is contained in a gas-shell so that if a rotational movement is imposed to the disc, a liquid film is brought upwards over the surface of the disc, thus providing a contact of the liquid film with the gas phase. After moving downwards the liquid film will be taken up again by the bulk of the liquid in the trough. The main advantage of such design is that the interfacial gas-liquid area is constant and known. In addition, the contact between phases is

generated by maintaining the liquid phase as thin film thus minimising the mass transfer resistances related to the liquid phase. More flexibility of the variables influencing mass transfer can be obtained compared to a gas-liquid stirred tank reactor. For example, in stirred vessels the gas flowrate used is limited by the flooding of the impeller (Sutter et al 1987, Tatterson and Morrison 1987). Modification of the size and dimensions of the gas shell can accommodate a wider range of gas flowrates. Most importantly, a RDR is suitable for scale-out. By increasing the number of discs the throughput can be increased by replicating an optimised unit, thus eliminating possible potential scale-up obstacles which usually occur during the scale-up of the conventional gas liquid reactor (i.e. bubble column, stirred tank vessels).

2.4.3.2 Film thickness measurements and correlations

The main issue related to operation of a RDR is the correlation of the film thickness formed on the disc with disc size and speed of rotation. Bintanja et al. (1975) used a simple experimental method to determine an average film thickness over the disc. In this method a curved screen wiper, bent in the middle into a V-shape, and pressed against the rotating disc over the total width of the wetted surface was used to wipe off the liquid film on the disc. The liquid of the film unties in the middle of the wiper and is collected in a small collecting vessel. A second wiper, placed beneath the first one, may serve to control the completeness of the collection of the liquid film. The reproducibility of the method amounts to ±5%. The liquid amount was collected and weighted and a mean average film thickness was calculated. Their experiment correlates the average film thickness as a function of liquid properties, disc radius and the speed of rotation:

$$\delta_g = k\left(\frac{\eta \cdot \omega \cdot R}{\rho \cdot g}\right)^{0.5} \qquad (2\text{-}2)$$

where, η is dynamic viscosity of the liquid, ω is speed of rotation, ρ is density, R is the radius of the disc, g is acceleration due to gravity and k is constant. A value of 0.93 was found for the constant k from fitting experimental measurements for δ as a function of $\omega^{0.5}$. Similar experiment was conducted by Zeevalkink et al. (1978). The amount of the liquid entrained by the discs was measured by holding sponges against the disc in the region of the ultimate film thickness, i.e. at the horizontal line passing through the disc center. After one or two rotations the increase of weight of the

sponges was measured. It is considered that the film velocity equals the disc velocity and the film thickness is uniform over the disc. They found that the mean film thickness is given by:

$$\delta_g = \frac{4}{15}\left(\frac{2\cdot\eta\cdot\omega}{\rho\cdot g}\right)^{0.5}\left(R^2 - H^2\right)^{0.25}$$

(2-3)

where H is the distance between the disc centre and the liquid level. The reproducibility of the method amounts to ±5%. Good comparison of the film thickness given by Equation (2-3) with experimental data was reported.

Bintanja et al. (1975) also examined the variation of the film thickness over the disc using the following method. After rotation was stopped small weighted filtering papers with a distinct surface area were pressed at several places against the wetted disc, using a screen wiper above it to prevent the filtering paper from contamination with water from other places of the disc. Forty measurements showed uniformity of the thickness of the water layer over the total surface within approx 6%.

Suga and Boongorsrang (1984) proposed that the liquid film thickness on the disc between the boundary-layer submerged and film exposed to the gas is different. The average submerged boundary-layer film thickness is given by

$$\delta_l = \frac{10}{3}\left(\frac{\eta}{2n}\right)^{1/2}\cdot Sc^{-1/3}$$

(2-4)

and the film thickness exposed to air is given by:

$$\delta_g = \frac{1}{3}\left(\frac{2\cdot\eta\cdot\omega\cdot r}{g}\right)^{1/2}$$

(2-5)

Zeevalkink et al (1978) also demonstrated that the thickness of a boundary-layer film, partly immersed in water, is larger than the film thickness exposed to the gas for the disc size 0.60m diameter, rotation speed 6-33rpm and depth of immersion 0.105-0.27m. However, the film thickness exposed to the gas increases with increase of the rotation speed and disc size and the boundary-layer thickness decreases with increase of the rotating speed. Therefore, for a certain value of the rotation speed and disc size, it is possible that boundary-layer thickness is smaller than the film thickness exposed the air.

2.4.3.3 Mass transfer

Bintanja et al. (1975) proposed an expression to calculate an average mass transfer coefficient in the liquid film:

$$K_L^{Film} = 2\sqrt{\frac{D}{\pi \cdot t_r}} \cdot \left[1 + 2\sqrt{\pi} \cdot \sum_{n=1}^{\infty} (-1)^n \cdot ierfc\left(\frac{n \cdot \delta}{\sqrt{D \cdot t_r}} \right) \right] \qquad (2\text{-}6)$$

where, ierfc(x) is the integral complementary error function calculated as

$$ierfc(x) = \left(1/\sqrt{\pi} \right) \exp\left(-x^2 \right) - x \cdot erfc(x) \qquad (2\text{-}7)$$

erfc(x) is complementary error function of x

$$erfc(x) = 1 - erf(x) \qquad (2\text{-}8)$$

erf(x) is error function of x

$$erf(x) = \frac{2}{\sqrt{\pi}} \int_0^x e^{-y^2} dy \qquad (2\text{-}9)$$

This correlation is well accepted by other researchers (Zeevalkink et al 1979, Suga and Boongorsarang 1984). For high speed of the rotation, when $\dfrac{\delta}{\sqrt{D \cdot t_r}} \geq 1.7$,

Equation 2-6 simplifies to:

$$K_L^{Film} = 2\sqrt{\frac{D}{\pi \cdot t_r}} \qquad (2\text{-}10)$$

and for low speed of rotation, when $\dfrac{\delta}{\sqrt{D \cdot t_r}} < 0.8$, Equation 2-6 simplifies to:

$$K_L^{Film} = \frac{\delta}{t_r} \qquad (2\text{-}11)$$

where the average contact time of the liquid on the disc with the gas phase is given in a good approximation by :

$$t_r = \frac{1}{\omega} \left(\frac{P_0 - (1/\pi) \cdot P_1}{P_0} \right) \qquad (2\text{-}12)$$

where, ω is disc rotation speed and

$$P_0 = 0.5\left(R^2 - H^2 \right) \qquad (2\text{-}13)$$

$$P_1 = 0.5R^2 \cdot \arccos\left(\frac{H}{R} \right) - 0.5R \cdot H \cdot \sqrt{1 - \left(\frac{H}{R} \right)^2} \qquad (2\text{-}14)$$

49

It can be seen that when $\dfrac{\delta}{\sqrt{D \cdot t_r}} \geq 1.7$, the average mass transfer coefficient is independent of the film thickness, while when $\dfrac{\delta}{\sqrt{D \cdot t_r}} < 0.8$, the mass transfer coefficient is proportional to the film thickness.

For intermediate speeds of rotation, $0.8 < \dfrac{\delta}{\sqrt{D \cdot t_r}} < 1.7$, the mass transfer coefficient is (Zeevalkink et al 1979):

$$K_L^{Film} = \left(2\sqrt{\dfrac{D}{\pi \cdot t_r}} \right) \cdot \left(1 - 4.21 \cdot \exp\left(-3.2 \cdot \dfrac{\delta}{\sqrt{D \cdot t_r}} \right) \right) \qquad (2\text{-}15)$$

In the boundary-layer forming on the disc inside the liquid bulk, the mass transfer coefficient can be calculated as (Suga and Boongorsrang 1984):

$$K_L^{Bulk} = \dfrac{D}{\delta_l} \qquad (2\text{-}16)$$

2.4.3.4 Mixing of the film in the trough

Bintanja et al (1975) assumed that the liquid film being entrained as the disc left the trough is stripped off and then mixed completely with bulk liquid, when the disc re-enters the trough. There is no experimental support for this assumption. Zeevalkink et al (1979) assumed that part of the film layer nearest to a disc adheres to the disc and does not mix with water in the trough. This assumption was investigated experimentally. The experiment was done by rotating a glass disc (diameter 30cm) through an aqueous solution containing 600mg/l methyl violet until a film of the solution adhered to the disc. The glass disc was then brought to a tank containing only water. The liquid on the glass was then collected and the mean methyl violet concentration was measured with a spectrophotometer. The immersion depth of the disc was always kept about 10cm. The experiment was conducted at rotation velocities of 15, 35 and 60rpm, while the maximum number of the rotation in the water tank amounted to 10, 15 and 25 respectively. The disappearance of methyl violet on the disc showed a linear relationship with the number of rotations which

demonstrates that only part of the film layer slowly mixes with water in the trough. They also suggested that about 25~50% of the water film on a disc adheres to the disc. They explained this incomplete mixing from a theoretical point of the view for the rotating disc reactor with disc size 0.60m diameter, rotation speed 6-33rpm and depth of immersion 0.105-0.27m. The rotation of the disc through the water in the trough caused a flow in the water which resulted in a boundary layer near the disc. The boundary layer thickness is larger than the film thickness above the water. Moreover, the flow caused by the disc is usually laminar at low rotation speed. Therefore, the water film does not mix completely with water in the trough after a revolution due to the growing thickness of the layer under water and the laminar flow conditions.

Suga and Boongorsrang (1984) also demonstrated that only part of film on the disc was mixed with liquid in the trough experimentally. A disc was rotated in the trough, into which blue blank ink had been poured to colour the water, until a liquid film was formed on the disc. Then the disc was transferred immediately to a tank of fresh water and rotated manually. The photographs of the pattern of the liquid film on the disc mixed with the liquid in the trough are shown in Figure 2-12. It is clearly shown in Figure 1 that the liquid film on the disc was stripped off partly from the disc and mixed with bulk in the trough when the disc emerged from the trough rather than when it re-entered.
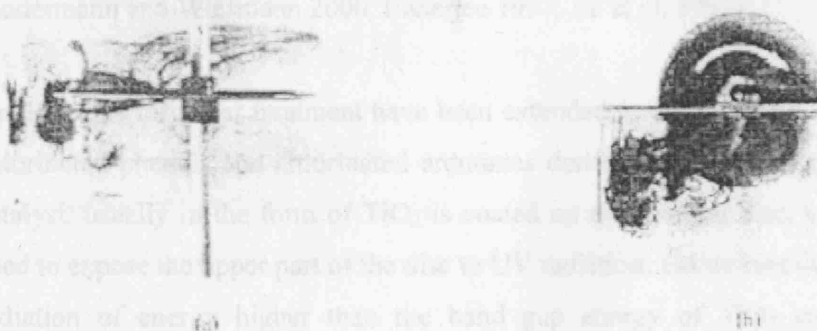
Figure 2-12 Photographs manifesting the mixing of liquid film when the disc emerges from the water reservoir: (a) top view, (b) side view. (Picture scanned from the paper by Suga and Boongorsrang 1984)

In order to improve the mixing of the liquid film with trough liquid, the following two means are suggested. First, a wiper is suggested to press against the disc at the position where the disc re-enters the liquid trough. In this way the liquid film can be wiped off by the wiper and mixed with trough liquid. Second, one can bubble gas through the trough liquid rather than flowing it above the liquid surface. The gas bubbles can reduce the boundary layer thickness and improve the mixing in the trough.

2.4.3.5 Applications

The principle of RDR for multiphase reactions has been applied successfully for several purposes. Many applications are for treatment of waste water because it is possible to obtain high performance in the removal of dissolved pollutants at the expense of less energy than using other conventional methods (Friedman et al. 1979). For this type of applications the RDR is also known as a *rotating biologic contactor*. Waste water with high concentrations of nitrogen compounds (i.e. ammonia, biological nitrogen) is biologically denitrified. The nitrogen compounds are reduced finally to molecular nitrogen by specific bacterial cultures. The constant rotation of the disc causes mixing of the liquid, and at the same time the disc surface alternately comes into contact between air and waste water acting as an aeration device for wastewater treatment. The RDR as biocontactor combines advantages of the aerobic rotating biological contactor: high biomass concentration, short hydraulic retention time, low energy consumption, operational simplicity, and advantages of the anaerobic process: no oxygen transfer limitation, low quantities of waste biological solids (Kubsad et al. 2004, Di Palma et al. 2003, Teixeira and Oliveira 2001, Lindermann and Wiesmann 2000, Banerjee 1997, Lu et al. 1997).

Applications for water treatment have been extended to photocatalytic degradation of chlorinated phenols and chlorinated aromatics derived from pesticides or dyes. The catalyst, usually in the form of TiO_2 is coated on the rotating disc, while lamps are used to expose the upper part of the disc to UV radiation. Ultraviolet illumination with radiation of energy higher than the band gap energy of TiO_2 creates a charge separation (electron-hole) pair. These charge carrier species interact with solvent molecules, usually water, and form hydroxyl radicals which are the primary oxidants of wastewater organics. Owing to the thin entrained liquid films, UV absorption by

substrate molecules or intermediates is reduced in comparison with slurry phase reactors (Dionysiou et al. 2002, Hamill et al. 2001, Dionysiou et al. 2000).

RDR has been used for citric acid production by aerobic fermentation using a bacterial culture. The oxygen distribution through the biofilm formed on the disc is of crucial importance for the rate of cell growth, and thus for the yield in citric acid. The advantages of a RDR with a conventional stirred tank reactor and airlift reactor is that the energy requirement is lower since it needs no aeration apparatus and the foaming which usually accompanies aeration in conventional reactors is eliminated (Sakurai et al. 1997).

Another application type for a RDR is in the area of thermoplastic polymer production such as polycarbonates, when a reaction by-product needs to be removed by gas stripping from the reaction mixture. For example, in the melt polycondensation of bisphenol A polycarbonate, the condensation by-product, phenol, can be efficiently removed from the highly viscous polymer melt using an inert gas in a RDR (Woo et al. 2001).

Glatzer et al. (2001, 1998) report a rotating disc reactor for a reacting liquid-liquid system. The disc carries a solid phase transfer catalyst, and is rotated about the horizontal axis which is located at the level of a liquid-liquid interface. Phase transfer catalysis is an important tool in the manufacture of pharmaceuticals and fine chemicals. Whenever the overall reaction is inhibited because its reactants are soluble in different phases, phase transfer catalysis offers a convenient way to bring the reactants together. The disc is positioned perpendicular to the liquid-liquid interface so that the catalyst is equally exposed to both bulk phases during one revolution. This reactor design was used for experimental investigation of mass transfer influence for the esterification of benzyl chloride with sodium acetate mediated by polymer-bound tributylmethylammonium chloride as immobilized phase transfer catalyst.

2.4.4 Membrane gas-liquid contactors

2.4.4.1 General characteristics

There has been active research on membrane processes for gas-liquid contact, such as membrane pervaporation (PV) (Lipnizki et al 1999, Jonquières et al 2002, Smitha et al

2004), membrane distillation (MD) (Godino et al 1996, Lawson and Lloyd 1997) and membrane air stripping (MAS) (Mahmud and Kumar 1998, Mahmud et al 2000), for the removal/separation/concentration of organics from aqueous solutions. The membrane acts as a fixed interface and keeps the gas-liquid phase separated while the transport of organics can take place through the membrane. Advantages membrane contactors offer over columns and other conventional mass transfer equipment include the following (Reed et al 1995, Gabelman and Hwang 1999).

- Membrane contactors provide a relatively large interfacial area between the two phases. The specific surface area of the membrane contactor can be as high as $6000m^2/m^3$ (He et al 2004), while the highest specific surface area of commonly used packing materials is about $600m^2/m^3$ (LaGrega et al 1994).

- There is no fluid-fluid dispersion. The flooding, foaming, and emulsion formation can be avoided in the membrane air stripping. The flowrates of the two fluids can be very high or very low.

- Interfacial area is constant, which allows performance to be predicted more easily than conventional dispersed phase contactors.

- Solvent hold up is low, which is attractive feature when using expensive solvents.

- Modular design of membrane contactor allows flexibility in plant operation and modification. Small and large capacity can be obtained by altering the number of modules.

- Scale up is more straightforward because membrane operation usually scales linearly.

On the other hand, membrane contactors have several disadvantages compared to conventional packed towers:

- The membrane introduces an additional resistance to mass transfer not found in conventional processes.

- Membranes are subject to fouling.

- Membranes have a finite life.

- Membrane pores may become wetted causing leakage across the membrane or reduced performance.

2.4.4.2 Membrane materials and contactor modules

The membrane is at the heart of every membrane process and can be considered as a permselective barrier or interface between two phases. The membrane can be thick or thin and its structure can be homogeneous or heterogeneous. Membranes can be made from a large number of different materials such as Polycarbonate, Polyvinylidenefluoride (PVDF), Polytetrafluoroethylene (PTFE), Polypropylene (PP), Polyamide, Cellulose-esters, Polysulfone (PSF), Poly(ether-imide), Polyetheretherketone (PEEK) and inorganic materials (Mulder 1996).

PTFE is highly crystalline and exhibits excellent thermal stability. It is not soluble in any common solvent and hence also shows high chemical resistance. PVDF shows good thermal and chemical resistance although not quite as good as PTFE. PVDF is soluble in aprotic solvents such as dimethylformamide (DMF), dimethylacetamide (DAMC) and in triethylphosphate (TEP). PP is an excellent solvent resistant polymer when it is in the isotactic configuration. The three polymers PTFE, PVDF and PP have some properties which are similar. They all exhibit good to excellent chemical and thermal stability. Because of their hydrophobic nature, water cannot wet these membranes spontaneously.

Another class of membrane polymers are the polyamides which have outstanding mechanical, thermal, chemical and hydrolytic stability. PSF possess very good chemical and thermal stability and is widely used as basic materials for ultrafiltation membranes and as support materials for composite membranes. Polyetherketones is a new group of chemically and thermally resistant polymers. PEEK is only soluble at room temperature in concentrated inorganic acids such as sulfuric acid or chlorosulfonic acid.

Inorganic materials generally possess superior chemical and thermal stability relative to polymeric materials. Four different types of inorganic materials frequently used may be distinguished: ceramic membranes; glass membranes; metallic membranes and zeolitic membranes. The high temperature resistance make inorganic membranes very attractive for gas separation at high temperatures, especially in combination with chemical reaction where the membrane is used as catalyst as well as a selective barrier to remove one of the components which has been formed. The chemical stability of

inorganic materials is superior and they can generally be applied at any PH and in any organic solvent. Another important factor is the ease of cleaning, especially in high fouling applications involving ultrafiltation and microfiltation. Another point to consider is that the life time of inorganic membranes is greater than that of organic polymer membranes.

A number of membrane module designs are possible and all are based on two types of membrane configuration: flat and tubular (Figure 2-13). Plate-and-frame and spiral-wound modules involve flat membranes whereas tubular, capillary and hollow fiber modules are based on tubular membrane configurations. The choice of the module is mainly determined by economic considerations. This does not mean that the cheapest configuration is always the best choice because the type of application is also very important. In fact, the functionality of a module is determined by the type of application. The characteristics of all the modules can be compared qualitatively in Table 2-3 (Mulder 1996).

Although the costs of the various modules may vary appreciably, each of them has its field of application. Despite being the most expensive configuration, the tubular module is well suited for application with high fouling tendency because of its good process control and ease of membrane cleaning. In contrast, hollow fiber modules are very susceptible to fouling and are difficult to clean. Pretreatment of the feed stream is most important in hollow fiber system. Because of the easy cleaning and membrane replacement, the plate and frame module is adoped in this work. Moreover, due to its micro-structured characteristics, the packing density of the plate-and-frame module can be high.
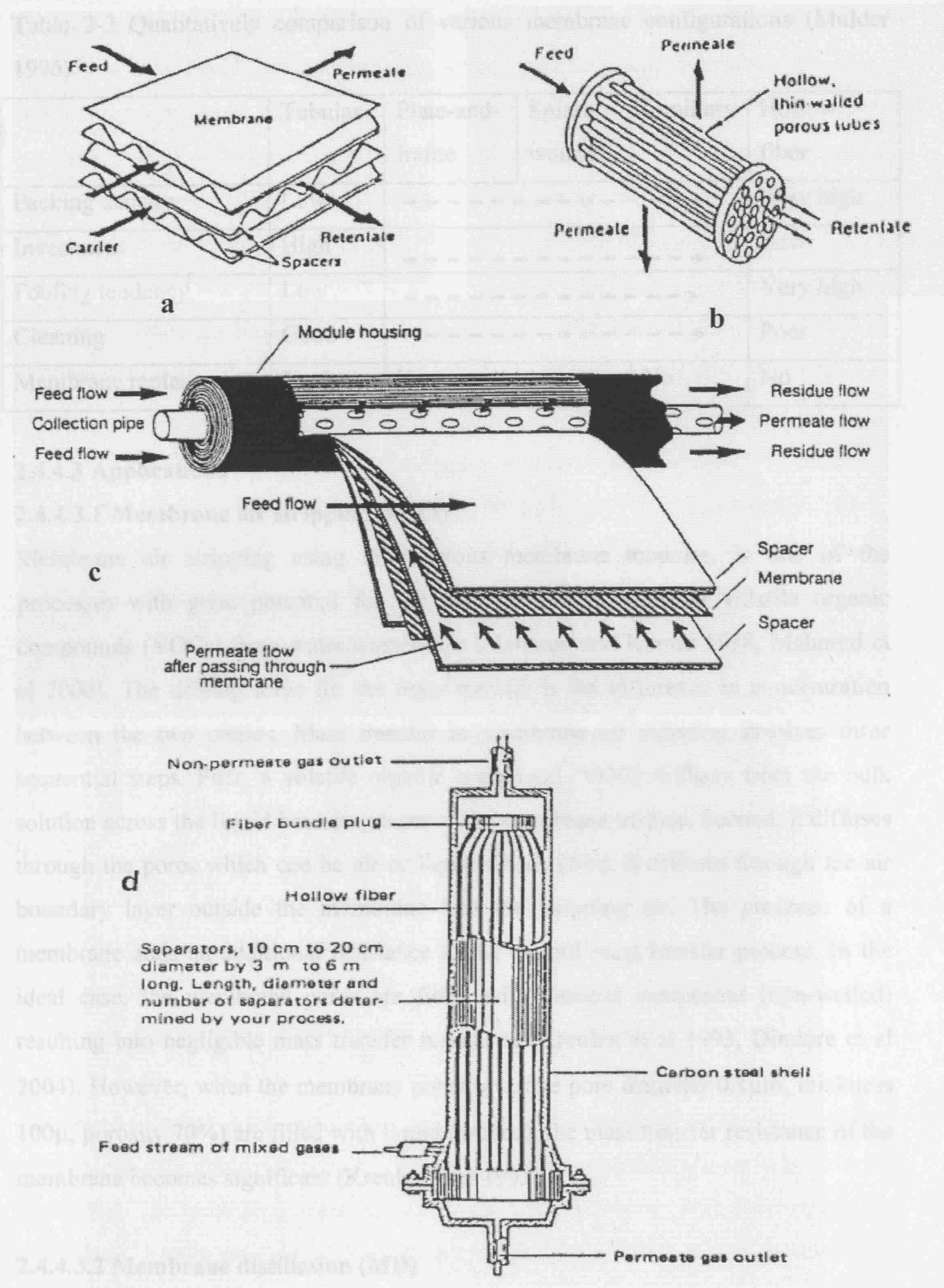
Figure 2-13 Membrane Modules (a) Plate-and-frame, (b) Tubular, (c) Spiral-wood, (d) Hollow fiber (Mulder 1996)

Table 2-3 Qualitatively comparison of various membrane configurations (Mulder 1996)

	Tubular	Plate-and-frame	Spiral-wound	Capillary	Hollow fiber
Packing density	Low	— — — — — — — — — — — — →			Very high
Investment	High	— — — — — — — — — — — — →			Low
Fouling tendency	Low	— — — — — — — — — — — — — →			Very high
Cleaning	Good	— — — — — — — — — — — — — →			Poor
Membrane replacement	Yes/no	Yes	No	No	No

2.4.4.3 Applications

2.4.4.3.1 Membrane air stripping (MAS)

Membrane air stripping using microporous membrane modules, is one of the processes with great potential for the removal and recovery of volatile organic compounds (VOCs) from water/wastewater (Mahmud and Kumar 1998, Mahmud et al 2000). The driving force for the mass transfer is the difference in concentration between the two phases. Mass transfer in membrane air stripping involves three sequential steps. First, a volatile organic compound (VOC) diffuses from the bulk solution across the liquid boundary layer to the membrane surface. Second, it diffuses through the pores which can be air or liquid filled. Third, it diffuses through the air boundary layer outside the membrane into the stripping air. The presence of a membrane adds an additional resistance to the overall mass transfer process. In the ideal case, the membrane pores are filled with gaseous component (non-wetted) resulting into negligible mass transfer resistance (Kreulen et al 1993, Dindore et al 2004). However, when the membrane pores (average pore diameter $0.1\mu m$, thickness 100μ, porosity 70%) are filled with liquid (wetted), the mass transfer resistance of the membrane becomes significant (Kreulen et al 1993).

2.4.4.3.2 Membrane distillation (MD)

Membrane distillation (Godino et al 1996, Lawson and Lloyd 1997) is a relatively new process that is being investigated worldwide as a low cost, energy saving alternative to conventional separation process. The driving force in membrane distillation is a vapour pressure difference across the membrane, which can be

imposed by temperature difference across the membrane, and can be aided by a vacuum or a sweep gas on the permeate side of the membrane. It requires the latent heat of vaporization to be supplied to achieve phase change. Figure 2-14 illustrates several common configurations of the MD process that may be utilized to establish the required driving force. The permeate side of the membrane may consist of a condensing fluid in direct contact with the membrane (DCMD) (Gryta et al 1997), a condensing surface separated from the membrane by an air gap (AGMD) (García-Payo et al 2000), a sweeping gas (SGMD) (Kharyet et al 2000, 2003, García-Payo et al 2002, Rivier et al 2002, Lee and Hong 2001), or a vacuum (VMD) (Bandini et al 1992). The sweeping gas membrane distillation is very similar to and is often confused to membrane air stripping. Sweeping gas membrane distillation is thermally driven process and there is temperature difference across the membrane, while membrane air stripping is isothermal process. The type of MD employed is dependent upon the permeate composition, flux, and volatility.
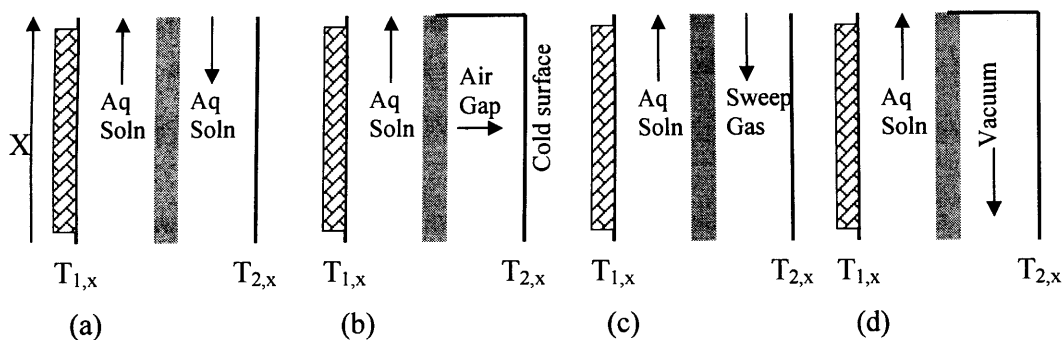
Figure 2-14 Membrane distillation (a) Direct contact membrane distillation, (b) Air gap membrane distillation, (c) Sweeping gas membrane distillation, (d) Vacuum membrane distillation , ▓ Membrane, $T_{1,x} > T_{2,x}$

Compared to other more popular separation process membrane distillation requires lower operating temperatures and pressure, reduces vapour spaces and provide significant interfacial area (Lawson and Lloyd 1997). However, MD also has several limitations, which have resulted in a lack of general interest in the process. The primary limitation arises from the defining phenomenon itself: the process solution should not wet the microporous membrane.

2.4.4.3.3 Membrane pervaporation (PV)

Membrane pervaporation is a process in which one component out of a fluid mixture selectively permeates through a dense membrane, driven by a gradient in partial vapour pressure, leaving the membrane as a vapour, which can be recovered in a condensed form as a liquid (Cardew and Le 1998). Pervaporation is unusual among membrane process in that transport across the membrane is accompanied by a phase change. The gradient in partial vapour pressure between the feed and permeate side of the membrane is maintained by a reduction of the permeate side partial vapour pressure by using a sweeping gas or vacuum. The separation is governed by the physical-chemical affinity between the membrane materials and species to pass through and thus by sorption and solubility phenomena. Invariably, permeation through the thin surface layer of the membrane is rate limiting (Cardew and Le 1998). The separation of compounds using pervaporation methods can be classified into three major fields: (i) dehydration of aqueous-organic mixtures (Reddy and Reineke 1998), (ii) removal of trace volatile organic compounds from aqueous solution (Bengtsson et al 1993) and (iii) separation of organic-organic solvent mixtures (Garcia-Villaluenge and Tabe-Mohammadi, 2000, Smitha et al 2004).

Pervaporation process is similar to and is often confused with vacuum membrane distillation (VMD). The fundamental difference between pervaporation and VMD is the role that membrane plays in the separation. VMD employs a microporous membrane that acts only as a support for a vapour-liquid interface. While the VMD membrane may impart some selectivity based on individual Knudsen diffusivities of diffusing species, the largest degree of the separation is determined by vapour-liquid equilibrium conditions at the membrane-solution interface. On the other hand, pervaporation uses a dense membrane, and the separation is based on the relative solubility and diffusivity of each component in the membrane material. Because of these differences, VMD typically achieves fluxes that are several orders of magnitude higher than pervaporation fluxes.

A comparison of the membrane air stripping (MAS), membrane distillation (MD) and pervaporation (PV) is summarized in the Table 2-4.

Table 2-4: Comparison of the membrane air stripping (MAS), membrane distillation (MD) and pervaporation (PV)

Membrane process	Membrane & wetability	Driving force	Separation mechanism
MAS	Microporous Wetting, non-wetting	Concentration gradient	Vapour –Liquid equilibrium difference
MD	Non-wetting	Partial pressure difference	Vapour –Liquid equilibrium difference
PV	Dense membrane	Partial pressure difference	Solubilities and diffusivities of the component in the membrane material

In the membrane distillation (MD) process, temperature gradient across the membrane is required. However, the catalyst for the asymmetric transfer hydrogenation will deactivate over 40°C. Therefore, MD is not suitable for the IPA-acetone system. The permeability is very low in PV process which is undesirable for the acetone removal during reaction where high acetone flux is required. Membrane air stripping can deal with both wetted and non-wetted membrane and it can be applied in lower temperature. Therefore, it can be ideal solution for stripping acetone from IPA. If the membrane pores are filled by the liquid for such system, the membrane resistance for the mass transfer becomes significant. Therefore, care must be taken to reduce the membrane thickness for membrane wetted by IPA.

2.4.4.3.4 Micro Gas-liquid contactors

Micro-contactors provide very efficient mixing, efficient heat exchange and large surface to volume ratio, which is excellent situation for stripping VOCs and gas-liquid reactions. Such contactors have been used for stripping or gas-liquid reaction as described below. The Institut für Mikrotechnik Mainz GmbH (IMM) designed a micro bubble column (MBC) for direct fluorination (Jähnisch et al 2000), which consisted of a mixing and a reaction unit whereby the mixer was equipped with 20μm deep gas and liquid feeding channels 7 and 20 μm wide, respectively. The reaction unit comprised of an array of parallel microchannels with two different sizes, either 50μm by 50μm or 300μm by 100μm channel cross-section, which allowed a continuous stream of small gas bubbles to flow through the liquid. The residence time of MBC is about 0.14-0.56s typically. The specific inner surface is $2830m^2/m^3$ per plate. Chambers et al (2005) designed a gas/liquid micro-reactor, for direct

fluorination reactions of diethyl malonate and Meldrum's acid using only common and inexpensive mechanical workshop techniques. The reactor is assembled by base block, PTFE gasket, bottom plate, channel plate, polychlorotrifluoroethylene (PCTFE) plate and steel top plate. The channel plate consists of stainless steel sheet (0.5mm) with the desired number of reaction channels, typically 3, 9 or 30 channels per plate. Cypes and Engstrom (2004) designed a microfabricated stripping column (MFSC) fabricated using standard Si processing techniques. The dimensions of the liquid and gas microchannels are approximately 3.35cm long ×920 (450) μm wide at the top (bottom) ×330μm deep. The MFSC offers overall capacity coefficients, K_La, an order of magnitude greater than the packed tower as found for stripping of toluene from water. IMM designed a falling film micro-reactor (FFMR) which includes a platelet comprising a large number of micro channels of 100μm by 300μm cross-section (Jähnisch et al 2000). The FFMR enabled the generation of a thin film of several 10μm thickness to flow. Yeong et al (2004) studied nitrobenzene hydrogenation over palladium in the falling film reactor. The K_La value of the system based on liquid volume was estimated to be 3-8 s^{-1} with interfacial surface area per reaction volume 9000-15000m^2/m$^3_{liq}$.

However, both of the above gas-liquid direct-contact microreactors have one disadvantage: the residence time is too short and it is not possible to use very high gas flowrate which is required for efficient VOC stripping. Wenn et al (2003) and Abdallah et al (2004) developed a mesh micro contactor which can offer residence time of more than a minute. Similar to membrane contactors, gas and liquid phases are separated by a micromesh which has uniform cylindrical pores. The reaction chamber depth is set at 100μm in the active area on the each side of the mesh. Roughly 20 to 25% of the mesh surface area is occupied by holes of 5μm diameter which leads to a gas-liquid interfacial area ca. 2000m^2/m$^3_{liq}$ well above the values (100-300m^2/m$^3_{liq}$) obtained in the traditional stirred tank reactors. Moreover, employing mesh separators with high open area (>20%) and with pore length to width ratio of a relatively low value (1:1) ensures that diffusive resistance through the mesh does not become dominant over that within the phases on either side of the separating structure, as can occur for conventional microporous and other membranes. Using stainless steel or nickel mesh can prevent the problem of membrane swelling which

results in the reduction of the membrane pore size and therefore, increases the membrane transport resistance (Mahmud et al 2002).

TeGrotenhuis et al (1998) summarized that the contactor plate mass transfer resistance in the micro-mesh contactor is a function of several parameters, including the thickness of the contactor plate, porosity, tortuosity and the solute diffusion coefficient in the wetting liquid filling the pores. Two thicknesses of micromachined contactor plates were used in the micro-mesh contactor, 25μm and 50μm. The holes were conical and made by laser drilling, averaging 25μm in diameter on one side and 35μm in diameter on the other side of the plate. Porosity was estimated at 26%. The micromachined contactors were coated with Teflon to make them more non-wetting to water.

James et al (1999) invented a method and apparatus for diffusive transfer between immiscible fluids. The invention is based on the concept of providing for a diffusive transfer process through an apertured or foraminous sheet wherein the fluids interfaces are created. Both fluids flow essentially parallel to the interface and rapid diffusion can take place across the interface. The invention provides in a first aspect an apparatus for carrying out a diffusive transfer process between two immisible fluids. A foraminous sheet with apertures height no greater than 200μm defined two fluids interface and a stable interface is formed between the fluids within each aperture. Diffusive transfer takes place across the interface and subsequently the fluids flow away from the region without mixing.

2.4.4.4 Design equations

Three idealized flow patterns for membrane gas-liquid contactor shown in Figure 2-15 have received considerable attention.
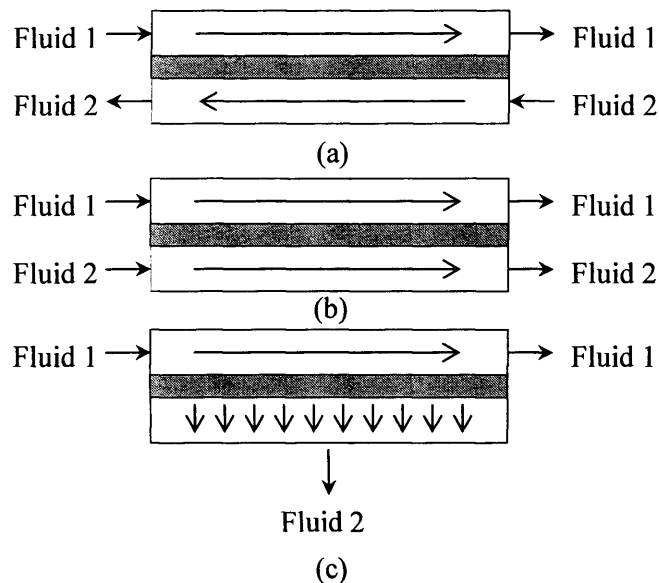
Figure 2-15 Idealized flow patterns in membrane modules: (a) countercurrent flow; (b) co-current flow; (c) crossflow

Wang and Cussler (1993) explained that conventional parallel flow modules offer true countercurrent flow and are preferred when the membrane or the tube side boundary layer resistance controls. However, with these modules mass transfer coefficients can be reduced and/or flows can become uneven if the shell side resistance is significant; in this case a crossflow design is preferred. Flow normal rather than parallel to the fibers leads to higher mass transfer coefficients, but the price is loss of efficiency compared to countercurrent designs. Some efficiency is regained by the use of baffled modules, which provide elements of both countercurrent and crossflow; efficiency increases as the number of baffles increases, but pressure drop increases as well, and the modules become more difficult to build.

Countercurrent operation is usually more efficient than a co-current flow configuration because of the larger driving force (Kreith and Black 1980). In the co-current flow, the effluent gas phase concentration can not exceed the concentration in equilibrium with the effluent liquid phase concentration. For countercurrent flow, on the other hand, the effluent gas phase concentration can approach the concentration in equilibrium with liquid influent. Clearly, at a given gas flowrate, a greater removal efficiency (a higher effluent gas concentration and a lower effluent liquid concentration) can be obtained in the countercurrent flow than in the co-current flow contactor.

Figure 2-16 a shows a counter-current flow membrane contactor for gas stripping and Figure 2-16 b shows the correspondent equilibrium curve and operating line. The slope of the operating line is:

$$\frac{L}{G} = \frac{y_1 - y_2}{x_1 - x_2} \qquad (2\text{-}17)$$

When the gas flowrate G increases, the slope decreases. Therefore, point A in operation curve moves towards to the equilibrium curve. When it reaches C, the gas phase concentration at exit y_1 becomes the equilibrium concentration corresponding to the liquid inlet concentration x_1. In this case, it takes an infinite number of stages for this equilibrium to be achieved. The corresponding minimum ratio of the gas flowrate and liquid flowrate $(G/L)_{min}$ can be calculated as:

$$\left(\frac{G}{L}\right)_{min} = \frac{x_1 - x_2}{y_{1e} - y_2} \qquad (2\text{-}18)$$

In practical operation, (G/L) should be larger than $(G/L)_{min}$ to provide sufficient driving force along the whole contactor.
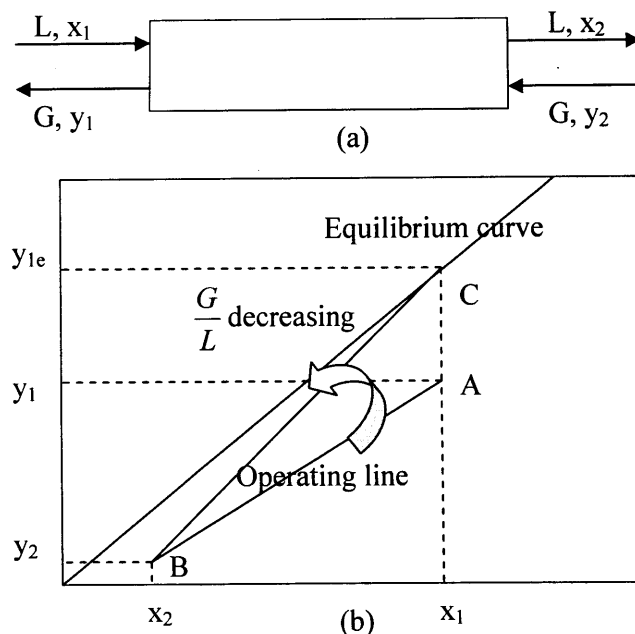
Figure 2-16 (a) Gas-liquid contactor in counter-current operation (b) Corresponding equilibrium curve and operating line

Figure 2-17 a shows a co-current flow membrane contactor for gas stripping and Figure 2-17 b shows the correspondent equilibrium curve and operating line. The slope of the operating line AB is:

$$-\frac{L}{G} = \frac{y_{2,B} - y_2}{x_{2,B} - x_2} \tag{2-19}$$

When the gas flowrate G increases, the slope increases. Therefore, point A in operating line moves from B to C. The corresponding liquid phase exit concentration decreases from $x_{2,B}$ to $x_{2,C}$ respectively. Therefore, lower $\frac{L}{G}$ is preferred in the co-current operation membrane contactor to obtain better stripping efficiency.
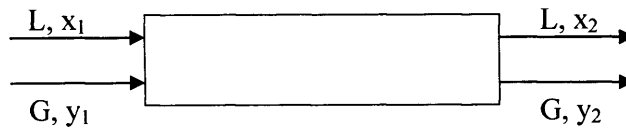
(a)
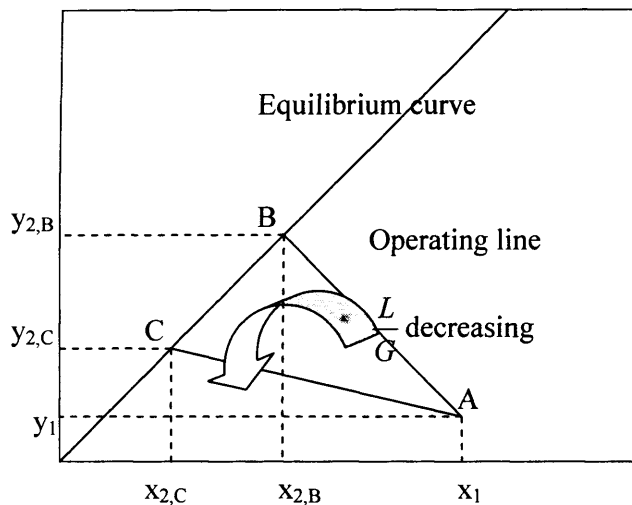
(b)

Figure 2-17 (a) Gas-liquid contactor in co-current operation (b) Corresponding equilibrium curve and operating line

Figure 2-18 shows the comparison for the co-current and counter-current operation in the membrane gas-liquid contactor. For certain gas/liquid inlet concentration (x_1, y_1) and outlet concentration (x_2, y_2), the minimum ratio of gas to liquid flowrate $\left(\frac{G}{L}\right)_{min}$ in co-current operation with infinite reactor length corresponds to operating

line AB, while it only needs one theoretical plate to achieve the same separation

results with this $\left(\dfrac{G}{L}\right)_{min}$ in counter-current operation (Operating line CD). The

$\left(\dfrac{G}{L}\right)_{min,counter-current}$ needed in the counter-current operation (Operating line CE) is

much smaller than the $\left(\dfrac{G}{L}\right)_{min,co-current}$ in co-current operation (Operating line AB) with

infinite reactor length.
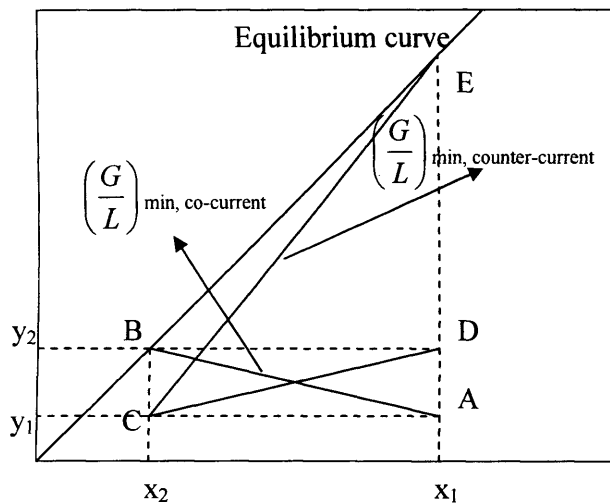
Figure 2-18 Comparison of co-current and counter-current operation

Figure 2-19 shows indicatively the pressure difference ΔP between gas and liquid phase in the membrane contactor with co-current and counter-current operation. As it can be seen the ΔP for the counter-current operation at the exit of the membrane contactor is larger than that for the co-current operation. This is due to opposite pressure profile along the reactor for co-current and counter-current operation. Larger pressure difference between the gas and liquid phase along the reactor makes phase breakthrough easier to take place.
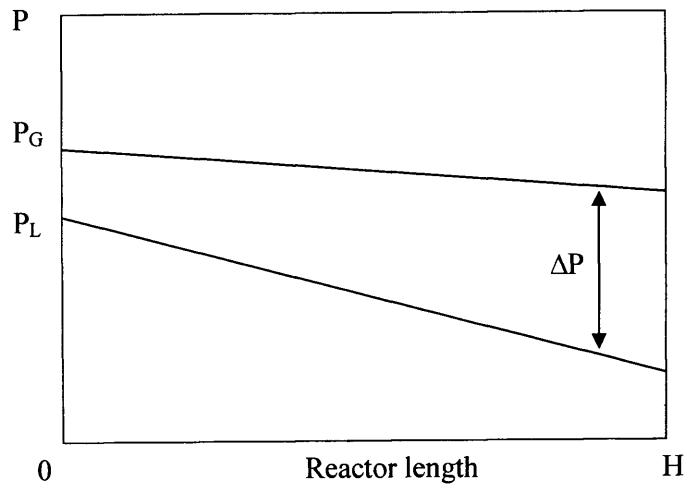
(a)
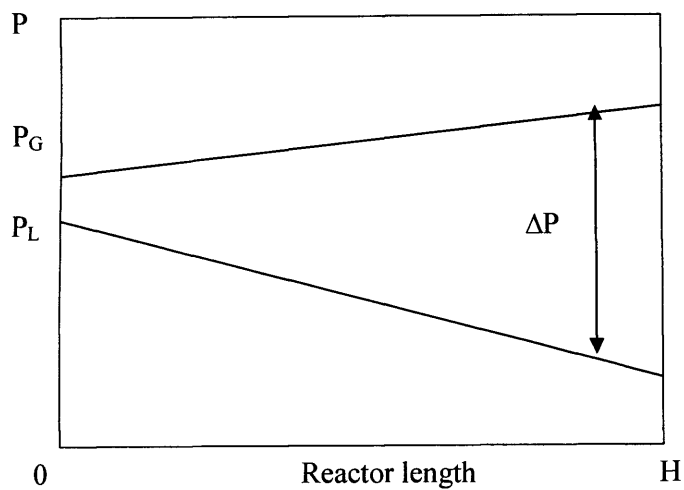
(b)

Figure 2-19 Pressure profiles in gas and liquid phases in (a) co-current operation and (b) counter-current operation membrane contactors

Hence, in this work, co-current operation is considered even though it is not as efficient as counter-current operation because it is less sensitive to breakthrough.

When considering using a membrane contactor, one needs to know the size of a unit for a specific job, or how good a separation can be achieved with a particular module. The basic equations for any dilute absorption or extraction are (See Appendix D):

$$H = HTU \bullet NTU \qquad (2\text{-}20)$$

where H is the module length, HTU is the height of a transfer unit, and NTU is the number of the transfer units.

Based on the vapor side driving force, HTU_G can be written as:

$$HTU_G = \frac{G}{K_y a} \qquad (2\text{-}21)$$

Where G $(mol/s \cdot m^2)$ is the gas flowrate, K_y $(mol/s \cdot m^2)$ is the overall mass transfer coefficient based on vapor side driving force and α $(m^2/m^3_{contactor})$ is the gas/liquid interfacial area.

NTU_G can be written as

$$NTU_G = \int_{y_1}^{y_2} \frac{dy}{y_e - y} \qquad (2\text{-}22)$$

Where y_1 and y_2 are inlet and outlet gas phase concentrations, y_e is the vapour concentration in equilibrium with liquid concentration x.

Based on the liquid side driving force, HTU_L can be written as:

$$HTU_L = \frac{L}{K_x a} \qquad (2\text{-}23)$$

Where L $(mol/s \cdot m^2)$ is liquid flowrate, K_x $(mol/s \cdot m^2)$ is overall mass transfer coefficient based on liquid side driving force and α $(m^2/m^3_{contactor})$ is gas/liquid interfacial area.

NTU_L can be written as

$$NTU_L = \int_{x_1}^{x_2} \frac{dx}{x_e - x} \qquad (2\text{-}24)$$

Where x_1 and x_2 is inlet and outlet liquid phase concentration, x_e is the liquid phase concentration in equilibrium with vapor phase concentration y.

The NTU are roughly parallel to the number of equilibrium stages in distillation, or the number of mixer-settlers in extraction. However, the NTU do not refer to the equilibrium limit commonly approached in staged distillation or extraction. In the

same sense, the HTU roughly parallels the length of a distillation stage, or the depth of a mixer-settler. The HTU are also equivalent to the height of a theoretical plate often used to describe analytical chromatography. Alternatively, one can think of the NTU indicating the difficulty of the separation and the HTU as measuring the efficiency of the equipment.

2.4.4.5 Mass transfer in membrane contactors

The mass transfer process in a membrane contactor mainly involved three steps which is shown in Figure 2-20 with membrane pores filled with liquid.

- Mass transfer from the liquid bulk to the liquid interface.
- Mass transfer through the membrane pores to the gas interface.
- Mass transfer from the gas interface to the gas bulk.
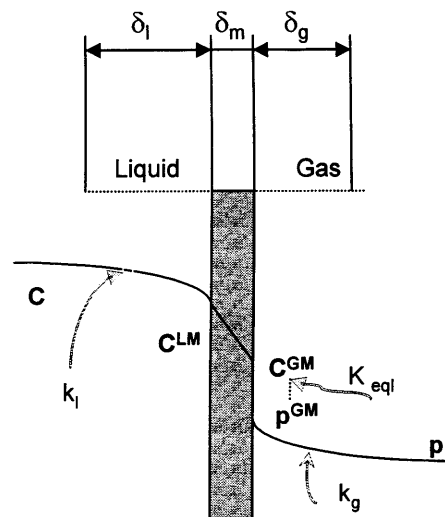
Figure 2-20 Concentration profiles of a compound diffusing in a membrane contactor

The overall mass transfer process consists of three resistances in series: the gaseous phase boundary layer, the membrane and the liquid phase boundary layer. The overall mass transfer in the gas-liquid membrane contactor can be described with the resistance-in-series model and the overall mass transfer resistance can be obtained by adding the partial resistances in series (see Appendix E):

$$\frac{1}{K_L} = \frac{1}{k_l} + \frac{1}{k_m} + \frac{K_{eq}}{k_g} \tag{2-25}$$

where K_L is the overall liquid-phase based mass transfer coefficient (m/s), k_l the local liquid-phase mass transfer coefficient (m/s), k_g the local air-phase mass transfer

coefficient (mol/s·m^2), k_m the membrane mass transfer coefficient (m/s), K_{eq} *is* the vapour-liquid equilibrium ratio (mol/m^3).

Usually, one of the three individual mass transfer coefficients is much smaller than the two others and the mass transfer is dominated by that phase. In many applications, the membrane resistance is the dominating factor because of low membrane permeability and relative large membrane thickness. Progress in membrane production technology and extensive research on membrane characteristics has greatly reduced the mass transfer resistance of modern membranes. In some cases, the membrane resistance is now negligible compared to resistance in the liquid phase (Yang and Cussler 1986, Semmens et al 1989; Kreulen et al 1993, Banat and Simandl 1996). The fact that the pores of the membrane are filled with gas contributes to reduce the membrane resistance. Bradley et al (1995) suggested two heuristics for the membrane selection to reduce the membrane resistance. The first heuristic is to choose the membrane so that it is wetted by the fluid in which the solute of interest is more soluble. For example, if the compounds of interest partitions more strongly into the solvent vs. water, then one needs to choose a membrane wetted by the solvent. If the compounds partitions more strongly into the aqueous feed than into the solvent, then one needs to choose a membrane wetted by water. The second heuristic is to choose a membrane which hinders solute diffusion as little as possible. In many cases, this has been realized by choosing a microporous membrane. Such a membrane is wetted by either the solvent or the feed. In either case, solute diffuses easily through the pores. Such a microporous membrane does risk convective flow through the pores. Such flow, a significant risk, can usually be eliminated by applying a static pressure.

Because the membrane introduces an additional mass transfer resistance, the overall mass transfer coefficient K_L obtained in the membrane contactor is usually about the same or even slightly smaller than that obtained in the traditional air stripping contactors. The larger K_La achieved in the membrane gas-liquid contactor is the contribution of larger gas-liquid interfacial area, which remains constant with changes in operating conditions or fluid physical properties. The specific surface area of the membrane contactor can be as high as 6000m^2/m^3 (He et al 2004), while the highest specific surface area of commonly used packing materials is about 600m^2/m^3 (LaGrega et al 1994). Membrane contactors offer up to 30 times more area than that

achievable in ordinary gas absorbers and 500 times than obtainable in liquid/liquid extraction columns (Cussler 1994). Reed et al. (1995) gave the following values of interfacial area per unit volume (ft^{-1}) for various types of contactors:

• Free dispersion columns: 1–10.

• Packed/trayed columns: 10–100.

• Mechanically agitated columns: 50–150.

• Membranes: 500–2000.

It is reported that membrane air stripping offers an order of magnitude higher overall volume specific mass transfer coefficient (K_La) than that of packed-tower air stripping (Qi and Cussler 1985). Several authors have compared mass transfer performance of membrane contactors to that of conventional equipment. For example, Ding et al. (1992) determined the mass transfer coefficient obtained with a hollow fiber contactor in the extraction of d-leucine from a racemic aqueous mixture into a 1-octanol solution of N-n-dodecyl-l-hydroxyproline, then compared their results to those reported by others for dispersed phase contactors. The K_La values were 0.053, 0.0007 and 0.00005 s^{-1} for the membrane contactor, a high-efficiency rotating column (Takeuchi et al, 1990) and a conventional extractor (Treybal 1980), respectively. Sims et al. (1996) used a membrane contactor to extract orange aroma into near-critical carbon dioxide, then compared their results to those obtained by Schultz et al. (1974) with a Schiebel column. The extract from the membrane contactor contained substantially higher levels of key components such as ethyl butyrate, ethyl acetate, octanol, terpinen-4-ol and citronellal, and the membrane contactor was reportedly an order of magnitude more efficient. Similarly, Seibert and Fair (1997) found that the extraction of hexanol from water into octanol was 10 times more efficient with a hollow fiber membrane contactor than with a column containing structured packing; the authors attributed the higher efficiency to the significantly greater mass transfer area.

Qi and Cussler (1985) explained that the HTUs obtained in conventional towers all tend towards the same value (within a factor of 10 or so). Generally for the conventional towers, the mass transfer coefficient increases with increasing flowrate and the interfacial area decreases with decreasing flowrate. As a result, the HTU

remains about the same over a wide range of flowrates. On the other hand, with membrane contactors the mass transfer coefficient drops slightly at low flow rate but the interfacial area remains unchanged, leading to very low values of HTU. Kreulen et al. (1993) compared the performance of a bubble column to that of a microporous polypropylene hollow fiber membrane contactor for the absorption of oxygen into glycerol/water solutions of various concentrations. The membrane module (interfacial area: 20 cm^2/cm^3; fiber length: 18 cm) had the same liquid hold-up and liquid height as the bubble column (diameter: 4 cm; liquid holdup: 200 cm^3). The K_La for the bubble column was actually higher than that of the membrane contactor at low glycerol concentrations. For example, with water alone the K_La was 0.20 s^{-1} for the bubble column vs. 0.023 s^{-1} for the membrane contactor. Both K_La values decreased with increasing glycerol concentration, but the value for the bubble column decreased faster. Values were higher for the membrane contactor at high glycerol concentrations, e.g., 0.002 and 0.0012 s^{-1} for the membrane contactor and the bubble column, respectively, at 80% glycerol. The authors explained that the increasing viscosity with increasing glycerol concentration led to a reduction in the mass transfer coefficient for both devices; however, the interfacial area decreased in the bubble column while it stayed the same in the membrane contactor, hence the slower degradation in K_La with the latter.

Prasad and Sirkar (1998) reported HTU values as a function of flow rate for liquid/liquid extractions with chemical systems covering a range of partition coefficients (0.013 ‒ 50) for both hydrophilic and hydrophobic membranes. Values as low as 23 cm were obtained, and HTU was found to be independent of interfacial tension. Similarly, Prasad and Sirkar (1990) reported HTU values of 3 ‒ 15 cm in the simultaneous extraction of 4-methylthiazole (MT) and 4-cyanothiazole (CNT) from an actual process stream provided by Merck (Rahway, NJ), using a hydrophobic membrane and either toluene or benzene as the extraction solvent. As explained by the authors, these HTU values were probably lower than any values reported in the literature on packed and agitated columns in solvent extraction service. The closest literature value reported was ~17 cm, obtained by Steiner and Hartland (1980) in their work with an enhanced coalescence plate agitated column operated at high agitator speed (250 rpm).

2.4.4.6 Phase breakthrough

Membrane contactors are devices that allow a gas and liquid or two immiscible liquid phases to come into contact with each other without dispersing one phase into the other. The breakthrough of one phase into another may cause unwanted froth, foam or emulsion. Such breakthrough can be controlled by applying a higher pressure on the phase which does not wet the pores. The pressure difference must not exceed a critical value, or the non-wetting fluid will penetrate the pores and contaminate the other fluid stream. This is the breakthrough pressure. To avoid one phase breaking through into the other, the gas-liquid or liquid-liquid interface should remain within the pores for the range of pressure differences existing between the two phases during operation and modified along the mesh due to pressure drop.

The term critical entry pressure of one phase refers to the pressure difference necessary for that phase to enter a pore. Even more important than critical entry pressure for the present work is the critical filling pressure difference of one phase ΔP_C, defined as the pressure difference necessary to completely fill the pores with that phase. Critical entry and filling pressures are identical for constant cross section pores and they differ for tapered pores where the wetting phase is on the small pore opening side. Thus, there are two critical filling pressures defined as critical filling pressure of the wetting phase $\Delta P_{C,W}$ and of the non-wetting phase $\Delta P_{C,NW}$,

$$\Delta P_{C,W} = (P_W - P_{NW})_{C,W} \tag{2-26}$$

$$\Delta P_{C,NW} = (P_{NW} - P_W)_{C,NW} \tag{2-27}$$

If the membrane resistance is significant, it is very important to fill the pores with the fluid offering the lower resistance to mass transfer. For instance, if the wetting phase offers low mass transfer resistance, operation pressure should be equal to or higher than the critical filling pressure of the wetting phase $\Delta P_{C,W}$ to make sure that the wetting phase fills the pores. However, the operation pressure difference should not exceed breakthrough pressure difference. There are two breakthrough pressures $\Delta P_{B,W}$ and $\Delta P_{B,NW}$ corresponding to breakthrough of the wetting and non-wetting phase respectively.

$$\Delta P_{B,W} = (P_W - P_{NW})_{B,W} \tag{2-28}$$

$$\Delta P_{B,NW} = (P_{NW} - P_W)_{B,NW} \tag{2-29}$$

Based on the above discussion, the operation pressure difference should be carefully controlled so that $\Delta P_{C,W} \leq \Delta P \leq \Delta P_{B,W}$ to allow wetting phase to fill the pore or $\Delta P_{C,NW} \leq \Delta P \leq \Delta P_{B,NW}$ to allow the non-wetting phase to fill the pore.

For the case of sufficiently small uniform cylindrical pores, various researchers used the Laplace-Young equation to calculate the pressure difference necessary for breakthrough or critical pore entry (Prasad and Sirkar 1992, Lawson and Lloyd 1997, Drioli et al 2005, Dindore et al 2004)

$$\Delta P = P_{NW} - P_W = \frac{2\gamma \cos\theta}{r} \tag{2-30}$$

where, ΔP is pressure difference; γ is surface tension of the liquid; θ is contact angle between the liquid and solid and r is the pore radius. Positive breakthrough pressure of wetting phases in membranes have been reported (Byoung-Sik and Harriot 1984, Prasad et al 1990, Vaidya et al 1994). These results seemingly contradict the prediction of the Laplace equation. However, as shown below, this is probably due to the fact that the solid wall inclination change of the pore ends (for regular pore membranes) or pore interior (for tortuous pore membranes) is not accounted for (Adam 1948). The above indicates that one needs to use with care the Laplace-Young equation.

The contact angle measured for a liquid advancing slowly across a surface, θ_A, exceeds that of the liquid receding on the surface, θ_R, and all intermediate contact angles correspond to metastable equilibrium states (Volpe et al 2002). This phenomenon is called contact angle hysteresis. The contact angle hysteresis is in general attributed to surface roughness and heterogeneity, solution impurities, swelling, rearrangement or alteration of the surface by the solvent (Adamson and Gast, 1997). Because of the contact angle hysteresis, the Laplace-Young equation is written as equation (2-31) to calculate the wetting phase critical filling pressure and equation (2-32) to calculate the non-wetting phase critical filling pressure:

$$\Delta P_{C,W} = -\frac{2\gamma \cos\theta_A}{r} \tag{2-31}$$

$$\Delta P_{C,NW} = \frac{2\gamma \cos\theta_R}{r} \tag{2-32}$$

where θ_A is advancing contact angle and θ_R is receding contact angle. The wetting phase critical filling pressure is negative, which indicates that filling the pore with wetting phase is spontaneous. Due to the fact that at the pore end the solid wall changes inclination from vertical to horizontal, an apparent contact angle needs to be defined. For an ax-symmetric straight pore, it is defined as the angle that the meniscus forms at the three phase contact line with vertical plane.

There are two mechanisms by which one phase can break through into the other:

i) *Breakthrough by spreading*

When the apparent contact angle becomes equal to the sum of advancing contact angle and maximum solid wall inclination at the pore ends inclination 90°, breakthrough by spreading takes place.

$$\theta_{APP} = \theta_A + 90 ° < 180 ° \qquad (2\text{-}33)$$

The wetting phase breaks through into the non-wetting phase by spreading out horizontally along the mesh. In this case, the breakthrough pressure difference is calculated by equation (2-34):

$$\Delta P_{B,W} = -\frac{2\gamma \cos(\theta_A + 90)}{r} \qquad (2\text{-}34)$$

Equation (2-34) indicates that $0 \le \Delta P_{B,W} \le \frac{2\gamma}{r}$. This is now consistent with positive breakthrough pressure measured by various researchers.

ii) *Breakthrough by maximum curvature*

The breakthrough by maximum curvature takes place when

$$\theta_{APP} = \theta_A + 90° \ge 180 ° \qquad (2\text{-}35)$$

The meniscus at the pore opening will reach its maximum curvature of hemispherical shape, which can accommodate the largest pressure difference between the two phases. Beyond this point, breakthrough happens by bubble/droplet formation. Equation 2-35 shows that breakthrough by maximum curvature is encountered only for breakthrough of a non-wetting phase in a wetting phase. The non-wetting phase breakthrough pressure difference can be calculated by:

$$\Delta P_{B,NW} = \frac{2\gamma \cos(0)}{r} = \frac{2\gamma}{r} \qquad (2\text{-}36)$$

Based on the above discussion, the meniscus position can be determined knowing pore geometry, θ_A and θ_R as follows (Table 2-5):

Table 2-5: Meniscus position as a function of apparent contact angle

Condition	Meniscus position
$0^\circ<\theta_{App}< \theta_R$	Pore end where wetting phase is
$\theta_R <\theta_{App} < \theta_A$	Any part of the pore
$\theta_A<\theta_{App}< \theta_A+90^\circ$	Pore end where non-wetting phase is

A cylindrical pore and a fluid pair with $\theta_A = 60^\circ$, $\theta_R = 30^\circ$ is considered by Amador et al (2005) for illustration of the shape and stability of the gas-liquid interface and reproduced in Figure 2-21. Figure 2-21 shows the dimensionless meniscus area and position versus the dimensionless pressure difference between the phases considering that the apparent contact angle can change from 0° at the wetting pore end to $\theta_A +$ $90^\circ= 150^\circ$ at the non-wetting pore end (see Table 2-5). At contact angles $\theta_R< \theta_{App} <$ θ_A, the meniscus is located at any part within the pore, at $\theta_{App} < \theta_R$ the meniscus is pinned at the wetting end and at $\theta_{App} > \theta_A$ at the non-wetting end. As the contact angle gets closer to 0° at the wetting end, small changes in the pressure difference modify the meniscus area and curvature significantly.

As shown in Equation (2-34) and (2-36), the interfacial tension (or surface tension) can affect phase breakthrough. As the interfacial tension increases, more energy is required to bring the two fluids together. Hence more pressure is needed to displace one fluid from the pores with the other.

A troublesome reduction in breakthrough pressure can occur in the presence of even trace levels of surfactant, which cause a reduction in the surface tension (Vaidya et al 1992). Three approaches to increase the breakthrough pressure have been suggested:

- Coat the microporous fibers with a thin, highly permeable polymer or gel (Ding et al 1992, Reed et al 1995). Such a layer effectively addresses the breakthrough issue by stopping flow through the pores.

- Add a compound which increases the interfacial tension (Prasad and Sirkar, 1989).

Based on the above discussion, the meniscus position can be determined knowing pore geometry, θ_A and θ_R as follows (Table 2-5):

Table 2-5: Meniscus position as a function of apparent contact angle

Condition	Meniscus position
$0°<\theta_{App}< \theta_R$	Pore end where wetting phase is
$\theta_R <\theta_{App} < \theta_A$	Any part of the pore
$\theta_A<\theta_{App}< \theta_A+90°$	Pore end where non-wetting phase is

A cylindrical pore and a fluid pair with $\theta_A = 60°$, $\theta_R = 30°$ is considered by Amador et al (2005) for illustration of the shape and stability of the gas-liquid interface and reproduced in Figure 2-21. Figure 2-21 shows the dimensionless meniscus area and position versus the dimensionless pressure difference between the phases considering that the apparent contact angle can change from $0°$ at the wetting pore end to $\theta_A + 90°= 150°$ at the non-wetting pore end (see Table 2-5). At contact angles $\theta_R< \theta_{App} < \theta_A$, the meniscus is located at any part within the pore, at $\theta_{App} < \theta_R$ the meniscus is pinned at the wetting end and at $\theta_{App} > \theta_A$ at the non-wetting end. As the contact angle gets closer to $0°$ at the wetting end, small changes in the pressure difference modify the meniscus area and curvature significantly.

As shown in Equation (2-34) and (2-36), the interfacial tension (or surface tension) can affect phase breakthrough. As the interfacial tension increases, more energy is required to bring the two fluids together. Hence more pressure is needed to displace one fluid from the pores with the other.

A troublesome reduction in breakthrough pressure can occur in the presence of even trace levels of surfactant, which cause a reduction in the surface tension (Vaidya et al 1992). Three approaches to increase the breakthrough pressure have been suggested:

- Coat the microporous fibers with a thin, highly permeable polymer or gel (Ding et al 1992, Reed et al 1995). Such a layer effectively addresses the breakthrough issue by stopping flow through the pores.

- Add a compound which increases the interfacial tension (Prasad and Sirkar, 1989).

- Use a smaller pore size. This can be easily deduced from equation (2-34) and (2-36).
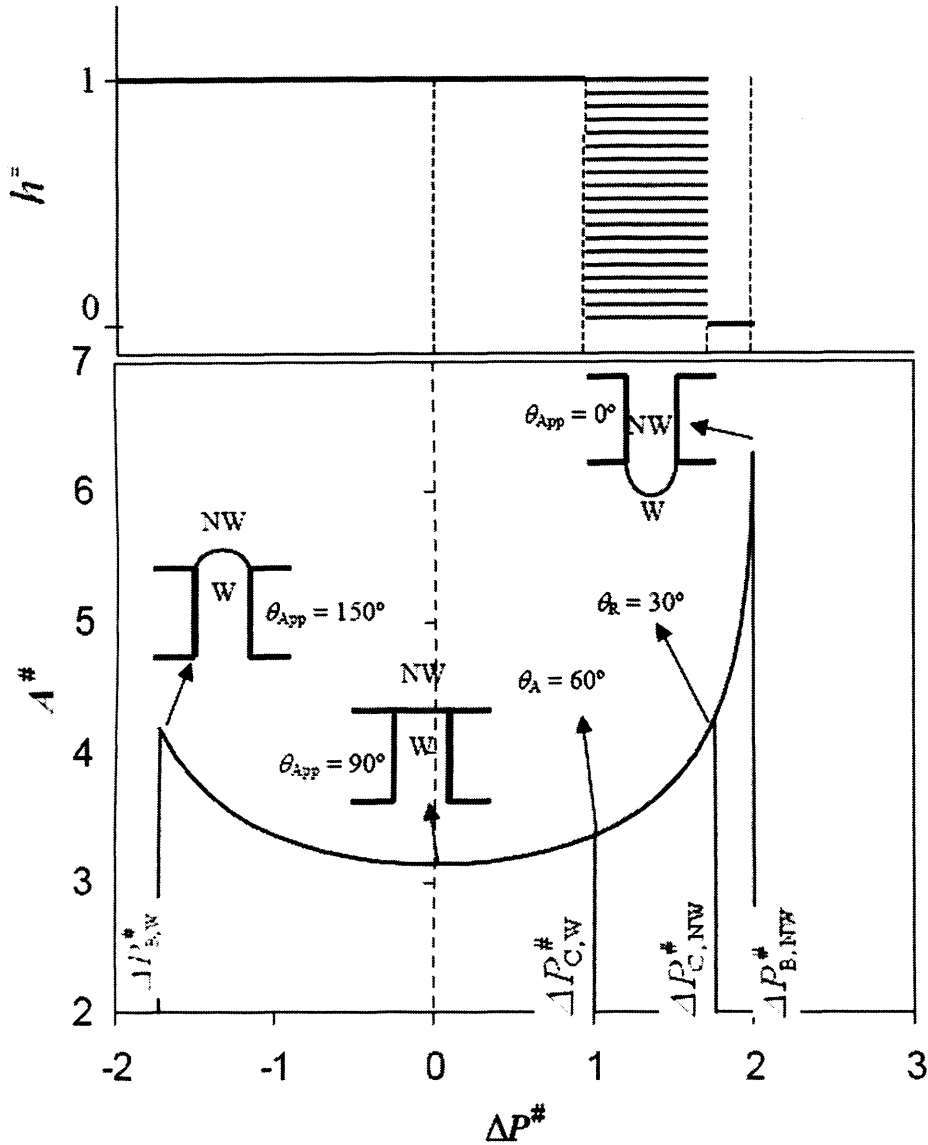
Figure 2-21 Meniscus location $h^{\#} = \dfrac{h}{l}$ (where h is distance of the three phase contact line from the pore end where the wetting phase is, l is pore length), $\Delta P^{\#} = \dfrac{\Delta P}{\dfrac{\gamma}{r}}$,

$A^{\#} = \dfrac{A}{r^2}$ (where A is meniscus area)

Microfabricated meshes often have supports which keep the mesh from bending (Wenn et al 2003). The supports can decrease the meniscus stability since they increase the effective diameter of the meniscus in the membrane pores adjacent to the supports as shown in Figure 2-22 (Amador et al 2005). A similar effect on meniscus stability can take place at the edges of the membrane, where gaskets or O-rings are used for sealing the two phases of the reactor. Moreover, small particles which can contaminate the membrane will increase the effective diameter as well. The increase of effective diameter thus will reduce the breakthrough pressure. Therefore, membranes must be carefully cleaned before use.
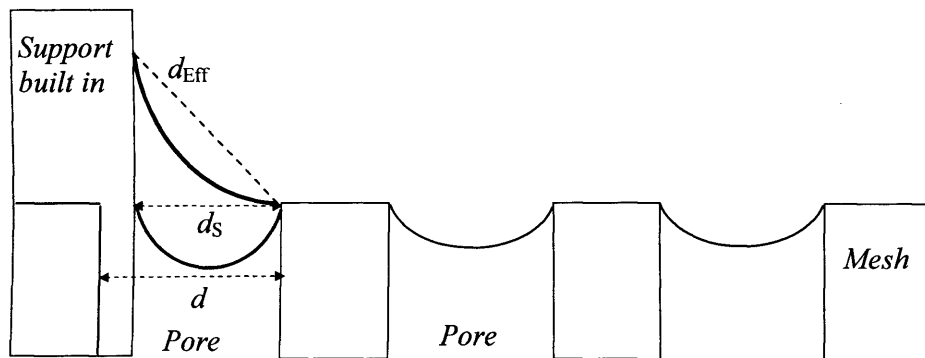
Figure 2-22 Illustration of effective diameter increase by built in support (*edge effect*)

Chapter 3

Batch Reactor for Catalytic Asymmetric Transfer Hydrogenation

3.1 Introduction

Batch reactors are widely used in the chemistry laboratory to investigate the reaction conditions and study the reaction kinetics. In this chapter, the behaviour of 1R, 2S-aminoindanol/pentamethylcyclopentadienylrhodium catalyst (Blacker and Mellor 1997, Blacker 1998) for acetophenone transfer hydrogenation is studied under various reaction conditions in the batch reactor. Studies of the CATHy^{TM}(Catalytic Asymmetric Transfer Hydrogenation) system with other ligands and other substrates can be found in (Blacker and Martin 2004). The reaction conditions investigation work in this chapter will give a deep understanding of the asymmetric transfer hydrogenation, the factor limiting the reaction conversion and selectivity, and provide fundamental experimental data for the kinetic study. The kinetic study will also provide guidelines for the later novel reactor design.

In order to understand the reaction, the reaction mechanism will be needed to be investigated first since it can be used to explain experimental phenomena and investigate kinetic models. Since the structure (Figure 3-1, a) of the CATHy^{TM} catalyst used in this work is similar to Noyori's catalyst (Figure 3-1, b), the metal-ligand bifunctional mechanism (Figure 2-5, Chapter 2) can be considered to be valid in this reaction system (Figure 3-2).

(a)   (b)
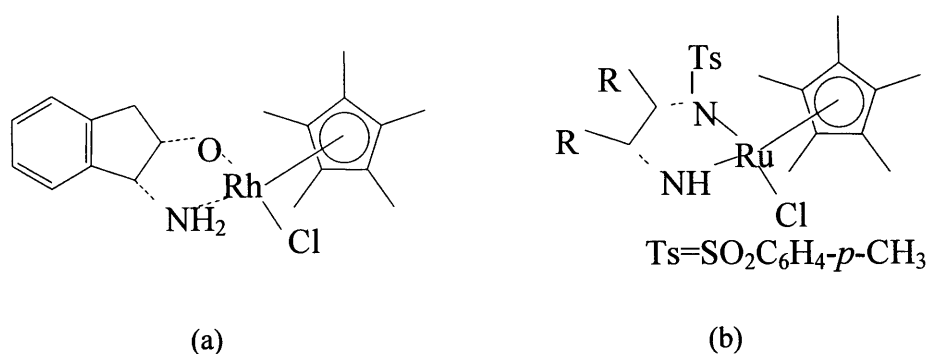
Figure 3-1 Catalyst structures (a) catalyst used in this work and (b) Noyori's catalyst

In the presence of a base, the catalytic species **4** is formed from precursor **3** by HX removal. This active catalytic species **4** facilitates the H-transfer from the solvent 2-propanol (isopropanol, IPA) to the substrate ketone through the formation of intermediate **5** and acetone. The catalyst cycle is restored by the reduction of ketone.
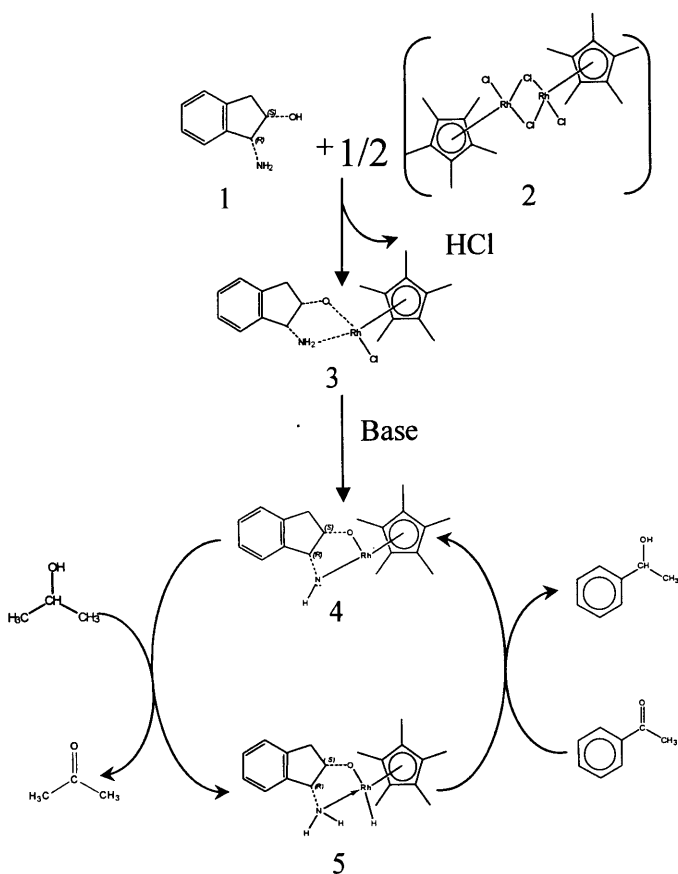
Figure 3-2 Metal-ligand bifunctional catalysis mechanism

3.2 Experimental details

11.2 mg (18.1μmol) pentamethylcyclopentadienylrhodium chloride dimer (Avecia), 5.6 mg (37.1μmol) 1R, 2S-aminoindanol (Avecia) and 100 ml (1.3mol) isopropanol (Aldrich 99.5%) were introduced into a 500ml 3-neck flask reactor with overhead stirrer for catalyst preparation. N_2 (BOC CP grade) bubbling through the solution with 1/8" PTFE tubing at a flow rate of 40ml/min was used to keep an inert blanket (Figure 3-3). The mixture was stirred overnight at room temperature. Temperature was measured by a thermometer. A deep red catalyst solution was obtained.
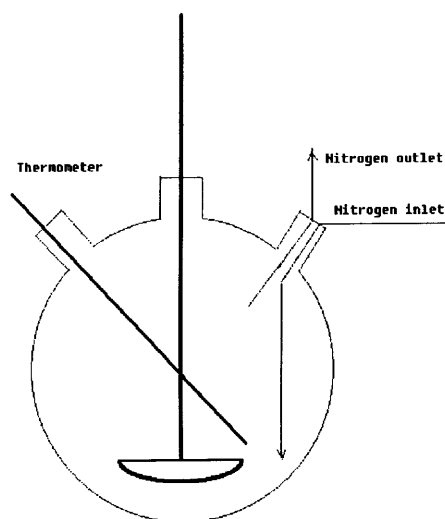
Figure 3-3 Batch reactor experimental set up

4.5g (37.1mmol) acetophenone (Aldrich 99%) was introduced into the reactor containing the catalyst solution along with 150 ml (1.95mol) isopropanol while stirring. Nitrogen flow rate was increased to 800ml/min. 3 ml 0.1M sodium isopropoxide in isopropanol solution was added by a syringe to the mixture, which was considered as reaction time zero. Temperature was kept constant at 30°C by a water bath. The above conditions represent the base case experiment where the catalyst concentration is 0.000144M, substrate concentration/catalyst concentration is 1000:1, sodium isopropoxide concentration/catalyst concentration is 8:1, reaction system volume is 250ml.

The reaction mixture was sampled at 2 minutes intervals in the first 10 minutes and subsequently every 10 minutes intervals in the first hour. A 0.4ml sample was withdrawn by a syringe into a vial containing 10μl acetic acid (Aldrich 99.7%) which was used to stop further reaction and then analysed by an Agilent 6890 GC system. The inlet temperature was 250°C, the inlet pressure 20psi, split ratio 200:1. An injection volume of 0.2μl was used in the autoinjector. A CYCLODEX-B capillary column (30.0m×250μm×0.25μm) was employed for the separation of the acetophenone, (R)-1-phenylethanol and (S)-1-phenylethanol, in order to estimate conversion and enantiomeric excess, along with a flame ionisation detector at 250°C. The oven temperature was kept at 110°C. The internal normalisation method (with

acetophenone) (Rouessac and Rouessac 2000) was used for quantification. Acetone concentration was determined using a DB-624 capillary column (30.0m×530μm×3.00μm) and a thermal conductivity detector at 250°C, with an oven temperature program: 60°C to 100°C at 10°C/min; 100°C for 4min; 100°C to 200°C at 40°C/min; 200°C for 2min.

The conversion of acetophenone was estimated as:

$$conversion = \frac{[Ap]_0 - [Ap]}{[Ap]_0} = \frac{[R] + [S]}{[Ap] + [R] + [S]}$$

where,

$[Ap]_0$ is initial acetophenone concentration,

$[Ap]$ is acetophenone concentration,

$[S]$ is (S)-1-phenylethanol concentration and

$[R]$ is (R)-1-phenylethanol concentration.

(After 60 mins, the deviation of [AP]+[R]+[S] from [AP]$_0$ is about 2%, after 240mins, the deviation becomes more than 13%)

The product enantioselectivity was characterised using enantiomeric excess (e.e.):

$$ee = \frac{[S] - [R]}{[S] + [R]}$$

Turnover frequency (TOF) was characterised as:

$$TOF = \frac{n_{product}}{n_{catalyst} * time}$$

Where:

$n_{product}$ is the number of moles of the product ((S)-1-phenylethanol and (R)-1-phenylethanol),

$n_{catalyst}$ is the number of moles of the catalyst and

time is the reaction time.

3.3 Results and discussion

3.3.1 Base case experiment

Conversion and e.e. as function of time for the base case experiment are shown in Figure 3-4. It can be seen that the initial reaction rate is very fast. Conversion reaches 80% in 20 minutes and 90% in 60 minutes. The average TOF are 2339 hr^{-1} and 905

hr^{-1} respectively. The reaction continued after 60 minutes and the conversion reached 97% in 240 minutes. The initial enantioselectivity obtained was 86.6% and afterwards it decreased with time to 85.1% after 240 minutes. Carrying out the base case experiments four times, it was established that the e.e. was reproducible within ±0.1% and conversion was reproducible within ±1.3%. Four injections were made for one sample to check the analysis. The analysis error on e.e. is within ±0.1% and on conversion is within ±0.07%.
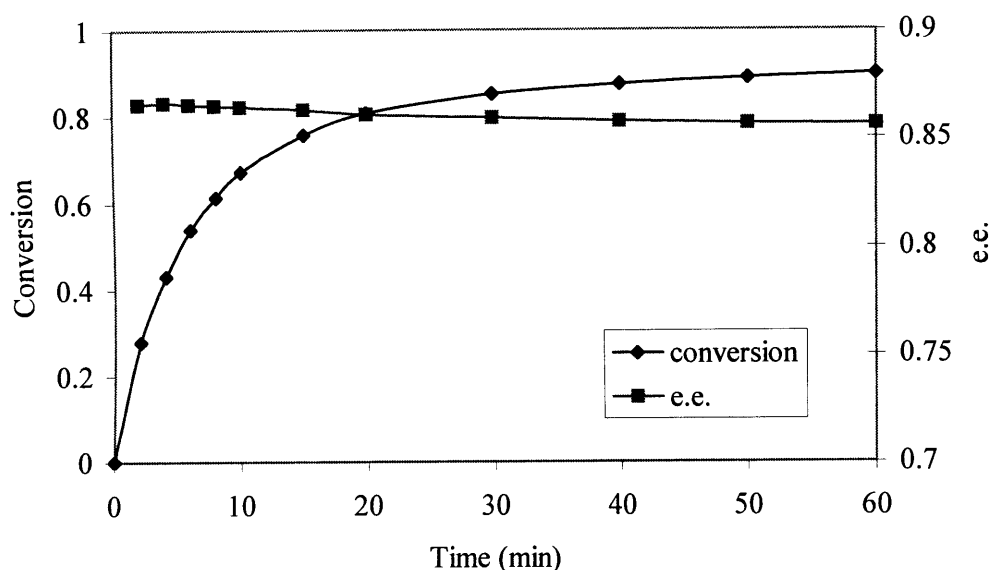
Figure 3-4 Conversion and e.e. vs reaction time for the base case experiment

(Reaction conditions: Temperature: 30°C; [Substrate]=0.14M;

[Substrate]/[Catalyst]=1000; Nitrogen flowrate=800ml/min.)

Other researchers have used different catalysts for the same reaction. Hashiguchi et al (1995) obtained (S)-1-Phenylethanol with 97% e.e. and 95% yield using 0.1M solution of acetophenone in isopropanol containing the in situ prepared Ru catalyst (S/C=200) and KOH (5 equiv to Ru atom) at room temperature in 15 hours. Palmer et al (1997) obtained (S)-1-phenylethanol in 70% isolated yield and 91% e.e. in 1.5 hours with 1mol% of (1R,2S)-(+)-cis-1-Amino-2-indanol in conjunction with 0.25 mol% of the ruthenium complex [RuCl$_2$(p-cymene)]$_2$ and 2.5 mol% of KOH in isopropanol ([ketone]=0.1M) at room temperature. The rhodium catalytic system in this work gives faster reaction rate, although slightly lower e.e. is obtained.

3.3.2 Blank experiments in the absence of substrate

According to Noyori's mechanism (Noyori et al 2001), acetone can be formed even without addition of substrate during formation of the metal hydride (Figure 3-2). In fact Haack et al (1997) isolated the hydride and confirmed its catalytic activity. Formation of acetone (and hence formation of the metal hydride) without closing the catalytic cycle was also confirmed in this work.

Firstly, in preliminary experiments it was observed that mixing of precursor 3 and acetophenone does not initiate any chemical reactions. Only after the addition of sodium isopropoxide, the presence of acetone and phenylethanol was detected. Secondly, mixing of precursor 3 and sodium isopropoxide with IPA in the absence of acetophenone generated traces of acetone. Two experiments in the absence of substrate were conducted using two ratios of sodium isopropoxide : precursor 3, namely 12:1 and 8:1. Peak areas of acetone measured with GC are given in Figure 3-5 as function of time. Due to the low concentrations, accurate absolute quantification of acetone concentration was not possible. However, it is obvious that acetone concentration increased with increasing sodium isopropoxide amount.
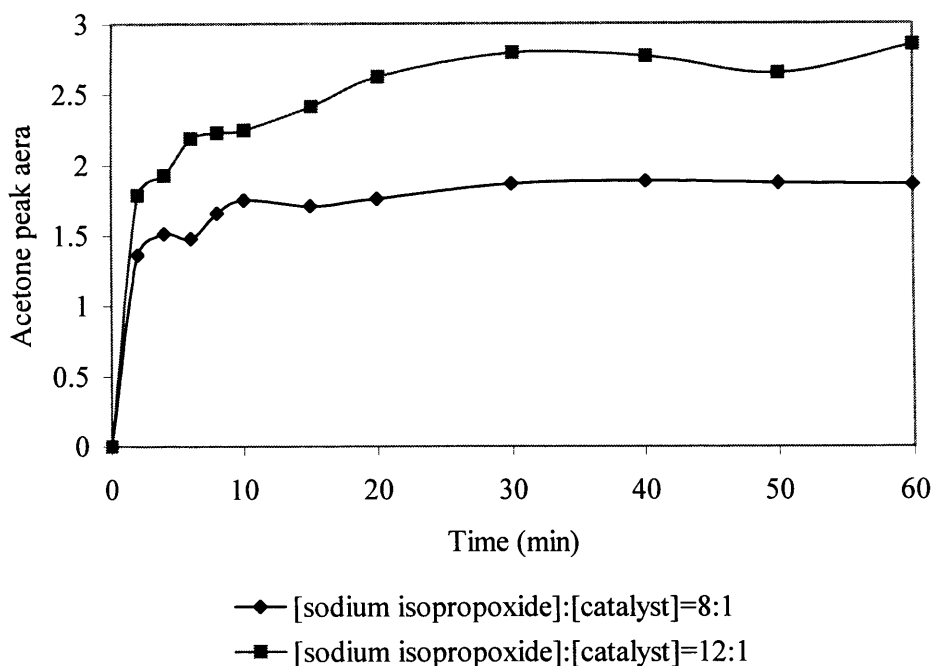
Figure 3-5 Acetone concentration vs. time in the absence of acetophenone at various ratios of initiator sodium isopropoxide to catalyst precusor

Theoretically, an amount of two equivalents of sodium isopropoxide is enough to form an equivalent of active catalyst species **4** (Figure 3-6). One equivalent is required to neutralise the HCl formed during the reaction forming precursor **3** and another equivalent is required to deprotonate the precursor **3** to form the active catalyst species **4**. However, the concentration of the catalytic species generated in situ remains unknown. It is reasonable to assume that the formation reactions of the active catalyst complex **4** are relatively fast, so an equilibrium is established quickly between catalyst precursor and active complex. Increasing sodium isopropoxide amount should firstly increase HCl consumption (Figure 3-6, step 1) increasing the amount of precursor **3**, which in turn shifts the equilibrium of step 3 (Figure 3-6) towards generating more active catalytic species **4**. Obviously, a higher concentration of active catalytic species **4** increases the concentration of formed acetone as experimentally observed (see Figure 3-2).

1	+ *(1/2)* **2**	$\rightleftharpoons$	**3**	+ **HCl**	(step 1)
HCl	+ **sodium isopropoxide**	$\rightleftharpoons$	**NaCl** + **IPA**		(step 2)
3	+ **sodium isopropoxide**	$\rightleftharpoons$	**4**	+ **NaCl**	(step 3)
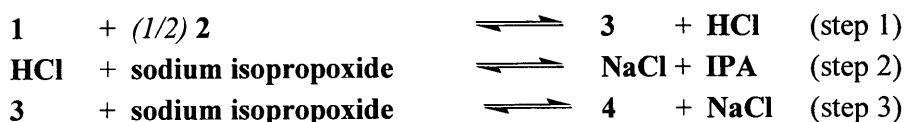
Figure 3-6 Catalyst activation by sodium isopropoxide (For compounds **1,2,3,4** refer to Figure 3-2)

3.3.3 Effect of addition sequence of reactants and catalyst solutions

The influence of addition sequence was another factor investigated. Catalytic precursor **3** was made in both cases in situ. The procedure for sequence 1 consisted of mixing catalyst precursor **3** and acetophenone in IPA and after 30mins stirring, adding sodium isopropoxide solution. Sequence 2 procedure consisted of mixing catalyst precursor **3** and sodium isopropoxide in IPA and after 30 minutes stirring, adding acetophenone. Conversion and enantioselectivity obtained from each addition sequence are shown in Figure 3-7.
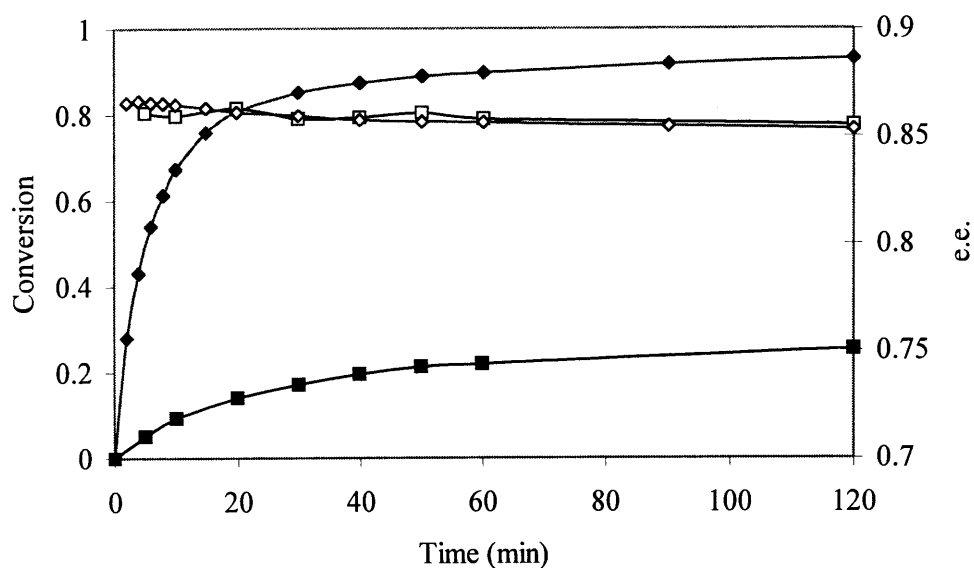
Figure 3-7   Effect of adding sequence of catalyst / acetophenone /sodium isopropoxide solution on conversion and enantioselectivity

It can be seen that the effect of addition sequence is significant on the conversion of acetophenone. Conversion for sequence 2 increases more slowly than conversion for sequence 1. In 60 minutes, conversion for sequence 1 reached almost 90%, while conversion for sequence 2 was just over 20%.

A possible reason of the effect of addition sequence on conversion is the following. In sequence 2, the active catalyst species **4** and catalyst intermediate **5** had been formed before addition of acetophenone, enhancing the extent of competitive reactions such as dimerisation which can form inactive compounds and limit the amount of rhodium available for transfer hydrogenation (Gladiali et al 1990). Another possible reason is that the central rhodium atom might combine with isopropoxide first, causing a loss of the catalyst ability to coordinate with acetophenone. Hence, the catalyst activity would decrease after staying with sodium isopropoxide for a long time. There was no obvious effect of addition sequence on enantioselectivity (Figure 3-7), consistent with the above hypothesis that sodium isopropoxide affects only the amount of active catalyst present.

Since the conversion of acetophenone was greatly affected by the addition sequence, with sequence 1 resulting in higher conversion, the rest of experiments were carried out by mixing catalyst solution and acetophenone prior to adding sodium isopropoxide solution.

3.3.4 Effect of presence of air

The asymmetric transfer hydrogenation is operated under inert atmosphere, usually N_2. An experiment was conducted to investigate the influence of air presence on the activity of the catalytic system by bubbling air (800ml/min) instead of N_2 into the reaction system. As can be seen from Figure 3-8, in the presence of air, 25% conversion was obtained compared to 95% with N_2 in 60 minutes. This suggests that catalyst might deactivate/decompose in the presence of air. However, there is still active catalyst available. The reaction sample was left for one week in the presence of air. The conversion went up to 58% and stabilised in another two weeks. The enantioselectivity of the catalyst was not affected by the presence of air. Although catalytic activity decreased, e.e. in both cases was 88% after 60 minutes.

- ◆ Bubbling N_2 (conversion)
- ◊ Bubbling N_2 (e.e.)
- ■ Bubbling air (conversion)
- □ Bubbling air (e.e.)
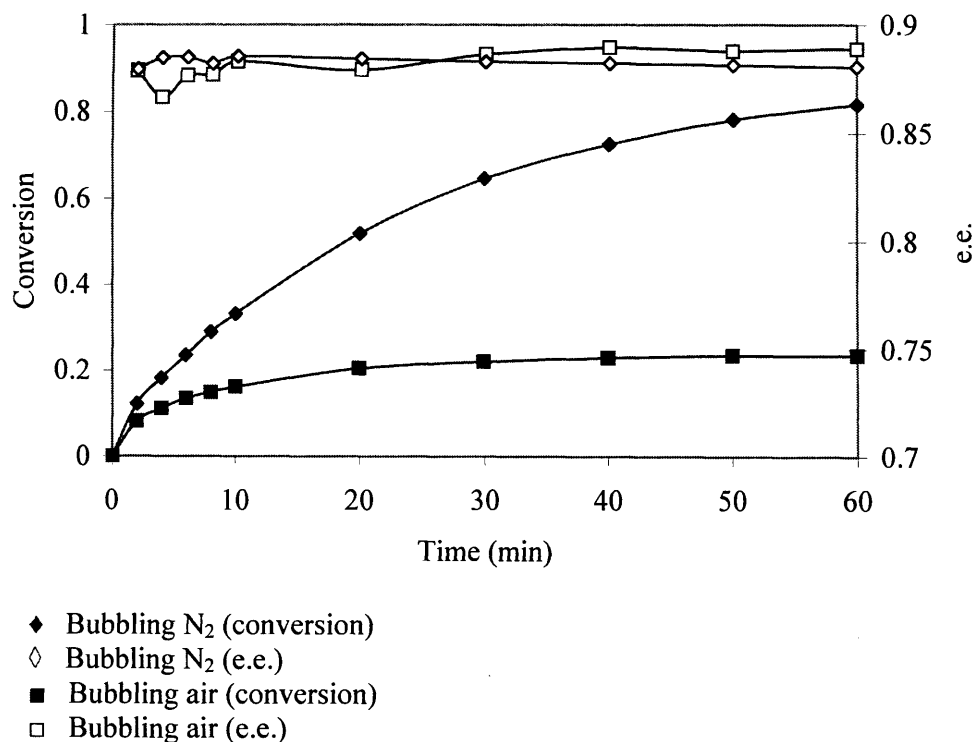
Figure 3-8 Effect of presence of air on conversion and enantioselectivity
(All the experiments conditions were the same as base case except temperature was 15°C and air was bubbled through the reaction mixture)

3.3.5 Effect of temperature

Experiments were conducted under different temperatures to study the effect of temperature on catalyst activity/selectivity. The results are shown in Figure 3-9 in terms of conversion (Figure 3-9a) and e.e. (Figure 3-9b). It can be seen that with increasing reaction temperatures, the initial reaction rate increased as expected. However, e.e. decreased slightly. From $0^\circ C$ to $30^\circ C$, the conversion increased with temperature. At $40^\circ C$ albeit the faster initial reaction rate, the conversion level dropped below that at $30^\circ C$ and levelled after 10 minutes, so that at 60 minutes it dropped below the value measured at $15^\circ C$, indicating catalyst deactivation. It can be concluded that $30^\circ C$ represents an optimum temperature with high reaction rate and good catalyst stability. Consequently, $30^\circ C$ was selected for the experimental studies. While in this work e.e. changed from 89% to 85% (in 60 minutes) for a temperature range 0 to $40^\circ C$, much larger and qualitatively different influence of temperature on e.e. has been observed by other researchers. Wills et al (1999) observed a change of e.e. to S-product from 13.5% to 94.4% for the reduction of α-chloroacetophenone by phosphinamide for the temperature range 40 to $110^\circ C$. Zassinovich et al (1992) observed change of e.e. from 2.2% to 24.9% for the range 65 to $83^\circ C$ for the reduction of acetophenone by [Rh$_2$(ac)$_4$.4H$_2$O] and (+)-(S)-3-sec-Butyl-1,10-phenanthroline.
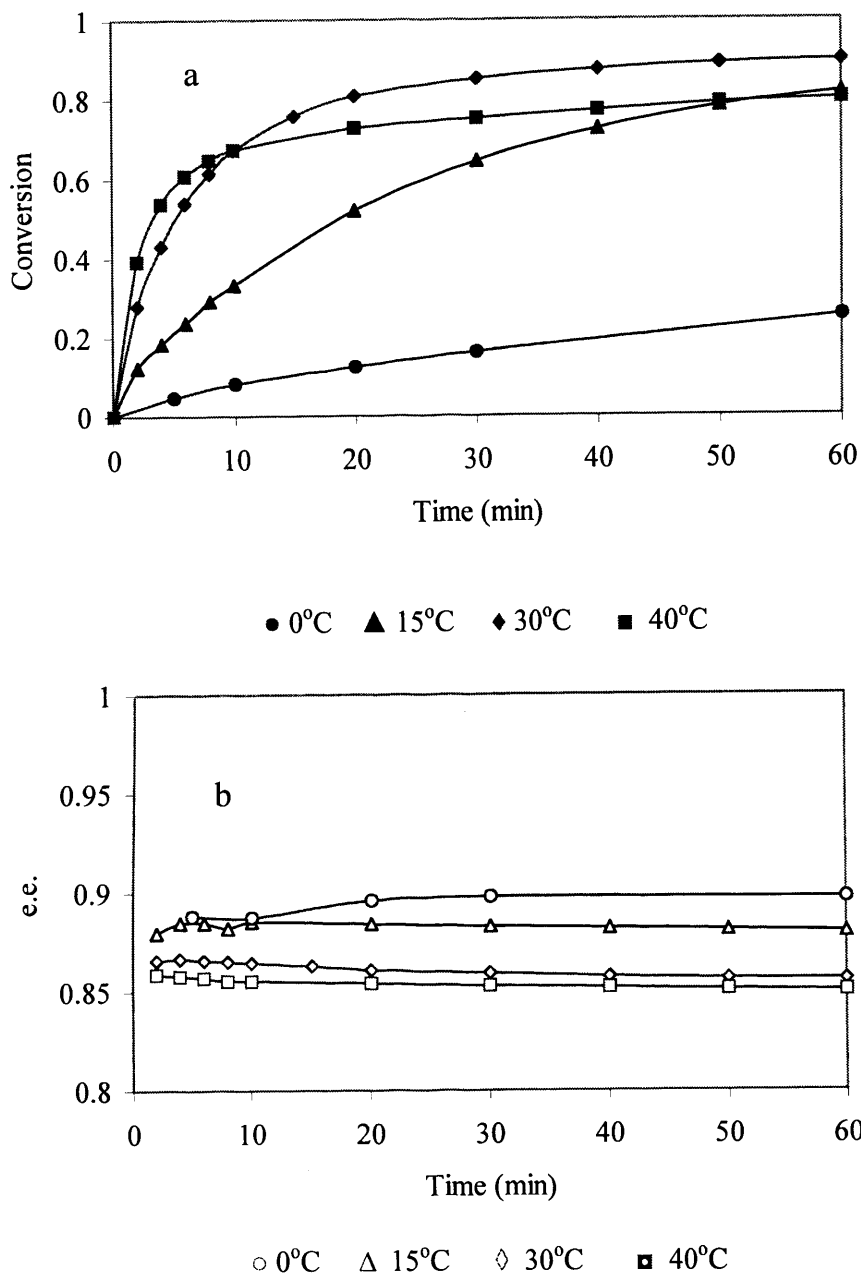
Figure 3-9 Effect of temperature on conversion and e.e. (a) Conversion vs. time for different temperatures; (b) Enantiomeric excess vs. time for different temperatures

3.3.6 Effect of acetone concentration

If the reaction steps in Figure 3-2 are reversible, removal of acetone is expected to affect reaction equilibrium. Consequently, the effect of acetone concentration on reaction performance was studied by adding acetone into the reaction mixture before

starting the reaction. Experiments were run at different initial acetone concentrations in the range 0M to 0.5M.

The results in terms of conversion vs. initial acetone concentration are presented in Figure 3-10a for selected reaction times. Figure 3-10b represents e.e. as a function of conversion for different initial acetone concentrations used, while Figure 3-10c gives acetone concentration profile. The results show that conversion decreased with increasing initial acetone concentration (Figure 3-10a). Although e.e. was not affected in the range of 0M to 0.1M throughout the whole conversion range, when initial acetone concentration was further increased to 0.5M, e.e. decreased significantly at high conversions (Figure 3-10b). For 0.5M initial acetone concentration conversion increased from 52.8% to 60.0% from 180 minutes to 520 minutes, and e.e. dropped from 86.1% to 84.0%. Because of very fast initial reaction rate, acetone concentration increased in the first 20 minutes for the range of initial acetone concentration 0M to 0.1M. Afterwards, it decreased slightly due to N_2 bubbling (Figure 3-10c).

The results suggest that acetone presence inhibits the reaction and does not have significant effect on enantioselectivity at least initially. The lower e.e. was obtained with 0.5M acetone initial concentration. The possible reason might be that reaction rate became slower with higher acetone initial concentration, and prolonged exposure of the product to the catalyst favors the reverse reactions (Noyori and Hashiguchi 1997). de Bellefon and Tanchoux (1998) observed that acetone inhibits the reaction as well for the [Rh(1,5-cyclooctadiene)Cl]$_2$/(1S,2S)-(-)-N,N'-dimethyl-1,2-diphenyl-1,2-ethanediamine catalyst system. However, increase of e.e. from 60% to 80% was observed when the initial acetone concentration increased from 0 to 0.9kmol/m^3.
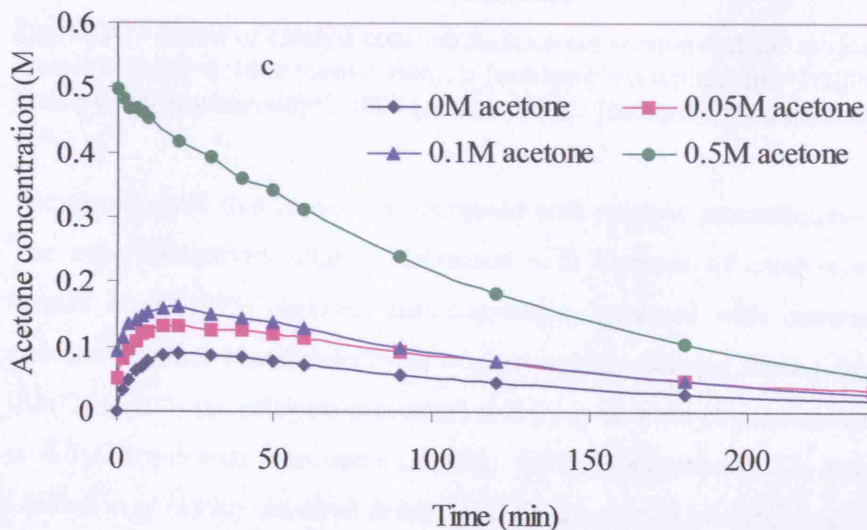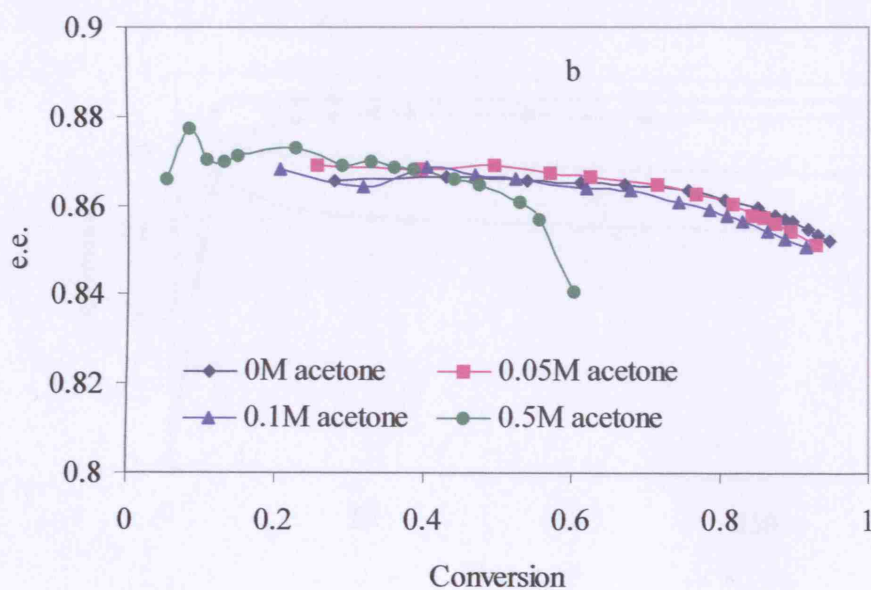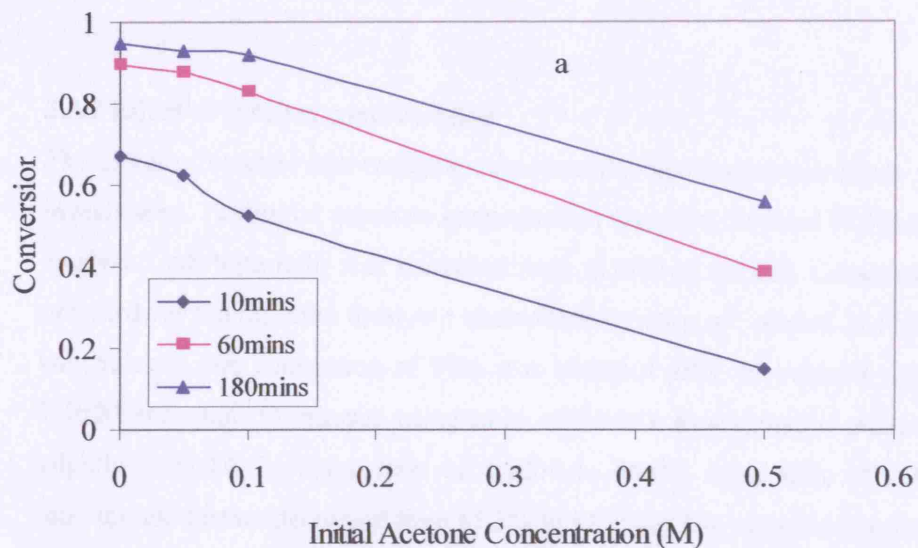
Figure 3-10 Effect of initial acetone concentration on reaction performance (a) Conversion at selected reaction time as function of initial acetone concentration; (b) e.e. vs. conversion for different initial acetone concentration; (c) Acetone concentration vs. time for different initial acetone concentration

3.3.7 Effect of catalyst concentration

The effect of catalyst concentration on conversion and enantioselectivity was further investigated. The initial substrate concentration was kept constant (0.14M), while the catalyst : substrate ratio was increased from 1:1000 to 2:1000. Conversion and e.e. obtained for the different catalyst : acetophenone ratios are plotted in Figure 3-11. It can be seen that conversion of 90% was obtained after 10 minutes using ratio of 2:1000 and after 30 minutes using ratio of 1:1000. Enantiomeric excess decreased slightly from 86.5% using ratio of 1:1000 to 85.0% using ratio of 2:1000 at 10 minutes and further decreased from 85.5% to 82.1% at 180 minutes respectively.
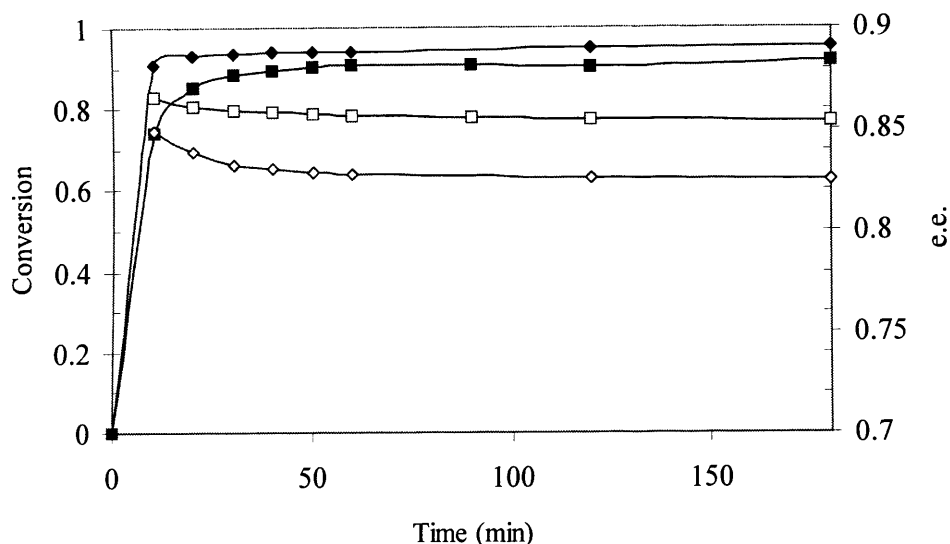
Figure 3-11 Effect of catalyst concentration on conversion and e.e. ■ [catalyst]:
[acetophenone]=1:1000 (conversion); □ [catalyst]:[acetophenone]=1:1000 (e.e.); ♦
[catalyst]:[acetophenone]=2:1000 (conversion); ◊ [catalyst]:[acetophenone]=2:1000
(e.e.)

The results show that conversion increased with catalyst concentrations as expected. The enantioselectivity slightly decreased with increase of catalyst concentration. Gamez et al (1995) observed that conversion increased with increase of catalyst concentration but enantioselectivity was not notably affected for the catalytic system $[Rh(C_6H_{10})Cl]_2$ (as catalytic precursor) and C_2 symmetric chiral diamines (as ligand) at 0.016M substrate concentration and 82°C Temperature). On the other hand, Gladiali et al (1990) observed decrease of e.e. as amount of catalyst increased for the system $[Rh(hd)Cl]_2$ and chiral phenanthrolines with 0.16M acetophenone in isopropanol.

3.3.8 Effect of initial substrate concentration at constant catalyst concentration

In this series of experiments, the catalyst concentration was kept constant while the substrate concentration varied over a range of 0.07M to 0.28M. The results obtained in terms of conversion and enantioselectivity are given in Figure 3-12. At low substrate concentrations much higher conversion was obtained (see Figure 3-12a) indicating that the reaction can not described by a simple first order kinetics. Figure 3-12b indicates that higher e.e. is obtained for smaller substrate concentrations at the same conversion. However, if one plots e.e. vs. S-(1)-phenylethanol concentration (see Figure 3-12c), it is evident that for the same amount of product required, it is better to operate at high substrate concentrations. In this way, if one operates far from equilibrium, forward reactions are enhanced and reverse reactions are minimised.
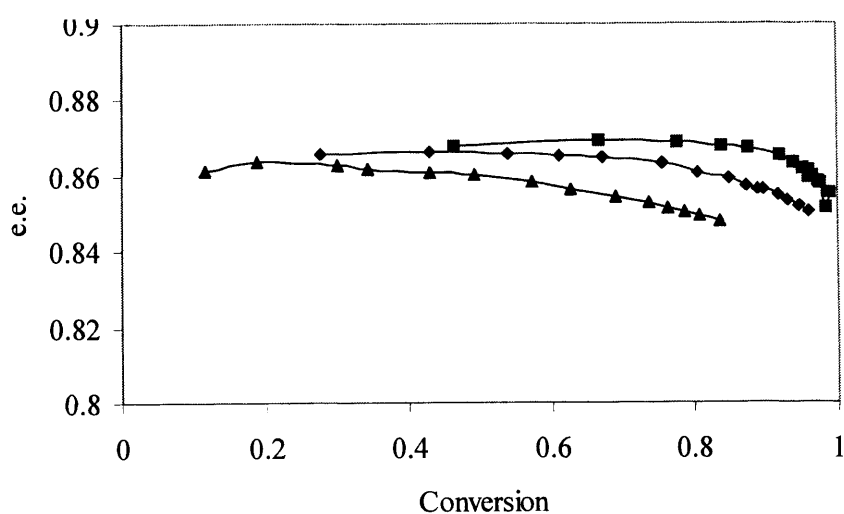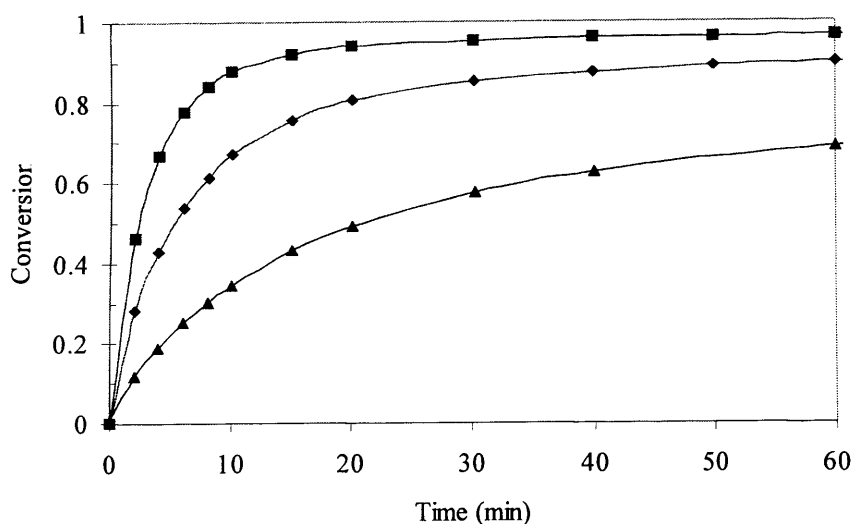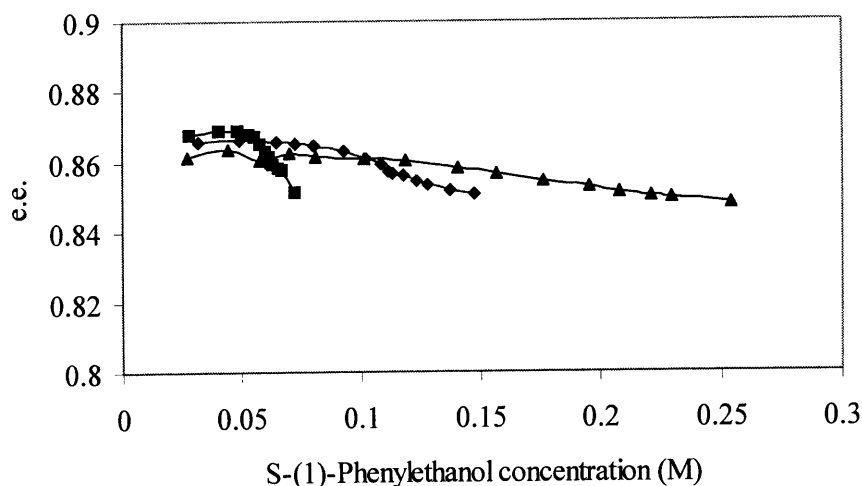
Figure 3-12 Effect of substrate concentration on conversion and e.e. at constant catalyst concentration; a: Conversion vs. time; b: e.e. vs. conversion; c: e.e. vs. S-(1)-Phenylethanol concentration; ■ [catalyst]:[acetophenone]=1:500; ◆[catalyst]: [acetophenone] =1:1000; ▲[catalyst]:[acetophenone]=1:2000

3.3.9 Effect of initial substrate concentration at constant substrate/catalyst ratio

From a cost point of view, a high substrate concentration would be advantageous. Keeping catalyst: acetophenone ratio constant, experiments were conducted with high acetophenone concentration. The results in terms of conversion vs. time are given in Figure 3-13a, while Figure 3-13b shows e.e. as a function of conversion for different initial substrate concentrations.

There was no significant effect on the final conversion when the initial acetophenone concentration was increased from 0.14M to 0.40M (Figure 3-13a). Final e.e. dropped considerably from 85.2% at 0.14M to 80.1% at 0.4M initial acetophenone concentration. When acetophenone concentration was further increased to 1M, both conversion and enantioselectivity exhibited a significant drop. At 1M initial acetophenone concentration, final e.e. dropped to 73.2% at 180 minutes.

The behaviour demonstrated in Figure 3-13 for increasing substrate concentration at constant catalyst/substrate concentration ratio is very similar to Figure 3-12 for increasing substrate concentration at constant catalyst amount. As observed in Figure 3-13c for certain S-(1)-phenylethanol concentration, the more concentrated (in substrate) solution provides higher e.e.. However, if high conversions are required, the more dilute (in substrate) solutions provide better final e.e. (Figure 3-13b). This is probably associated with higher equilibrium conversions for lower substrate concentrations (Noyori and Hashiguchi 1997) as also indicated by Figure 3-13a.
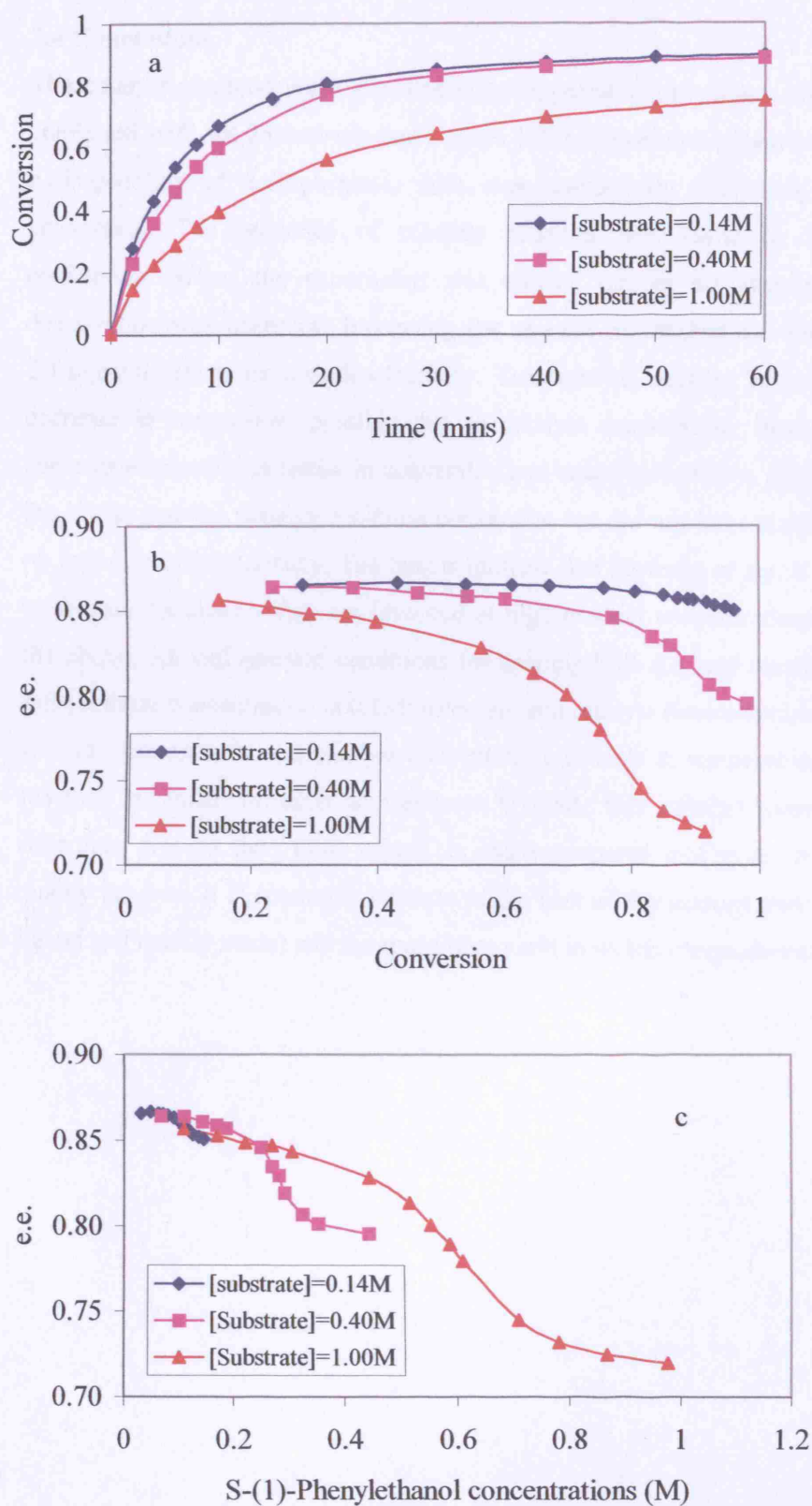
Figure 3-13   The effect of initial acetophenone concentration on conversion and e.e.; a: Conversion as function of reaction time; b: e.e. as function of conversion; c: e.e. as function of S-(1)-Phenylethanol concentration

3.4 Conclusions

The catalyst obtained when pentamethylcyclopentadienylrhodium chloride dimer is combined with 1R,2S-aminoindanol gives fast reaction rate of asymmetric transfer hydrogenation of acetophenone, with enantioselectivity decreasing slightly with conversion. The sequence of reactant addition was found to affect reactant conversion. When the experiment was carried out in air atmosphere, catalyst deactivation was observed. Increasing the amount of catalyst and temperature had detrimental effects on enantioselectivity. Temperature increase beyond 30°C led to decrease in conversion, possibly due to catalyst deactivation. Increasing reactant concentration led to decrease in conversion and enantioselectivity. Adding acetone to the initial reaction mixture inhibited conversion but did not have a significant effect on initial enantioselectivity. The results indicate that decrease of e.e. is primarily due to reverse reactions which are favoured at high product concentrations. Considering the above, optimal reaction conditions for keeping high e.e. and reaction rate would be: substrate concentration is 0.1M; substrate and catalyst concentration ratio is 1000; sodium isopropoxide and catalyst concentration ratio is 8; temperature is 30°C; the reaction is under nitrogen atmosphere. Overall, this catalyst provides a more economic process than most others, is easily prepared and gives consistent high quality product. It is economic because of the cost of the catalyst (low usage, cheap ligand and readily made) and the space/time yield in which the product can be made.

Chapter 4

Kinetic Studies for Catalytic Asymmetric Transfer Hydrogenation

4.1 Introduction

The chemical reactions taking place in the chemical reactor form the heart of any chemical process. Reaction kinetics are the translation of the understanding of the chemical process into a mathematical rate expression that can be used in reactor design. Because of the importance of correct and safe design of chemical reactors, chemical reaction kinetics is a key aspect of research and development in chemical industries, in research institutions, and academic centres, as well as in industrial laboratories.

Kinetics is simply a technical term used to describe the rate of chemical process, such as a catalytic reaction, as a function of the conditions. Knowledge of the rate of a catalytic reaction and its selectivity as a function of the process conditions and reactant concentrations is essential for the application of the catalyst in a commercial reactor. More specifically, the kinetics of the reaction are required in the form of a mathematical rate expression that can be used reliably to translate laboratory and pilot scale data into the design of commercial scale unit. The importance of a reaction's kinetics is that the rate and selectivity of reaction determine the size of the catalytic reactor for an overall production rate. Without a reliable means to predict the reaction rate, the reactor design could be highly speculative (Berger et al 2001).

One commonly used reaction rate expressions is the power law expression. For an irreversible reaction A+B→C, the reaction rate can be represented by an expression of the form (Fogler 1999):

$$r = kC_A^m C_B^n \qquad (4\text{-}1)$$

where r is reaction rate, C_A and C_B are concentrations of reactant A and B, k is reaction rate constant, m and n are termed the orders of the reaction. The power law expression is commonly used because of its simplicity and its property that it frequently fits the data rather easily. However, in catalysis this expression is not based on a sound physicochemical theory, and therefore the reliability of the results and predictions is limited to the range of conditions under which the kinetic experiments were performed.

A common approach to build kinetic models from theoretical and mechanistic considerations of the reaction is the so-called elementary step approach where the reaction mechanism is described by a set of single events, to each of which can be ascribed a rate equation, or a term in a single rate equation. This clearly has the potential to lead to very complex models with large numbers of fitting parameters. If this technique is used properly, the mechanistic understanding can in fact lead to simple models and equations through the rational elimination of some of the steps in order to focus on the rate-limiting steps and key competitive process in the case of parallel reactions (Fogler 1999).

4.2 Kinetic model

In the metal-ligand bifunctional catalysis mechanism shown in Figure 3-2 (Chapter 3), it is assumed that the catalyst preparation $1+2\rightarrow3$ is an irreversible reaction and 100% conversion is reached after overnight preparation. The second step, the activation of the catalyst by sodium isopropoxide, is assumed to be an irreversible reaction and takes place spontaneously. Therefore, it is assumed that the reaction from rhodium complex 2 and ligand 1 to active catalytic species 4 reaches completion fast and the amount of the 4 can be calculated based on the amount of 10 and 11 used. Based on the catalyst cycle shown in Figure 3-2 (Chapter 3), the following kinetic models were developed and evaluated. Comparing how well these models fit the experimental data, one can chose the best for reactor design.

4.2.1 Equilibrium model

In this model, it is assumed that the overall reaction proceeds according to the following steps (see Figure 3-2, Chapter 3):
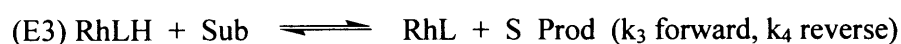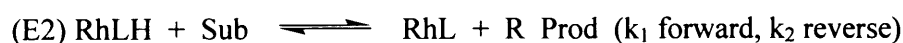
(E1) $RhL + IPA \rightleftharpoons RhLH + Acetone$ (fast equilibrium K_{ec})

(E2) $RhLH + Sub \rightleftharpoons RhL + R\_Prod$ (k_1 forward, k_2 reverse)

(E3) $RhLH + Sub \rightleftharpoons RhL + S\_Prod$ (k_3 forward, k_4 reverse)

(In which RhL=Active catalyst, RhLH= catalytic intermediate, IPA=isopropanol, Sub=substrate (acetophenone), R_Prod =(R)-1-phenylethanol, S_Prod=(S)-1-Phenylethanol)

101

In this model, the first reaction is assumed to be in an equilibrium while reactions (E2) and (E3) are reversible but not in equilibrium. The equilibrium constant K_{ec} is calculated as:

$$K_{ec} = [RhLH][Acetone]/[RhL][IPA] \tag{4-2}$$

The mass balance for the Rhodium is:

$$[Rh]_0 = [RhLH] + [RhL] \tag{4-3}$$

The mass balance for the substrate is:

$$[Sub]_0 = [Sub] + [R\_Prod] + [S\_Prod] \tag{4-4}$$

The following can be obtained by combining equation (4-2) and (4-3):

$$[RhLH] = K_{ec}[Rh]_0[IPA]/([Acetone] + K_{ec}[IPA]) \tag{4-5}$$

$$[RhL] = [Rh]_0[Acetone]/([Acetone] + K_{ec}[IPA]) \tag{4-6}$$

The rate equations of R_Prod and S_Prod are:

$$r_{R\_Prod} = k_1[RhLH][Sub] - k_2[RhL][R\_Prod] \tag{4-7}$$

$$r_{S\_Prod} = k_3[RhLH][Sub] - k_4[RhL][S\_Prod] \tag{4-8}$$

Substituting the [RhLH] and [RhL] with Equation 4-5 and 4-6, the expression of the rate equations of [R_Prod] and [S_Prod] can be written as following:

$$r_{R\_Prod} = \frac{[Rh]_o(k_1 K_{ec}[Sub][IPA] - k_2[R\_Prod][Acetone])}{K_{ec}[IPA] + [Acetone]} \tag{4-9}$$

$$r_{S\_Prod} = \frac{[Rh]_o(k_3 K_{ec}[Sub][IPA] - k_4[S\_Prod][Acetone])}{K_{ec}[IPA] + [Acetone]} \tag{4-10}$$

The instantaneous enantiomeric excess can be calculated as

$$E.E. = \frac{r_{S\,Prod} - r_{R\,Prod}}{r_{S\,Prod} + r_{R\,Prod}} = \frac{K_{ec}(k_3 - k_1)[IPA][Sub] + k_2[R\_Prod][Acetone] - k_4[S\_Prod][Acetone]}{K_{ec}(k_3 + k_1)[IPA][Sub] - k_2[R\_Prod][Acetone] - k_4[S\_Prod][Acetone]}$$

$$(4\text{-}11)$$

The reaction rate based on substrate can be calculated as:

$$r_{Sub} = \frac{Rh_0(K_{ec}(k_3 + k_1)[IPA][Sub] - k_2[R\_Prod][Acetone] - k_4[S\_Prod][Acetone])}{K_{ec}[IPA] + [Acetone]}$$

$$(4\text{-}12)$$

When time t=0, [acetone], [R_Prod] and [S_Prod] = 0. Therefore, the initial E.E. can be calculated as

$$E.E._{\cdot initial} = \frac{k_3 - k_1}{k_3 + k_1} \qquad (4\text{-}13)$$

and the initial reaction rate can be calculated as

$$r_{Sub} = Rh_0(k_3 + k_1)[Sub] \qquad (4\text{-}14)$$

It can be seen that the initial E.E. is independent of the substrate and catalyst concentration. It is only a function of reaction rate constants. This theoretical calculation agrees well with experimental findings which are shown in Table 1. The same initial e.e. was achieved when the substrate and catalyst concentration varies in the batch reactor.

The initial reaction rate is a function of both substrate and catalyst concentration. It increases with increase of catalyst and initial substrate concentration. Experimental findings in the batch reactor confirmed that the initial reaction rate increased with increase of catalyst concentration. However, the initial experimental reaction rate (Table 4-1) is independent of the substrate concentration which contradicts the theoretical predictions (Equation 4-14). For this reason, this model is not acceptable.

Table 4-1: Initial reaction rate and E.E. for different initial conditions

	[Substrate] M	[Catalyst] M	E.E.$_{initial}$ %	r$_{initial}$ M/min
1	0.07	0.00014	86.79	0.015
2	0.14	0.00014	86.56	0.016
3	0.28	0.00014	86.14	0.013
4	0.33	0.00033	86.43	0.044

([R_Prod]$_0$=0M, [S_Prod]$_0$=0M, [Acetone]$_0$=0M, T=30°C, where the initial reaction

rate is calculated as: $r_{initial} = \dfrac{[Substrate]_{t=0} - [Substrate]_{t=2\min}}{2\min}$)

4.2.2 Non-equilibrium model

In this model, it is assumed that the overall reaction proceeds according to the following steps and the first reaction is not considered to be at equilibrium:
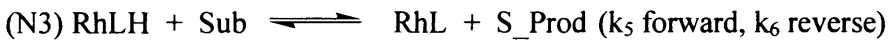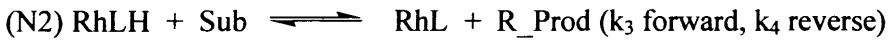
(N1) RhL + IPA $\rightleftharpoons$ RhLH + Acetone (k_1 forward, k_2 reverse)

(N2) RhLH + Sub $\rightleftharpoons$ RhL + R_Prod (k_3 forward, k_4 reverse)

(N3) RhLH + Sub $\rightleftharpoons$ RhL + S_Prod (k_5 forward, k_6 reverse)

(In which RhL=Active catalyst, RhLH= catalytic intermediate, IPA=isopropanol, Sub=substrate (acetophenone), R_Prod =(R)-1-phenylethanol, S_Prod=(S)-1-Phenylethanol)

In this model, it is assumed that intermediate RhLH exists in trace level and its net rate of formation is negligible (Bodenstein approximation). Therefore, applying steady-state approximation to RhLH:

d[RhLH]/dt=k_1[RhL][IPA]-k_2[RhLH][Acetone]-k_3[RhLH][Sub]+

k_4[RhL][R_Prod]-k_5[RhLH][Sub]+k_6[RhL][S_Prod]   (4-15)

=0

and the mass balance for Rhodium is:

[Rh]$_0$= [RhLH]+ [RhL]   (4-16)

Combining equations (4-15) and (4-16):

$$[RhL] = \frac{[Rh]_0(k_1[IPA] + k_4[R\_Prod] + k_6[S\_Prod])}{k_1[IPA] + k_2[Acetone] + k_3[sub] + k_4[R\_Prod] + k_5[Sub] + k_6[S\_Prod]}$$

(4-17)

$$[RhLH] = \frac{[Rh]_0(k_2[Acetone] + k_3[sub] + k_5[Sub])}{k_1[IPA] + k_2[Acetone] + k_3[sub] + k_4[R\_Prod] + k_5[Sub] + k_6[S\_Prod]}$$

(4-18)

The reaction rate equations of R_Prod and S_Prod are:

$$r_{R\_Prod} = k_3[RhLH][Sub] - k_4[RhL][R\_Prod]$$

(4-19)

$$r_{S\_Prod} = k_5[RhLH][Sub] - k_6[RhL][S\_Prod]$$

(4-20)

Substituting the [RhLH] and [RhL] with Equation 4-17 and 4-18, the expression of the rate equations of R_Prod and S_Prod can be derived as follows:

$$r_{R\_Prod} = \frac{[Rh]_0(k_1k_3[IPA][Sub] + k_6k_3[S\_Prod][Sub] - k_4k_2[R\_Prod][Acetone] - k_4k_5[R\_Prod][Sub])}{k_1[IPA] + k_2[Acetone] + k_3[Sub] + k_4[R\_Prod] + k_5[Sub] + k_6[S\_Prod]}$$

(4-21)

$$r_{S\_Prod} = \frac{[Rh]_0(k_1k_5[IPA][Sub] + k_4k_5[R\_Prod][Sub] - k_6k_2[S\_Prod][Acetone] - k_6k_3[S\_Prod][Sub])}{k_1[IPA] + k_2[Acetone] + k_3[Sub] + k_4[R\_Prod] + k_5[Sub] + k_6[S\_Prod]}$$

(4-22)

The instantaneous enantiomeric excess can be calculated as:

$$E.E. = \frac{r_{S\_Prod} - r_{R\_Prod}}{r_{S\_Prod} + r_{R\_Prod}} =$$

$$\frac{(k_1k_5 - k_1k_3)[IPA][Sub] + 2k_4k_5[R\_Prod][Sub] - k_6k_2[S\_Prod][Acetone] + k_2k_4[R\_Prod][Acetone] - 2k_3k_6[S\_Prod][Sub]}{(k_1k_5 + k_1k_3)[IPA][Sub] - k_6k_2[S\_Prod][Acetone] - k_2k_4[R\_Prod][Acetone]}$$

(4-23)

and the reaction rate of substrate can be calculated as:

$$r_{Sub} = \frac{Rh_0\{(k_1k_5 + k_1k_3)[IPA][Sub] - k_6k_2[S\_Prod][Acetone] - k_2k_4[R\_Prod][Acetone]\}}{k_1[IPA] + k_2[Acetone] + k_3[sub] + k_4[R\_Prod] + k_5[sub] + k_6[S\_Prod]}$$

(4-24)

When time t=0, [acetone], [R_Prod] and [S_Prod] = 0. Therefore, the initial E.E. can be calculated as

$$E.E._{initial} = \frac{k_5 - k_3}{k_5 + k_3}$$

(4-25)

and the initial reaction rate can be calculated as

$$r_{initial} = \frac{Rh_0(k_1k_5 + k_1k_3)[IPA][Sub]}{k_1[IPA] + (k_3 + k_5)[Sub]}$$

(4-26)

It can be seen that the initial E.E. is independent of the substrate and catalyst concentration. It is only function of the reaction rate constant. This theoretical calculation agrees well with experimental findings which is shown in Table 1. The same initial E.E. was achieved when the substrate and catalyst concentration varies in the batch reactor.

The initial reaction rate is a function of both substrate and catalyst concentration. It increases with increase of catalyst concentration. As shown in Table 4-1 experimental findings in the batch reactor confirmed that the initial reaction rate increased with increase of catalyst concentration. However, experimental results show that the initial reaction rate is independent of the substrate concentration which can be obtained by this model if $k_1[IPA] << (k_3+k_5)[Sub]$. Then the initial reaction rate becomes:

$$r_{initial} = Rh_0 \cdot k_1 \cdot [IPA]$$

(4-27)

Note that IPA is solvent in the system and that [IPA] is constant. The initial reaction rate is then only function of the catalyst concentration and reaction rate constant k_1.

A set of experiments (Table 4-2) were run in the batch reactor with different reactants and products initial concentrations to obtain experimental data for the kinetic parameters estimation. The kinetic parameter estimation was carried out using

gPROMS. The estimated parameters are summarised in Table 4-3 and the fittings between the experimental data and model simulation data are shown in Figure 4-1.

Table 4-2 Experiments and corresponding conditions used for parameter estimation

	[Sub]$_0$, M	[Acetone]$_0$, M	[Sub]/[Cat]
BR-30T-Base case	0.14	0	1000
BR-30T-005Acetone	0.14	0.05	1000
BR-30T-Double sub	0.28	0	2000
BR-30T-Half sub	0.07	0	500
Br-30T-01Acetone	0.14	0.1	1000

(Reaction conditions: Temperature=30°C, Nitrogen flowrate=800ml/min bubbling inside the liquid phase. [R_Prod]$_0$=0, [S_Prod]$_0$=0, [catalyst]=0.000144M)

Table 4-3 Reaction rate constant estimated by gPROMS based on non-equilibrium model at 30°C

	k, (mol/l)$^{-1}$min^{-1}	95% t-value
k$_1$	8.62	0.00163
k$_2$	17395.44	0.00024
k$_3$	862.61	0.00017
k$_4$	39.77	0.00005
k$_5$	12491.29	0.00016
k$_6$	183.81	0.00021

(Reference t-value (95%):1.65673; A 95% t-value for a parameter component smaller than the reference t-value indicates that the data is not sufficient to estimate this parameter precisely.)

Based on the reaction rate constants (Table 4-3) estimated by gPROMS, the initial e.e. can be calculated as:

$$e.e._{initial} = \frac{k_5 - k_3}{k_5 + k_3} = \frac{1201.61 - 89.76}{1201.61 + 89.76} = 86.1\% \qquad (4\text{-}28)$$

As it can be seen, this is very close to the experimental value (Table 4-1)

Next, the denominator terms in Equation 4-24 are calculated

$$k_1[IPA]= 8.62 \times 13 = 112.06 \, \text{min}^{-1} \quad (4\text{-}29)$$

and

$$(k_3+k_5)[Sub]= (862.61 + 12491.29) \times 0.14 = 1869.55 \, \text{min}^{-1} \quad (4\text{-}30)$$

therefore, the initial reaction rate can be approximated by

$$r_{Sub} = Rh_0 \cdot k_1 \cdot [IPA] = 0.000144 \times 8.62 \times 13 = 0.016 \, (\text{mol/l})/\text{min} \quad (4\text{-}31)$$

which is also very close to the experimental value (Table 4-1) and is independent of substrate concentration.

The fact that k_1 is very small indicates that the rate-limiting step is the hydrogen transfer from hydrogen donor, IPA, to the catalyst. In order to increase the reaction rate, acetone removal is an efficient way to help slow down the reverse reaction.

The agreements between experimental data and model simulation results used for the kinetic parameter estimation are reasonably satisfactory (Figure 9). However, due the fact that acetone has been removed during the experiments, experimental data only in first 15 minutes were used for the parameter estimation, in which the amount of acetone removed is very small and can be neglected due to in this period, acetone production rate is larger than the acetone removal rate.

However, message "A 95% t-value for a parameter component smaller than the reference t-value indicates that the data is not sufficient to estimate this parameter precisely" is shown in the gPROMS estimation results. The 95% t-value is determined by the probability (0.05 for a 95% confidence interval) and the degrees of freedom (Sokal and Rohlf 1995). This is probably due to the fact that the experiments carried out in the batch reactor were not carefully designed, so the experimental data obtained are not enough for kinetic parameter estimation.
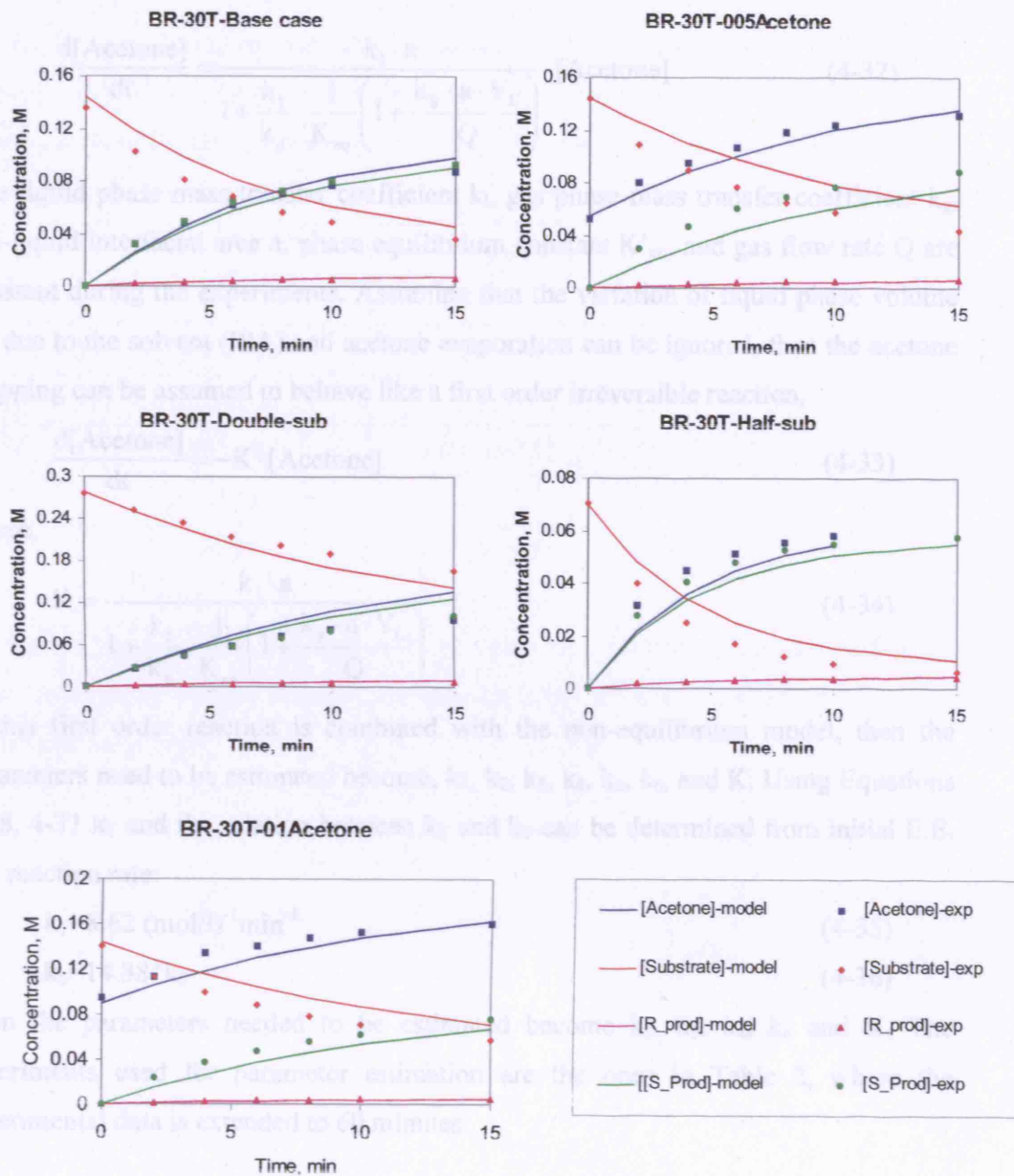
Figure 4-1 Comparison between experimental data and non-equilibrium model simulation results used for kinetic parameter estimation (for reaction conditions, see Table 4-2 and for kinetic parameters, see Table 4-3)

4.2.3 Non-equilibrium model with acetone stripping

Due to the fact that acetone concentration can affect the reaction rate significantly, acetone stripping in the batch reactor has to be considered for the kinetic parameters estimation. An acetone stripping model has been derived in Appendix A:

$$\frac{d[\text{Acetone}]}{dt} = \frac{-k_1 \cdot a}{1 + \frac{k_1}{k_g} \cdot \frac{1}{K_{eq}'}\left(1 + \frac{k_g \cdot a \cdot V_L}{Q}\right)} \cdot [\text{Acetone}] \tag{4-32}$$

The liquid phase mass transfer coefficient k_l, gas phase mass transfer coefficient k_g, gas-liquid interfacial area a, phase equilibrium constant K'_{eq}, and gas flow rate Q are constant during the experiments. Assuming that the variation of liquid phase volume V_L due to the solvent (IPA) and acetone evaporation can be ignored, then the acetone stripping can be assumed to behave like a first order irreversible reaction,

$$\frac{d[\text{Acetone}]}{dt} = -K \cdot [\text{Acetone}] \tag{4-33}$$

where,

$$K = \frac{k_1 \cdot a}{1 + \frac{k_1}{k_g} \cdot \frac{1}{K'_{eq}}\left(1 + \frac{k_g \cdot a \cdot V_L}{Q}\right)} \tag{4-34}$$

If this first order reaction is combined with the non-equilibrium model, then the parameters need to be estimated become, k_1, k_2, k_3, k_4, k_5, k_6, and K. Using Equations 4-28, 4-31 k_1 and the relation between k_3 and k_5 can be determined from initial E.E. and reaction rate:

$$k_1 = 8.62 \ (\text{mol/l})^{-1}\text{min}^{-1} \tag{4-35}$$

$$k_5 = 14.38 * k_3 \tag{4-36}$$

Then the parameters needed to be estimated become k_2, k_3, k_4, k_6 and K. The experiments used for parameter estimation are the ones in Table 2, where the experimental data is extended to 60 minutes.

The parameters to be estimated by gPROMS are shown in Table 4-4. The comparison of experimental data with model simulation results is shown in Figure 4-2. As it can be seen, K=0.01 min^{-1} which is much smaller than k_1=8.62 min^{-1} (The K value calculated according to Equation 4-34 is 0.0109min^{-1} which is very close to the K value estimated by gPROMS). This indicates that acetone stripping rate is much slower than the acetone producing rate, especially in the beginning of the reaction where acetone concentration is very low. The backwards reaction, which is acetone plus catalytic intermediate gives IPA and active catalyst (Reaction (N1)), is the fastest reaction in the reaction network. One way to reduce this reaction rate is by using large

excess of IPA, therefore, the reaction is preferred in dilute solution with IPA as solvent. Another way is to increase the acetone stripping rate.

Table 4-4 Reaction rate constant estimated by gPROMS based on non-equilibrium plus acetone stripping model at $30^{\circ}C$

	k, $(mol/l)^{-1}min^{-1}$	95% t-value
k_1	8.62	--
k_2	58070.42	0.000052
k_3	2856.11	0.000055
k_4	101.08	0.000131
k_5	41070.86	--
k_6	88.82	0.000111
K	0.01 (min^{-1})	0.000490

(Reference t-value (95%):1.65185; A 95% t-value for a parameter component smaller than the reference t-value indicates that the data is not sufficient to estimate this parameter precisely.)
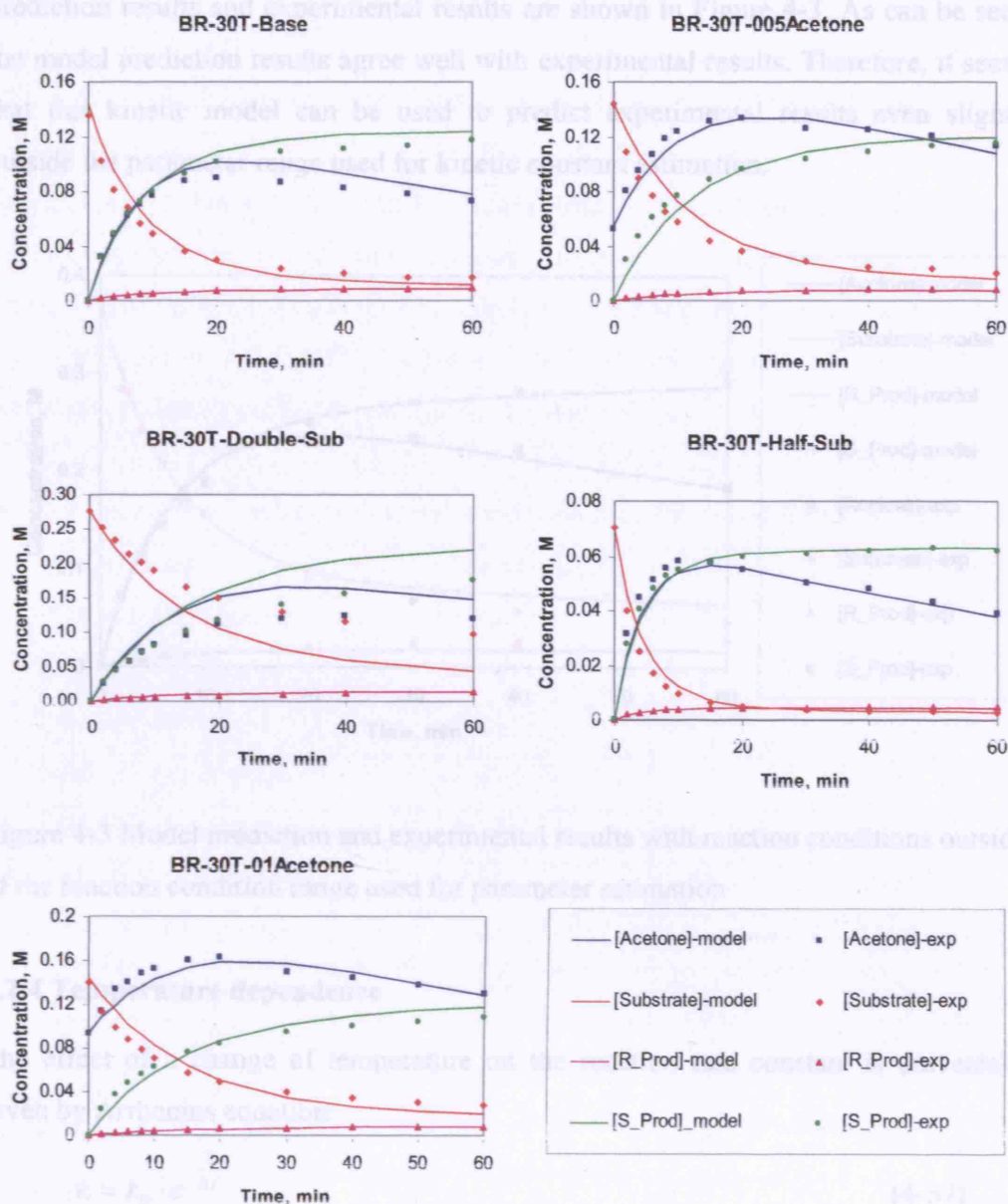
Figure 4-2 Comparison between experimental data and non-equilibrium model with acetone stripping simulation results used for the kinetic parameter estimation (for reaction conditions, see Table 4-2 and for kinetic parameters, see Table 4-4)

In order to check if this non-equilibrium model plus acetone stripping can be used to predict experimental results or not, an experiment was conducted in the batch reactor with reaction conditions outside of the reaction conditions range used for the kinetic parameter estimation shown in Table 4-4. The substrate concentration was selected as 0.37M and the substrate to catalyst concentration ratio was kept as 1000. The model

112

prediction results and experimental results are shown in Figure 4-3. As can be seen, the model prediction results agree well with experimental results. Therefore, it seems that this kinetic model can be used to predict experimental results even slightly outside the parameter range used for kinetic constant estimation.
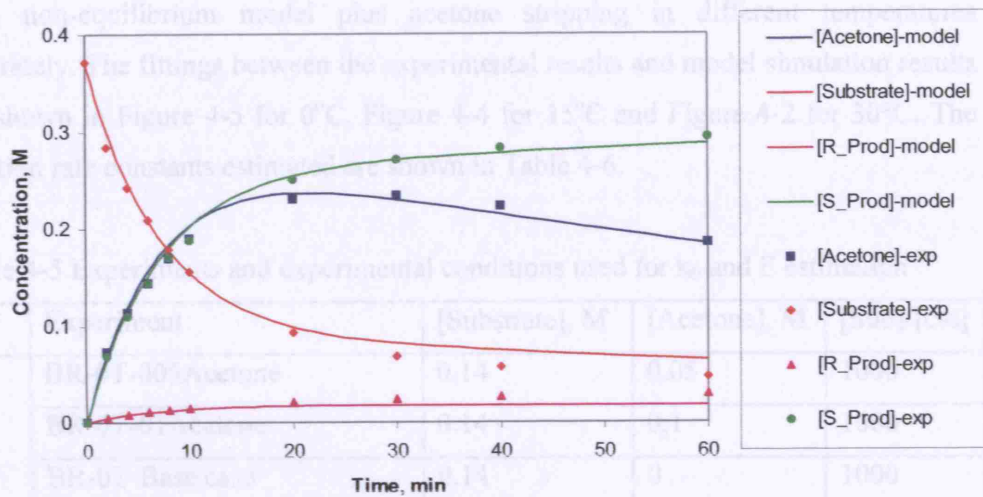
Figure 4-3 Model prediction and experimental results with reaction conditions outside of the reaction condition range used for parameter estimation

4.2.4 Temperature dependence

The effect of a change of temperature on the reaction rate constant is universally given by Arrhenius equation:

$$k = k_0 \cdot e^{-\frac{E}{RT}} \tag{4-37}$$

where, k_0 is the pre-exponential factor, R is ideal gas constant, T is absolute temperature and E is activation energy.

The determination of activation energy from data on the temperature dependence of the rate constant is accomplished by a simple graphical analysis of the Arrhenius equation. Taking logarithms of both sides:

$$\ln(k) = \ln(k_0) - \frac{E}{RT} \tag{4-38}$$

Thus, a plot of the logarithm of the rate constant versus the reciprocal of the temperature is linear with slop $-(E/R)$ and intercept $\ln(k_0)$.

113

In order to determine the activation energy and pre-exponential factor, experiments were carried out at 0°C, 15°C and 30°C with different reactant and product concentrations (Table 4-5). The reaction rate constants were estimated by gPROMS with non-equilibrium model plus acetone stripping in different temperatures separately. The fittings between the experimental results and model simulation results are shown in Figure 4-5 for 0°C, Figure 4-4 for 15°C and Figure 4-2 for 30°C. The reaction rate constants estimated are shown in Table 4-6.

Table 4-5 Experiments and experimental conditions used for k_0 and E estimation

	Experiment	[Substrate], M	[Acetone], M	[Sub]/[cat]
0°C	BR-0T-005Acetone	0.14	0.05	1000
	BR-0T-01Acetone	0.14	0.1	1000
	BR-0T-Base case	0.14	0	1000
	BR-0T-Double sub	0.28	0	2000
	BR-0T-Half sub	0.07	0.1	500
15°C	BR-15T-005Acetone	0.14	0.05	1000
	BR-15T-01Acetone	0.14	0.1	1000
	BR-15T-Base case	0.14	0	1000
	BR-15T-Double sub	0.28	0	2000
	BR15T-Half sub	0.07	0.1	500
30°C	BR-30T-005Acetone	0.14	0.05	1000
	BR-30T-01Acetone	0.14	0.1	1000
	BR-30T-Base case	0.14	0	1000
	BR-30T-Double sub	0.28	0	2000
	BR-30T-Half sub	0.07	0.1	500

(Reaction conditions: Nitrogen flowrate=800ml/min bubbling inside the liquid phase. [R_Prod]$_0$=0, [S_Prod]$_0$=0, [catalyst]=0.000144M)

Table 4-6 Reaction rate constants at different temperatures, activation energy and pre-exponential factor for nonequilibrium model with acetone stripping

	0°C $(mol/l)^{-1}min^{-1}$	15°C $(mol/l)^{-1}min^{-1}$	30°C $(mol/l)^{-1}min^{-1}$	E J/mol	k_0 $(mol/l)^{-1}min^{-1}$
k_1	0.77	3.41	8.62	55603	3.5472E+10
k_2	9.42	5531.27	58070.42	201681	6.1299E+39
k_3	1.50	57.90	2856.11	173047	1.6781E+33
k_4	0.86	9.32	101.08	109287	6.5686E+20
k_5	30.54	1051.63	41070.86	165116	1.0658E+33
k_6	0.11	24.46	88.82	155114	9.1762E+28

BR-15T-Base

BR-15T-005Acetone

BR-15T-Double-Sub

BR-15T-Half-Sub

BR-15T-01Acetone

[Acetone]-model — [Acetone]-exp ■
[Substrate]-model — [Substrate]-exp ♦
[R_Prod]-model — [R_Prod]-exp ▲
[S_Prod]-model — [S_Prod]-exp ●
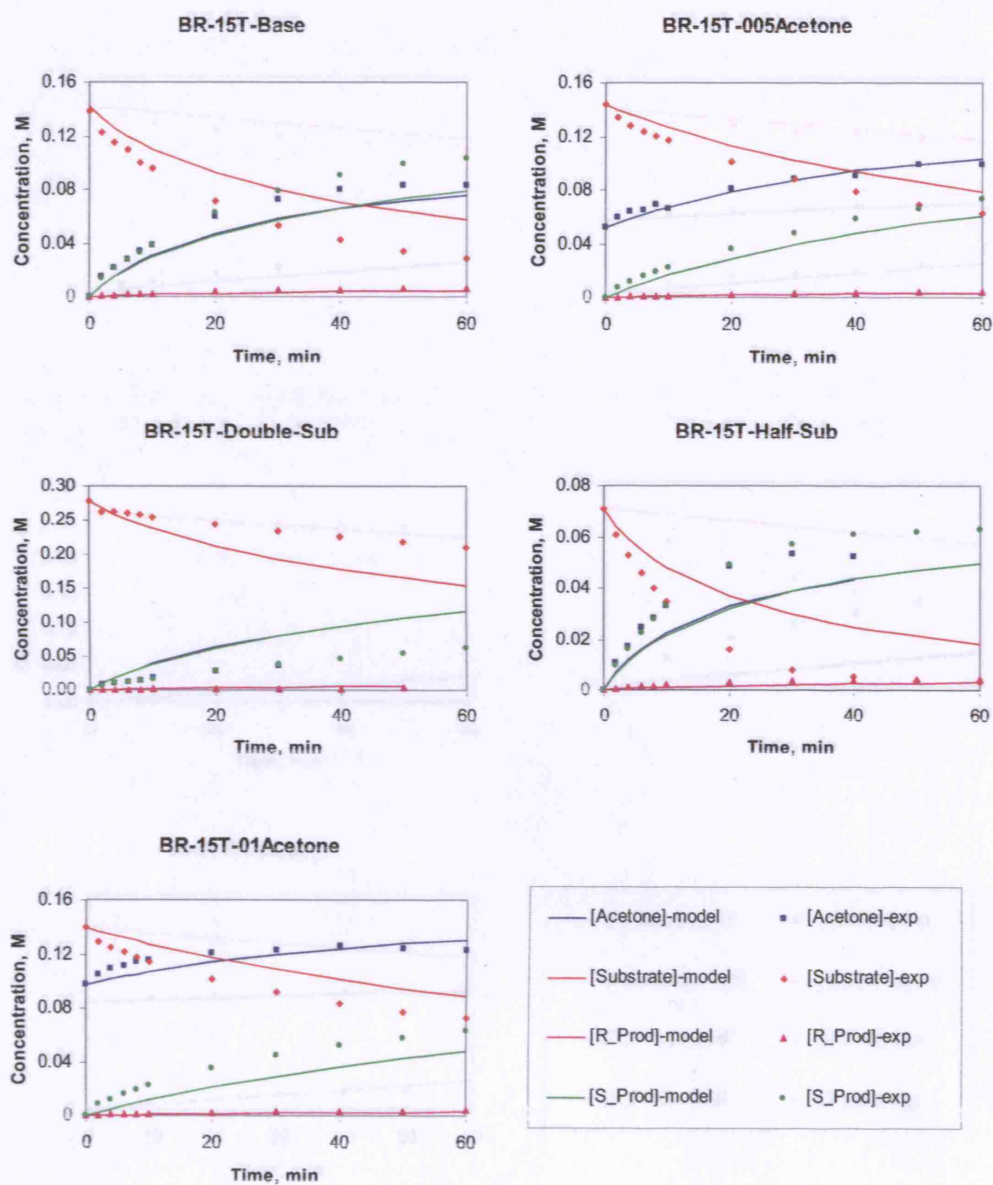
Figure 4-4 Comparison between experimental data (15°C) and non-equilibrium model with acetone stripping simulation results used for kinetic parameter estimation (for reaction conditions, see Table 4-5 and for kinetic parameters, see Table 4-6)
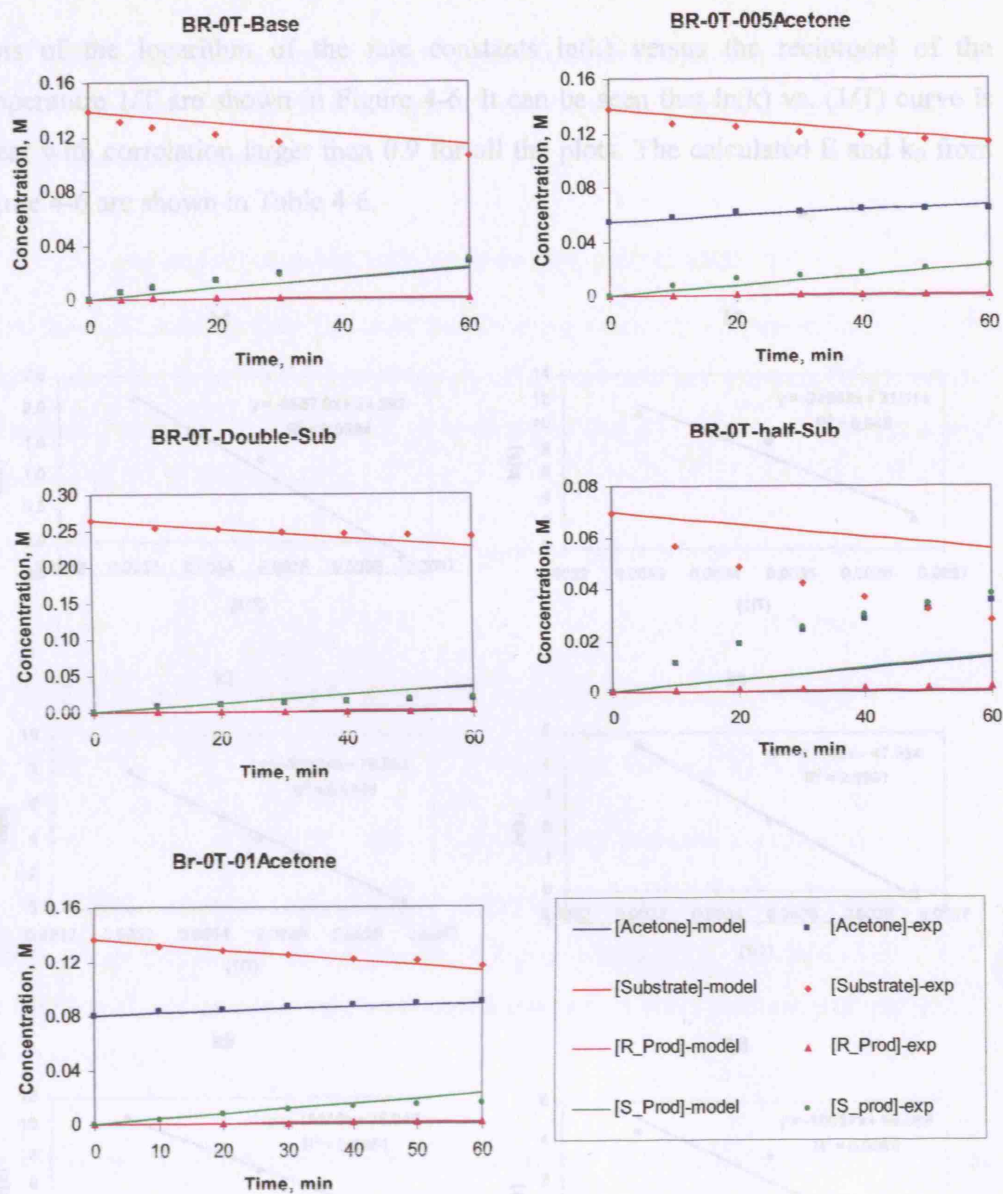
Figure 4-5 Comparison between experimental data (0°C) and non-equilibrium model with acetone stripping simulation results used for kinetic parameter estimation (for reaction conditions, see Table 4-5 and for kinetic parameters, see Table 4-6)

Plots of the logarithm of the rate constants ln(k) versus the reciprocal of the temperature 1/T are shown in Figure 4-6. It can be seen that ln(k) vs. (1/T) curve is linear with correlation larger than 0.9 for all the plots. The calculated E and k_0 from Figure 4-6 are shown in Table 4-6.
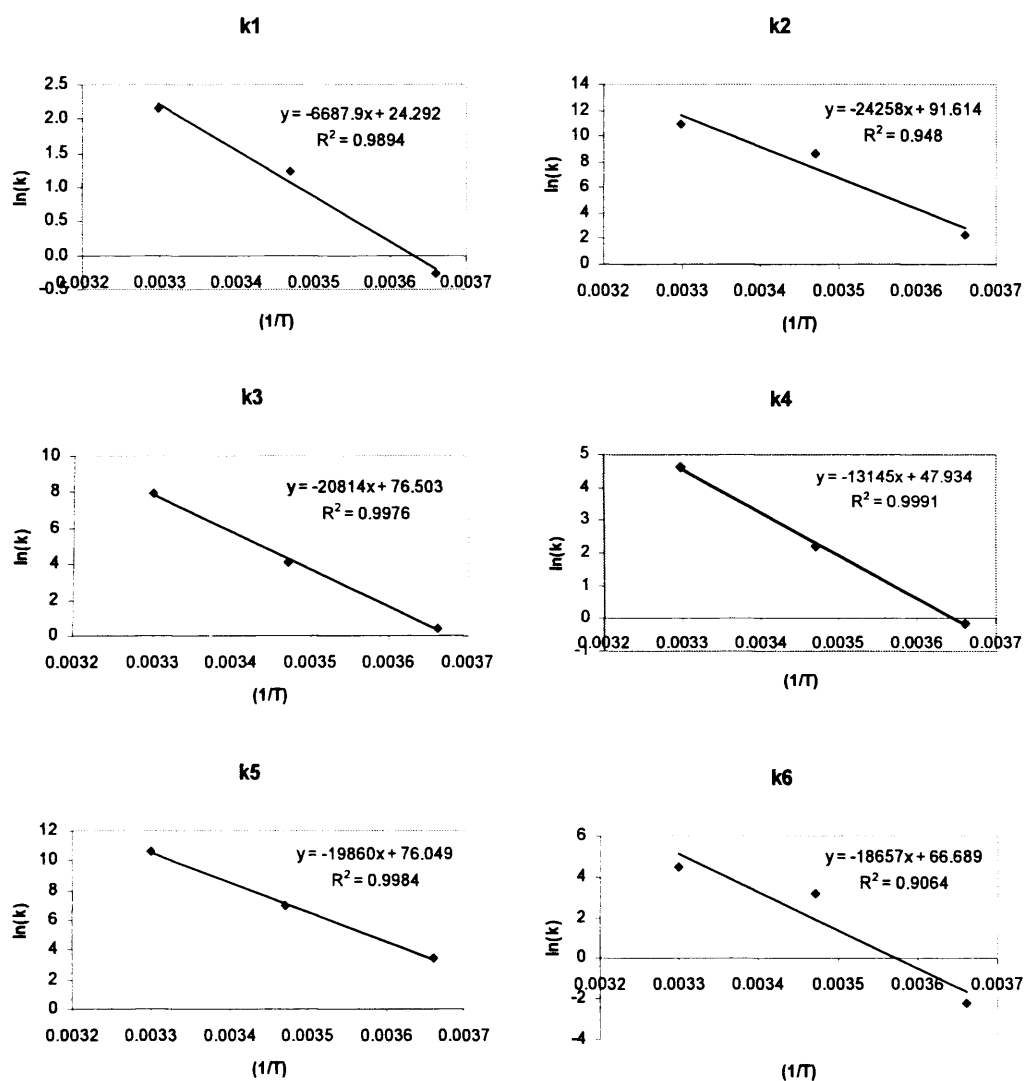
Figure 4-6 Arrhenius plots for reaction rate constants of non-equilibrium model with acetone stripping

For the initial enantioselectivity:

$$e.e._{initial} = \frac{k_5 - k_3}{k_5 + k_3} = 1 - \frac{2}{\frac{k_5}{k_3} + 1} = 1 - \frac{2}{\frac{k_{0,5}}{k_{0,3}} \cdot e^{\frac{E_3 - E_5}{RT}} + 1}$$ (4-39)

From Table 4-6, it can be seen that $E_3>E_5$, therefore, with decrease of temperature, the initial e.e. increases. This indicates that low reaction temperature is beneficial for e.e. as observed experimentally.

4.2.5 Ten reactions mechanism with acetone stripping model

A ten reaction mechanism with acetone stripping model is attempted to reduce the 95% t-value, improve the fittings of the experimental data and improve the parameter estimation precision. In this model, it is assumed that the overall reaction proceeds according to the following steps:

(T1) RhL + IPA $\rightleftharpoons$ RhLH + Acetone (k_1 forward, k_2 reverse)

(T2) RhLH + Sub $\rightleftharpoons$ SIM (k_3 forward, k_4 reverse)

(T3) RhLH + Sub $\rightleftharpoons$ RIM (k_5 forward, k_6 reverse)

(T4) SIM $\rightleftharpoons$ RhL + S_Prod (k_7 forward, k_8 reverse)

(T5) RIM $\rightleftharpoons$ RhL + R_Prod (k_9 forward, k_{10} reverse)
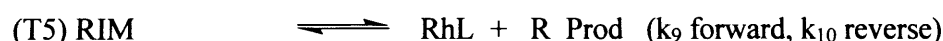
(In which RhL=actived Catalyst, RhLH=catalyst intermediate, IPA=isopropanol, Sub=substrate (acetophenone), S_Prod=(S)-1-phenylethanol, R_Prod=(R)-1-phenylethanol, acetone stripping was considered as first order reaction and reaction rate constant is K)

The experiments used for parameter estimation are the ones in Table 4-2, where the experimental data is extended to 60 minutes. The parameters estimated by gPROMS are shown in Table 4-6. The comparison of experimental data with model simulation results are shown in Figure 4-7. The agreement between experimental data and model simulation results used for the kinetic parameter estimation is reasonably satisfactory. However, a 95% t-value for a parameter component is still smaller than the reference t-value, which indicates that the data are not sufficient to estimate this parameter precisely.

Table 4-7 Reaction rate constant estimated by gPROMS based on ten reactions
mechanism with acetone stripping model at 30°C

Parameter	k	Units	95% t-value
k_1	0.877	$(mol/l)^{-1}sec^{-1}$	0.10917
k_2	179.72	$(mol/l)^{-1}sec^{-1}$	0.11100
k_3	308.23	$(mol/l)^{-1}sec^{-1}$	0.17204
k_4	0.0033	sec^{-1}	0.22057
k_5	112.07	$(mol/l)^{-1}sec^{-1}$	0.00052
k_6	9.50	sec^{-1}	0.01651
k_7	11.32	sec^{-1}	0.00093
k_8	2176.37	$(mol/l)^{-1}sec^{-1}$	0.00093
k_9	2.39	sec^{-1}	0.00035
k_{10}	2.88	$(mol/l)^{-1}sec^{-1}$	0.00104

(Reference t-value (95%):1.6499; A 95% t-value for a parameter component smaller
than the reference t-value indicates that the data is not sufficient to estimate this
parameter precisely.)
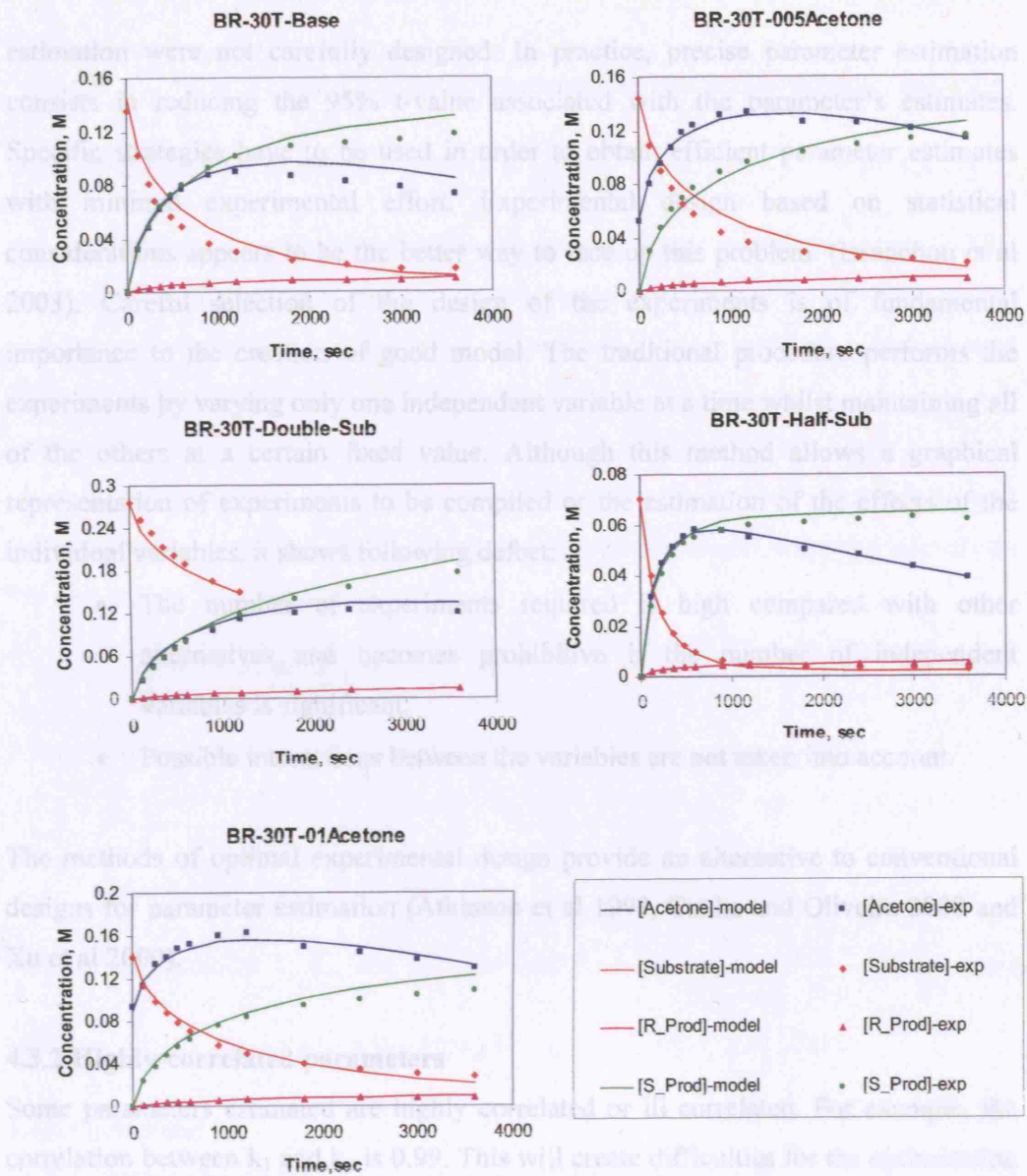
Figure 4-7 Comparison between experimental data and ten reaction mechanism with acetone stripping model simulation results used for kinetic parameter estimation (for reaction conditions, see Table 4-2 and for kinetic parameters, see Table 4-7)

4.3 Problems during the parameter estimation

4.3.1 Large confidence intervals

As shown earlier, a 95% t-value for a parameter component smaller than the reference t-value indicates that the data is not sufficient to estimate this parameter precisely, which is probably due to the fact that the experiments performed for the parameter

estimation were not carefully designed. In practice, precise parameter estimation consists in reducing the 95% t-value associated with the parameter's estimates. Specific strategies have to be used in order to obtain efficient parameter estimates with minimal experimental effort. Experimental design based on statistical considerations appears to be the better way to face up this problem. (Issanchou et al 2003). Careful selection of the design of the experiments is of fundamental importance to the creation of good model. The traditional procedure performs the experiments by varying only one independent variable at a time whilst maintaining all of the others at a certain fixed value. Although this method allows a graphical representation of experiments to be compiled or the estimation of the effects of the individual variables, it shows following defect:

- The number of experiments required is high compared with other alternatives and becomes prohibitive if the number of independent variables is significant.

- Possible interactions between the variables are not taken into account.

The methods of optimal experimental design provide an alternative to conventional designs for parameter estimation (Atkinson et al 1998, Cunha and Oliveira 2000 and Xu et al 2000).

4.3.2 Highly-correlated parameters

Some parameters estimated are highly correlated or ill correlated. For example, the correlation between k_1 and k_2 is 0.99. This will create difficulties for the optimization program.

Re-parameterization is an efficient way to reduce the correlations between parameters. For example, for the Arrhenius equation,

$$k = k_0 \cdot e^{-\frac{E}{RT}}$$

the two parameters k and E are strongly correlated because of the imbalance in their relative influence on the model. This can create numerical difficulties for the optimization program. The Arrhenius equation can be re-parameterized as:

$$k = k_{ref} \cdot e^{-\frac{E}{RT^*}}$$

where, $k_{ref} = k_0 \cdot e^{-\frac{E}{RT_{ref}}}$ and T* is the reparameterized reaction temperature, calculated

from the reaction temperature according to $\frac{1}{T^*} = \frac{1}{T} - \frac{1}{T_{ref}}$. Here T_{ref} is an arbitrarily

chosen reference temperature within the experimental temperature range. This reparameterization strongly reduces the interdependency between activation energy and the pre-exponential factor, which enhances the fitting procedure (Berger et al 2001, Buzzi-Ferraris 1999).

Another example is reparameterizing Langmuir-Hinshelwood-Hougen-Watson (LHHW) type expressions by removing the kinetic parameters from the numerator. The original LHHW expression is:

$$r = \frac{kK_A P_A K_B P_B^2}{1 + K_A P_A + K_B P_B^2}$$

After reparameterization, the expression becomes:

$$r = \frac{P_A P_B^2}{\dfrac{1}{kK_A K_B} + \dfrac{P_A}{kK_B} + \dfrac{P_B^2}{kK_A}}$$

Therefore, instead of k, K_A and K_B, the combinations $\dfrac{1}{kK_A K_B}$, $\dfrac{1}{kK_B}$ and $\dfrac{1}{kK_A}$ are

estimated which also enhances the fitting procedure (Berger et al 2001).

4.4 Conclusions

In this chapter, kinetic models of asymmetric transfer hydrogenation were developed and reaction rate constants were estimated using gPROMS. The metal-ligand bifunctional mechanism was selected to develop the kinetic model. Based on this mechanism, two kinetic models were studied initially, namely the equilibrium model and the non-equilibrium model. The equilibrium model can not capture the independence of the initial reaction rate on the initial substrate concentration. The parameters were estimated based on the non-equilibrium model. An improvement to the non-equilibrium model was to include acetone stripping which was treated as pseudo first-order reaction. The reaction rate constants show that hydrogen transfer from hydrogen donor isopropanol to the catalyst is the rate limiting step. The acetone stripping rate is much slower compared to the acetone producing rate. The non-

equilibrium model successfully predicted the initial enantiomeric excess and initial reaction rate. The model was validated by predicting the experimental results in which reaction conditions were outside the range of experimental conditions used for the parameter estimation.

The effect of temperature on reaction rate and initial enantiomeric excess was investigated. The reaction rate constants were estimated at 0°C, 15°C and 30°C. The activation energy and pre-exponential factor were calculated based on the Arrhenius plot $\ln(k) \sim (1/T)$. The experimental increase of initial enantiomeric excess with decrease of temperature was related to the different activation energies of the two reactions where the two enantiomers were formed.

A ten-reaction model with acetone stripping was attempted to reduce the 95% t-value for the parameters estimated. The results showed no improvement. In all cases considered, a 95% t-value for a parameter component smaller than the reference t-value indicated that the data were not sufficient to estimate kinetic parameters with confidence. The parameters were also highly correlated. Optimal experimental design and reparameterization are recommended to reduce this problem. Moreover, deep understanding of the statistic terms such as confidence intervals, correlation matrix, 95% t-value are crucial for choosing the strategy to improve the parameter estimation.

Chapter 5

Single Phase Tubular Reactor and Gas-liquid Slug Flow Reactor for Catalytic Asymmetric Transfer Hydrogenation

5.1 Introduction

Tubular reactors are tubes commonly constructed of metal or plastic. As narrow-bore tubes, the high surface area-to-volume ratio allows for rapid heat transfer and control of reaction temperature. Most tubular reactors are relatively inexpensive, portable, and useful for the laboratory, pilot plant and manufacturing. They are ideal for gases and liquids, but efficient fluid flow can be limited by the presence of solid. Such difficulties may be exacerbated by small apertures and by narrow channels. Pressure drop can limit productivity as well. However, some of these difficulties can be eliminated by adjusting flowrates, by selecting solvents to ensure good dissolution, or by selecting higher-boiling solvents so that evaporation does not increase reactor pressure. In this chapter, the single phase tubular and the gas-liquid two-phase slug flow reactors were investigated. Mixing sequence of the catalyst, substrate and sodium isopropoxide solution were studied, since they can have a significant effect on reaction conversion and enatioselectivity. Mixing in the micromixer and union tee were compared. Other parameters such as effect of liquid flowrate, residence time, gas flowrate were also investigated in this chapter.

5.2 Single phase tubular reactor

5.2.1 Experiment set up

A schematic of the single phase tubular reactor set up is shown in Figure 5-1. Two single-syringe infusion pumps (RAZEL A-99.FJZ) are used to drive the liquids through the reactor. 10mL 0.00028M catalyst solution (prepared by 2.24mg rhodium complex and 1.12mg ligand in 25.6ml isopropanol) which is pumped by syringe pump 1 and substrate solution (containing 0.28M acetophenone and 0.00224M sodium isopropoxide in isopropanol) which is pumped by syringe pump 2 are premixed in a micromixer (Standard Slit Interdigital Micro Mixer SSIMM from IMM) before being fed into the single phase tubular reactor. The single phase tubular reactors are made of PFA tubing with 1mm or 1.65mm inner diameter and 1.56mm or 3.45mm outer diameter respectively (see Table 5-1). The reactor length ranges from 0.13m to 3.9m. Flowrates of both syringes were the same and varied in the range 0.025~0.1ml/min. The temperature of the reactor system was controlled by a water bath. A first sample was taken after three residence times, a second sample was taken after four residence times and the third sample after five residence times to ensure the operation is in the steady state. The residence time is defined as volume of PFA tubing over total

volumetric flowrate varied between 0.025ml/min and 0.2ml/min. The sample was collected at the outlet of the tubular reactor in a 2.5ml vial. Evaporation is minimised by putting the vial in an ice bath. An Agilent 6890 GC system was used for analysis, according to the procedure described in Chapter 3.
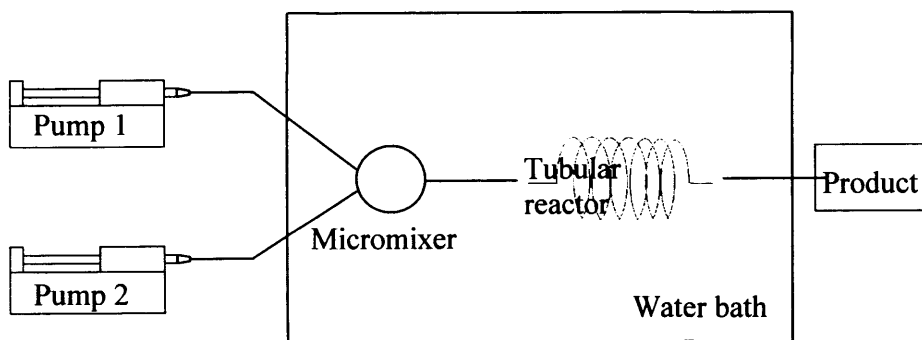
Figure 5-1   Single phase tubular reactor system set up

Table 5-1 Characteristics of the tubular reactors used

Reactor	ID (mm)	L (m)	Re	Pe	De
1	1	0.13	0.15	1311	0.39
2	1	0.26	0.15	1311	0.55
3	1	0.39	0.15	1311	0.67
4	1	0.52	0.15	1311	0.78
5	1	0.65	0.15	1311	0.87
6	1	1.3	0.15	1311	1.23
7	1	1.95	0.15	1311	1.5
8	1	2.6	0.15	1311	1.74
9	1	3.25	0.15	1311	1.95
10	1	3.9	0.15	1311	2.13
11	1.65	1.5	0.36	3177	0.976

($Re = \dfrac{du\rho}{\mu}$, $Pe = \dfrac{ud}{D}$, $De = \left(\dfrac{du\rho}{\mu}\right)\cdot\left(\dfrac{L}{2R}\right)^{1/2}$, where, d=diameter, L=length, μ=viscosity, u=velocity, D=diffusion coefficient, R=radius of curvature of bend, liquid flowrate=0.05ml/min)

5.2.2 Results and discussion

5.2.2.1 Effect of mixing sequence

As known from the batch reactor experimental results, the adding sequence of materials has a significant effect on reaction conversion. The catalyst reactivity of hydrogenation of acetophenone will decrease dramatically if the catalyst and sodium isopropoxide were mixed prior to adding substrate into the reaction system. The following experiments with different mixing sequences have been carried out in the tubular reactor as listed in Table 5-2 to investigate the effect on the reaction conversion and e.e.. In mixing sequence 1, the isopropanol solution of catalyst and substrate (acetophenone) were premixed first, and then mixed with sodium isopropoxide solution. In mixing sequence 2, the isopropanol solution of substrate and sodium isopropoxide were premixed first and then mixed with catalyst solution. In mixing sequence 3, the isopropanol solution of catalyst and sodium isopropoxide were premixed first and then mixed with substrate solution. The concentration of various compounds in the final solution obtained after the micromixer is the same as the base case in the batch reactor.

Table 5-2 Different mixing sequences investigated in the tubular reactor

	Sequence 1	Sequence 2	Sequence 3
Pump 1	Catalyst: Metal(2.24mg)+ligand(1.12mg) Acetophenone: 0.9g IPA: 25ml	Catalyst: Metal(2.24mg)+ ligand (1.12mg) IPA: 25.6ml	Catalyst: Metal(2.24mg)+ligand (1.12mg) Sodium isopropoxide solution: 0.6ml IPA: 25ml
Pump 2	Sodium isopropoxide solution: 0.6ml IPA: 25ml	Sodium isopropoxide solution: 0.6ml Acetophenone: 0.9g IPA: 24.4ml	Acetophenone: 0.9g IPA: 25ml

(Concentration of sodium isopropoxide solution is 3M in isopropanol)

All experiments were carried in the tubular reactor made from PFA tubing with 1.5m length and 1.65mm inner diameter. 0.1 ml/min flow rate was applied to both pump 1 and pump 2. The residence time was 16 minutes. Results and also the performance of the batch reactor for the corresponding mixing sequences are given in Table 5-3.

Table 5-3 Results of different mixing sequences for tubular reactors and batch reactor

	Tubular reactor		Batch reactor	
	Conversion (%)	ee(%)	Conversion (%)	ee(%)
Sequence 1	45.3	86.8	75.79	86.31
Sequence 2	72.7	85.9	---	---
Sequence 3	12.46	86.95	14.07	86.31

(Temperature= 30°C; [Substrate]=0.144M; [Substrate]/[Catalyst]=1000, [Sodium Isopropoxide]/[Catalyst]=8; Tubular reactor: ID: 1.65mm, length: 1.5m, flowrate: 2×0.1ml/min, residence time: 16min; Batch reactor: nitrogen flowrate =800ml/min, liquid volume=250ml.)

As shown in Table 5-3, the effect of the sequence is significant on the conversion of acetophenone. In 16 minutes, only 12.46% conversion was achieved with sequence 3, while about 72.7% conversion was achieved with mixing sequence 2. However, the mixing sequence does not have any effect on the enantioselectivity. Slightly lower e.e. obtained with mixing sequence 2 is due to the fact that e.e. decreases when conversion increases.

The lowest conversion was obtained with mixing sequence 3 (mixing catalyst and sodium isopropoxide firstly). This confirmed the results of batch reactor experiments where mixing catalyst and sodium isopropoxide prior to substrate was found to reduce catalytic activity (Chapter 3). A possible explanation is that the active catalyst species and catalyst intermediate had been formed before addition of acetophenone, enhancing the extent of competitive reactions such as dimerisation which can form inactive compounds and limit the amount of rhodium available for transfer hydrogenation (Gladiali et al 1990). Another possible reason is that the central rhodium atom might combine with isopropoxide firstly, causing a loss of the catalyst ability to coordinate with acetophenone. Hence, the catalyst activity would decrease after staying with sodium isopropoxide for a long time.

Better conversion was obtained by using sequence 2 and sequence 1. However, much higher conversion was obtained by using sequence 2 rather than sequence 1. It is worth noting that for sequence 2 during preparation of the mixture for pump 2, by

mixing of sodium isopropoxide solution with acetophenone solution, the resulting solution was yellow-green, even though the initial solutions were clear. This is probably due to some complex reactions (e.g. aldol condensation) taking place. However, the reason for low conversion of sequence 1 as compared to sequence 2 and batch reactor experiments is not clear. The conversion in the batch reactor (sequence 3) is slightly higher than that in the tubular reactor. This was probably due to acetone removal in the batch reactor experiments). Since the conversion of acetophenone was greatly affected by the mixing sequence, with mixing sequence 2 resulting in higher conversion, the rest of experiments were carried out by mixing acetophenone and sodium isopropoxide prior to the catalyst.

The experiment with mixing sequence 2 was repeated twice to check the reproducibility. Samples were taken after 3, 4 and 5 residence times in each experiment. The results are summarised in Table 5-4 and show that conversion is reproducible within 2.2% and e.e. is reproducible within 0.23%. It can also be seen that the conversion and e.e. for 3, 4 and 5 residence times is same in both experiments which indicates that the experiments reached steady state already after 3 residence times.

Table 5-4 Experimental reproducibility in single phase tubular reactor (mixing sequence 2)

	Experiment 1			Experiment 2		
	3 RT	4 RT	5 RT	3 RT	4 RT	5 RT
Conversion (%)	71.4	72.9	72.5	73.0	72.6	72.7
e.e. (%)	85.9	85.9	85.7	85.8	85.8	85.9

(RT: Residence time; Tubular reactor: ID=1.65mm, length=1.5m,

flowrate=2×0.1ml/min, RT=16mins; Temperature= 30°C; [Substrate]=0.144M;

[Substrate]/[Catalyst]=1000, [Sodium Isopropoxide]/[Catalyst]=8)

5.2.2.2 Effect of mixing method

It is very important that the catalyst solution and substrate solution can be mixed perfectly before entering the reactor. Micromixers are currently widely used to obtain good mixing in very short time. The SSIMM micromixer can achieve good mixing on

the microscale by splitting a main stream into a large number of substreams. Ehrfeld et al (1999) investigated mixing in micromixers and compared the mixing quality in micromixer and union Tee by a test reaction. They found that the micromixer has better performance than union Tee. Mixing in micromixer (SSIMM) and Union Tee (1/8", Swaglok) were also investigated in our reaction system. The results for sequence 2 are shown in table 5-5 where the residence time was altered by changing reactor length.

Table 5-5: Effect of mixing method on conversion and enantioselectivity

Residence time (min)	2		10	
Mixing method	Micromixer	Union tee	Micromixer	Union tee
Conversion (%)	22.68	11.81	57.25	50.81
e.e. (%)	86.69	86.65	86.66	86.96

(ID=1mm; Flowrate= 2×0.025ml/min; Temperature=30°C; [Substrate]=0.144M; [Substrate]/[Catalyst]=1000; [Sodium Isopropoxide]/[Catalyst]=8)

It can be seen from table 5-5 that 22.68% and 11.81% conversion was obtained in the experiment with the micromixer and union tee in 2 min respectively. Much higher conversion was obtained with micromixer than with union tee in short residence time which is probably due to the fact that the initial reaction rate is very fast and it is mixing controlled process in the short residence time. However, after 10 min, the difference between micromixer and union tee became less. This is because the reaction rate became slow after 10 minutes and the mixing is not very important compared with long residence time i.e. the process became kinetically controlled. Another possible reason is that mixing took place inside the tube which results in higher conversion.

The effect of tube size is studied by conducting the experiments in the PFA tube with 1mm ID and 1.65mm ID by keeping other experimental conditions same. The results are summarised in Table 5-6. As can be seen, the tube size does not have any effect on the reaction conversion and enantioselectivity in the ID range 1-1.65mm. this is due to high Pe number for both tubes i.e. both reactors behave as PFR with low

dispersion. It is worth noting that transverse vortexes can help mixing, but are not expected to be present, since Dean number is smaller than 140.

Table 5-6 Effect of tube size

Tube size (ID)	Conversion (%)	e.e. (%)
1mm	71.5	86.0
1.65mm	72.7	85.8

(Flowrate=2×0.025ml/min; Residence time=16min; Temperature=30°C; [Substrate]=0.144M; [Substrate]/[Catalyst]=1000; [Sodium Isopropoxide]/[Catalyst]=8)

5.2.2.3 Effect of sodium isopropoxide amount

As recognized with several other transfer hydrogenation catalysts, the catalyst is sensitive to water (de Bellefon et al 1998). Presumably, as demonstrated with similar complexes, water molecules are able to coordinate with the activated catalyst. Laue et al (2001) found, in a continuous application, that depending on the concentration of water in the feed stream, significant deactivation took place. This deactivation was reversible and could be compensated by a continuous low sodium isopropoxide dosage. The role of the sodium isopropoxide concentration was to replace coordinated water molecules with catalyst.

There is about 0.05% (wt%) water in isopropanol which is used as solvent in the reaction system. Sodium isopropoxide is used to activate the catalyst. It might be desirable to eliminate the water effect on the catalyst using a high excess of sodium isopropoxide. Theoretically, two equivalents of sodium isopropoxide are enough to activate the catalyst. Usually an excess of sodium isopropoxide is utilized in the reaction. However, high concentrations of isopropoxide were observed to result in a decreased enantioselectivity of the catalyst, possibly due to abstraction of the second chloride, which might cause a change in the catalyst geometry (Laue et al 2001). Therefore, the effect of sodium isopropoxide amount on the reaction conversion and e.e. was investigated and the results are summarised in table 5-7.

132

Table 5-7 Effect of sodium isopropoxide amount on conversion and enatioselectivity

| | [Sodium isopropoxide]: [Catalyst] | Tubular reactor | | Batch reactor | |
		Conversion (%)	e.e. (%)	Conversion (%)	e.e. (%)
Experiment 1	4	73.9	85.5	---	---
Experiment 2	8	72.7	85.9	75.79	86.31
Experiment 3	24	72.3	85.8	---	---

(Tubular reactor: ID= 1.65mm, Length= 1.5m, Flowrate= 2×0.1ml/min, RT= 16min; Temperature= 30°C; [Substrate]=0.144M; [Substrate]/[Catalyst]=1000)

The results show that the sodium isopropoxide concentration does not affect the reaction conversion and enantioselectivity. Sodium isopropoxide concentration four times larger than the catalyst concentration is enough to avoid deactivation of the catalyst by water. Moreover, the CATHy^{TM} catalyst shows good stability even when high excess of sodium isopropoxide amount is used (see Table 5-7). Gladiali et al (1990) observed only minor differences in rate and enantioselectivity on varying the concentration of KOH between KOH/Rh ratio of 3 and 24. However, Gamez et al (1995) observed an increase of conversion with KOH concentration while an optimum in enantioselectivity for a KOH/Rh ration between 6 and 10. Their explanation is that when a large excess of KOH is used, it can be assumed that iPrO⁻ is formed in the reaction medium and the alcoholate and OH⁻ can compete with diamine ligands which could decrease the e.e..

5.2.2.4 Effect of catalyst and substrate age

For continuous operation, it is important to find if the catalyst solution is deactivated or not when left standing for sometime. Therefore, the effect of catalyst and substrate solution age on reaction conversion and e.e. was investigated. Experiments were carried out with fresh catalyst/substrate solution and one day old solution in the single phase tubular reactor. The results are shown in Table 5-8. It can be seen that conversion is much lower with one day old catalyst solution, which indicates the

133

catalyst might be deactivated after one day. Therefore, fresh catalyst should be prepared for experiments conducted on different days.

Table 5-8: Effect of catalyst and substrate age

Catalyst solution	Fresh	1day	1 day
Substrate+IPA+sodium isopropoxide	Fresh	1day	Fresh
Conversion (%)	57.25	42.59	39.84
e.e. (%)	86.66	86.85	86.92

(ID=1mm; Length=0.65m; Residence time=10min; Flowrate= 2×0.025ml/min; Temperature= 30°C; [Substrate]=0.144M, [Substrate]/[Catalyst]=1000, [Sodium isopropoxide]/[Catalyst]=8)

It can be seen that one day old substrate+IPA+sodium isopropoxide solution gave better conversion than fresh one when one day old catalyst solution was used. When sodium isopropoxide and substrate are mixed together, the colour of the solution changed from colourless to light yellow-green immediately. The colour changed more dramatically with higher substrate concentration and also with time. So a reaction (probably aldol condensation) must be occurring after sodium isopropoxide is mixed with substrate. Therefore, the substrate concentration was measured in fresh and one day old substrate+IPA+sodium isopropoxide solution which was prepared and analysed by GC immediately (fresh), and then the same solution was kept in a sealed flask for an analysis after one day. The results are shown in Table 5-9.

Table 5-9 Effect of Substrate+IPA+sodium isopropoxide solution age on substrate concetration

Substrate+IPA+sodium isopropoxide	Fresh	1day
Substrate concentration (M)	0.274	0.261

There is no new chemical species detected by GC. However, slightly decrease of substrate concentration was observed (Table 5-5). The small change of substrate concentration is not enough to explain this behaviour.

5.2.2.5 Effect of residence time

The effect of different residence time was studied in the tubular reactor. The tube diameter and liquid flowrates were kept the same to obtain the same Reynolds number (0.15). The reactor volume was changed by changing tube length. Experimental results are shown in table 5-10.

Table 5-10: Effect of residence time on conversion and e.e.

RT (min)	2	4	6	8	10	20	30
Length (m)	0.13	0.26	0.39	0.52	0.65	1.3	1.95
Conversion (%)	22.68	37.55	45.72	52.88	57.25	77.45	82.25
e.e. (%)	86.69	86.64	86.66	86.70	86.66	86.64	86.42

(RT=Residence Time; ID=1mm; Flowrate=2×0.025ml/min; Temperature= 30°C; [Substrate]=0.144M; [Substrate]/[Catalyst]=1000, [Sodium Isopropoxide]/ [Catalyst]=8)

As shown in Table 5-10, conversion increased with increasing residence time. Enantioselectivity did not change with different residence time. A comparison between the single phase tubular reactor and batch reactor on the asymmetric transfer hydrogenation is shown in Figure 5-2 for the same reaction/residence time.

Higher reaction rate is obtained in the batch reactor than in the single phase tubular reactor. The possible reason is that there was some acetone being removed by bubbling nitrogen which drives the reaction towards forwards direction. Slightly lower e.e. was obtained in the batch reactor. As already known from batch reactor experiments, e.e. decreases with conversion. Conversion is higher in the batch reactor than in the tubular reactor, therefore, lower e.e. is not surprising.
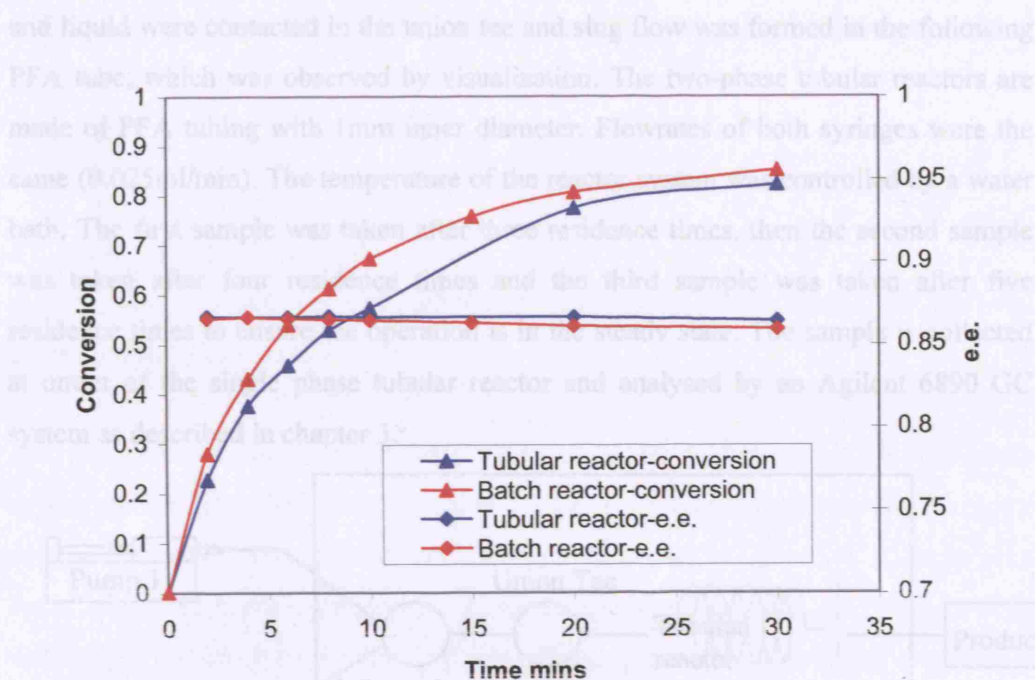
Figure 5-2 Comparison of single phase tubular reactor and batch reactor results
(Temperature= 30°C; [Substrate]=0.144M; [Substrate]/[Catalyst]=1000, [Sodium
Isopropoxide]/[Catalyst]=8; Single phase tubular reactor: ID=1mm; Flowrate =
2×0.025ml/min; Batch Reactor: nitrogen bubbling into liquid phase at flow rate
800ml/min)

5.3 Gas-liquid slug flow reactor

5.3.1 Experimental set-up

A schematic of the two-phase tubular reactor set up is shown in Figure 5-3. Two
single-syringe infusion pumps (RAZEL A-99.FJZ) are used to drive the liquids
through the reactor. 10mL 0.00028M catalyst solution (prepared by 2.24mg rhodium
complex and 1.12mg ligand in 25.6ml isopropanol) which is pumped by syringe pump
1 and substrate solution (containing 0.28M acetophenone and 0.00224M sodium
isopropoxide in isopropanol) which is pumped by syringe pump 2 are premixed in a
micromixer (Standard Slit Interdigital Micro Mixer SSIMM from IMM), see Table 5-
2, sequence 2. Nitrogen gas controlled by a mass flow controller was introduced into
the reactor system by a union tee (1/8" Swagelok). A PFA tube with 1.65mm inner
diameter and 5cm length was used to connect the union tee and the micromixer. Gas

and liquid were contacted in the union tee and slug flow was formed in the following PFA tube, which was observed by visualization. The two-phase tubular reactors are made of PFA tubing with 1mm inner diameter. Flowrates of both syringes were the same (0.025ml/min). The temperature of the reactor system was controlled by a water bath. The first sample was taken after three residence times, then the second sample was taken after four residence times and the third sample was taken after five residence times to ensure the operation is in the steady state. The sample is collected at outlet of the single phase tubular reactor and analysed by an Agilent 6890 GC system as described in chapter 3.
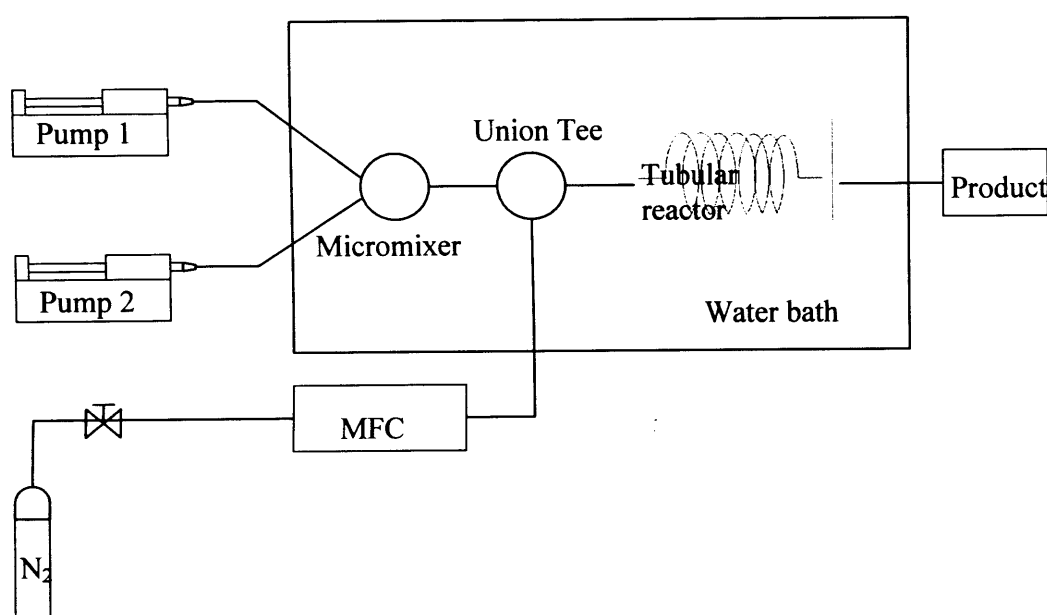
Figure 5-3 Two-phase tubular reactor experimental set-up. (MFC: mass flow controller)

5.3.2 Results and discussion

As discussed earlier, acetone inhibits the reaction. Therefore, acetone removal can shift the reaction equilibrium and possibly improve the enantioselectivity. During slug flow, very good mass transfer between gas and liquid can be achieved. Therefore, it is expected that the two-phase tubular reactor can give better performance for acetone removal. Experiments with different nitrogen flowrate in the range of 0-3ml/min flowrate were studied in tubular reactor with 1mm inner diameter PFA tubing. When nitrogen flowrate is 0, the two-phase tubular reactor becomes the single phase tubular reactor. The total liquid flowrate is 0.05ml/min. The mixing efficiency in the

137

connection tube (ID=1.65mm, Length=5cm) between the micromixer and union tee of the tubular reactor is calculated. The Fourier number is:

$$Fo = \frac{\dfrac{L}{U}}{\dfrac{d^2}{D}} = \frac{\dfrac{0.05m}{1.95 \times 10^{-4} m/s}}{\dfrac{1.65 \times 10^{-3} m^2}{0.81 \times 10^{-9} m^2/s}} = 0.75 \qquad (5\text{-}1)$$

It is between 0.1 and 1 which indicates that complete mixing should be achieved before the slug flow starts.

The experimental results for the asymmetric transfer hydrogenation in two phase tubular reactor are summarized in Table 5-11 and the comparison with batch reactor experiments which were described in Chapter 3 are shown in figure 5-4. It can be seen from Table 5-11 that e.e. decreases with increase of conversion. In the 10m tube with 0.05ml/min liquid flowrate and 3ml/min nitrogen flowrate, conversion could only reach 67.66%. If higher conversion is required, much longer tube has to be used. Another way to achieve higher conversion with less tube length is to reduce the nitrogen flowrate. However, small nitrogen flowrate might affect the acetone stripping efficiency.

Table 5-11 Asymmetric transfer hydrogenation in two-phase tubular reactors

Liquid flowrate ml/min	N_2 flowrate ml/min	Reactor length m	Conversion %	e.e. %
0.05	3	1.95	32.95	85.94
0.05	3	5	62.93	85.19
0.05	3	10	67.66	84.68
0.05	1	5	82.02	82.91

(Temperature 30°C, [Substrate]=0.33M, [Catalyst]/[Substrate]=1:1000.
[Sodium Isopropoxide]/[Catalyst]=8; Single phase tubular reactor: reactor ID=1mm; Liquid flowrate=2×0.025ml/min; Batch Reactor: nitrogen bubbling into liquid phase at flow rate 800ml/min)
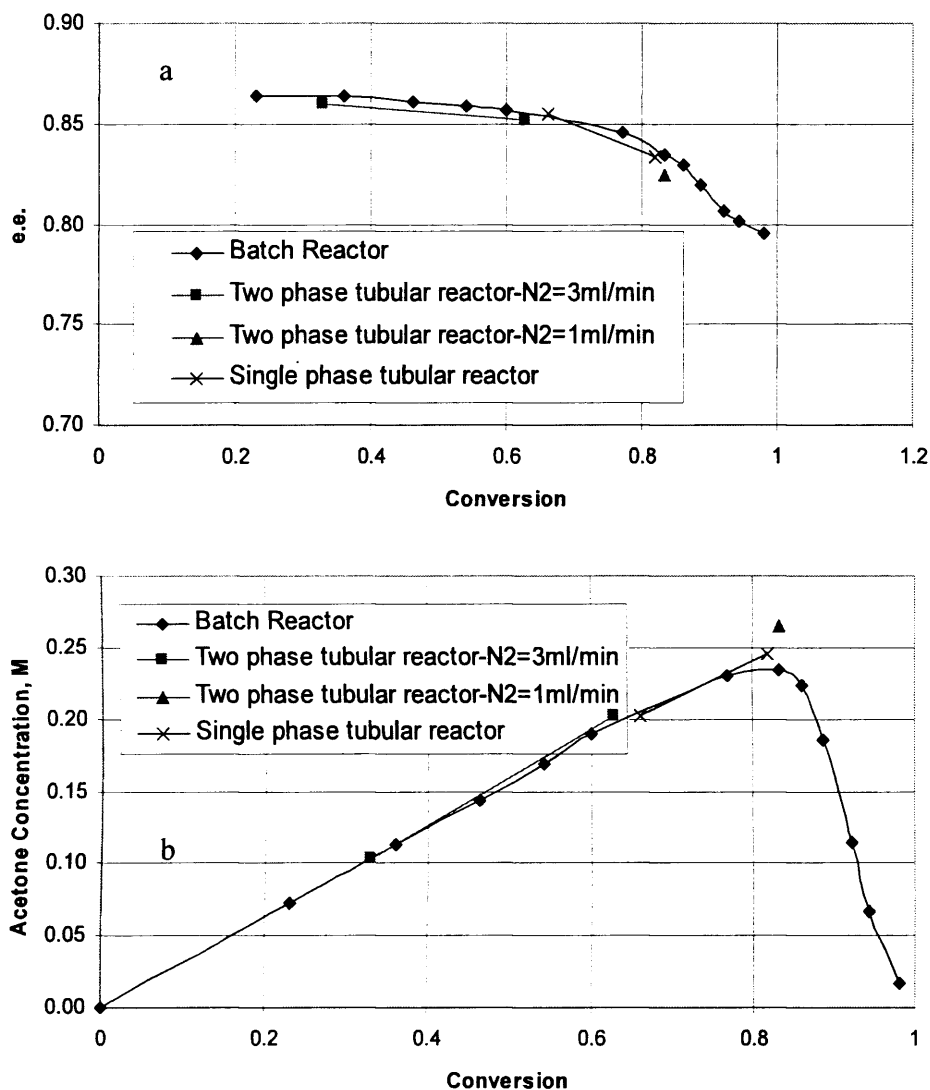
Figure 5-4 Comparison between batch reactor and tubular reactor experimental result
(Temperature=30°C, [Substrate]=0.33M, [Catalyst]/[Substrate]=1:1000.
[Sodium Isopropoxide]/[Catalyst]=8; Single phase tubular reactor: ID=1mm; Liquid
flowrate=2×0.025ml/min; nitrogen flowrate=0-3ml/min)

Figure 5-4a shows e.e. as function of conversion in different reactors. It can be seen
that e.e obtained before 80% conversion in the two-phase tubular reactor with
3ml/min nitrogen flowrate and single phase tubular reactor is similar to the batch
reactor. This is probably due to the fact that before 80% conversion, reaction rate is
much faster than the acetone removal rate. It can also be seen in Figure 5-4b which
shows acetone concentration as function of conversion that acetone concentration is
the same in the tubular reactor with 3ml/min nitrogen flowrate, single phase tubular

reactor and in the batch reactor when the conversion is lower than 80%. However, lower e.e. was obtained in the tubular reactor with 1ml/min nitrogen flowrate at about 80% conversion than in the batch reactor. This is probably due to the fact that higher acetone concentration is obtained in the two phase tubular reactor which can be seen in Figure 5-4b. This result can be explained by the fact that higher gas flowrate per liquid volume was achieved in the batch reactor. Assuming in acetone-isopropanol system without any reaction, initial acetone concentration is C_0. Acetone is removed by gas stripping. The acetone concentration decay in a batch reactor is given by (see Appendix A)

$$\frac{C}{C_0} = exp\left(- \frac{t}{\frac{1}{k_l \cdot a} + \frac{K_{eq}}{k_g \cdot a} + K_{eq} \frac{V_l}{F_{gas}}} \right) \qquad (5\text{-}2)$$

For the batch reactor experiment, the following parameters (Table 5-12) can be used for comparison (see Appendix A for calculations):

Table 5-12 Parameters for the Equation 5-2 in batch reactor

Mass transfer coefficient in the liquid phase	$k_l = 2.38 \times 10^{-4}$ m/s
Mass transfer coefficient in the gas phase	$k_g = 1.19$ mol/(m^2 s)
Equilibrium constant	$K_{eq} = 1.174 \cdot 10^4$ mol/m^3
Interfacial area (500ml flask, 250ml initial volume)	$a = 50.2$m^{-1}
Gas flowrate	$F_{gas} = 800$ml/min
$\dfrac{1}{k_l \alpha}$	83.7 (s)
$\dfrac{K_{eq}}{k_g \cdot \alpha}$	196.5 (s)
$K_{eq} \dfrac{V_l}{F_{gas}}$	5473 (s)

For the parameters in Table 5-12, $\dfrac{1}{k_l \alpha} < \dfrac{K_{eq}}{k_g \cdot \alpha} <<< K_{eq} \dfrac{V_l}{F_{gas}}$ and consequently

$\dfrac{C}{C_0} \rightarrow exp\left(- \dfrac{F_{gas}}{K_{eq} \cdot V_l} t \right)$. Thus the limitation in the batch reactor is not given by the interfacial area or by the mass transfer coefficients. The stripping performance is

determined by the ratio $\dfrac{F_{gas}}{K_{eq} \cdot V_l}$. The higher this ratio the better the acetone removal

becomes. Since the equilibrium constant (solubility) is the same, a comparison between batch reactor and two-phase tubular reactor should be provided in terms of $\dfrac{F_{gas}}{V_l}$. It took 40 mins to reach 80% conversion in the batch reactor. Therefore, for the

batch reactor: $\dfrac{F_{gas} \cdot t}{V_l} = \dfrac{800ml/min \times 40\,min}{250ml} = 128$; for the tubular reactor,

$\dfrac{F_{gas}}{F_{liquid}} = \dfrac{1ml/min}{0.05ml/min} = 20$. Therefore, higher acetone removal rate should be achieved in the batch reactor. This results in lower acetone concentration in the batch reactor than in the two-phase tubular reactor. The acetone removal rate dependence on the gas flowrate per liquid volume will be also demonstrated in the Chapter 6. Therefore, in order to increase the acetone removal efficiency, higher ratio of the gas flowrate to liquid flowrate should be used. However, this will result in much longer tube to achieve enough liquid residence time in the two-phase tubular reactor.

4.4 Conclusions

Asymmetric transfer hydrogenation has been conducted in a single-phase tubular reactor. Different mixing sequences of reactant, catalyst and sodium isopropoxide have significant effect on the reaction conversion. Catalyst deactivation took place when the substrate and catalyst were premixed before mixing with sodium isopropoxide. The mixing sequence 2 in which substrate and sodium isopropoxide were premixed before mixing with catalyst gave the best conversion and thus was applied in the experiments in the tubular reactor.

Experiments where mixing was achieved by a SSIMM micromixer showed higher conversion than using a union tee (1/8" Swagelok) especially at low residence time, where mixing was not completed for the latter. Tube size did not have any effect on conversion and enantioselectivity in the inner diameter range 1-1.65mm because in this range the tubular reactor behaves like a PFR. A large excess of sodium isopropoxide was used in the reaction to eliminate any effect of a minor amount of water in isopropanol. When the sodium isopropoxide to catalyst ratio was in the range 4-24, there was no effect on the reaction conversion and e.e.. The catalyst age affected

conversion which might be due to catalyst deactivation taking place with time. Fresh catalyst should be prepared in experiments conducted in different days.

The two-phase tubular reactor showed similar performance on the asymmetric transfer hydrogenation as the batch reactor. No advantage in acetone removal was observed. Furthermore, much longer tubes have to be used to achieve high conversion. Overall, the tubular reactor is not a promising reactor for the asymmetric transfer hydrogenation and for this reason it was not investigated further.

Chapter 6

Rotating Disc Reactor for Acetone Stripping and Catalytic Asymmetric Transfer Hydrogenation

6.1 Introduction

In asymmetric transfer hydrogenation acetone removal is beneficial for the reaction. The rate of acetone removal in a batch reactor is related to acetone solubility, ratio of gas flowrate/liquid volume and gas-liquid interfacial area, which will be discussed in this chapter. When the process is scaled up or the height of the liquid increases in the batch reactor, the ratio of surface area to volume decreases. Therefore, a batch reactor may not be the best means for the asymmetric transfer hydrogenation. A contactor that provides much larger surface area, such as a thin film contactor, is better suited. The aim of thin film contactors is to generate thin films of liquid that can be brought in contact with the gas phase, thus minimising the mass transfer resistances either for transferring a component from the gas phase to the liquid phase or to remove a component from the liquid phase. Generation of thin liquid films can be obtained in falling films (Tales-Alesson 1999, Dabir et al. 1996, Davis et al. 1979) and rotating/spinning discs. The latter uses one or more rotating discs to generate the thin liquid film, with a significant contribution of the centrifugal and viscous forces. A spinning disc consists of a disc mounted on a vertical shaft (Novakovic 2004, Aparício et al. 2002, Wang et al. 2002, Brechtelsbauer et al. 2001, Boodhoo and Jachuck 2000, Fei et al. 2000) while a rotating disc contactor consists of a disc mounted on a horizontal shaft (Woo et al. 2001, Zeevalink et al. 1979, Bintanja et al.1975). A wide range of the ratio of the gas flowrate/liquid volume can be applied to the rotating disc contactor. In this work, a rotating disc contactor/reactor is designed and used to remove acetone due to the following advantages: i) It is easy to operate in both batch and continuous mode, ii) The reproducibility is high, iii) The energy requirement is low; iv) The gas-liquid interfacial area is constant and known.

6.2 Acetone stripping in rotating disc contactor

6.2.1 Reactor description and experimental set-up

The rotating disc contactor consists of a single stainless steel disc with a radius of 70 mm, mounted on a stainless steel horizontal shaft with 10mm diameter. A stainless steel ring spacer, with radius of 75 mm and thickness of 10 mm is flanged between two glass lids, shaping a thin cylindrical chamber that contains the disc. The sealing between shaft and glass lids is achieved by two mechanical seals on each side of lids. The sealing between glass lids and the stainless steel spacer ring is achieved by two PTFE gaskets with thickness 1mm. There are four ports on each lid located at 90 °

144

between them so that their location is symmetrical related to the liquid level. The lower part of the chamber can be easily filled with liquid, while the gas flow can be directed through the upper part of the chamber which functions as gas-shell. The ports are used for feeding the gas or liquid phase in the reactor, connecting to the vacuum, and for sampling of the liquid phase. The schematic of the rotating disc reactor and reactor specifications are shown in Figure 6-1.

Component	Value (mm)
Disc radius	70
Disc thickness	2
Spacer ring radius	75
Spacer ring thickness	10
Shaft diameter	10
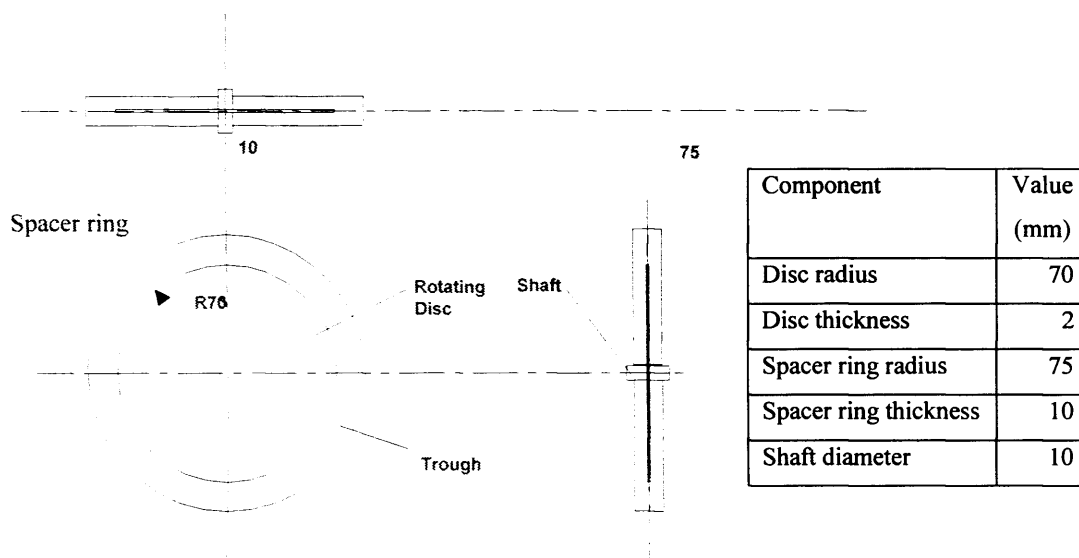
Figure 6-1 Schematic and reactor specifications of the rotating disc contactor

A picture and a schematic diagram of the bench scale rotating disc contactor experimental set up are shown in Figure 6-2a and b respectively. The reactor was operated in batch mode related to the liquid phase, while nitrogen was flown continuously. The liquid was charged to the reactor with volume 30-70ml using a Peristaltic pump (Gilson, Model: miniplus 3, France). Disc submergence in the liquid bulk was 17%~40%. The lower part of the reactor was placed in a water bath in order to maintain the temperature constant. The nitrogen flowrate was controlled between 200-800 ml/min by a mass flow controller (MFC Model: Brooks 5850; flowrate range: 0-1000ml/min; Readout Model: Brooks 0154/BC1A1). The disc was rotated with a variable speed from 0-100 rpm by a 180 W electric motor. A coupling was used to connect the shaft and motor to allow flexibility for the alignment between the shaft and motor. The rotation speed was measured by a digital tachometer (Lutron DT-2236). A syringe connected to 1/16" PTFE tube which was immersed in the bulk

145

liquid was used to withdraw samples from the liquid trough. The sample was put into sampling vial where acetic acid was used to quench the reaction. It was analysed by an Agilent 6890 GC system as described in Chapter 3.

(a)

(b)
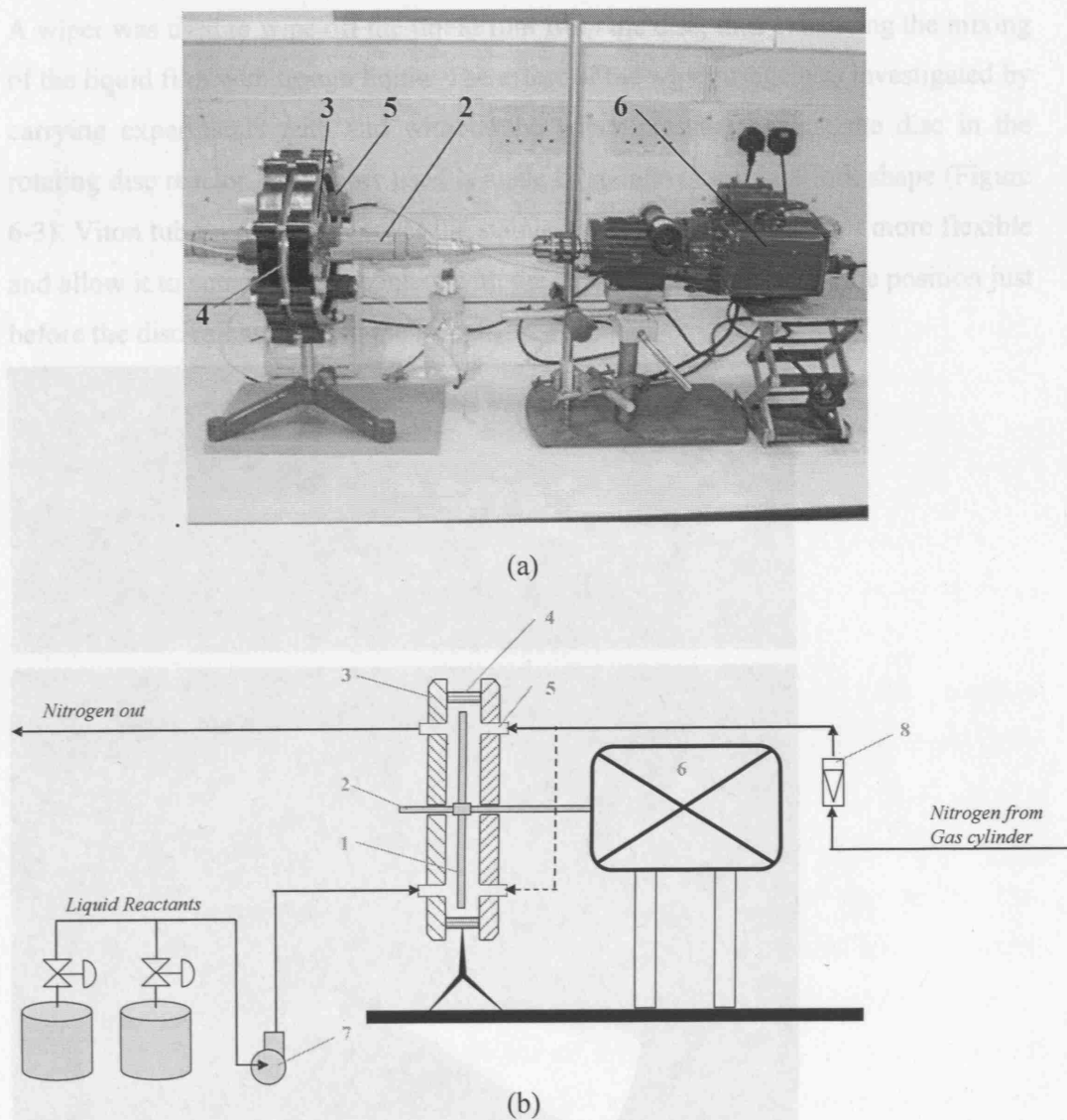
Figure 6-2 Rotating disc contactor (a) and set-up (b).

1. Disc; 2. Shaft; 3. Lid; 4. Ring spacer; 5 Ports for feed and sampling; 6. Motor; 7. Liquid pump; 8. Mass flow controller.

The effect of wiper, gas flowrate, initial liquid load in the reactor, speed of rotation, as well as the method for introducing the gas phase (either above the liquid or bubbled through the liquid phase) were investigated. In all experiments an initial concentration of acetone of 0.1M was utilised.

6.2.2 Results and Discussion

6.2.2.1 Effect of wiper and experimental reproducibility

A wiper was used to wipe off the liquid film from the disc, thus enhancing the mixing of the liquid film with trough liquid. The effect of the wiper usage was investigated by carrying experiments with and without the wiper pressing against the disc in the rotating disc reactor. The wiper used is made of stainless steel in a fork shape (Figure 6-3). Viton tubes are used to cover the stainless steel to make the wiper more flexible and allow it to come in close contact with the disc. The wiper is set at the position just before the disc re-entered into the trough.
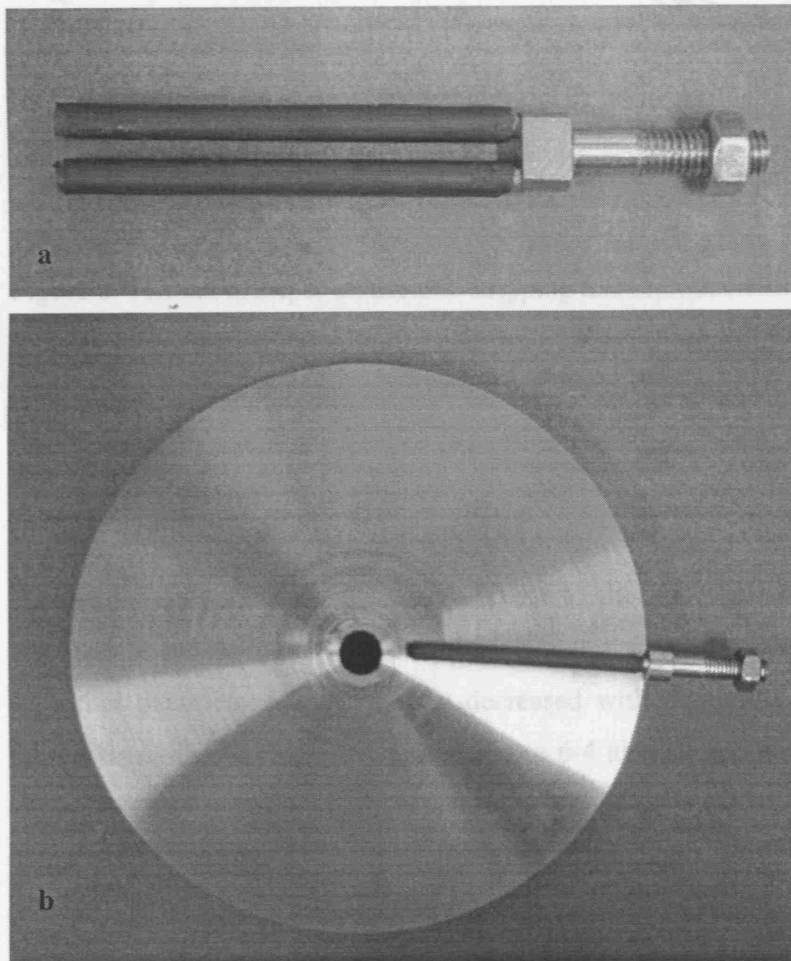
Figure 6-3 Picture of (a) the wiper and (b) the disc showing also the wiper location
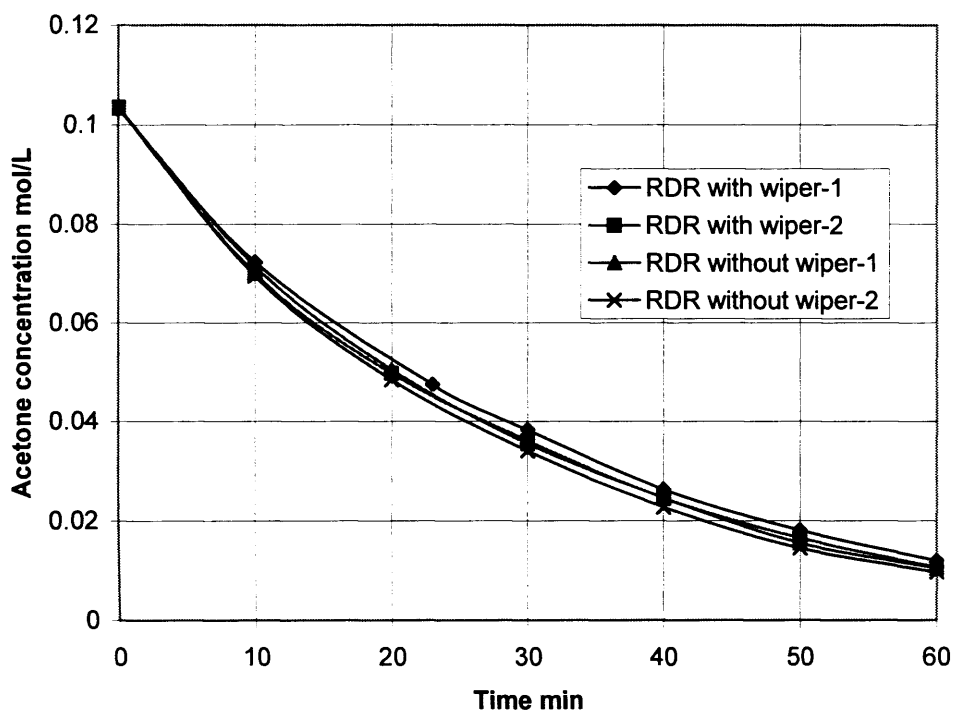
Figure 6-4 Effect of wiper on acetone stripping and reproducibility

(Nitrogen flowrate=800ml/min, liquid initial volume=50ml; disc rotation speed=50rpm; Temperature=30°; Initial acetone concentration=0.1M; Nitrogen flow above the liquid surface)

The experiments with wiper and without wiper were carried out in the rotating disc contactor and each experiment was run twice to check the reproducibility. The results are summarised in Figure 6-4. The experimental reproducibility is with ±1%. It can be seen that the acetone concentration decreased with time. About 90% acetone was removed in 60 minutes for all cases. Figure 6-4 also shows that the results obtained with wiper and without wiper are the same within experimental error. The following explanations maybe offered for the observed behaviour.

First, the objective of the wiper is to wipe off the liquid film on the disc and mix it with liquid in the trough. The same results obtained in both cases (with wiper and without wiper) suggest that the liquid film on the disc might mix up with liquid in the trough even without wiper. However, this is unlikely, since both Suga and

148

Boongorsrang (1984) and Zeevalkink et al (1979), demonstrated experimentally that only part of the liquid film on the disc is mixed with liquid in the trough.

Second, is it possible that the rate limiting step is the mass transfer of acetone from the film on the disc exposed to the gas rather than from the submerged boundary-layer? If this is true, then there should be no difference on the acetone stripping with or without wiper. In order to answer this question, the film thickness and mass transfer coefficient are calculated in the liquid film exposed to the gas and submerged boundary-layer. The average film thickness exposed to the gas and boundary-layer submerged are calculated based on equation (2-5) and (2-4). The average mass transfer coefficient in the film exposed to the gas is calculated using equation (2-10)

since $\dfrac{\delta_g}{\sqrt{D \cdot t_r}}$ =10 for the condition used which is larger than 1.7. The average mass

transfer coefficient in the submerged boundary-layer is calculated using equation (2-16). The calculated film thickness and mass transfer coefficient are summarised in Table 6-1. It can be seen that the film thickness exposed to gas is smaller than the submerged boundary-layer thickness. The mass transfer resistance in the gas can be ignored due to the large mass transfer coefficient. The average mass transfer coefficient in the film exposed to gas is larger than the submerged boundary-layer. These results indicate that the mass transfer limitation is located in the submerged boundary-layer and complete mixing of the liquid film with trough liquid should increase the acetone stripping performance.

Table 6-1 Film thickness and mass transfer coefficient in the film exposed to the gas, in the film submerged in the liquid phase and in the gas phase

	Film thickness (μm)	Mass transfer coefficient $\times 10^{-6}$(m/s)
Liquid film exposed to the gas	δ_g=108	K_L^{Film} =8.68
Submerged boundary-layer (Equation 2-16)	δ_L=275	K_L^{Bulk} =0.29
Gas phase	--	2130

(Mass transfer coefficient in the gas phase is calculated based on the equation: $Sh = 0.66 \cdot Re^{1/2} \cdot Sc^{1/3}$, disc rotating speed is 50rpm)

The third reason might be that the wiper only wiped off part of the liquid film on the disc exposed to the gas. The amount of the liquid wiped off from the film by the wiper may be close to the amount of the liquid stripped off by the rotation of the disc without wiper. If this is true, there should not be any difference for the acetone stripping with or without usage of the wiper. This might be possible because the wiper is made of stainless steel. Although it is covered with Viton tube to make the surface of the wiper more flexible and achieve better contact with disc, it is still not possible to wipe off all the liquid on the disc due to the roughness of the disc and very thin liquid film (about 108 μm).

In order to investigate if the film forms on the disc and if the wiper wipes off the liquid film completely, experiments were carried out with isopropanol dyed with blue ink. Liquid volume was 50ml and rotation speed was 50rpm. The photographs shown in Figure 6-5 were taken at different disc locations by a Fuji Finepix 6800 digital camera. It can be seen from Figure 6-5b that the liquid does form a film on the disc. The colour becomes deeper at the position closer to the edge of the disc. These results indicate that the film on the disc is not uniform. The film thickness increases with increase of the radial position. Figure 6-5a shows a photograph taken at the location where the wiper sits. It shows that the liquid film is wiped off from the disc and flows along the spacer ring wall to the trough. Most liquid was wiped off from the position near the disc edge due to large thickness at that part of the disc. Figure 6-5c shows a photograph taken at the location between the wiper and trough liquid surface. It can be seen that there is still some blue film attached on the disc which indicates that only part of the liquid film was wiped off by the wiper. These experiments provide evidence for the third assumption made above that only part of the film on the disc has been wiped off by the wiper.
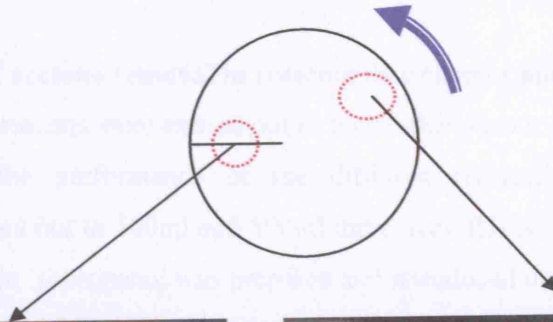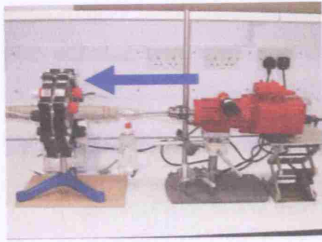
(a)
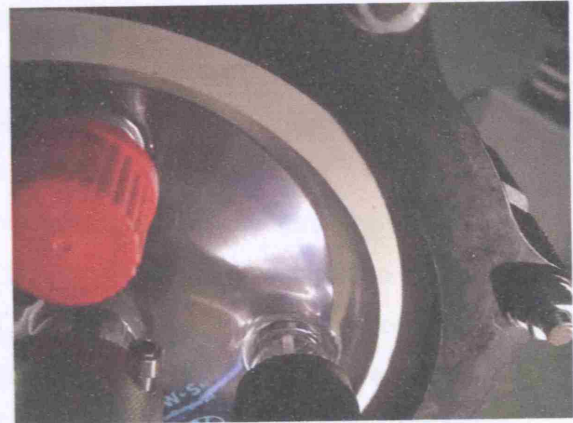
(b)
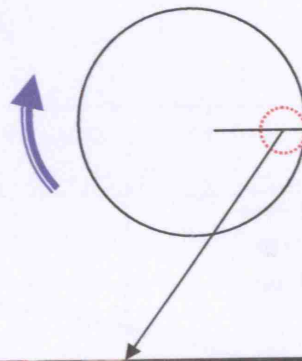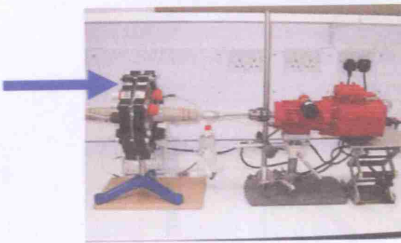
(c)

Figure 6-5 Photographs of different disc locations in the experiments with dyed isopropanol: a) Position where the wiper is located; b) position where the disc just emerges from the trough; c) position same as (a) but in opposite side.

6.2.2.2 Comparison of acetone removal in rotating disc reactor and batch reactor

Acetone stripping experiments were carried out in both batch reactor and rotating disc reactor to compare the performance of the different reactors. Batch reactor experiments were carried out in 500ml and 100ml three neck flasks. 250ml and 50ml 0.1M acetone solution in isopropanol was prepared and introduced into the 500ml and 100ml batch reactor respectively. The overhead stirrer was used to control the stirrer speed at 360rpm. Nitrogen flow at 800ml/min bubbled through the liquid phase through a glass frit. The temperature of the batch reactor was controlled by a water bath at 30°C. Samples were taken every 10 minutes and analysed by the GC. In the RDR experiments, 50ml 0.1M acetone solution in isopropanol was introduced in the RDR by a peristaltic pump. Rotation speed of the disc was controlled at 50rpm by the motor. The temperature was controlled at 30°C by the water bath. Nitrogen flowed at 800ml/min above the liquid surface. Sample was taken every 10 minutes and analysed by the GC. The results of acetone concentration as function of the time in different reactors are summarised in Figure 6-6.
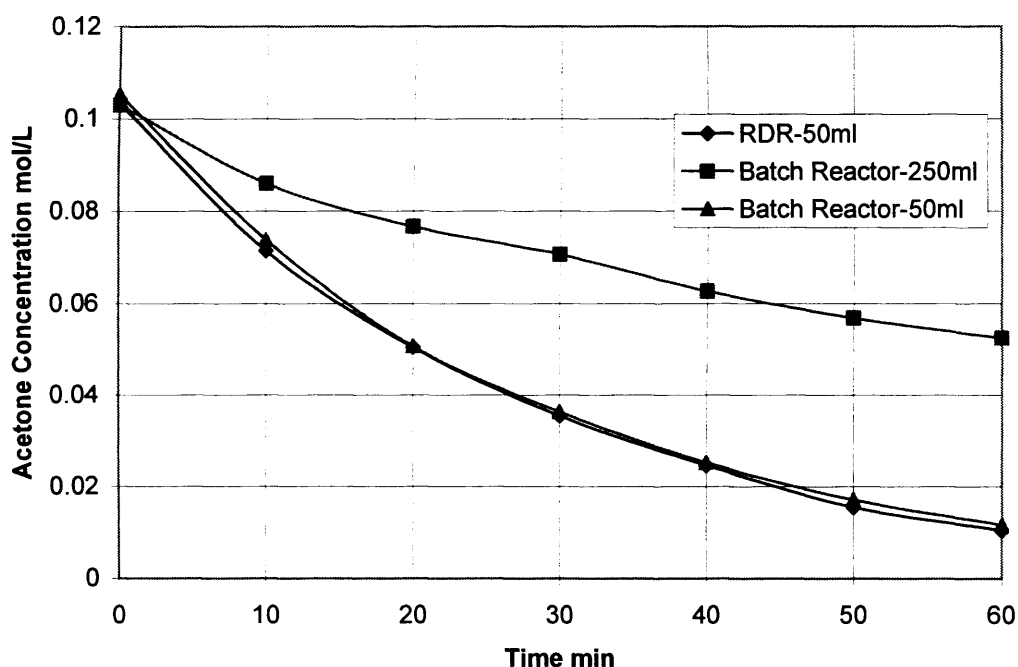
Figure 6-6 Comparison of acetone stripping in batch reactor and rotating disc reactor (Temperature=30°; Initial acetone concentration=0.1M. Batch reactor: Nitrogen flowrate=800ml/min; Liquid initial volume =50ml and 250ml; Stirrer rotation speed= 360rpm; RDR: Nitrogen flowrate=800ml/min; liquid initial volume=50ml; disc rotation speed=50rpm; Nitrogen flowed above the liquid surface)

It can be seen that about 90% of acetone is removed with 50ml initial liquid volume and about only 40% acetone is removed with 250ml initial liquid volume in the batch reactor. This result can be explained by the fact that higher gas flowrate per liquid volume was achieved with 50ml initial liquid volume. As discussed in Chapter 5 that acetone stripping rate depends on $\dfrac{F_{gas}}{V_l}$. Therefore, for the batch reactor volume:

50ml
$$\frac{F_g}{V_l} = \frac{800ml/\min}{50ml} = 16\min^{-1}$$

250ml
$$\frac{F_g}{V_l} = \frac{800ml/\min}{250ml} = 3.2\min^{-1}$$

The much higher ratio of gas flowrate/ liquid amount is provided with less initial liquid amount which results in better acetone removal.

Based on above analysis, it is not surprising that the same performance was obtained in both batch reactor with 50ml liquid volume and rotating disc reactor, which is due to the fact that the same ratio of gas flowrate/liquid volume was used in both cases. The highest gas flowrate that can be achieved in the batch reactor is limited by impeller flooding, while there is no limitation for the gas flowrate in the rotating disc reactor. Therefore, the rotating disc reactor is still a promising gas liquid contactor and worthy to be further investigated.

As shown earlier, acetone stripping performance depends on the gas flowrate/ liquid volume ratio. Therefore, the performance of the rotating disc reactor on the acetone stripping is further investigated by changing this ratio by two different means: i) varying the gas flowrate and keeping the liquid volume constant; ii) varying the liquid volume and keeping gas flowrate constant.

6.2.2.3 Effect of nitrogen flow rate at constant liquid initial volume

The effect of the nitrogen flowrate was studied by keeping constant the initial liquid volume at 50 ml and varying the nitrogen flowrate between 200-800 ml/min. The model simulation results based on Equation 5-2 and experimental results are summarised in Figure 6-7.
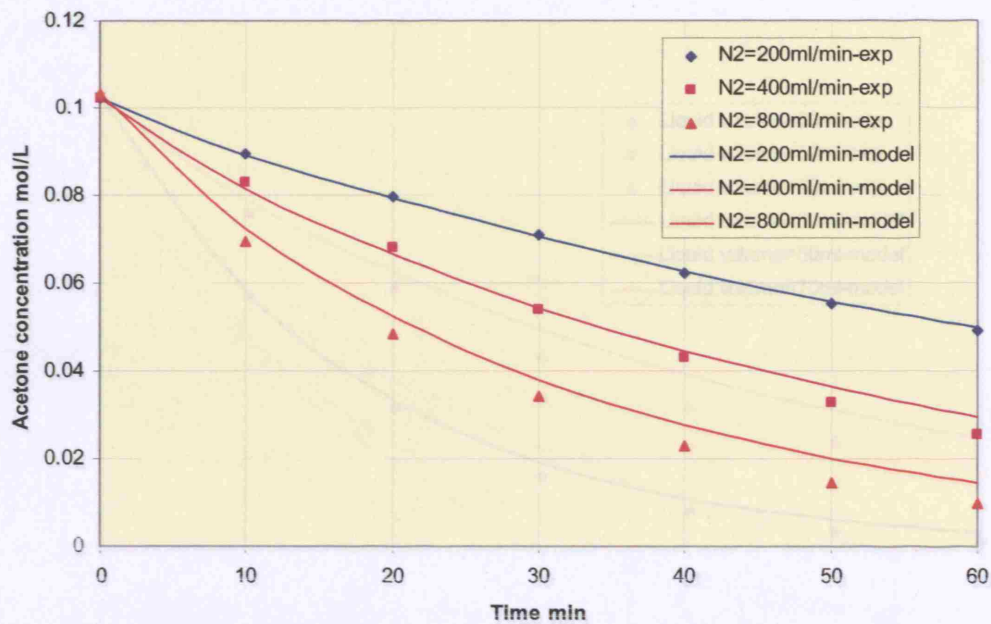
Figure 6-7 Effect of nitrogen flowrate on acetone removal in the rotating disc reactor (Liquid initial volume=50ml; disc rotation speed=50rpm; Temperature=30°; Initial acetone concentration=0.1M; Nitrogen flowed above the liquid surface)

It can be seen that acetone removal rate increased with increase of nitrogen flowrate. When the gas flowrate/liquid volume ratio increased from 4, 8 to 16 min^{-1} by changing gas flowrate from 200, 400, 800ml/min, the percent of the acetone removed in 60 minutes increased from 50%, 70% to 90%. It can also be seen that the model simulation results agree well with experimental results.

6.2.2.4 Effect of liquid amount at constant gas flow rate

The effect of different initial liquid volume was studied by keeping constant the nitrogen flowrate at 800 ml/min and varying the initial liquid volume between 30–70ml using in the rotating disc reactor. The results are summarised in Figure 6-8.

Figure 6-8 Effect of the liquid initial volume on acetone removal in the rotating disc reactor (Nitrogen flowrate=800ml/min; disc rotation speed=50rpm; Temperature=30°; Initial acetone concentration=0.1M; Nitrogen flowed above the liquid surface)

It can be seen that the lower acetone concentration was obtained with less liquid volume. When the gas flowrate/liquid volume ratio increased from 11.4, 16.0 to 26.7 min^{-1} by changing liquid initial volume from 70, 50, 30ml, the percent of the acetone removed in 60 minutes increased from 82%, 90% to 98%. It can also be seen that the model simulation results agree well with experimental results. Another effect of the liquid initial volume is that the disc submergence decreases with decrease of the liquid initial volume. The disc area exposed to the gas increases with decrease of the submergence. Therefore, gas-liquid interfacial area, which is the film area on the disc exposed to the gas, per liquid volume increased.

6.2.2.5 Effect of rotating speed

The rotation speed of the disc is one of the most important factors for the rotating disc reactor because it can affect the film thickness, contact time, mass transfer and mixing. The effect of rotation speed on the acetone removal is investigated by varying the rotation speed between 10-100rpm and keeping other conditions the same. The results are summarised in Figure 6-9.

155
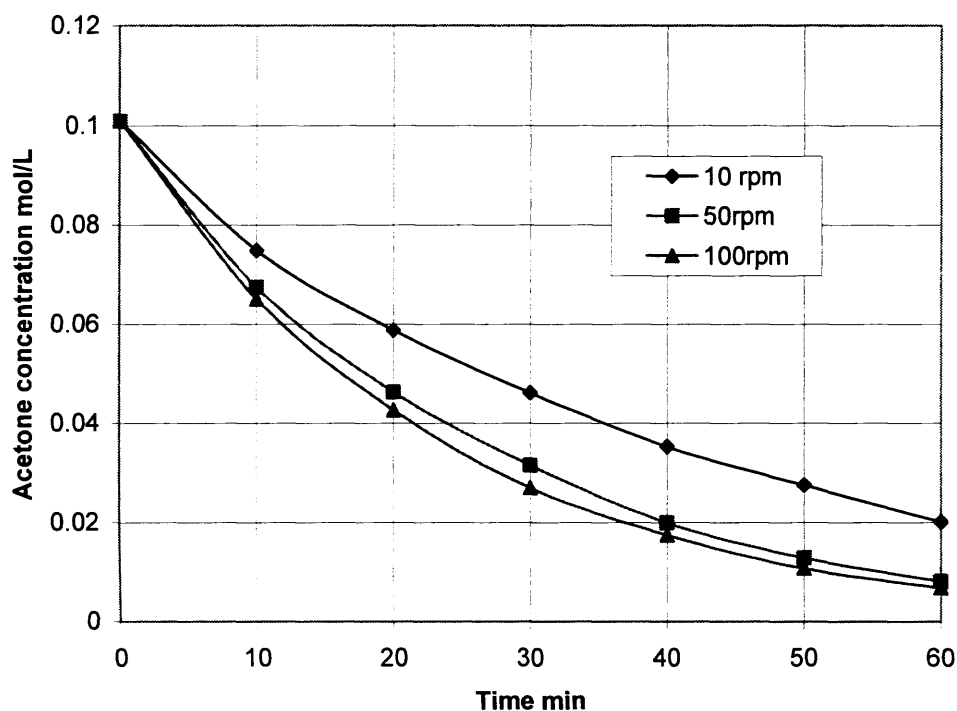
Figure 6-9 Effect of the rotation speed on acetone removal in the rotating disc reactor (Nitrogen flowrate=800ml/min; liquid initial volume=50ml; Temperature=30°; Initial acetone concentration=0.1M; Nitrogen flowed above the liquid surface)

It can be seen that acetone removal rate increases with increase of the rotation speed. The film thickness and mass transfer coefficients are calculated (Table 6-2) for the liquid film exposed and submerged boundary-layer to explain these results. It can be seen that film thickness exposed to the gas increased with increase of the rotation speed. This improved the rate of the liquid up-taking from the trough. The mass transfer coefficient in the film exposed to the gas increased with increase of the rotation speed due to the fact that the contact time (the time liquid on the disc is in contact with gas, Equation 2-12) decreased with increase of the rotation speed. The mass transfer coefficient in the boundary-layer submerged increased with increase of the rotation speed due to the boundary-layer thickness decrease with increase of the rotation speed. The increase of the mass transfer coefficients in both films thus improved the acetone stripping performance.

Table 6-2 Liquid film thicknesses, mass transfer coefficients and contact times for different rotation speed

Rotation speed (rpm)	δ_g, μm (Equation 2-5)	δ_l, μm (Equation 2-4)	K_L^{Film} $\times 10^{-6}$m/s (Equation2-10)	K_L^{Bulk} $\times 10^{-6}$m/s (Equation 2-16)	Contact time,s (Equation 2-12)
10	48	608	3.93	0.133	0.668
50	108	275	8.68	0.294	0.137
100	153	194	12.31	0.417	0.068

6.2.2.6 Effect of disc rotation and nitrogen flow configuration

In the rotating disc reactor, the disc provides the gas-liquid interfacial area by the film formed on it. In order to assess the disc function, the following experiments were conducted in the rotating disc reactor. The first experiment (50rpm-above) was conducted by flowing nitrogen gas only above the liquid trough while disc rotated with speed of 50rpm. The second experiment (0rpm-bubbling) was conducted by bubbling nitrogen in the trough liquid through a 1.65mm PTFE tube inserted into the bottom port while the disc was kept stationary (rotation speed 0 rpm). The third experiment (50rpm-bubbling) was conducted by bubbling nitrogen gas in the trough liquid while the disc was rotated with speed of 50rpm. The results are summarised in Figure 6-10.

It can be seen that acetone stripping with nitrogen bubbling in the trough liquid is more efficient than the gas flow above the liquid surface. This is because the mass transfer limitation exists in the boundary-layer in the trough when nitrogen flows above the liquid surface (see Table 6-1). The nitrogen bubbling through the trough liquid improved the mixing in the liquid trough (see Figure 6-11), thus enhancing the mass transfer.
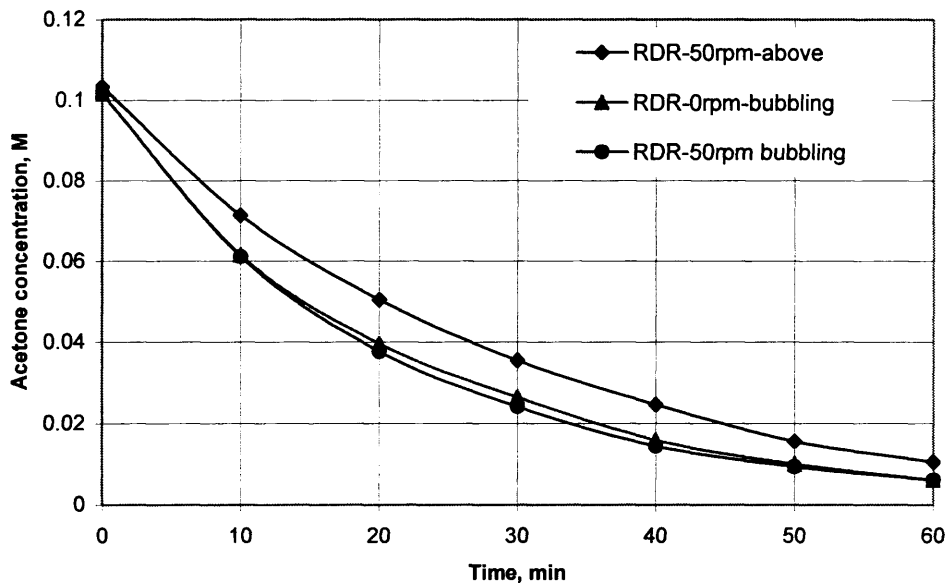
Figure 6-10 Effect of the disc rotation speed in conjunction with nitrogen flow configuration on acetone removal (Nitrogen flowrate=800ml/min, liquid initial volume=50ml; Temperature=30°; Initial acetone concentration=0.1M; Above means flowing nitrogen gas only above the liquid trough; bubbling means bubbling nitrogen in the trough liquid)

Figure 6-11 shows a photograph of the rotating disc reactor when nitrogen is bubbling into dyed IPA. It can be seen that nitrogen creates turbulence in the trough liquid which enhances mixing. The results for the "0rpm-bubbling" and "50rpm-bubbling" are similar which indicates that acetone removal mainly took place by the gas bubbles in the liquid trough rather than the liquid film formed on the disc. Acetone removed from the liquid film on the disc reaches its thermodynamic limit since the gas phase is already enriched in the volatile components when it leaves the liquid bulk. This result agrees with the assumptions of Woo and Choi (2001) who studied phenol removal by nitrogen sweeping in a rotating disc reactor. They assumed that phenol is mostly removed by the gas bubbles and that the amount of phenol removed from the polymer layers at the surface of the rotating disc is negligibly small. The model derived based on this assumption agreed well with their experimental findings.
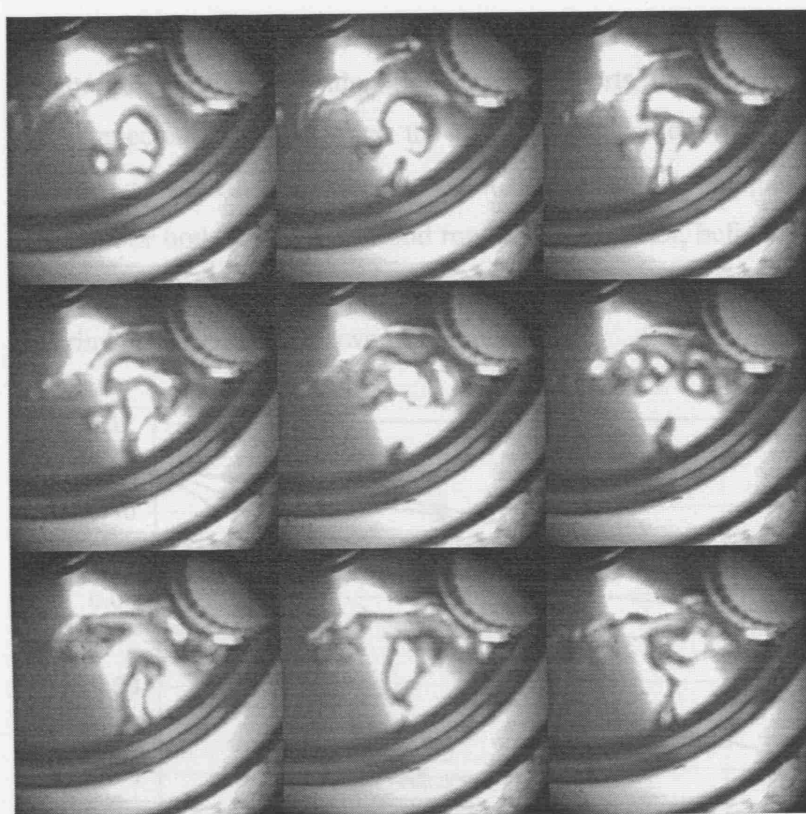
Figure 6-11 Mixing patterns in the trough when nitrogen was bubbled into trough liquid

6.2.2.7 Acetone stripping using vacuum

Vacuum distillation is often used for distillation of heat sensitive compounds. The catalyst utilised in the asymmetric transfer hydrogenation is sensitive to high temperature and it deactivates over 40°C. Therefore, vacuum stripping was attempted to remove acetone at low temperature for both RDR and batch reactor. The comparison for the acetone removal with vacuum and nitrogen stripping in the RDR and batch reactor are summarised in Figure 6-12. The experimental procedure for the acetone removal with nitrogen stripping is discussed earlier. For the acetone stripping with vacuum, the experimental procedure in the batch reactor is as follows. 250ml 0.1M acetone-IPA solution was introduced in the 500ml three-neck flask. A mechanical stirrer was put into the reactor through the middle neck. A rubber septum was put on one of the side neck where the sample was taken from by syringe. Another side neck was connected to the vacuum line. Vacuum was generated by a water vacuum pump. The experimental procedure in the RDR with vacuum stripping is as

159

follows. 50ml acetone-IPA solution was introduced in the RDR, followed by sealing the six ports on the glass lids. For the two left ports, the one above the liquid surface was connected to vacuum and the one whose position was lower than the liquid surface was sealed with rubber septum through which samples were taken with a syringe. For both batch reactor and rotating disc reactor, before sampling the vacuum was broken and the reactor was filled with air to atmospheric pressure. The experimental results are shown in Figure 6-12.
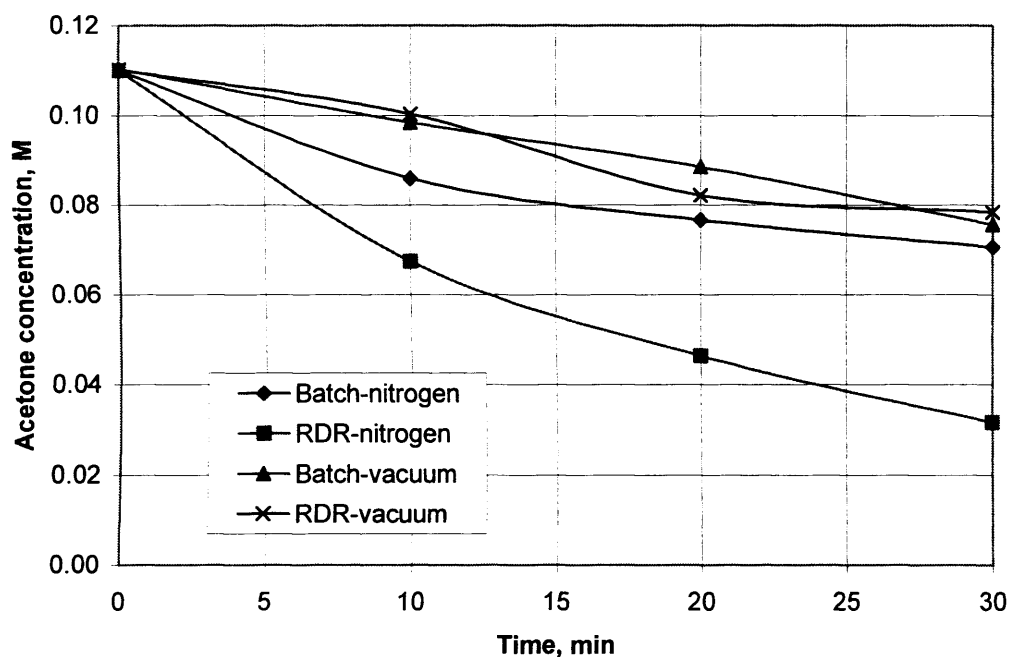
Figure 6-12 Comparison of the acetone removal with vacuum and nitrogen gas stripping in batch reactor and rotating disc reactor (Nitrogen flowed above the liquid surface in RDR. Nitrogen was introduced in the batch reactor through a glass frit. Nitrogen flowrate was 800ml/min in both reactors)

It can be seen that acetone removal is worse with vacuum than with nitrogen stripping in both RDR and batch reactor. The possible reason is that the vacuum is not very high which is only 26 inch Hg and the vacuum capacity is limited by the water flowrate which produced the vacuum. Moreover, leaking of the reactor due to poor sealing may result to low vacuum as well.

6.3 Catalytic asymmetric transfer hydrogenation in rotating disc reactor

6.3.1 Experimental procedure

A schematic and picture of the experimental set-up is shown earlier in Figure 6-2. A base case experimental procedure is described as following: 25ml 0.00028M catalyst solution (prepared by 11.2mg rhodium complex and 5.6mg ligand in 125ml isopropanol) is introduced into the rotating disc reactor by a peristaltic pump (Gilson, Model: mimiplus 3, France). 25ml 0.28M substrate solution is introduced in immediately after by the same pump. Then the motor is started to drive the disc at 100rpm to allow the catalyst and substrate solution to mix for 10 minutes. 0.6ml sodium isopropoxide solution was injected into the reactor by a syringe to start the reaction and nitrogen flow is initiated. Nitrogen gas controlled by a mass flow controller at 800ml/min is bubbled into the liquid trough. The rotation speed of the disc is adjusted to 50rpm after 1 minute. Temperature is controlled by means of water bath at 30°C. Sample is taken by a syringe from the liquid trough every 10 minutes and analysed by an Agilent 6890 GC system (see Chapter 3).

6.3.2 Results and discussion

6.3.2.1 Comparison of the batch reactor and rotating disc reactor

In this section, the experimental results of asymmetric transfer hydrogenation in batch reactor and rotating disc reactor are compared with regards to conversion, enantioselectivity, acetone concentration etc. The reaction solution volume is 250ml in the batch reactor and 50ml in the rotating disc reactor. The experimental procedure for the rotating disc reactor is described above while the experimental procedure for the batch reactor is described in Chapter 3 (section 3.2). Base case experiments were conducted in both batch reactor and rotating disc reactor. Since in chapter 3 it was shown that enantioselectivity decreased faster with conversion at higher substrate initial concentration, it seems preferable to perform asymmetric transfer hydrogenation in dilute solutions. However, from an economic point of view, it is better to run the reaction at high substrate concentration. Efficient acetone removal achieved in the rotating disc reactor might be able to prevent the backwards reaction, thus preventing enantioselectivity decrease. Thus, experiments with high initial substrate concentration at constant substrate/catalyst concentration ratio have been conducted in both reactors. The catalyst used for the asymmetric transfer hydrogenation is rather expensive. It will be more economical if one could utilise the

same amount of organometallic catalyst to catalyze the asymmetric transfer hydrogenation reaction with higher substrate concentrations. Therefore, experiments with substrate concentrations 0.28M were conducted while the ratio of the substrate concentration/catalyst concentration was increased to 2000. The reaction conditions for those experiments are summarised Table 6-4:

Table 6-3 Comparison of the reaction conditions in rotating disc reactor and batch reactor

	[Substrate] (M)	[Substrate]/ [Catalyst] (M)	Reaction mixture volume (ml)	
			Batch reactor	Rotating disc reactor
Experiment 1	0.14	1000	250	50
Experiment 2	0.33	1000	250	50
Experiment 3	0.28	2000	250	50

([Sodium isopropoxide]/ [Catalyst])=8; Temperature=30°; Nitrogen bubbled into the liquid phase in both batch reactor and rotating disc reactors. Nitrogen flowrate=800ml/min)

The results obtained for different reaction conditions in terms of conversion, acetone concentration and e.e. are given in Figure 6-13.
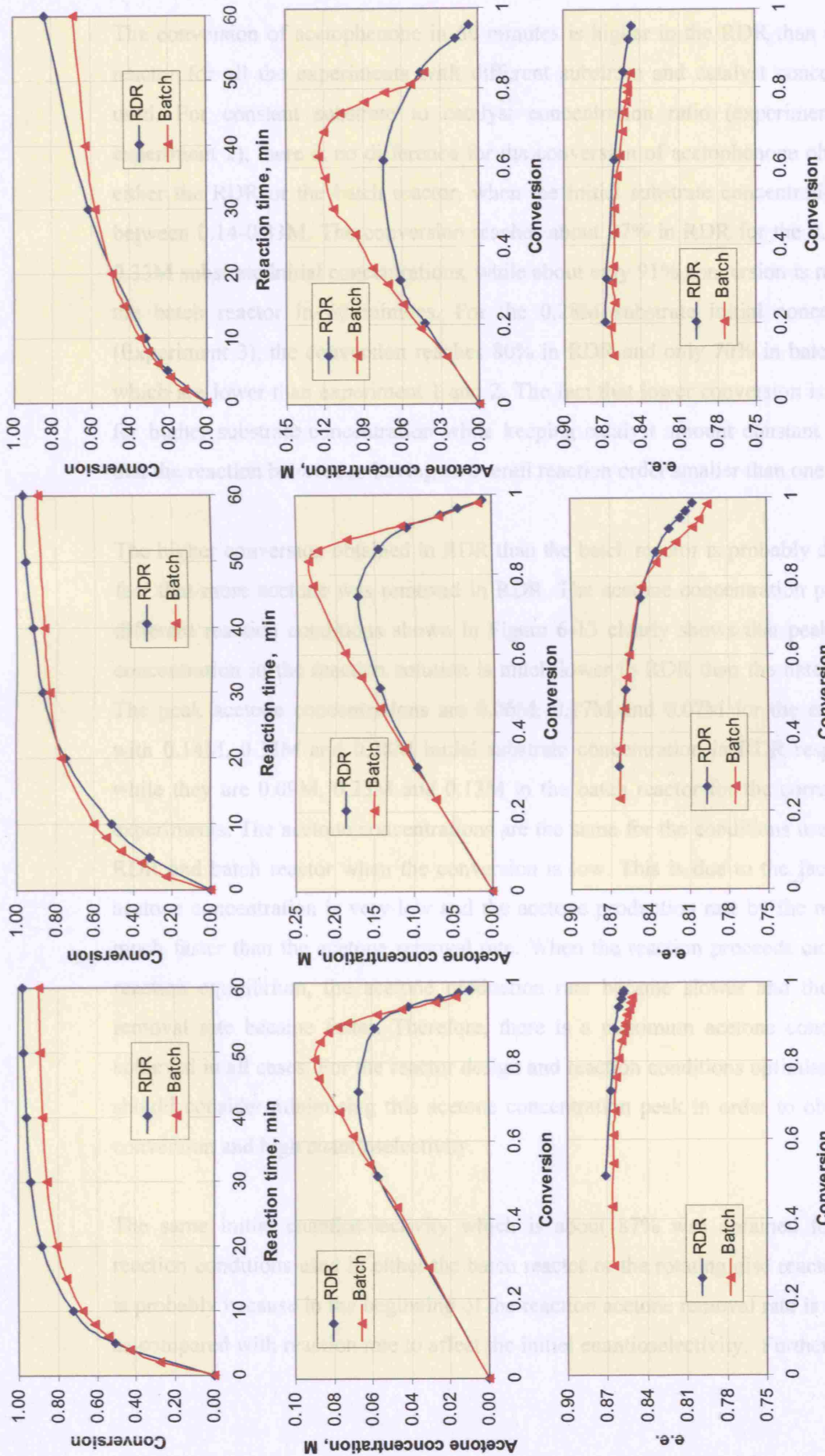
＊

Figure 6-13 Comparison of the rotating disc reactor and batch reactor at different reaction conditions (see Table 6-3)

The conversion of acetophenone in 60 minutes is higher in the RDR than the batch reactor for all the experiments with different substrate and catalyst concentrations used. For constant substrate to catalyst concentration ratio (experiment 1 and experiment 2), there is no difference for the conversion of acetophenone obtained in either the RDR or the batch reactor, when the initial substrate concentration varies between 0.14-0.33M. The conversion reaches about 97% in RDR for the 0.14M and 0.33M substrate initial concentrations, while about only 91% conversion is reached in the batch reactor in 60 minutes. For the 0.28M substrate initial concentrations (Experiment 3), the conversion reaches 80% in RDR and only 70% in batch reactor which are lower than experiment 1 and 2. The fact that lower conversion is obtained for higher substrate concentration while keeping catalyst amount constant indicates that the reaction behaves as having an overall reaction order smaller than one.

The higher conversion obtained in RDR than the batch reactor is probably due to the fact that more acetone was removed in RDR. The acetone concentration profile for different reaction conditions shown in Figure 6-13 clearly shows that peak acetone concentration in the reaction solution is much lower in RDR than the batch reactor. The peak acetone concentrations are 0.06M, 0.17M and 0.07M for the experiment with 0.14M, 0.33M and 0.28M initial substrate concentration in RDR respectively, while they are 0.09M, 0.23M and 0.13M in the batch reactor for the corresponding experiments. The acetone concentrations are the same for the conditions used in both RDR and batch reactor when the conversion is low. This is due to the fact that the acetone concentration is very low and the acetone production rate by the reaction is much faster than the acetone removal rate. When the reaction proceeds close to the reaction equilibrium, the acetone production rate became slower and the acetone removal rate became faster. Therefore, there is a maximum acetone concentration achieved in all cases. For the reactor design and reaction conditions optimisation, one should consider minimising this acetone concentration peak in order to obtain high conversion and high enantioselectivity.

The same initial enantioselectivity which is about 87% was obtained for all the reaction conditions used in either the batch reactor or the rotating disc reactor, which is probably because in the beginning of the reaction acetone removal rate is too small as compared with reaction rate to affect the initial enantioselectivity. Furthermore, no

products were present in the beginning of the reaction. This would lead to enantioselectivity erosion by the backwards reaction. The enantioselectivity decreased with conversion in all cases. However, the enantioselectivity decreased much faster at high substrate concentration and high ratio of the substrate concentration/catalyst concentration. For all the conditions used, enatioselectivity obtained in the RDR is higher than which obtained in the batch reactor. The possible reason for this is that in the rotating disc reactor acetone has been removed more efficiently which resulted in encouraging the forward reaction (acetone reacting with isopropanol gives phenylethanol and acetone) and preventing the backward reaction (acetone reacting with phenylethanol gives isopropanol and acetophenone). More efficient acetone removal in the rotating disc reactor is due to the fact that the ratio of nitrogen flowrate/liquid volume used in the rotating disc reactor was 16 as compared to the batch reactor.

6.3.2.2 Reproducibility of rotating disc reactor

Experiment 1 and experiment 3 have been repeated twice to check the reproducibility. It is established that conversion was reproducible within 2.8%, e.e. was reproducible within 0.2% and acetone concentration was reproducible within 4.5% (Figure 6-14).
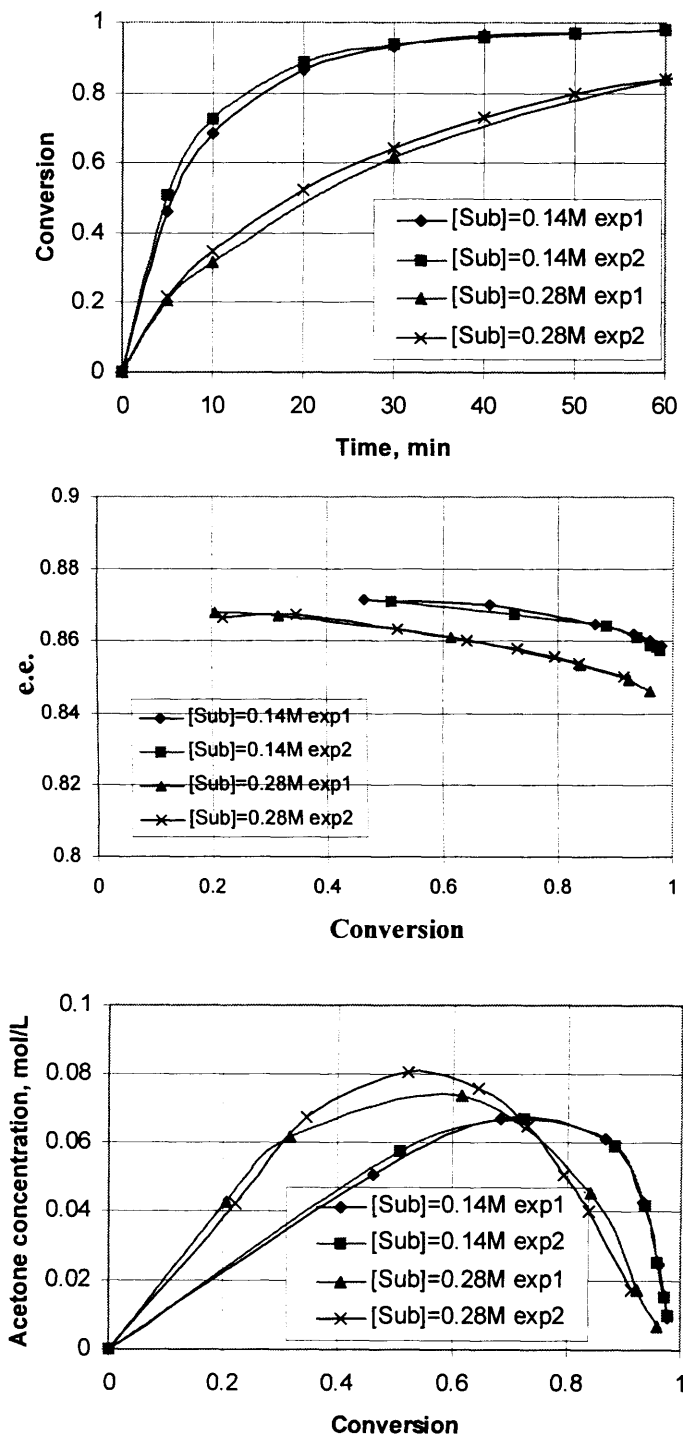
Figure 6-14 Reproducibility of the asymmetric transfer hydrogenation in RDR

(a) Conversion as function of time, (b) e.e. as function of conversion, (c) Acetone concentration as function of conversion ([Catalyst]=0.000144M; [Sodium Isopropoxide]/ [Catalyst]=8; Temperature=30°; Nitrogen flowrate=800ml/min bubbling into the liquid phase)

166

6.3.2.3 Experiments with and without isopropanol top-up

During acetone evaporation, part of isopropanol is simultaneously evaporated if the isopropanol partial pressure in the nitrogen gas is lower than isopropanol vapour pressure. Isopropanol evaporation will concentrate the reaction solution which will lead to the reduction of the enantioselectivity. Therefore, it is necessary to top-up the lost solvent in the reaction solution if one wants to keep the concentration constant. In this experiment, fresh isopropanol is introduced during reaction by a syringe pump (RAZEL A-99 FJZ).

The fresh IPA top up rate is calculated based on the isopropanol loss during the experiments. For the 50ml initial reaction solution volume, it decreased to 35ml after 60 minutes operation with 800ml/min nitrogen flowrate. Therefore, the IPA top-up rate is determined as $\dfrac{50ml - 35ml}{60\min} = 0.25ml/\min$. Experimental results with and without IPA top-up in the rotating disc reactor are summarised in Figure 6-15.
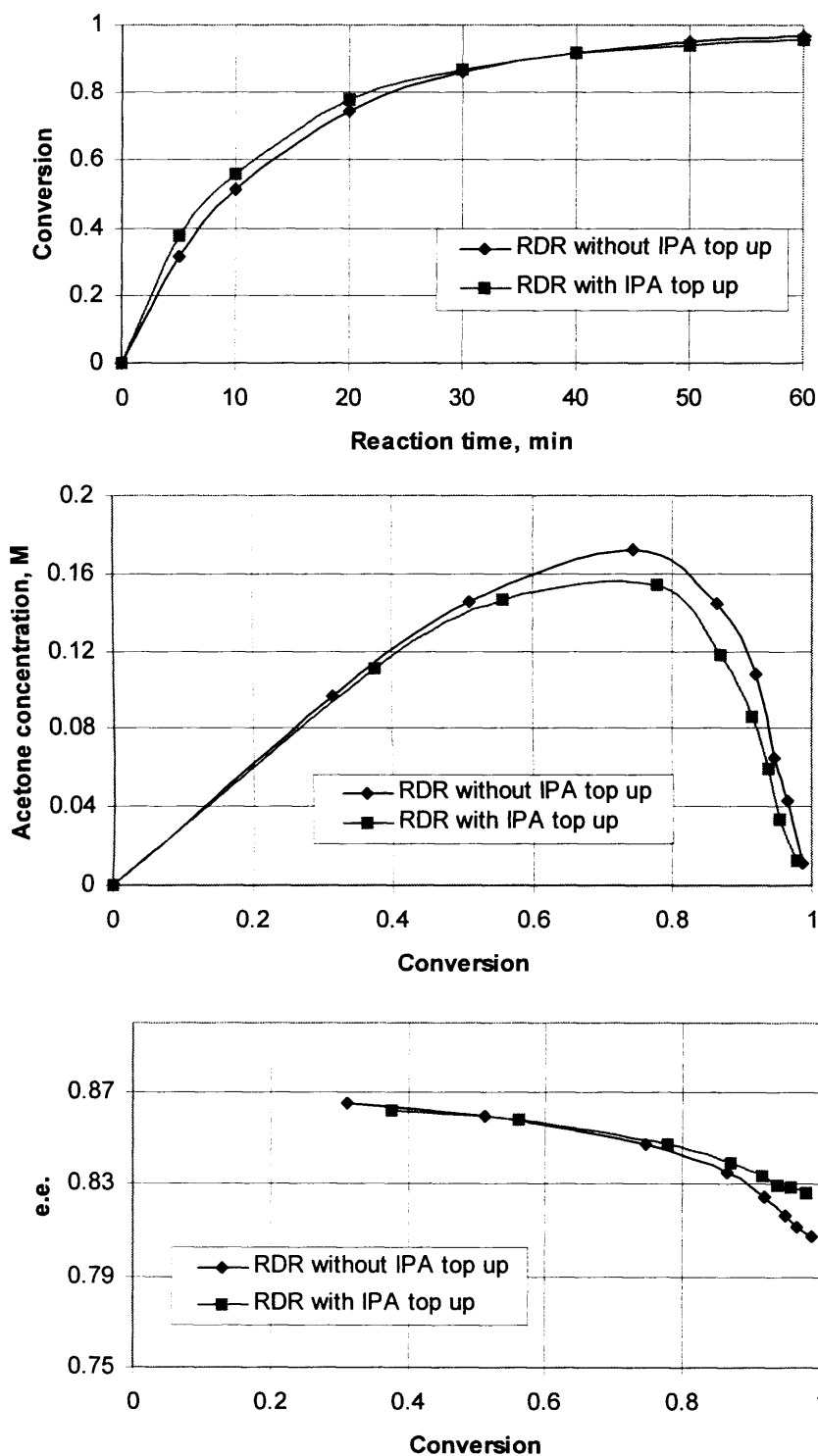
Figure 6-15 Effect of isopropanol top-up in the rotating disc reactor (a) Conversion as function of time, (b) Acetone concentration as function of conversion, (c) e.e. as function of conversion. ([Substrate]=0.33M; [Substrate]/[Catalyst]=1000; Temperature=30°; [Sodium Isopropoxide]/ [catalyst]=8; N_2 flowrate=800ml/min bubbling into the liquid phase)

Conversion as function of time is plotted in Figure 6-15a. It can be seen that 97% conversion was reached in both experiments with and without IPA top up in 60 minutes. As shown earlier, the conversion is the same for different substrate concentration when the ratio of substrate concentration/ catalyst concentration ratio is kept constant. Isopropanol loss only concentrated the reaction solution without changing the ratio of substrate concentration/ catalyst concentration. Therefore, the IPA top up did not change the conversion with conditions used.

Figure 6-15b shows acetone concentration against conversion for the experiments with and without IPA top. Slightly lower acetone concentration was obtained in the experiment with IPA top up which indicates that IPA loss during the experiment concentrated the reaction solution. Figure 6-15c shows the e.e. as function of conversion. It can be seen that initial e.e. is the same for both experiments which is due to the fact that IPA loss is insignificant at the beginning of the reaction. The final e.e. obtained in the experiment with IPA top-up (82.58%) is higher than without IPA top-up (80.73%). This is due to the fact that IPA loss concentrated the reaction solution and backwards reaction was favoured at high concentration which leads to a reduction of the e.e..

6.4 Conclusions

A rotating disc reactor (RDR) has been employed for acetone removal from binary mixtures of acetone-isopropanol and asymmetric transfer hydrogenation of acetophenone. The reactor consists of a 70mm radius and 2mm thickness stainless steel disc mounted on a horizontal shaft, accommodated in a cylindrical shell with 75mm radius and thickness 10mm.

First, acetone removal from acetone-isopropanol mixtures by nitrogen and vacuum stripping was investigated. A wiper incorporated to wipe off the liquid film from the disc does not have any effect on the acetone stripping which was attributed to the fact that liquid film is not completely wiped off by the wiper. The mass transfer limitation was located in the submerged boundary-layer rather than the film on the disc exposed to the gas. Acetone stripping performance is very much dependent on the ratio of the gas flowrate/liquid volume. If the ratio is the same, the acetone removal performance

is the same for the batch reactor and rotating disc reactor. However, the rotating disc reactor can still offer other advantages such as wide range of the gas flowrate to liquid volume ratio and potential scale out. Acetone stripping performance is improved by increasing the rotating speed. If the gas is first bubbled through the liquid phase, the contribution of the rotating disc for acetone removal is insignificant, due to saturation of the gas phase in volatile components after it leaves the liquid trough. Comparing with gas flow above the liquid surface, acetone removal is better when the gas is bubbled into the liquid phase which is due to the gas bubble enhancing the mixing in the liquid trough. Acetone removal by vacuum stripping has been attempted but was not successful.

Asymmetric transfer hydrogenation was also carried out. The comparison of the batch reactor with 250ml liquid volume and RDR with 50ml liquid volume shows that higher conversion and higher e.e. were obtained in the RDR due to more efficient removal of the acetone from RDR. Pure solvent, isopropanol top-up can keep the reaction solution concentration constant, thus resulting to better e.e. than the case without solvent top-up.

Chapter 7

Micro-mesh Gas-Liquid Reactor for Acetone Stripping and Catalytic Asymmetric Transfer Hydrogenation

7.1 Introduction

In this Chapter, acetone stripping and asymmetric transfer hydrogenation were conducted in a membrane/mesh reactor. A membrane/mesh provides an interface for the gas and liquid to be contacted. As discussed earlier, acetone removal can shift the reaction equilibrium and increase the enantioselectivity. Its removal depends on the gas flowrate to liquid volume ratio. In a mesh reactor, gas flowrate to liquid flowrate ratio can be much higher than in the batch reactor, two phase tubular reactor and rotating disc reactor.

One problem for the operation of the mesh reactor is phase breakthrough from one side of the mesh to the other. Therefore, breakthrough was investigated first in the mesh reactor to establish the operation pressure difference between gas and liquid phase. Acetone stripping was then conducted in the mesh reactor. Various conditions were investigated such as membrane type, gas and liquid flowrate, acetone initial concentration, isopropanol top-up, etc. in the mesh reactor. Asymmetric transfer hydrogenation was subsequently conducted. Various reaction conditions were investigated such as substrate concentration, substrate to catalyst concentration ratio, temperature. In the last section of the Chapter, scale out and scale up of the mesh reactor were studied and preliminary experiments were conducted.

7.2 Breakthrough studies in membrane contactors

7.2.1 Experimental set-up

The heart of the experimental set-up is the mesh reactor which is built in a layer structure (Figure 7-1). The reactor measures 3×8cm in size. The gaskets utilised to define the gas and liquid flow channels are made from brass. The reactor is sealed by top and bottom plates made from Perspex. The dimensions of the top and bottom plates are 3×8×1.5cm (W×L×H). The dimensions of the gaskets are 3×8×0.02cm (W×L×H) outside and 2×6×0.02cm (W×L×H) inside. The inlet and outlet of the gas and liquid are 1/8" stainless steel tubes connected by Swagelok fittings to the top and bottom plates. The top gasket defined the gas flow channel and the bottom gasket defined the liquid flow channel. The membrane is placed between two gaskets and contains the gas liquid interface. Two flow configurations were implemented as shown in Figure 7-1 to allow other types of experiments to be performed (for example,

IPA top up experiments and scale out experiments). However, the flow configuration did not have any effect on the breakthrough experiments.

The liquid phase used is isopropanol which has very strong wettability. It was difficult to find a membrane which was not wetted. The alternative solution is to stabilize the gas liquid interface by applying a pressure difference across the phases. The Perspex cover plates of the contactor allow visualisation of the hydrodynamics (Figure 7-2). However, the Perspex plates cracked when they came in prolonged contact with the liquid such as ethanol and isopropanol, which can be seen from the places where the inlet and outlet sit. Therefore, for subsequent experiments, Perspex cover plates were replaced by stainless steel plates to prevent the cracking as shown in Figure 7-2.
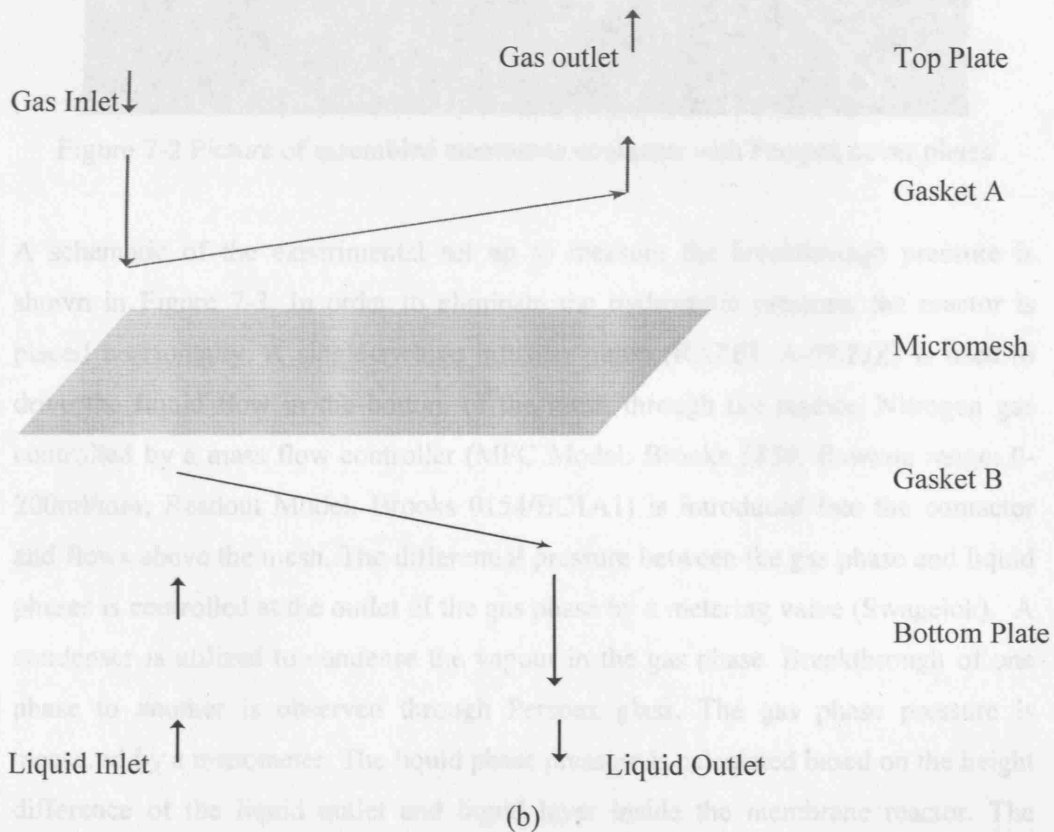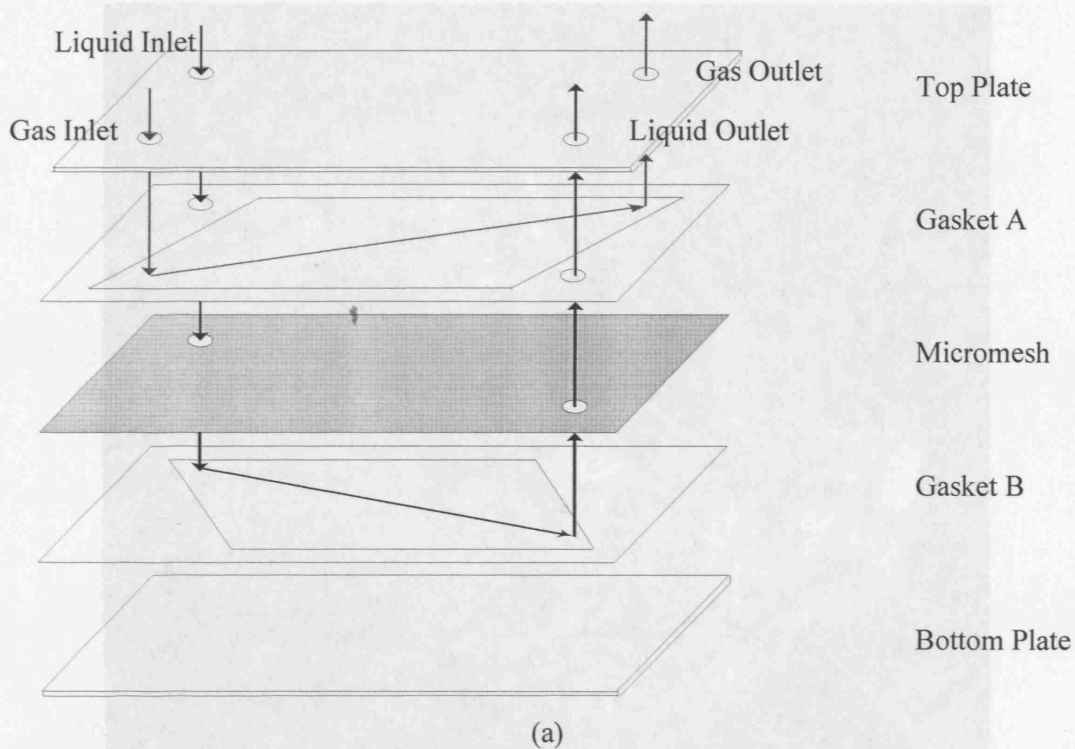
Figure 7-1 The layer structure of the membrane contactor (a) Flow configuration A (b) Flow configuration B

174
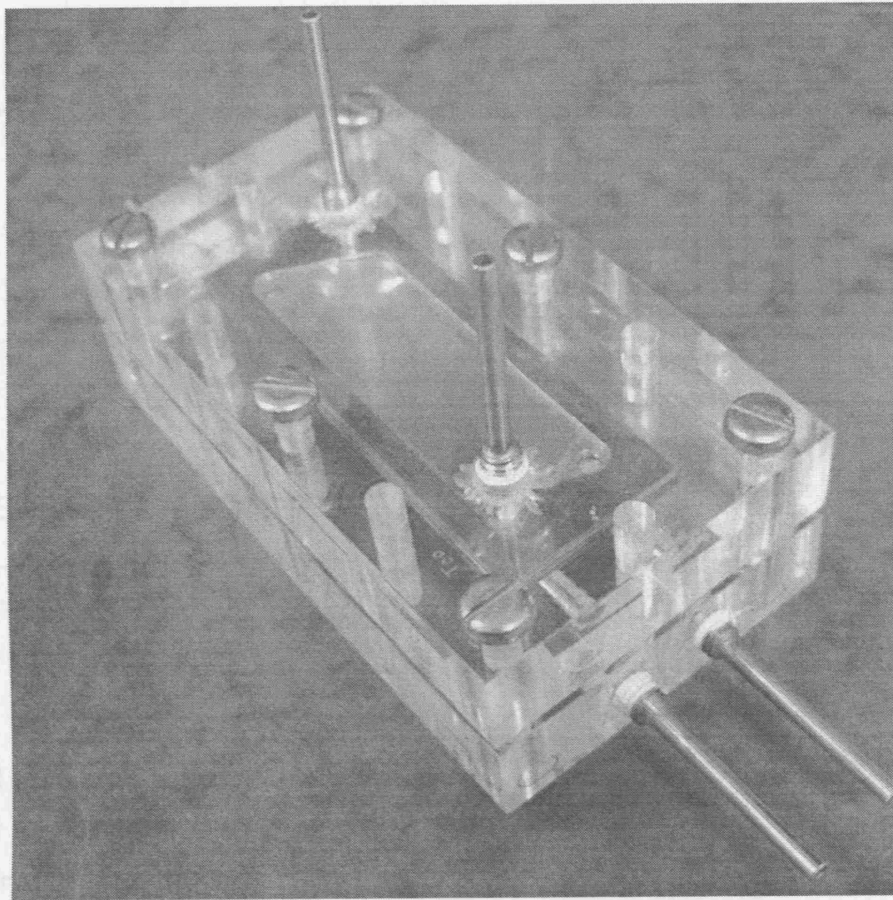
Figure 7-2 Picture of assembled membrane contactor with Perspex cover plates

A schematic of the experimental set up to measure the breakthrough pressure is shown in Figure 7-3. In order to eliminate the hydrostatic pressure, the reactor is placed horizontally. A single-syringe infusion pump (RAZEL A-99.FJZ) is used to drive the liquid flow in the bottom of the mesh through the reactor. Nitrogen gas controlled by a mass flow controller (MFC Model: Brooks 5850; flowrate range: 0-200ml/min; Readout Model: Brooks 0154/BC1A1) is introduced into the contactor and flows above the mesh. The differential pressure between the gas phase and liquid phases is controlled at the outlet of the gas phase by a metering valve (Swagelok). A condenser is utilized to condense the vapour in the gas phase. Breakthrough of one phase to another is observed through Perspex glass. The gas phase pressure is measured by a manometer. The liquid phase pressure is calculated based on the height difference of the liquid outlet and liquid layer inside the membrane reactor. The breakthrough pressure is calculated as the difference of the gas and liquid phase pressure.
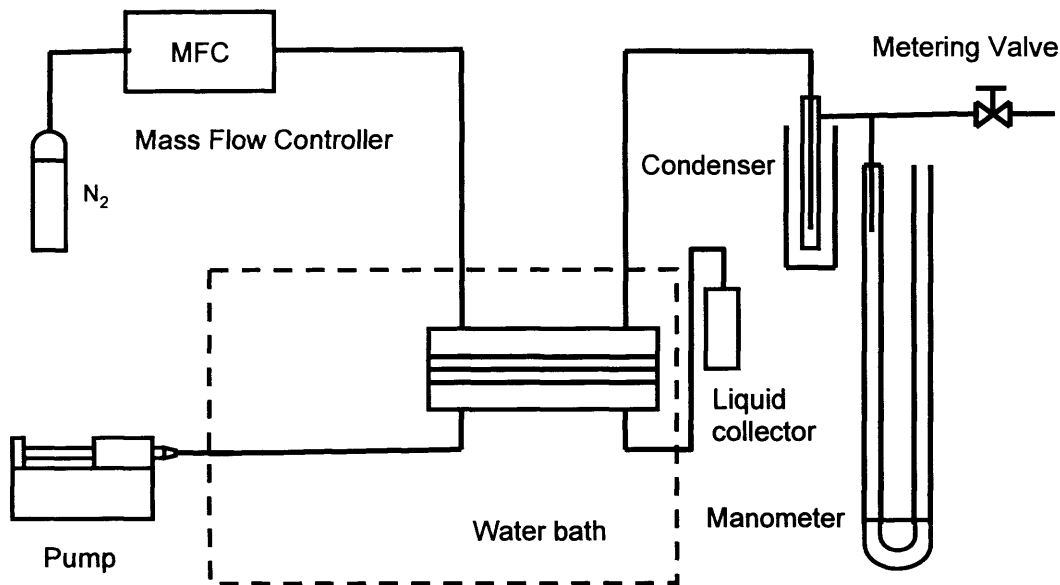
Figure 7-3 Experimental set up of the mesh contactor

7.2.2 Membranes and meshes description

Four membranes with different pore size, thickness and material have been studied. Their principal characteristics are listed in Table 7-1:

Table 7-1: Principal characteristics of the membranes investigated

Membrane	Average pore size $(\mu m)^a$	Maximum pore size $(\mu m)^b$	Thickness $(\mu m)^a$	Open area	Material	Supplier
Internetmesh	76	100	50	23%^{a}	Stainless steel 304	Internetmesh
Laser mesh	30	50	200	8%^{b}	Stainless steel 316	Liverpool University
PTFE	5	10	200	20%^{b}	PTFE	Bohlender
Mott	5	10	1574	30%^{b}	Stainless steel 316	Mott Corp.

(^{a}: From manufacturer, ^{b}: Determined from optical/SEM pictures)

The Mott membrane is produced by compressing fine metal particles together. The Internetmesh is made by a chemical etching method while the Laser mesh is made by laser drilling. The Mott membrane is a porous metal plate while Internetmesh and Laser mesh are plates with straight holes. Figures 7-4 (a) and (b) show optical microscope images of Internetmesh and Laser mesh. Figures 7-4 (c), (d) and (e) show SEM images of Mott membrane and PTFE membranes with magnification of ×500.

176

The average pore sizes of the membranes range from 5~76μm. The maximum pore sizes are between 10-~100μm and the open areas are between 8~30%. The PTFE membrane seems to have been affected after contacting with organic solvents. Figure 7-4 (e) shows PTFE membrane after one month using for acetone stripping. It can be seen that the membrane pore size and open area changed significantly.
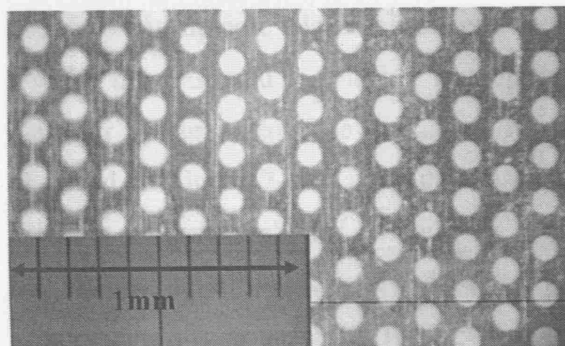
(a) Internetmesh
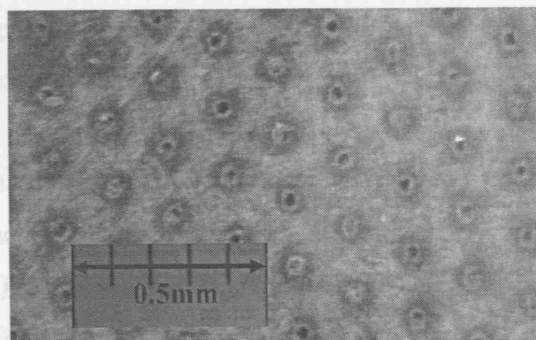
(b) Laser mesh
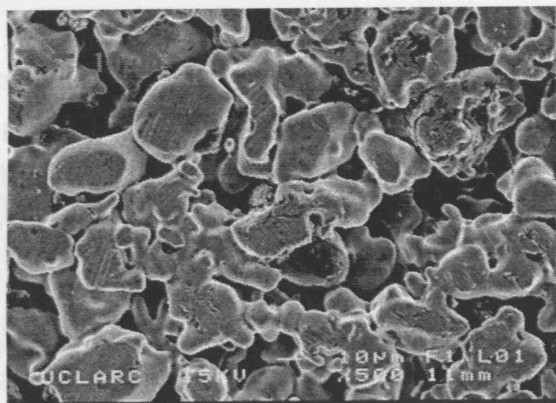
(c) Mott membrane
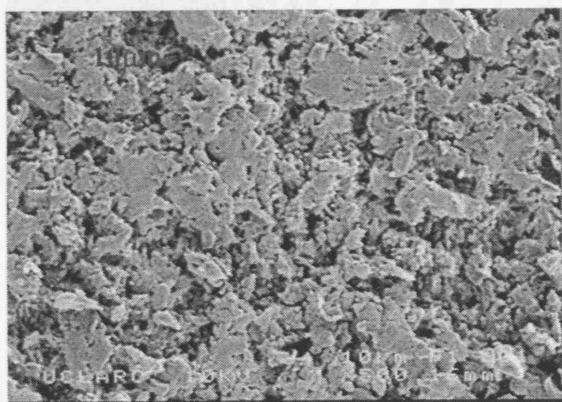
(d) New PTFE membrane
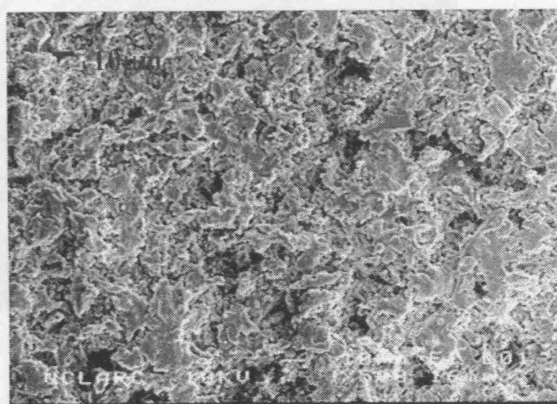
(e) Used PTFE membrane

Figure 7-4 Microscope images of membranes

7.2.3 Results and discussion

When one drop of isopropanol is placed on a stainless steel plate by a needle, the drop spreads immediately. This phenomenon indicates that the contact angle of isopropanol and stainless steel is close to zero. When a drop of isopropanol is placed on an Internetmesh with 23% area occupied by 76µm pores, the drop stayed on the mesh and ca 36° angle was observed (Figure 7-5). This is probably due to meniscus contortion at the pore edges as discussed in Chapter 2. The meniscus contortion can also be demonstrated by placing isopropanol on a stainless steel post 12.5mm in diameter (Figure 7-6). The maximum rotation should reach 90° in this case as observed in Figure 7-6. Using the Cassie Equation Equation (7-1) which gives apparent contact angle for a liquid on a surface contains different materials for heterogeneous surfaces (Cassie and Baxter, 1944) and assuming the mesh behaves as a heterogeneous surface with $f_1=0.23$, $\theta_1=90°$, $f_2=0.77$ and $\theta_2=0°$, one obtains θ_{APP} =39° which is close to 36° measured experimentally.

$$\cos\theta_{APP} = f_1 \cdot \cos\theta_1 + f_2 \cdot \cos\theta_2 \qquad (7\text{-}1)$$

where θ_1 is the contact angle for component 1 with area fraction f_1 (pore area) and θ_2 is the contact angle for component 2 with area fraction f_2 (solid area).
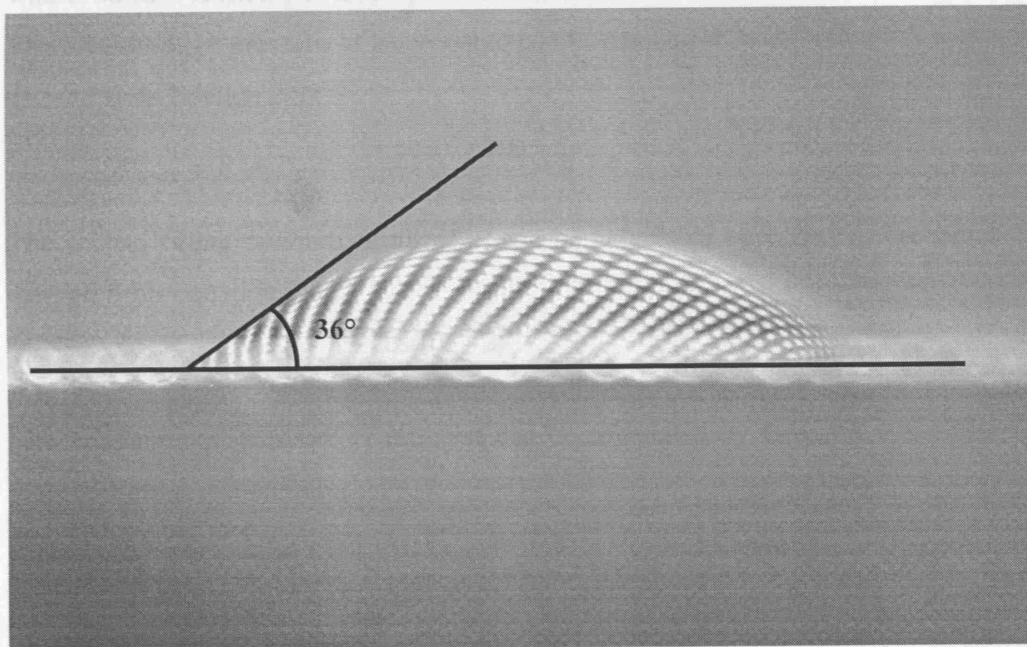
Figure 7-5 Isopropanol drop on internetmesh
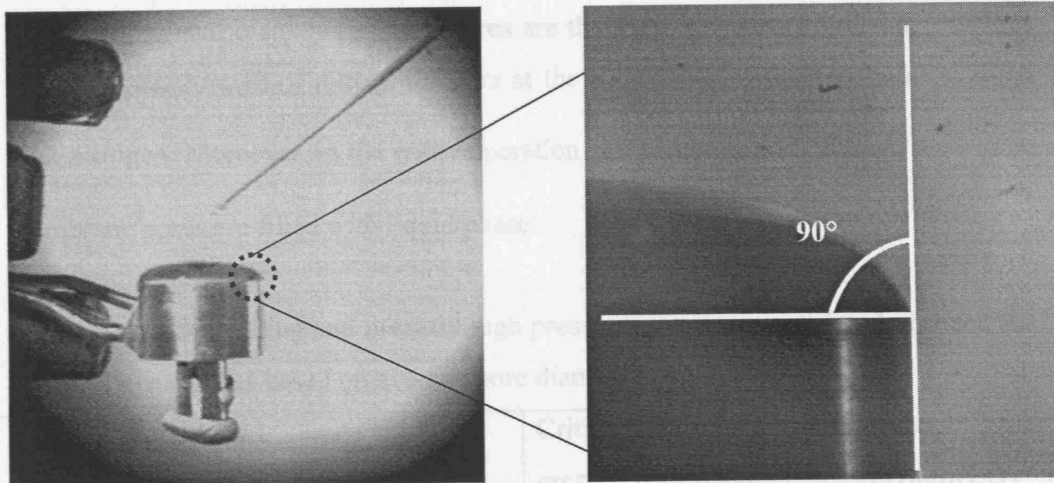
Figure 7-6 Meniscus rotation at the stainless steel post edge

Based on above analysis, it is reasonable to assume that $\theta=\theta_R=\theta_A=0°$. Therefore, the critical filling pressure of isopropanol can be calculated by equation 7-2 which is derived from Equation 2-31:

$$\Delta P_{C,IPA} = P_L - P_G = -\frac{2\gamma\cos(0)}{r} = -\frac{2\gamma}{r} \qquad (7-2)$$

where, surface tension γ of isopropanol is 0.021N/m.

The breakthrough pressure of isopropanol can be calculated by Equation 7-3 which is derived from Eqation 2-34:

$$\Delta P_{B,IPA} = P_L - P_G = -\frac{2\gamma\cos(0+90)}{r} = 0 \qquad (7-3)$$

The critical filling pressure of nitrogen can be calculated by equation 7-4 which is derived from Equation 2-32:

$$\Delta P_{C,N_2} = P_G - P_L = \frac{2\gamma\cos(0)}{r} = \frac{2\gamma}{r} \qquad (7-4)$$

The breakthrough pressure of nitrogen can be calculated by Equation 7-5 which is derived from Equation 2-36:

$$\Delta P_{B,N_2} = P_G - P_L = \frac{2\gamma\cos(0)}{r} = \frac{2\gamma}{r} \qquad (7-5)$$

Table 7-2 shows the calculated critical filling and breakthrough pressures for isopropanol and nitrogen for different membranes based on average membrane pore sizes. When $-\frac{2\gamma}{r} \leq P_L - P_G \leq 0$, isopropanol fills the pores spontaneously. The

critical filling and breakthrough pressures are the same for nitrogen, which indicates that the breakthrough of nitrogen occurs at the same time when the pores are filled with nitrogen. Moreover, in the entire operation pressure range, $0 \leq P_G - P_L \leq \dfrac{2\gamma}{r}$, the membrane pores are filled with liquid phase.

Table 7-2 Critical filling and breakthrough pressures for isopropanol and nitrogen for different membranes based on average pore diameter

Membranes		Critical filling pressure(mmH$_2$O)	Breakthrough pressure(mmH$_2$O)
Internetmesh	Isopropanol	-110	0
	Nitrogen	110	110
Laser mesh	Isopropanol	-280	0
	Nitrogen	280	280
PTFE	Isopropanol	-1680	0
	Nitrogen	1680	1680
Mott	Isopropanol	-1680	0
	Nitrogen	1680	1680

Table 7-3 shows a comparison of breakthrough pressure between the experimental results and prediction from Equation (7-3) and (7-5). The theoretical predictions agree better with experimental results when maximum pore size is used for calculations. This is due to the fact that the breakthrough takes place firstly at the biggest pore. The results show that the breakthrough pressure of nitrogen decreased with increase of membrane pore size as expected. Therefore, in order to obtain wider operation pressure range, a membrane with smaller pore size has to be used. In all the experiments, the breakthrough of isopropanol is spontaneous and it occurred firstly at the location where the gasket came in contact with the membrane. This can be explained by the edge effect (see Chapter 2).

Table 7-3: Breakthrough pressure of the different membranes for the IPA-N$_2$ system

Membrane	Breakthrough pressure (G---->L) P$_G$-P$_L$ (mm H$_2$O)			Breakthrough pressure (L---->G) P$_L$-P$_G$ (mm H$_2$O)	
	Experiment	Equation (7-5) based on maximum pore size	Equation (7-5) based on average pore size	Experiment	Equation (7-3)
Internetmesh	70~80	84	110	-5	0
Laser mesh	150~160	168	280	-5	0
PTFE	740~760	840	1680	-5	0
Mott	860~910	840	1680	-5	0

(Liquid flowrate: 0.1ml/min Isopropanol (IPA); dry N$_2$ flowrate: 70ml/min, θ=0°.)

7.3 Acetone stripping in membrane contactors

7.3.1 Experimental set-up

In the following experiments, the top and bottom plate of the reactors are made of stainless steel (Figure 7-7) to prevent cracking of the Perspex plates as mentioned in Section 7.2.1.

Pictures of the assembled and disassembled membrane contactors are shown in Figure 7-7. Both flow configurations shown in Figure 7-1 are utilized. The experimental set up is identical as the one described in section 7.2.1. Constant temperature was achieved by placing a reactor in a water bath. Samples from liquid side are collected in liquid collector which was placed in an ice bath (Figure 7-3). They were analysed by an Agilent 6890 GC system as described in Chapter 3.
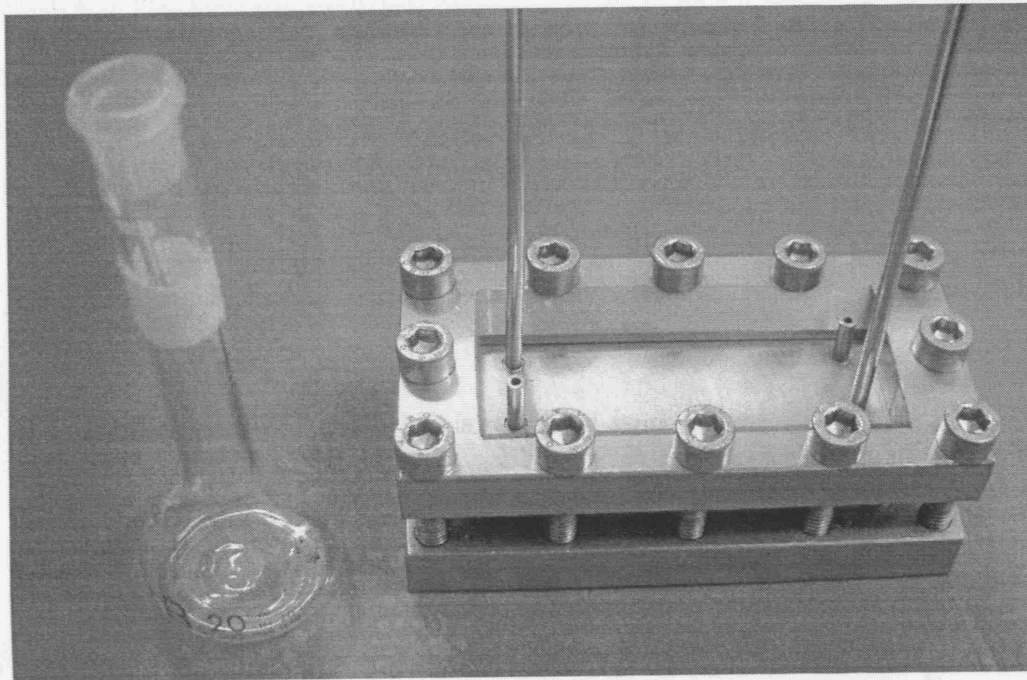
(a)
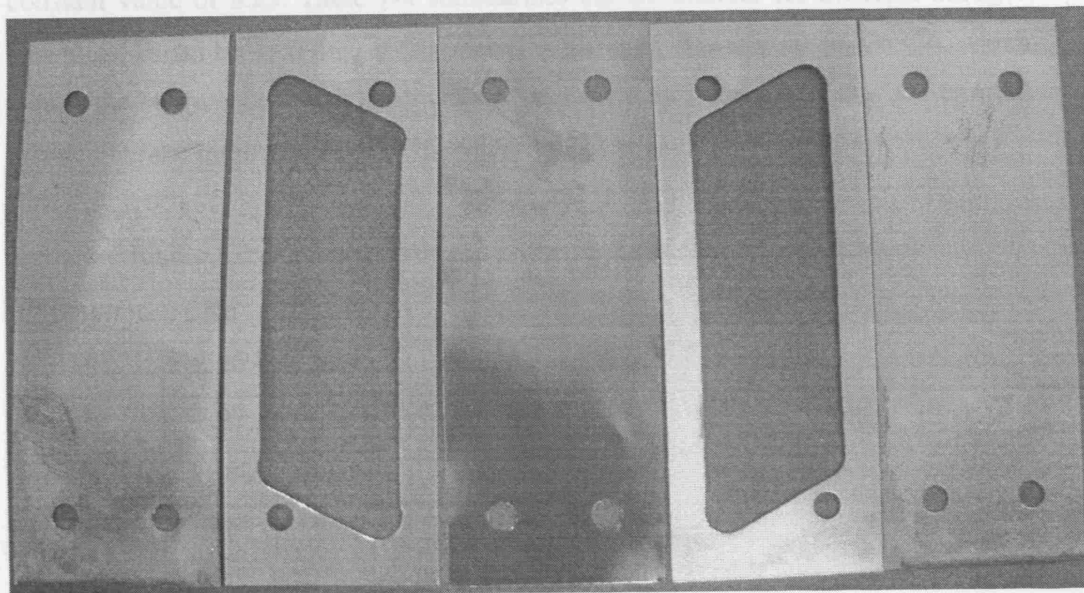
(b)

Figure 7-7 Picture of the mesh contactor (a) Assembled, (b) Disassembled (in this picture the Internetmesh is employed as membrane)

7.3.2 Mathematical model formulation

The following equation was developed to calculate the outlet acetone concentration in the liquid phase of the membrane contactor C_{out} as function of the inlet concentration

C_{in}, the contactor length H and two dimensionless parameters β and Ω (for details see Appendix D):

$$\frac{x_2}{x_1} = \frac{C_{out}}{C_{in}} = \frac{1}{1+\Omega}\left\{1+\Omega\cdot\exp\left[-\beta\cdot\left(1+\frac{1}{\Omega}\right)H\right]\right\} \tag{7-6}$$

$$\Omega = \frac{F_g}{F_l}\cdot\frac{P}{R_gT}\cdot\frac{1}{K_{eq}}, \tag{7-7}$$

$$\beta = \frac{K_T\cdot\tau_l}{h_l\cdot H} \tag{7-8}$$

The overall mass transfer coefficient is calculated as:

$$\frac{1}{K_T} = \frac{1}{k_l}+\frac{1}{k_m}+\frac{K_{eq}}{k_g} \tag{7-9}$$

Skelland (1974) suggested that the laminar flow in parallel plates will be fully developed when $Gz = \frac{Re\cdot Sc\cdot 2\delta}{L} < 20$. Then the Sherwood number ($\frac{k\cdot 2\delta}{D}$) has constant value of 8.23. Table 7-4 summarizes the Gz number for different nitrogen flowrates. It can be seen that in the operation nitrogen flowrate range, Gz<20, which means the laminar flow is fully developed and constant Sherwood value can be used to calculate the mass transfer coefficient in the gas phase.

Table 7-4 Re, Sc, Gz numbers in the gas phase for different nitrogen flowrates

F_{N2} ml/min	Re	Sc	Gz
70	3.96	1.296	0.034
140	7.92	1.296	0.068
210	11.88	1.296	0.102
280	15.85	1.296	0.136

The mass transfer coefficient in the liquid phase can be calculated by Sh= $\frac{k\cdot 2\delta}{D}$ =8.23 due to the fact that in the entire flowrate range Gz < 20 (Skelland 1974) (Table 7-5) which indicates that the laminar flow in parallel plates will be fully developed.

Table 7-5 Re, Sc, Gz number in the liquid phase for different liquid flowrates during acetone stripping in the membrane contactors

Liquid flowrate ml/min	Re	Sc	Gz
0.05	0.0189	2717	0.0855
0.1	0.0378	2717	0.3423
0.2	0.0756	2717	1.3693
0.3	0.1512	2717	4.1081

The mass transfer coefficient in the membrane was calculated from Equation 7-10 because the membrane is filled with liquid as discussed in Section 7.2.

$$k_m = \frac{D_{Acetone-isopropanol} \cdot \varepsilon}{\delta_m \cdot \tau} \qquad (7\text{-}10)$$

where k_m is mass transfer coefficient in the membrane, $D_{acetone\text{-}isopropanol}$ is diffusion coefficient, ε is porosity, δ is the thickness of the membrane, τ is residence time.

7.3.3 Results and discussion

7.3.3.1 Reproducibility

In this set of experiments, dry N_2 (CP grade), which is obtained directly from N_2 cylinder, was used. Initial acetone concentration was selected as 0.1M which is close to the amount of acetone generated in the asymmetric transfer hydrogenation of acetophenone under base case conditions (Chapter 3). The experimental conditions are listed in Table 7-6:

Table 7-6: Experimental conditions used for reproducibility experiments

N_2 flow rate (F_g) ml/min	70
Liquid flow rate (F_l) ml/min	0.1
Average N_2 residence time (τ_g) min	0.0035
Average liquid residence time (τ_l) min	2.4
Acetone initial concentration M	0.106
Reactor gas chamber volume V_g ml	0.24
Reactor liquid chamber volume V_l ml	0.24
Temperature °C	30

(solvent: isopropanol; $\tau_g = \dfrac{V_g}{F_g}, \tau_l = \dfrac{V_l}{F_l}$)

The experiments are conducted three times with the same conditions to check the reproducibility and results are summarized in Table 7-7. As it can be seen the experiments are reproducible within ±2.6%.

Table 7-7 Reproducibility experiments for acetone stripping with N_2 in mesh reactor

	$C_{Ac,in}$, M	$C_{Ac,out}$, M
Exp 1	0.106	0.036
Exp 2	0.106	0.038
Exp 3	0.106	0.037

(Internetmesh, dry N_2; T=30°C; solvent: isopropanol; liquid inlet flowrate=0.1ml/min, N_2 flowrate=70ml/min; ΔP: pressure difference $(P_{gas}-P_{liquid})$=30mmH$_2$O; $C_{Ac,in}$ =Acetone concentration in the contactor liquid inlet; $C_{Ac,out}$: acetone concentration in the contactor liquid outlet)

7.3.3.2 Effect of membrane type

In order to select a suitable membrane and operation pressure for the membrane contactor, acetone stripping has been carried out in the mesh reactor with different membranes and pressure difference. The experimental conditions are listed in Table 7-6 and the results for the acetone stripping with different membranes and different pressure are summarised in Table 7-8.

Table 7-8: Acetone removal with different membranes at different pressures

Membrane	Thickness	Porosity	Tortuosity	ΔP	$C_{Ac,out}$ /$C_{Ac,in}$	$C_{Ac,out}$ /$C_{Ac,in}$
	mm	ε	τ	mm H$_2$O	Exper.	Model Eq 7-6
Internetmesh				10	0.346	0.325
Internetmesh	0.05	0.23	1	30	0.346	0.325
Internetmesh				50	0.364	0.325
Internetmesh				60	0.336	0.325
Mott	1.5	0.3	3.3[a]	30	0.770	0.965
Mott				660	0.780	0.965
Laser mesh	0.2	0.08	1	30	0.670	0.804
Laser mesh				100	0.623	0.804
PTFE	0.2	0.3	3.3[a]	30	0.752	0.783
PTFE				510	0.761	0.783

($C_{Ac,in}$=0.106M, ΔP: pressure difference $(P_{gas}-P_{liquid})$; $C_{Ac,in}$: acetone concentration in the liquid inlet; $C_{Ac,out}$: acetone concentration in the liquid outlet of the reactor; a: tortuosity is calculated as $\tau = 1/\varepsilon$ (Iversen et al 1997)

It can be seen that the Internetmesh gives the best performance on acetone evaporation. At the liquid flowrate 0.1ml/min, about 70% acetone was removed using the Inernetmesh membrane while only 15~32% acetone was removed using other membranes. This can be explained by the mass transfer coefficient values. Table 7-9 shows the individual mass transfer coefficients for liquid phase, gas phase and membrane and the total mass transfer coefficient for all membranes. It can be seen that the mass transfer coefficient in the liquid phase k_l and mass transfer coefficient in the gas phase k_g/K_{eq} are constant which is due to the same flow conditions. Mass transfer coefficient in the membrane varies for different membranes due to the different thickness, porosity and tortuosity. For all membranes used the mass transfer coefficients in the gas phase and in the liquid phase are much larger than that in the membrane. Therefore mass transfer coefficient k_l and k_g/K_{eq} can be neglected and the overall mass transfer coefficient is determined by the mass transfer coefficient in the membrane k_m. k_m increases with decrease of the membrane thickness and increase of the porosity. In order to obtain faster mass transfer in the membrane contactor, it is better to select thinner membrane with higher porosity. The tortuosity value of porous membranes is usually larger than 1. This results in an increase of the mass transfer length inside the membrane, thus increasing the mass transfer resistance. Therefore, membrane with straight pores which gives tortuosity value 1 is preferred due to its shorter mass transfer path.

Table 7-9 Mass transfer coefficients for different membranes

	k_l ($\times 10^{-5}$ m/s)	k_g/K_{eq} ($\times 10^{-5}$ m/s)	k_m ($\times 10^{-5}$ m/s)	K_T ($\times 10^{-5}$ m/s)
Internetmesh	1.667	80.4	0.3726	0.3033
Laser Mesh	1.667	80.4	0.0324	0.0317
PTFE	1.667	80.4	0.0368	0.0359
Mott Membrane	1.667	80.4	0.00491	0.0049

(Diffusion coefficient for the liquid is 0.81×10^{-9} m^2/s and diffusion coefficient for the gas is 1.136×10^{-5} m^2/s)

As shown in Table 7-8, the model prediction for $C_{Ac,out}/C_{Ac,in}$ agrees well with experimental data for the Internetmesh. However, the model prediction is higher that

the experimental data for other membranes. For the PTFE and Mott membranes this is probably due to incorrect values for the tortuosity of the membrane used in the calculations. For the Laser mesh this may be due to pores being not completely open as shown in Figure 7-4.

In all cases, the pressure difference does not have any effect on the acetone evaporation. It is known that the pressure difference will slightly affect the solubility of the acetone in isopropanol. Table 7-10 summarizes the effect of the pressure on the solubility of the acetone in isopropanol based on equation 7-11 (See Appendix B).

$$K_{eq} = \frac{P_{total}}{P^{vap}} \cdot \frac{1}{\gamma} \cdot C_{total} \qquad (7\text{-}11)$$

where, P_{total} is system pressure, P_{Vap} is vapour pressure of isopropanol, γ is the activity coefficient of isopropanol and C_{total} is total concentration.

Table 7-10 Effect of pressure difference on the solubility of the acetone

Membrane	ΔP	K_{eq}
	mmH_2O	mol/m^3
Internetmesh	10	11744
Internetmesh	30	11767
Internetmesh	50	11790
Internetmesh	60	11801

It can be concluded that the effect of the pressure on the solubility is very small and can be ignored in the pressure range of operation.

7.3.3.3 Effect of contactor orientation

The contactor orientation can affect the hydrostatic pressure in the system. In order to study the effect of the contactor orientation on the acetone stripping and gas-liquid interface stability, experiments were carried out by placing the reactor vertically, horizontally with gas on the top, horizontally with liquid on the top, and gas on the top with slope 30°. The results are summarised in Table 7-11.

Table 7-11: Effect of the contactor orientation on the acetone removal:

Position	$F_{L\text{-}in}$	F_{N2}	$C_{Ac,in}$	$C_{Ac,out}$
	ml/min	ml/min	M	M
Vertical	0.1	70	0.104	0.036
Horizontal(G-UP)	0.1	70	0.104	0.038
Horizontal(L-UP)	0.1	70	0.104	0.036
Slope(G-UP)=30°	0.1	70	0.104	0.036

(Internet mesh; With dry N_2; T=30°C; solvent: isopropanol; $F_{L\text{-}in}$: liquid inlet flowrate, F_{N2}: N_2 flowrate; $C_{Ac,in}$: acetone concentration in the liquid inlet; $C_{Ac,out}$: acetone concentration in the liquid outlet of the reactor; ΔP: pressure difference (P_{gas}-P_{liquid}) range used are from 20~60mmH$_2$O; The gas phase pressure is measured by a manometer. The liquid phase pressure is calculated based on the height difference of the liquid outlet and liquid layer inside the membrane reactor. ΔP is calculated as the difference of the gas and liquid phase pressure.)

The results indicate that the reactor position does not have any effect on acetone stripping. As long as the flow conditions in the liquid and gas phases are kept the same, the overall mass transfer coefficient is the same. Therefore, any orientation can be used as long as the operation is in the range of pressure differences where no phase breakthrough takes place. However, for scale up or scale out of the mesh reactor, the pressure drop and gravity should be taken into consideration to prevent phase breakthrough.

7.3.3.4 Effect of nitrogen flowrate

It can be seen from the model that sweeping gas flowrate is a very important factor for acetone stripping performance. In order to study the effect of nitrogen flowrate on the acetone stripping, experiments were carried out by changing the nitrogen flowrate from 70ml/min to 280ml/min and keeping all other conditions the same. The results are summarised in Table 7-12.

Table 7-12: Effect of the nitrogen flowrate on the acetone removal

F_{N2}	$C_{Ac,out}/C_{Ac,in}$
ml/min	Exper.
70	0.346
140	0.270
210	0.243
280	0.216

(Internetmesh; dry N_2; T=30°C; solvent: isopropanol; Liquid inlet flowrate 0.1ml/min, F_{N2}: N_2 flowrate; ΔP: pressure difference (P_{gas}-P_{liquid})=30mmH$_2$O; Acetone concentration in the liquid inlet is 0.1M; $C_{Ac,out}$: acetone concentration in the liquid outlet of the reactor)

As can be seen, acetone removal rate increased with increase of N_2 flowrate. These results can be explained by the mass transfer driving force and the ratio of the gas/liquid flowrate. The mass transfer coefficient in the gas phase did not change with nitrogen flowrate since the Sherwood number is constant (see Section 7.3.2). It is worth emphasizing that the mass transfer coefficient in the gas phase k_g/K_{eq}>>k_l>k_m, therefore, mass transfer resistance can be ignored for the operation conditions used. The effect of nitrogen flowrate on the driving force can be demonstrated in Figure 7-8. Figure 7-8 shows the operating line for different nitrogen flowrate and equilibrium curve y=mx, where m is vapour liquid equilibrium ratio. When the equilibrium curve is a straight line, the average driving force under different nitrogen flowrate can be calculated as (Chen et al 1989)

$$\Delta y_m = \frac{\Delta y_1 - \Delta y_2}{\ln \frac{\Delta y_1}{\Delta y_2}}$$

(7-12)

where Δy_1=mx_1-x_1 is inlet driving force and Δy_2=mx_2-L/G*(x_1-x_2) is the driving force when x=x_2, L is liquid flowrate and G is gas flowrate.

It can be seen that when the nitrogen flowrate increases, the slope of the operating line increases. The driving force Δy_2 increases, thus the average driving force increases. The average driving force increase with increase of nitrogen flowrate is shown from Table 7-13 which summarizes the average driving force for different nitrogen flowrate at x=0.00284 which is the outlet acetone mole fraction in the liquid phase at

189

70ml/min nitrogen flowrate. The driving force increased about 28% when the nitrogen flowrate increased from 70ml/min to 140ml/min. When the nitrogen flowrate increased further to 280ml/min, the driving force did not improve much. This agrees well with experimental results. Much more acetone has been removed when the nitrogen flowrate increased from 70ml/min to 140ml/min. However, acetone removal did not improve much when nitrogen flowrate increased further to 280ml/min. Figure 7-8 also demonstrates that the increase of gas/liquid flowrate ratio decreases the minimum possible outlet acetone concentration which corresponds to the intersection of the equilibrium curve with the operating line.
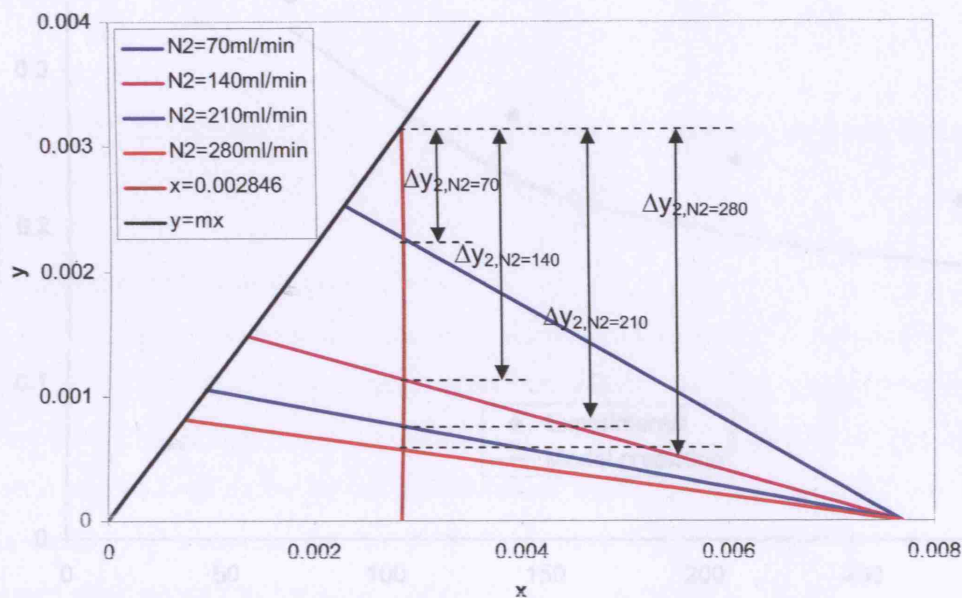
Figure 7-8 Effect of the ratio of gas-liquid flowrate (m=1.11, x is acetone mole fraction in liquid phase, y is acetone mole fraction in gas phase)

Table 7-13 Driving force for different gas flowrates

F_{N2} (ml/min)	Δy_m
70	0.00350
140	0.00453
210	0.00482
280	0.00496

Figure 7-9 shows a comparison of the experimental results and modelling results for different nitrogen flowrates. It can be seen that the model prediction is lower than the experimental results. This is probably due to the fact that the model did not take into consideration that IPA has been removed from the system which results in not only higher acetone concentrations, but also higher residence time. Also as Re increases, the flow is expected to go in a more straight line from inlet to outlet, bypassing the corner of the gaskets.
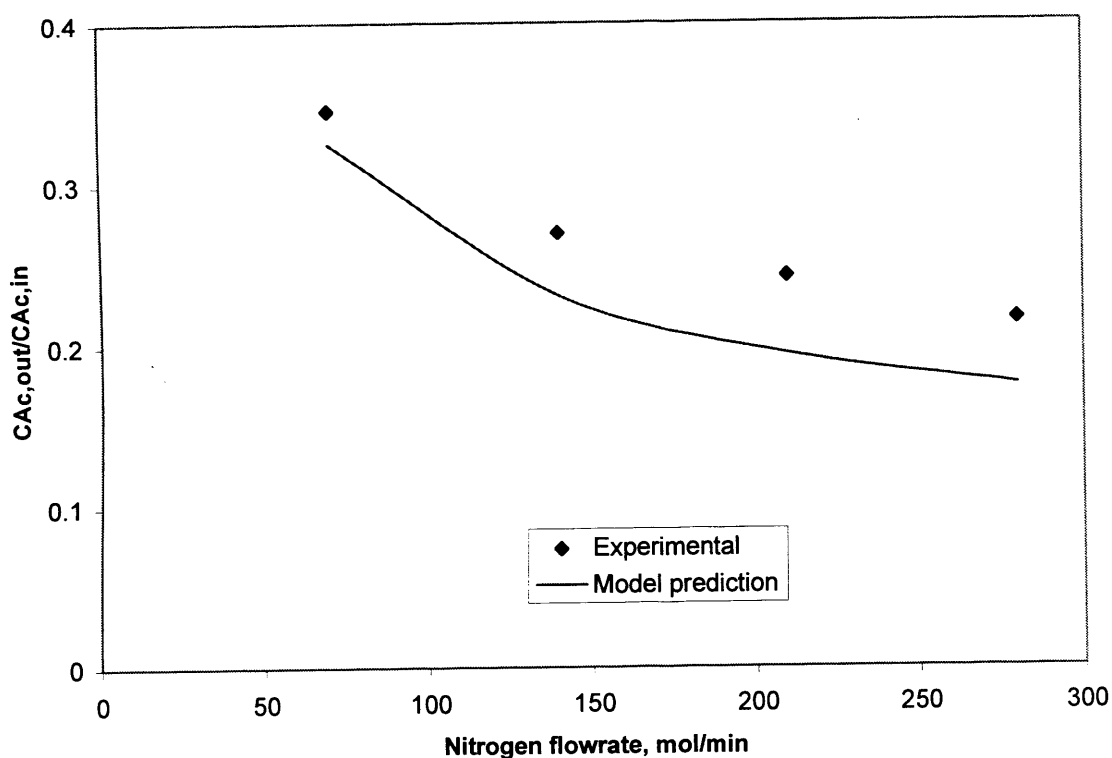
Figure 7-9 Comparison of the experimental and model prediction results for acetone stripping in mesh contactor (Internetmesh; dry N_2; T=30°C; solvent: isopropanol; liquid inlet flowrate 0.1ml/min, ΔP: pressure difference $(P_{gas}-P_{liquid})$=30 mm H_2O; Acetone concentration in the liquid inlet=0.1M)

Figure 7-10 shows acetone axial concentration profile for acetone stripping with different nitrogen flowrates. As can be seen, acetone concentration in the liquid phase decreases with increase of the reactor length. With the experimental conditions used, there are still some possibilities that more acetone can be removed if the reactor length can be extended. Alternatively, counter-current flow can be employed, if breakthrough conditions are not reached.

191
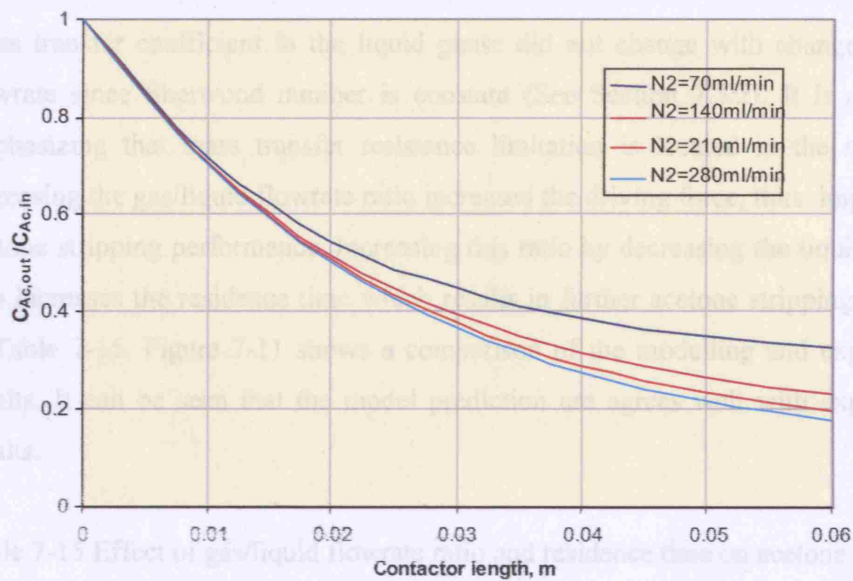
Figure 7-10 Simulated acetone axial concentration profiles for different nitrogen flowrates

7.3.3.5 Effect of liquid flowrate

As shown earlier, nitrogen flowrate has significant impact on acetone removal by changing the gas and liquid flowrate ratio. Another way to change this ratio is by changing the liquid flowrate and keeping gas flow constant. In this way, the residence time is altered keeping the contactor volume constant. The effect of liquid flowrate was studied by changing the liquid flowrate from 0.05ml/min to 0.3ml/min and keeping other conditions constant. The results are summarised in Table 7-14. It can be seen that the ratio $C_{Ac,out}$ /$C_{Ac,in}$ increases with increase of liquid flowrate.

Table 7-14: Effect of liquid flowrate on the acetone removal

F_{L-in}, ml/min	Residence time, min	$C_{Ac,out}$ /$C_{Ac,in}$
0.05	4.8	0.160
0.1	2.4	0.350
0.2	1.2	0.585
0.3	0.8	0.698

(Internetmesh, dry N_2; T=30°C; solvent: isopropanol; F_{L-in}: liquid inlet flowrate, N_2 flowrate=70ml/min; ΔP: pressure difference (P_{gas}-P_{liquid})=30mmH$_2$O; Acetone concentration in the liquid inlet=0.1M; $C_{Ac,out}$: acetone concentration in the liquid outlet of the reactor)

Mass transfer coefficient in the liquid phase did not change with change of liquid flowrate since Sherwood number is constant (See Section 7.3.2). It is also worth emphasizing that mass transfer resistance limitation is located in the membrane. Increasing the gas/liquid flowrate ratio increased the driving force, thus improved the acetone stripping performance. Increasing this ratio by decreasing the liquid flowrate also increases the residence time which results in further acetone stripping as shown in Table 7-15. Figure 7-11 shows a comparison of the modelling and experimental results. It can be seen that the model prediction are agrees well with experimental results.

Table 7-15 Effect of gas/liquid flowrate ratio and residence time on acetone stripping

F_G/F_L	F_L (ml/min)	F_G (ml/min)	Residence time (min)	$C_{Ac,out}/C_{Ac,in}$
700	0.1	70	2.4	0.349
1400	0.1	140	2.4	0.270
	0.05	70	4.8	0.160
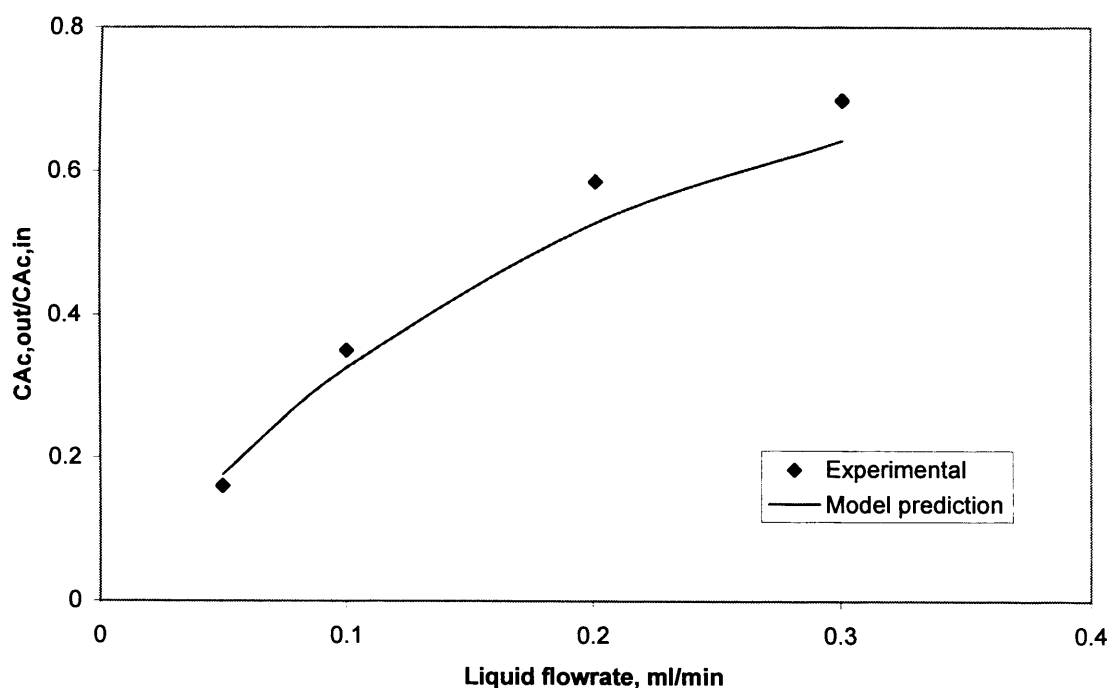
Figure 7-11 Comparison of the model and experimental results for acetone stripping in mesh reactor (Internetmesh; dry N_2; T=30°C; solvent: isopropanol; Nitrogen flowrate 70ml/min, ΔP: pressure difference $(P_{gas}-P_{liquid})$=30 mm H_2O; liquid inlet acetone concentration =0.1M)

Figure 7-12 shows acetone axial concentration profiles in the mesh reactor for acetone stripping with different liquid flowrates. As can be seen, acetone concentration decreases with increase of the reactor length. When liquid flowrate is higher than 0.1ml/min, there is still possibility that more acetone can be removed by increasing the reactor length. However, when the liquid flowrate is lower than 0.05ml/min, only very little acetone is removed in the reactor between 0.04 and 0.06m. Therefore, the reactor might be over designed for the acetone stripping when the liquid flowrate is lower than 0.05ml/min.
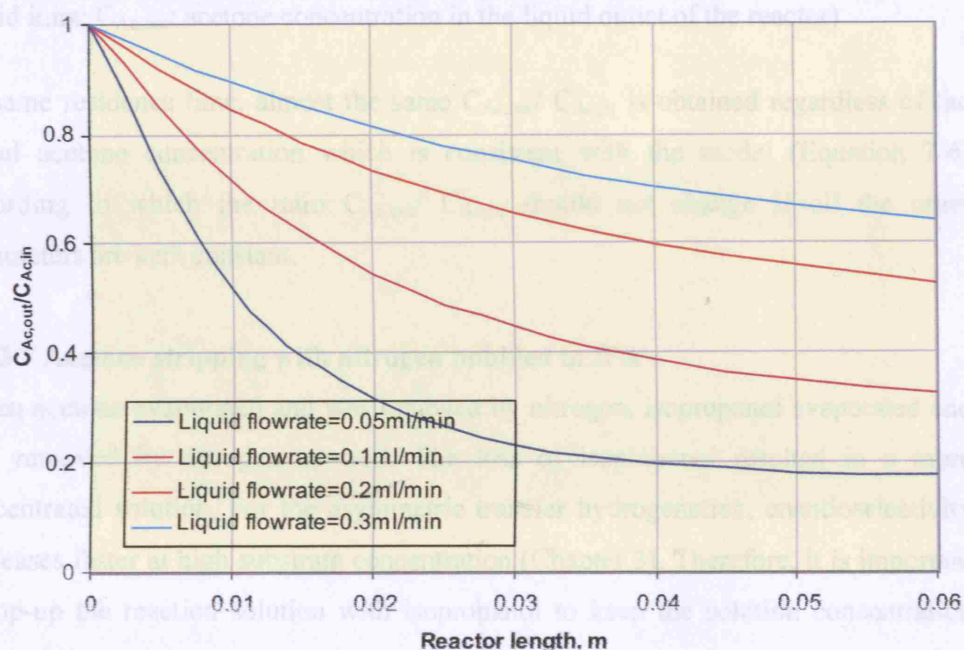
Figure 7-12 Theoretical Acetone axial concentration profile for different liquid flowrates during acetone stripping in mesh contactor (Internetmesh, dry N_2; T=30°C; solvent: isopropanol; Nitrogen flowrate 70ml/min, ΔP: pressure difference ($P_{gas}-P_{liquid}$)=30mmH$_2$O; Acetone concentration in the liquid inlet=0.1M)

7.3.3.6 Effect of the liquid phase inlet acetone concentration

From an industrial point of view, running the asymmetric transfer hydrogenation with higher substrate concentration is preferred. However, high substrate concentration results in high acetone concentration. In order to examine the performance of the mesh contactor with high initial acetone concentration, the experiments were carried out by changing acetone concentration from 0.1M to 0.4M while keeping other conditions the same. The results are summarised in Table 7-16.

194

Table 7-16: Effect of the composition in the liquid phase inlet on acetone removal

$F_{L\text{-}in}$	F_{N2}	ΔP	$C_{Ac,in}$	$C_{Ac,out}$	$C_{Ac,out}/ C_{Ac,in}$
ml/min	ml/min	mm H_2O	M	M	
0.1	70	30	0.109	0.038	0.349
0.1	70	30	0.227	0.075	0.330
0.1	70	30	0.323	0.115	0.356
0.1	70	30	0.413	0.154	0.373

(Internet mesh; dry N_2; T=30°C; solvent: isopropanol; $F_{L\text{-}in}$: liquid inlet flowrate, F_{N2}: N_2 flowrate; ΔP: pressure difference (P_{gas}-P_{liquid}); $C_{Ac,in}$: acetone concentration in the liquid inlet; $C_{Ac,out}$: acetone concentration in the liquid outlet of the reactor)

At same residence time, almost the same $C_{Ac,out}/ C_{Ac,in}$ is obtained regardless of the initial acetone concentration which is consistent with the model (Equation 7-6) according to which the ratio $C_{Ac,out}/ C_{Ac,in}$ should not change if all the other parameters are kept constant.

7.3.3.7 Acetone stripping with nitrogen bubbled in IPA

When acetone evaporated and was removed by nitrogen, isopropanol evaporated and was removed by nitrogen as well. The loss of isopropanol resulted in a more concentrated solution. For the asymmetric transfer hydrogenation, enantioselectivity decreases faster at high substrate concentration (Chapter 3). Therefore, it is important to top-up the reaction solution with isopropanol to keep the solution concentration constant. In order to top up IPA into the reactor system, two methods were emloyed.

First, an IPA top up plate is introduced to the two phase membrane contactor as shown in Figure 7-13:

Liquid out

Nitrogen out

Nitrogen in

Liquid in

IPA top up

Left Block   Gasket A   Membrane   Gasket B   Top-up   Right Block
plate

(a)

(b)
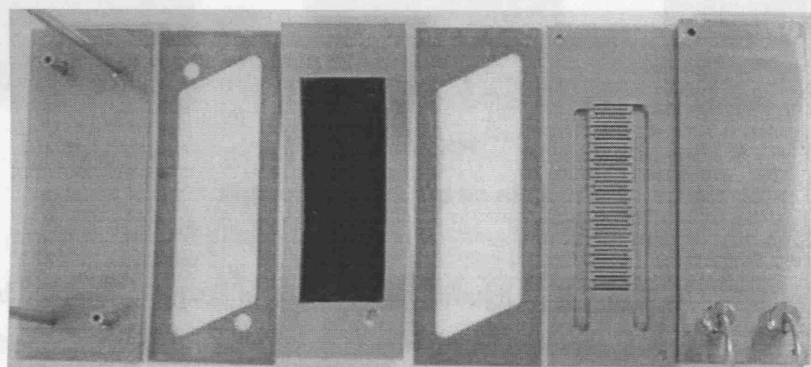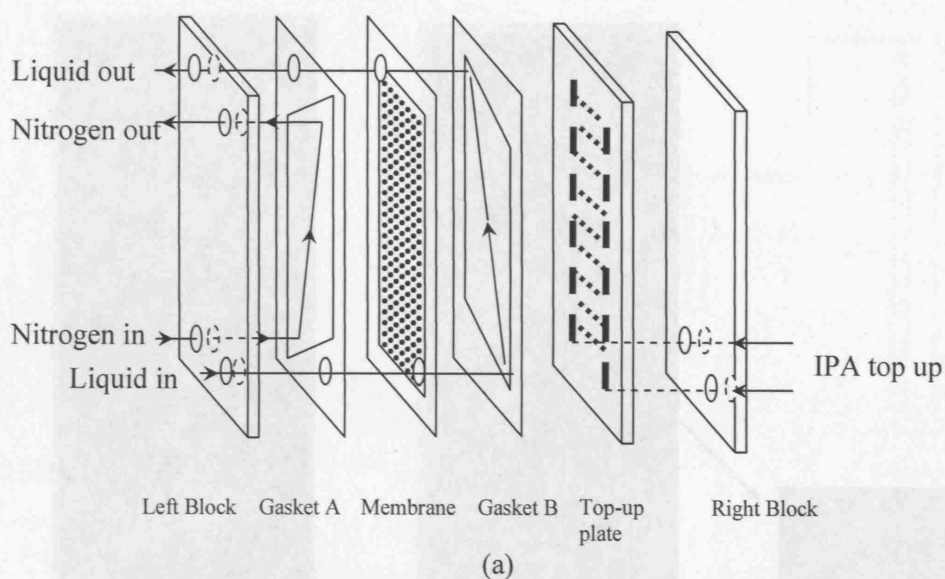
Figure 7-13 Configuration of the two phase membrane contactor with IPA top-up plate (a) schematic (b) picture of the disassembled contactor (membrane shown is laser mesh)

The top-up plate (Figure 7-14) is made of stainless steel. Two main channels with 4mm width, 2mm depth and 50mm length are divided into 44 sub-channels with 0.5mm width, 2mm deep and 10mm length. There are 200μm diameter holes in each sub-channel. IPA is topped up to the reaction solution through these holes. However, for this kind of configuration, the IPA distribution is not very uniform. Most IPA comes out from the holes in the channels on the top of the plate.

196

Front view   Back view
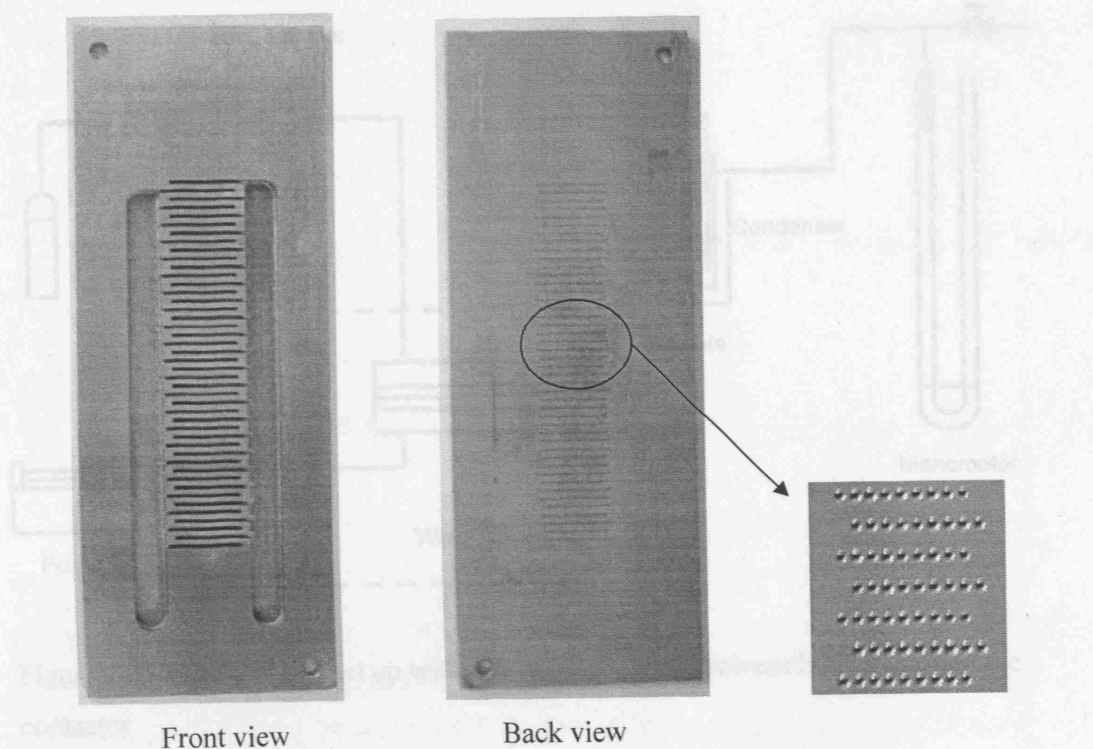
Figure 7-14 IPA top up plate

The second method is by passing the nitrogen through an IPA container (Figure 7-15). This is the easiest way to top-up isopropanol without changing the reactor configuration. Before nitrogen flows into the mesh reactor, it is fed by a 1.65mm ID PTFE tube to a cylindrical glass container (Volume: 250ml) which contains 150ml of pure isopropanol at 30°C. The container was placed in a water bath while the tubes were left in atmosphere at room temperature. Nitrogen bubbled in isopropanol, and then it entered the mesh reactor. Condensation of the IPA vapour was observed in the tube between the IPA container and mesh contactor which indicates that nitrogen was saturated with IPA at room temperature. However, it was not certain if nitrogen was saturated at 30°C when it just came out from the IPA container. The IPA condensed in the tube was carried by nitrogen and flowed into the mesh contactor, which might introduce an nonuniform IPA top-up mechanism in the system.

Mass Flow Controller

MFC

N₂

IPA

Pump

Water bath

Condenser

Sample

Manometer
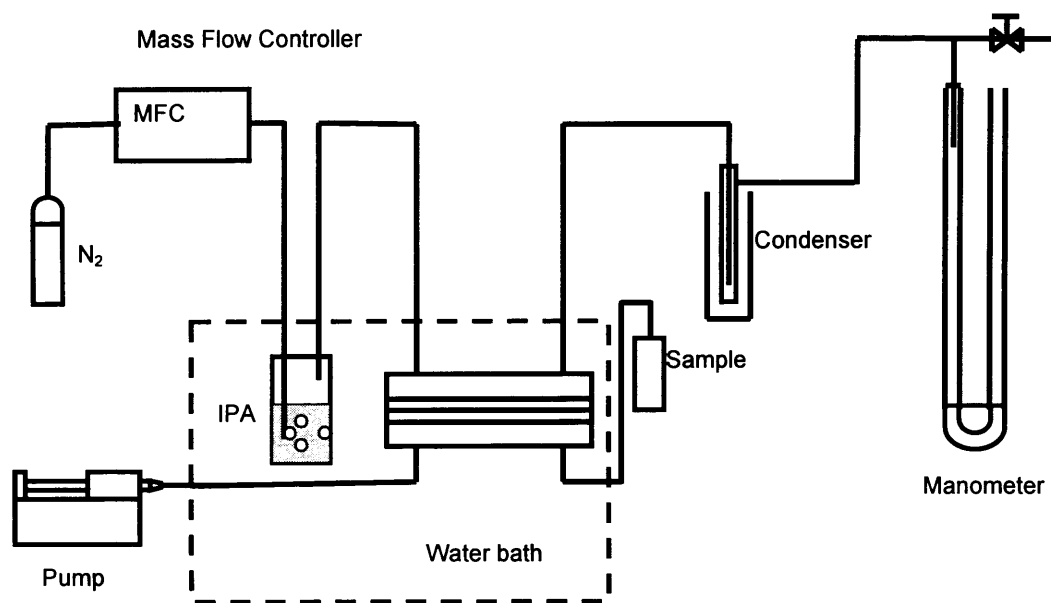
Figure 7-15 Experimental set up with nitrogen bubbled in solvent before entering the contactor

A comparison of acetone removal with dry nitrogen without IPA top-up and with IPA top up by nitrogen bubbled in isopropanol is summarised in Table 7-17.

Table 7-17: Effect of N_2 bubbled in IPA on acetone removal

N_2	F_{L-in}	F_{N2}	ΔP	$C_{Ac,in}$	$C_{Ac,out}$	F_{L-out}	Acetone removed
	ml/min	ml/min	mm H₂O	M	M	ml/min	mol/min
Dry	0.1	70	30	0.107	0.037	0.079	0.0077
	0.1	70	30	0.108	0.038	0.078	0.0079
Bubbled in IPA	0.1	70	30	0.102	0.044	0.098	0.0059
	0.1	70	30	0.102	0.045	0.097	0.0058

(Internetmesh; T=30°C; solvent: isopropanol; F_{L-in}: liquid inlet flowrate, F_{N2}: N_2 flowrate; ΔP: pressure difference ($P_{gas}-P_{liquid}$); $C_{Ac,in}$: acetone concentration in the liquid inlet; $C_{Ac,out}$: acetone concentration in the liquid outlet of the reactor; F_{L-out}: Liquid outlet flowrate)

The outlet liquid flowrate was measured by collecting the outlet flow for 35 minutes after starting the experiments. The sample vial was placed in an ice bath to prevent acetone evaporation. Acetone removed was calculated by a mass balance: $F_{removal}C_{Ac,removal} = F_{L-in} C_{Ac,in} - F_{L-out} C_{Ac,out}$. The outlet liquid flowrate could also be calculated based on the assumption that nitrogen was saturated after it flowed through the mesh reactor.

IPA mole fraction in the gas phase can be calculated as:

$$y = \frac{P^{Vap}}{P^{Total}} = \frac{8157}{101325} = 0.0805$$

IPA lost into the nitrogen stream can be calculated as

$$F_{N_2} \cdot \frac{P}{RT} \cdot y = 70 \times 10^{-6} \times \frac{101325}{8.314 \times 303} \times 0.0805 = 0.227 \times 10^{-3} \, mol/min = 0.017 ml/min$$

Therefore, the outlet liquid flowrate can be calculated as:

$$F_{L-out,cal} = 0.1 - 0.017 = 0.083 ml/min$$

which is close to the experimental value 0.079ml/min.

It can be seen that outlet acetone concentration is slightly higher, corresponding to less acetone being removed by using nitrogen bubbled in isopropanol. The possible reason is that both acetone and isopropanol were removed with dry nitrogen. Therefore, the flowrate decreased (see Table 7-17) and the residence time was extended. This can be independently confirmed by observing the outlet flowrate decrease. Overall, more acetone is removed with dry nitrogen. When the N_2 was saturated with IPA, there was no IPA concentration gradient, and hence the driving force for IPA mass transfer. The experimental results show that using nitrogen bubbled in isopropanol, the flowrates of the inlet and outlet of the reactor are almost the same, which indicates that solvent loss is avoided and the concentration of the reactant+products will be kept constant if it is applied to the asymmetric transfer hydrogenation of the acetophenone. However, from economic point of view, the recycle of the IPA in the N_2 flow has to be considered for operation in the large scale.

7.3.3.8 Comparison of acetone stripping in the batch reactor and micro-mesh contactor

Acetone removal was also conducted in the 500ml batch reactor. The reactor set up is the same as presented in Chapter 3. Temperature was controlled at 30°C by means of water bath. Nitrogen flowrate controlled at 800ml/min by a mass flow controller is introduced into the system through a frit. 800ml/min flowrate was chosen because the limitation for the mass flow controller is 1000ml/min. (70ml/min nitrogen flowrate was chosen in the mesh contactor due to the fact that the gas phase breakthrough to liquid phase took place at higher nitrogen flowrate). The reactor was filled with 250ml initially with 0.1M acetone concentration. Figure 7-16 shows the comparison of the

mesh reactor and batch reactor experiments. It can be seen that within 5 minutes about 90% of acetone was removed in the mesh reactor while only about 10% acetone was removed in the batch reactor.
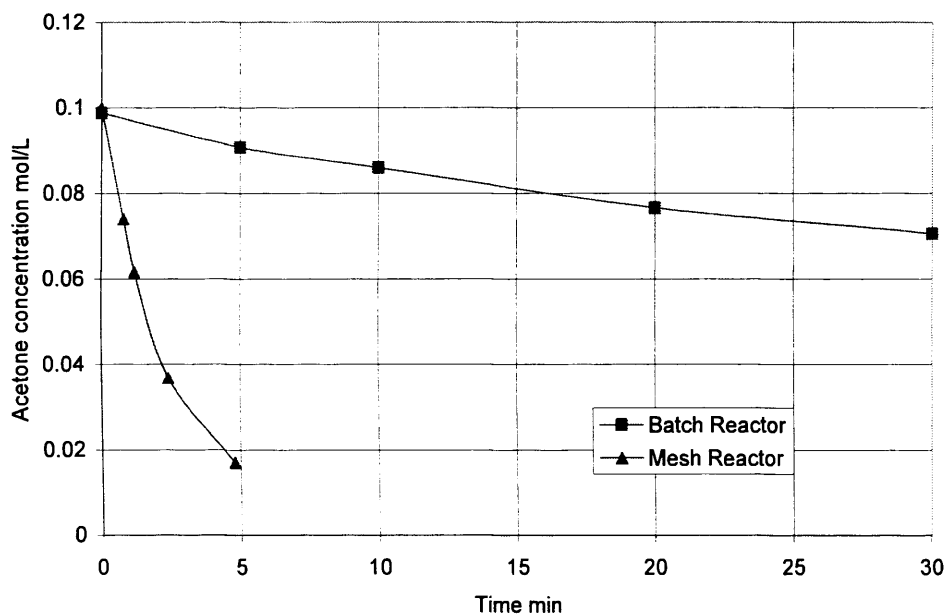
Figure 7-16 Comparison of acetone removal in batch and mesh contactors
(Mesh reactor: Dry N_2 flowrate: 70ml/min; ΔP=50mmH2O; Temperature=30°C;
Batch reactor: Dry N2 flowrate: 800ml/min; Liquid volume:250ml; temperature=30°C)

As shown in Chapter 5, acetone stripping in the batch reactor is determined by the ratio $\dfrac{F_{gas}}{K_{eq} \cdot V_l}$. The higher this ratio the better the acetone removal becomes. Since the equilibrium constant (solubility) is the same, a comparison between batch and membrane reactor should be provided in terms of $\dfrac{F_{gas}}{V_l}$. Therefore, for the residence time of $\tau = 5$ min :

Batch Reactor :
$$\frac{V_g}{V_l} = \frac{F_g \cdot \tau}{V_l} = \frac{800ml/min \cdot 5min}{250ml} = 16$$

Membrane Reactor
$$\frac{V_g}{V_l} = \frac{F_g}{F_l} = \frac{70ml/min}{0.05ml} = 1400$$

Two orders of magnitude of the ratio: gas amount/ liquid amount is provided in the mesh reactor which results in better acetone removal.

7.4 Asymmetric transfer hydrogenation in mesh reactor

7.4.1 Experimental set-ups

The schematic and picture of the assembled and disassembled reactor are given in 7-7. A schematic of the mesh reactor set up is shown in Figure 7-17. Two single-syringe infusion pumps (RAZEL A-99.FJZ) are used to drive the liquids through the reactor. 10ml of 0.00028M catalyst solution (prepared by 11.2mg rhodium complex and 5.6mg ligand in 125ml isopropanol) which is pumped by syringe pump 1 and substrate solution (containing 0.28M acetophenone and 0.00224M sodium isopropoxide in isopropanol) which is pumped by syringe pump 2 are premixed in a micromixer (Standard Slit Interdigital Micro Mixer SSIMM from IMM) before being fed into the mesh reactor. Flowrates of the both syringes were the same and varied in the range 0.01~0.3ml/min. Nitrogen gas which is controlled by a mass flow controller (MFC Model: Brooks 5850; flowrate range: 0-200ml/min; Readout Model: Brooks 0154/BC1A1) is introduced into the reactor. The liquid phase is kept separated from gas phase by a stainless steel mesh (Internetmesh, USA) whose characteristics are given in Table 7-1. The differential pressure between gas phase and liquid phase is controlled at the outlet of the gas phase by a metering valve (Swagelok) to prevent gas breakthrough to the liquid phase and liquid breakthrough to the gas phase. A manometer is used to measure the gas phase pressure. A start-up procedure was established where both sides of the reactor were filled with reaction solution, then nitrogen was introduced and its outlet pressure was adjusted so that the top reactor chamber was filled with gas and the gas-liquid interface stabilised inside the mesh. A condenser containing ice is used to condense the vapour in the gas phase. Temperature control is by means of a water bath. The sample vial (in the ice bath) is placed in such a way so that the exit of the liquid outlet tube is 2cm higher than the mesh. The sample is analysed by an Agilent 6890 GC system as described in Chapter 3.
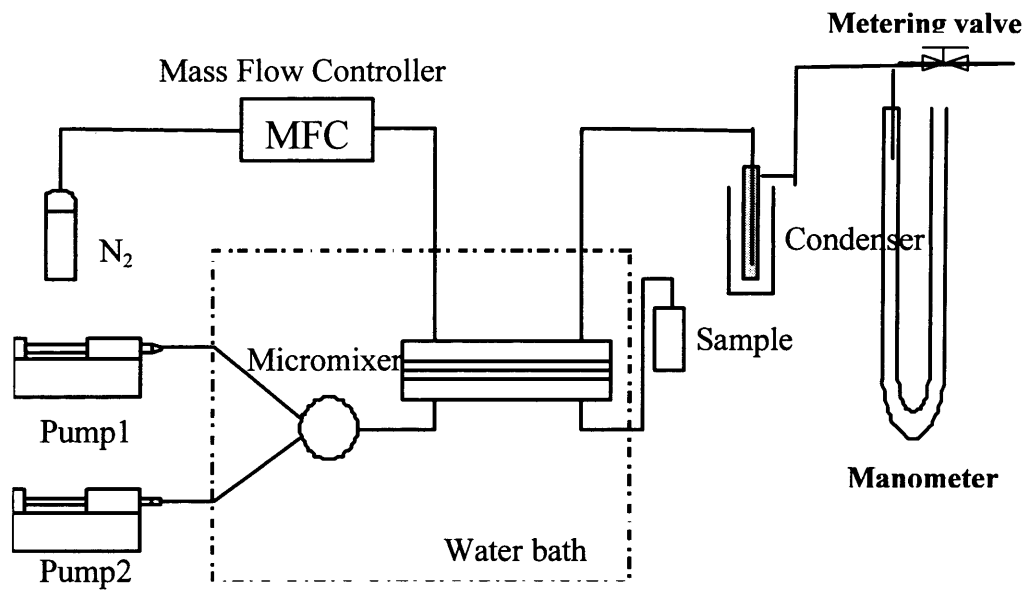
Figure 7-17 Experimental set up of the mesh reactor

A single phase plate reactor was used to established the base case where no stripping of acetone took place. It consists of top stainless steel plate (3×8×0.5cm), copper gasket (3×8×0.02cm outside and 2×6×0.02cm inside) and bottom stainless steel plate (3×8×0.5cm) (Figure 7-18). The gasket defined the liquid flow channel and no gas phase exists in the system.

Top Plate

Gasket

Bottom Plate

Figure 7-18 Schematic and picture of disassembled single phase plate reactor

The experimental set-up for the single phase plate reactor is shown in Figure 7-19. Two streams, (a) catalyst solution in IPA and (b) substrate and sodium isopropoxide solution in IPA, are mixed in a micromixer and then flow to the reactor. The residence time is determined by the liquid flowrate. The sample is collected from the outlet of the reactor and analysed by GC.

Figure 7-19 Experimental set up for single phase plate reactor

7.4.2 Results and discussion

7.4.2.1 Effect of acetone removal in different reactors

The experimental conditions in the mesh gas-liquid reactor, single phase plate reactor and batch reactor that was used for comparison are summarised in Table 7-18.

Table 7-18: Experimental conditions and reactor configurations for asymmetric transfer hydrogenation

Reaction conditions	Temperature=30°C; [Substrate]=0.33M; [Substrate]/[Catalyst] =1000; [Sodium isopropoxide]/[Catalyst]=8
Batch Reactor	N_2 flowrate=800ml/min, Reactor volume=500ml; Reaction solution volume=250ml.
Single Phase Reactor	Gasket dimension (Width×Length×Depth, cm)=3×8×0.02 (outside) and 2×6×0.02 (inside); Top and Bottom plate= 3×8×0.5; Reactor volume = 0.24ml; Inlet volume = 0.042ml; Outlet volume=0.031ml
Mesh Reactor	N_2 flowrate=70ml/min (bubbled in IPA); gasket dimension (Width×Length×Depth, cm) =3×8×0.02 (outside) and 2×6×0.02 (inside); Top and Bottom plate=30×80×5; Mesh: Internetmesh, stainless steel, 0.05mm thickness and 0.076mm average pore size; Liquid phase reactor volume=0.24ml; Gas phase reactor volume=0.24ml; Inlet volume=0.042ml; Outlet volume=0.031ml ; $\Delta P=P_G-P_L$ =30mmH$_2$O.

Note that the reaction takes place not only inside the reactors, but also in the tubing between the mixer and the reactor (inlet volume) as well as the reactor and the sample container (outlet volume). The residence time in the mesh reactor and single phase reactor is calculated as reactor volume (reactor liquid volume, liquid inlet and outlet volume) divided by liquid flowrate. The maximum residence time for the mesh reactor was ca 15 min. Beyond that it was difficult to start up the reactor and stabilise the gas-liquid interface. Because of reactor size and flowrate limitation, the maximum residence time that can be achieved in the single phase reactor was 30 minutes.

The experimental results for the batch reactor, single phase plate reactor and mesh reactor are compared in Figure 7-20.
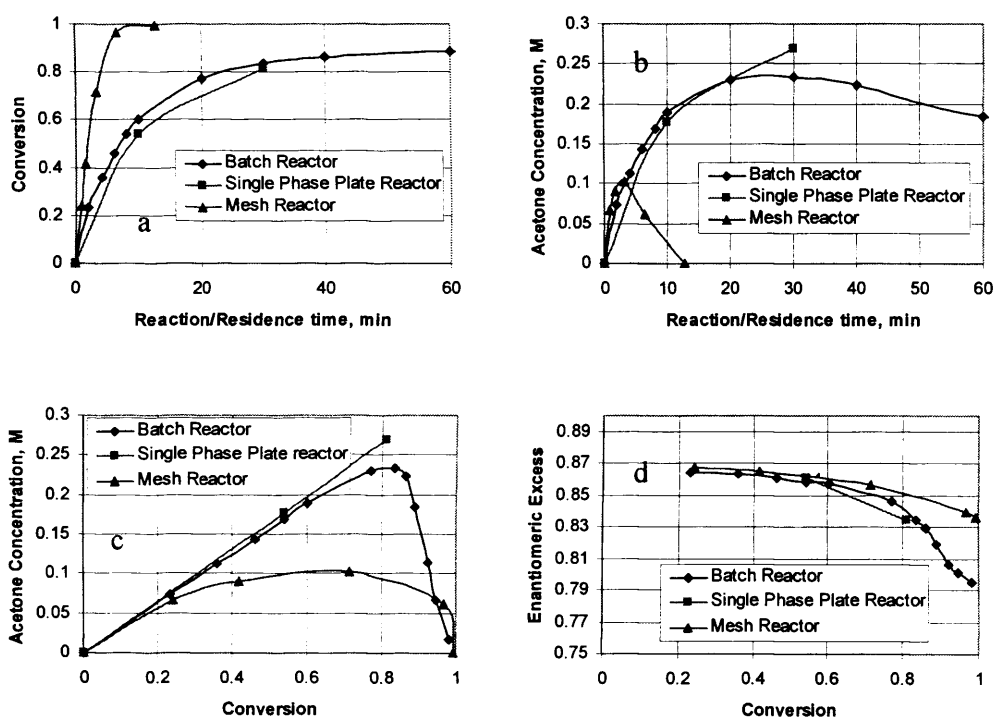
Figure 7-20 Comparison of batch reactor, single phase plate reactor and mesh reactor for asymmetric transfer hydrogenation; a: Conversion as function of time; b: Acetone concentration as function of reaction/residence time; c: Acetone concentration as function of conversion; d: Enantiomeric Excess as function of conversion (Temperature: 30°C, [Substrate]: 0.33M, [Substrate]/[Catalyst]=1000, N_2 bubbled in IPA in mesh reactor. For more details, see Table 7-18)

Figure 7-20a shows conversion as function of residence time for the asymmetric transfer hydrogenation in different reactors. In the mesh reactor, the reaction reached about 100% conversion within 15 minutes. In batch reactor, only 88% conversion is

obtained in 60 minutes, and it takes more than three hours to complete the reaction. In single phase reactor, almost the same conversion was obtained in 30 minutes as the batch reactor. The fact that fastest reaction rate was obtained in the mesh reactor is due to the fastest acetone removal from the reaction system. This can be confirmed from Figure 7-20b and Figure 7-20c. The batch reactor showed slightly better performance than the single phase plate reactor because in the latter no acetone removal occurred. However, the two reactors showed similar performance which is related to similar acetone concentration profiles (see Figure 7-20 b and c).

Figure 7-20c shows acetone concentration at reactor outlet for mesh reactor and single phase plate reactor or at reaction time t in the batch reactor as function of conversion. In the single phase plate reactor, acetone concentration keeps increasing due to the fact that no acetone removal takes place. In the batch reactor, the acetone concentration keeps increasing before reaching 85% conversion, and then it decreases afterwards and reaches almost zero concentration in three hours. The peak acetone concentration in the batch reactor is about 0.23M which happens at about 85% conversion. The possible reason is that the reaction rate is very fast in the beginning of the reaction and acetone removal rate is relatively slow, therefore, acetone concentration increased. When the reaction continued, the decrease of the reactant concentration and the increase of products concentration result in decrease of the reaction rate. The increase of acetone amount produced results in the increase of the acetone removal rate. When the acetone removal rate is faster than acetone producing rate, acetone concentration decreases. Therefore, a maximum in acetone concentration occurred. In the mesh reactor acetone concentration keeps increasing to 0.1M and decreases afterwards. In less than 15 minutes, the acetone concentration reaches zero (Figure 7-20b). The acetone concentration in the batch reactor is very close to that of the single phase plate reactor before 60% conversion which indicates that not much acetone has been removed in the batch reactor. However, significant amount of acetone has already been removed before 60% conversion in the mesh reactor. The peak acetone concentration has been significantly reduced from 0.23 M to 0.1M in the mesh reactor and it has been brought forward to about 70% conversion in the mesh reactor.

Figure 7-20d shows enantioselectivity as function of conversion in different reactors. It can be seen that the same initial enantioselectivity was obtained in all reactors, which is probably because in the beginning of the reaction acetone removal rate is too low as compared to the reaction rate to affect the initial enantioselectivity. Furthermore, no products are available in the beginning of the reaction where backwards reaction with acetone would erode the enantioselectivity. The enantioselectivity decreased with conversion in all cases, especially after 80% conversion. However, the final enantioselectivity varies significantly in different reactors. The highest final enantioselectivity was obtained in the mesh reactor. The possible reason for this is that in the mesh reactor acetone was removed most efficiently encouraging the forward reaction (acetone reacting with isopropanol to give phenylethanol and acetone) and preventing the backward reaction (acetone reacting with phenylethanol to give isopropanol and acetophenone). Moreover, because the reaction is complete in 15 minutes in the mesh reactor, there is not enough time for the backward reaction to take place.

7.4.2.2 Effect of substrate concentration at constant catalyst/substrate ratio in the mesh reactor

Batch reactor experimental results showed that enantioselectivity decreased faster with conversion at higher substrate initial concentration. Therefore, it seems to be preferable to perform asymmetric transfer hydrogenation in dilute solutions. However, from economic point of view, it is better to run the reaction at high substrate concentration. Efficient acetone removal achieved in the mesh reactor might be able to prevent the backwards reaction, thus preventing the enantioselectivity decreasing. Thus, experiments with different initial substrate concentration at constant substrate/catalyst concentration ratio have been conducted in the mesh reactor. The results are summarised in Figure 7-21.

Figure 7-21a shows the conversion as function of residence time for different initial substrate concentrations. It can be seen that when the substrate concentration is 0.14M, the conversion reached 90% conversion within 15 minutes in the mesh reactor. When the substrate concentration increased to 0.33M, reaction rate became much faster and 96% conversion was reached within 7 minutes. However, when the substrate concentration was further increased to 0.5M, the reaction rate decreased and the

results are similar to the substrate concentration at 0.14M. The possible reason for these is that at substrate concentration 0.14M, the reaction solution is very dilute and acetone removal does not have big effect on the reaction conversion. When the substrate concentration is 0.5M, the acetone removal is not efficient enough; there is still a large amount of acetone left in the reaction solution (see Figure 7-21b). In the batch reactor, there was no significant effect on the conversion when the initial substrate concentration increased from 0.14M to 0.33M. This is still due to the acetone removal effect as mentioned above. However, acetone removal is less efficient in the batch reactor than in the mesh reactor, therefore, conversion with 0.33M initial substrate concentration is only close to the conversion with 0.14M substrate concentration in the batch reactor. Conversion with 0.33M initial substrate concentration is higher than the conversion with 0.14M substrate concentration in the mesh reactor indicating that the optimal interaction between acetone removal and reaction rate is achieved close to 0.33M.

Figure 7-21b shows acetone concentrations as function of reaction time and Figure 7-21c show acetone concentrations as function of conversion in the mesh reactor and batch reactor. A similar trend is observed in both mesh reactor and batch reactors. Higher acetone concentrations are obtained with higher substrate initial concentrations. However, acetone concentration is much lower in the mesh reactor than in the batch reactor due to more efficient acetone removal in the mesh reactor.

Figure 7-21d shows enantioselectivity as function of conversion for different initial substrate concentrations. The initial enantioselectivity is similar for all cases in both mesh reactor and batch reactor. The final enantioselectivity decreased with increase of the initial substrate concentration, which is similar to the batch reactor experiments. The enantioselectivity decrease rate became faster with conversion at higher initial substrate concentration which indicates that the effect of the backwards reaction became more significant at higher initial substrate concentrations due to presence of more acetone and phenylethanol in the reaction solution (Figure 7-21c).
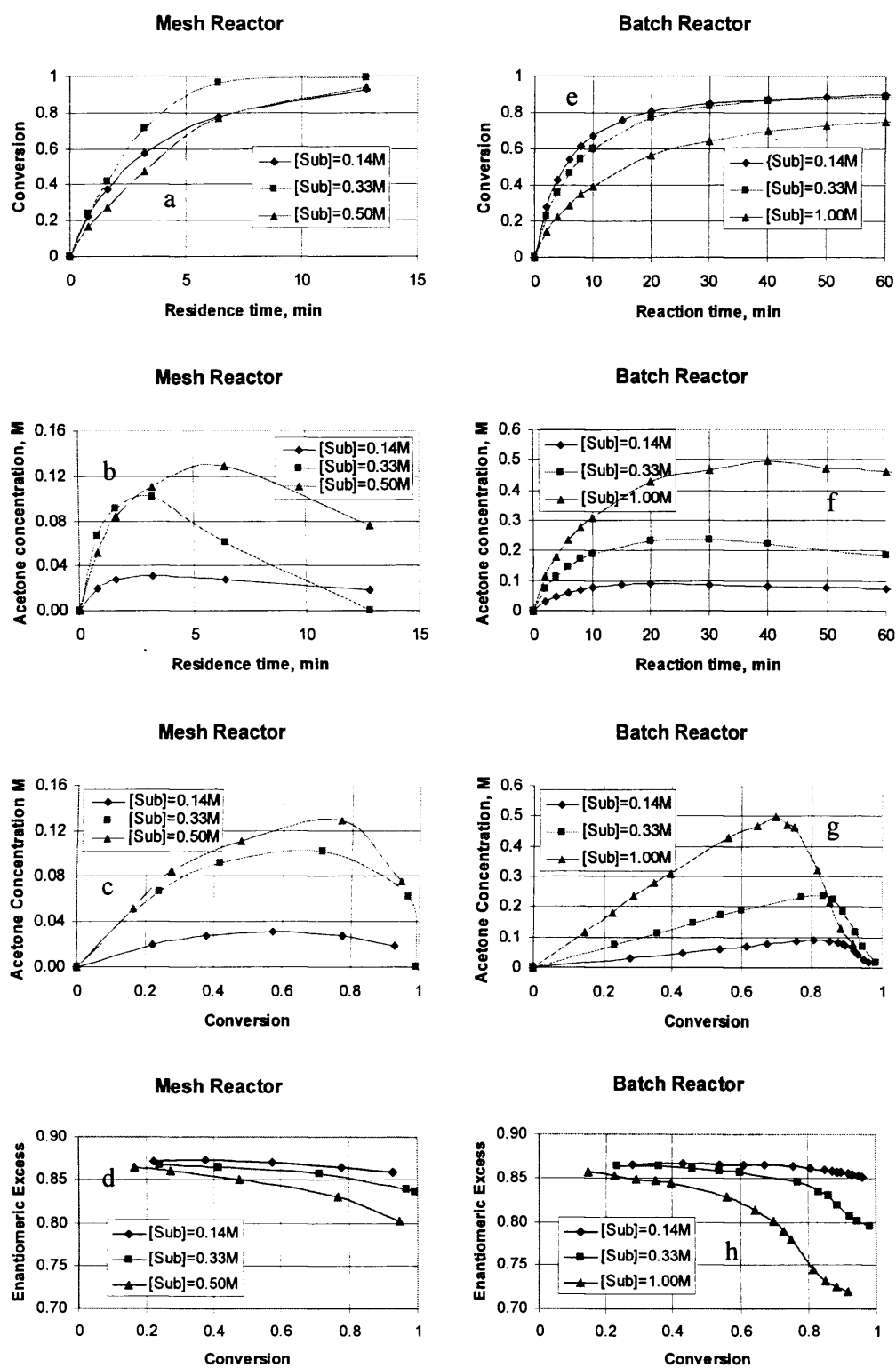
Figure 7-21: Effect of substrate concentration at constant catalyst/substrate ratio
a: Conversion as function of time; b: Acetone concentration vs. residence time;
c:Acetone concentration vs. conversion; d: Enantiomeric excess as function of
conversion (Temperature: 30°C, Nitrogen flowrate: 70ml/min, bubbled in IPA,
[substrate]/[catalyst]=1000)

7.4.2.3 Effect of substrate concentration at constant catalyst concentration in the mesh reactor

The catalyst used for the asymmetric transfer hydrogenation is organometallic catalyst which is often very expensive. It will be more economical if one could utilise the same amount of organometallic catalyst to catalyze the asymmetric transfer hydrogenation reaction with higher substrate concentrations. In this series of experiments, the catalyst concentration was kept constant, while two substrate concentrations were examined (0.14M and 0.28M). The results obtained in terms of conversion, acetone concentration and e.e. are given in Figure 7-22.

Similar to batch reactor experimental results (Figure 7-22a), it can be seen that much higher conversion was obtained at 0.14M substrate concentration due to catalyst/substrate ratio (1:1000) which is two times higher than at 0.28M substrate concentration (1:2000). However, the average catalyst turnover frequency (TOF) for the reaction with 0.28M substrate concentration in the first 13 minutes is $6230hr^{-1}$ which is higher than $4364hr^{-1}$, at 0.14M substrate concentration in the mesh reactor. This is due to more efficient acetone removal taking place with 0.28M substrate concentration which increases the reaction rate. However, in the batch reactor, very similar catalyst TOF $3712hr^{-1}$ and $3691hr^{-1}$ are achieved for the reaction with 0.28M and 0.14M substrate concentration respectively within the first 10 min. This indicates acetone removal is poor in the batch reactor even at higher substrate concentration.

Figure 7-22c shows that more acetone was present at 0.28M substrate concentration before 60% conversion. However, this is reversed above 60% conversion. This can be explained by the residence time difference for reaching 65% conversion for the two different substrate concentrations. For 0.14M substrate concentration this time is less than 5 min while it takes 12 min to reach it with 0.28M substrate concentration. In 7 min significant amount of acetone has been removed in the experiments with 0.28 M which results in lower acetone concentration in the reaction solution (Figure 7-22c). Another way of demonstrating the more efficient acetone removal for 0.28M substrate concentration is by looking at Figure 7-22c, where the acetone produced is also shown, assuming a 1:1 substrate: acetone stoichiometry. The difference between acetone in solution and acetone produced is the amount of acetone removed, which is clearly larger for 0.28M substrate concentration specially for residence time larger than 4min.

Figure 7-22d indicates that higher e.e. was obtained for low substrate concentration at the same conversion. The possible reason is that the products concentration produced is higher at the same conversion with higher substrate initial concentration, which favoured the backwards reaction and decreased the e.e.. Another reason is that to reach the same conversion, a longer time is needed at high substrate concentration, which might decrease the e.e. as well.

Three sets of experiments with the same batch of catalyst and one week old sodium isopropoxide solution were conducted in the same day in the mesh reactor with 0.28M substrate concentration to check the reproducibility. Conversion was reproducible within ±2.8%, e.e. was reproducible within ±0.2% and acetone concentration was reproducible within ±4.5% as shown in Figure 7-23.
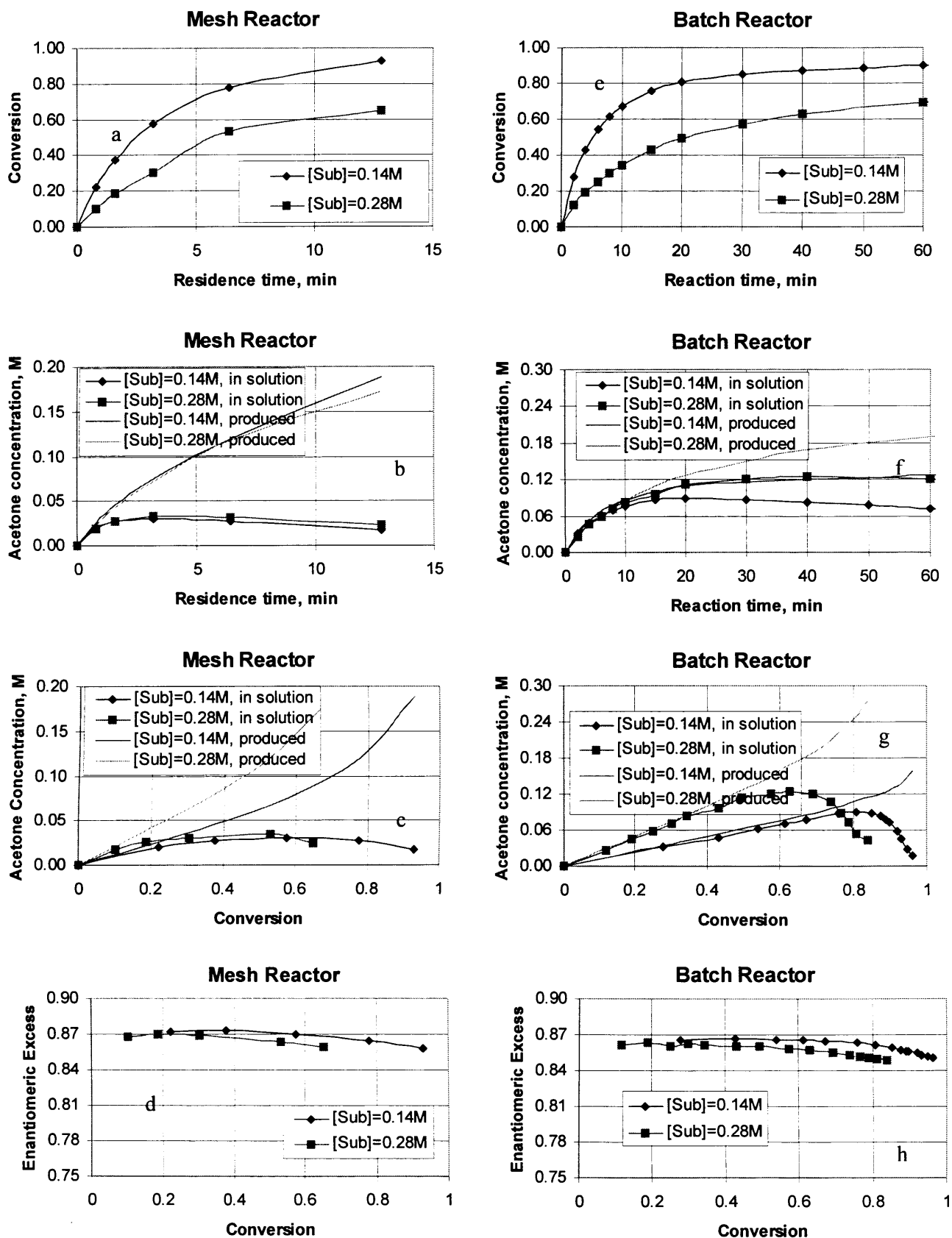
Figure 7-22 Effect of substrate concentration at constant catalyst concentration
a: Conversion as function of time; b: Acetone concentration vs. residence time;
c: Acetone concentration vs. conversion; d: Enantiomeric excess as function of
conversion (Temperature: 30°C, Nitrogen flowrate: 70ml/min, bubbled in IPA,
[Catalyst]: 0.00014M)
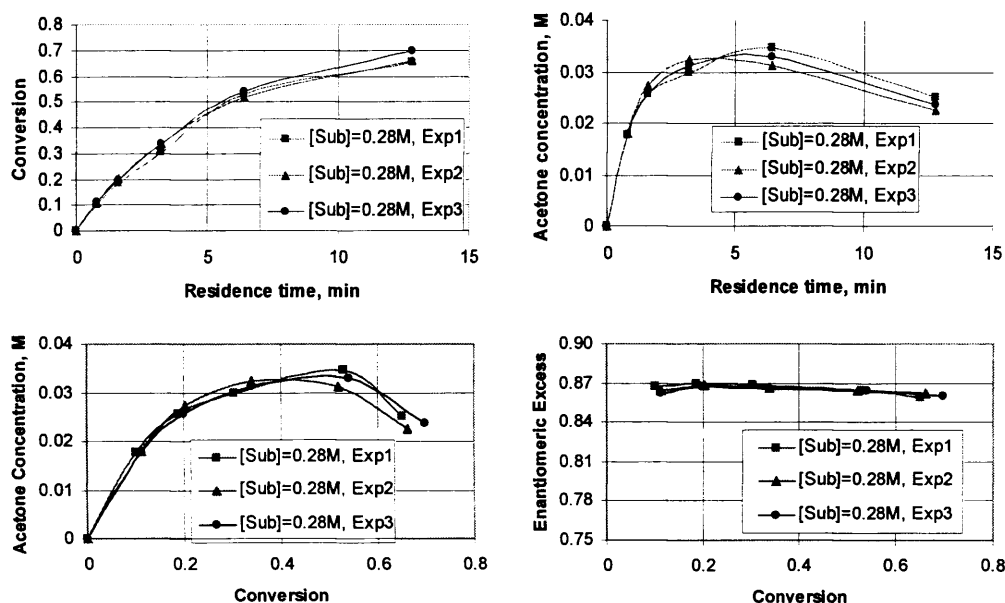
Figure 7-23 Reproducibility of experiments in the mesh reactor a: Conversion as function of time; b: Acetone concentration vs. residence time; c: Acetone concentration vs. conversion; d: Enantiomeric excess as function of conversion (Temperature: 30°C, Nitrogen flowrate: 70ml/min, bubbled in IPA, [Substrate]=0.28M, [Catalyst]=0.00014M)

7.4.2.4 Effect of temperature in the mesh reactor

In order to reach higher initial enantioselectivity, the asymmetric transfer hydrogenation has to be conducted at lower temperature. Experiments were conducted under different temperatures to study the effect of temperature on catalyst activity/selectivity. The results are shown in Figure 7-24.

It can be seen that with increasing reaction temperature, the initial reaction rate increased as expected (Figure 7-24a). At 40°C albeit faster initial reaction rate, conversion dropped below that at 30°C at the same residence time, indicating catalyst deactivation. Compared with batch reactor experimental results at 15°C, higher reaction rate was obtained in the mesh reactor, still due to the efficient acetone removal (Figure 7-24b). However, due to the residence time limitation in the mesh reactor, only 13 minutes residence time can be reached in continuous mode.

In order to achieve longer residence time, stop-flow mode was applied in the mesh reactor. The reaction solution was pumped through the reactor with 0.1ml/min total flowrate and N_2 flowed through the reactor at 70ml/min. When the operation reached steady state, the liquid pumping was stopped while N_2 flowrate was still kept at 70ml/min. After 60 minutes, the gas phase outlet was closed and liquid inside the reactor was pushed out by N_2 to the liquid outlet where a sample was collected. Lower acetone concentration was obtained in the stop-flow mode than in the batch reactor which is due to the fact that much higher ratio of gas flowrate to liquid volume was used in the stop-flow mode. However, compared to continuous flow, acetone concentration was higher with stop-flow mode which is probably due to the fact that no removal of acetone took place in the reactor dead zones (i.e. reactor exit tube, volume 0.031ml) which do not come in contact with gas phase when operated in stop-flow mode in the mesh reactor. The same conversion as the batch reactor for the same reaction time was obtained in the stop-flow mode although much lower acetone concentration was obtained. This is probably due to the fact that more isopropanol was lost in the stop-flow mode which resulted to highly concentrated solution. Hence, conversion was lower due to high concentration. Moreover, highly concentrated solution resulted in slightly lower e.e in the stop-flow mode as well. It is worth emphasizing that the batch reactor was operated with 800ml/min nitrogen flowrate.
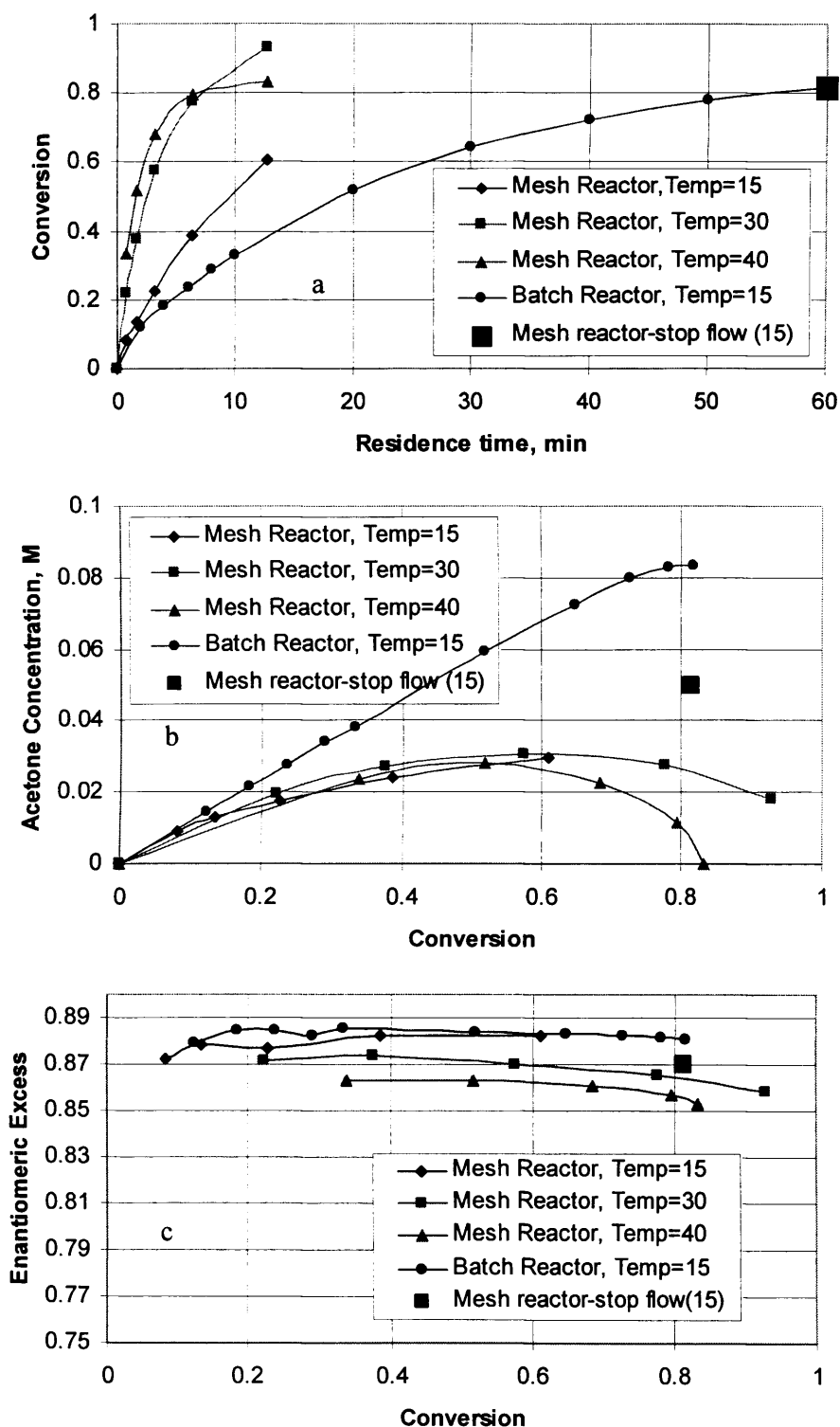
Figure 7-24: Effect of temperature on the reaction in the batch and mesh reactor
a: Conversion as function of time; b: Acetone concentration as function of conversion; c: Enantiomeric excess as function of conversion; ([Substrate]: 0.14M, Nitrogen flowrate: 70ml/min, bubbled in IPA)

Figure 7-24b shows acetone concentration as function of conversion. Up to 60% conversion, similar acetone concentration was obtained for all reaction temperatures in the mesh reactor. Theoretically, 0.084M acetone should be produced at 60% conversion if there was no acetone removal from the system. However, only 0.030M acetone remained in the system. Hence, about 60% of the acetone produced was removed at 60% conversion. In order to reach 60% conversion, it took 2 minutes at 40°C, 4 minutes at 30°C and 13 minutes at 15°C in the mesh reactor (Figure 7-24a). Therefore, much faster acetone removal was achieved at higher temperature. The possible reason is that at lower temperature, the vapour pressure of acetone became smaller. Figure 7-25 shows vapour pressure as function of temperature for acetone, isopropanol, substrate and product (The data were obtained from the software Component Plus 3.4.0.1, Pure Component Database Manager, Prosim Sa, www.prosim.net). The stripping of acetone became more difficult at low temperature. In this case, operation under vacuum will be ideal solution. However, because of IPA's strong mesh wettability, applying vacuum in the mesh reactor will result in breakthrough of the liquid phase to gas phase.
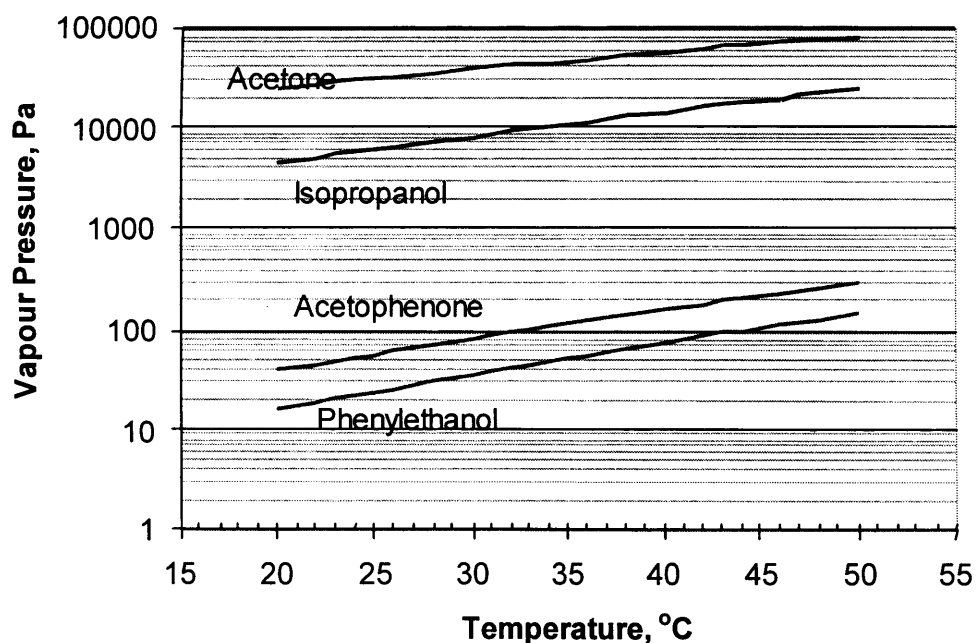
Figure 7-25 Vapour pressure as function of temperature for acetone, isopropanol, acetophenone and phenylethanol

Similar to the batch reactor experimental results (chapter 3), e.e. decreased with increase of the temperature (Figure 7-24c).

7.4.2.5 Effect of substrate concentration at lower temperature in the mesh reactor

As shown earlier enantioselectivity decreases with increase of substrate concentration and increases with decrease of temperature. Higher substrate concentration is preferred from cost point of view. Therefore, experiments with high substrate initial concentration at lower temperature were attempted to increase the enantioselectivity at high substrate initial concentration. The catalyst/substrate ratio was kept constant at 1:1000 while two substrate concentrations, 0.14M and 0.50M were examined at 15°C. The results are summarized in Figure 7-26.

Similarly to batch reactor experimental results (chapter 3), Figure 7-26a shows that lower conversion was obtained at high substrate concentration. This is probably due to the fact that a large amount of products were produced at higher substrate concentration which favoured the backwards reaction. Acetone concentration as function of conversion is plotted in Figure 7-26b. For 0.14M substrate concentration, acetone concentration increased with conversion which indicates that acetone production rate is faster than the acetone removal rate. For 0.5M substrate concentration, acetone concentration increases up to 30% conversion, which indicates that reaction rate is faster than the acetone removal rate at this stage, then it decreased which is due to acetone removal rate becoming faster than the acetone producing rate. There was a maximum in acetone concentration at 0.5M substrate concentration at about 30% conversion while there was not at 0.14M substrate concentration. This is because the residence was not long enough for acetone to reach maximum concentration with 0.14M substrate initial concentration.
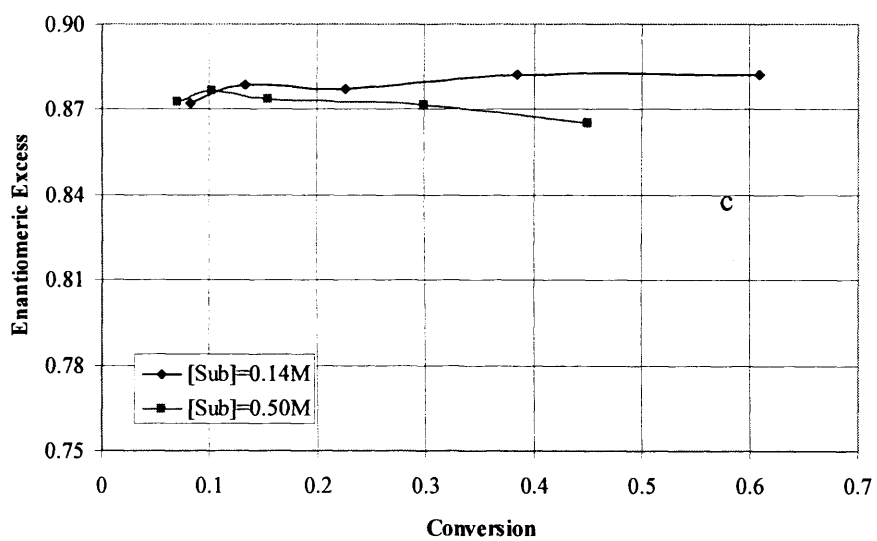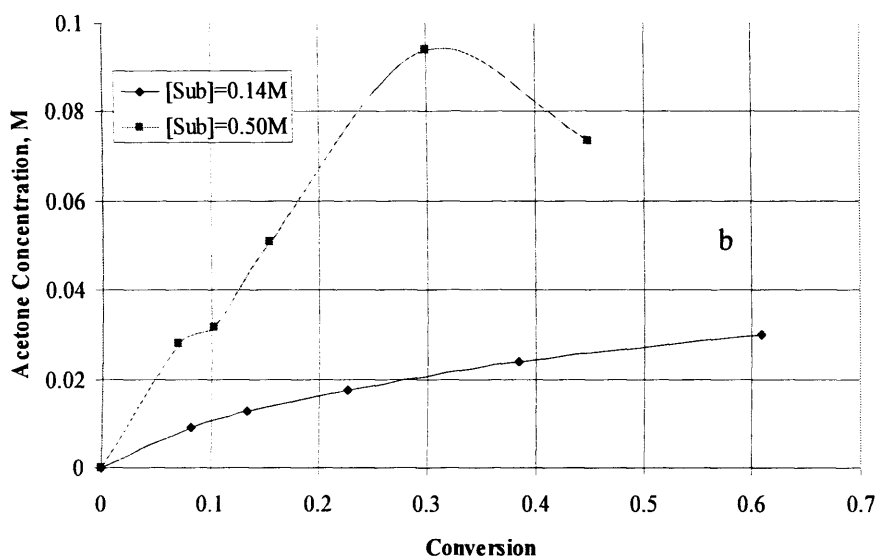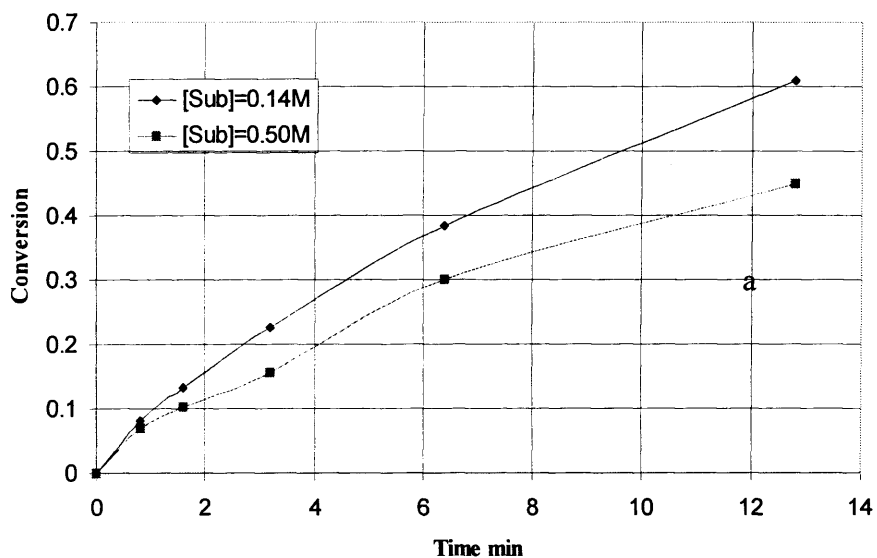
Figure 7-26 Effect of substrate concentration in the mesh reactor at 15°C
a: Conversion as function of time; b:Acetone concentration vs. conversion; c: e.e. as function of conversion. (Nitrogen flowrate: 70ml/min, bubbled in IPA; [Substrate]/[Catalyst]=1000)

Figure 7-26c shows the e.e. as function of conversion. It can be seen that the same initial e.e. was obtained with different substrate concentrations. e.e. dropped much faster with conversion at high substrate concentrations. Similar behaviour was observed at 30°C (see Figure 7-21). As can be seen from Table 7-19, e.e. dropped 0.7% and 1.2% in 12 minutes with [Substrate]=0.14M and 0.5M at temperature 15°C respectively. While at 30°C, e.e. dropped 1.4% and 6.1% in 12 minutes with [Substrate]=0.14M and 0.5M respectively. The reaction rate was higher at higher temperature, but e.e. dropped faster at higher temperature as well. Higher substrate concentration also results in lower e.e.. Comparing performance at 15°C with that obtained at 30°C, e.e. improved, but to the detriment of large reaction times. In order to select optimal reaction conditions, one must take both reaction rate and e.e. drop into consideration.

Table 7-19 Enantiomeric excess obtained for different temperature and substrate initial concentrations in the mesh reactor

Temperature °C	Concentration M	Conversion %	e.e. %	Time min	e.e. drop %
15	0.14	8	87.7	12	0.7
		60	87.0		
	0.5	10	87.7	12	1.2
		45	86.5		
30	0.14	22	87.2	12	1.4
		93	85.8		
	0.5	16	86.4	12	6.1
		95	80.3		

(Nitrogen flowrate: 70ml/min, bubbled in IPA; [Substrate]/[Catalyst]=1000, time is the time needed from conversion 1 to conversion 2; e.e. drop is the difference between e.e. at convesion 1 and e.e. at conversion 2)

7.4.2.6 Effect of different IPA concentration in the sweeping gas

During acetone evaporation, part of isopropanol is simultaneously evaporated if the isopropanol partial pressure in the sweeping gas is lower than isopropanol vapour pressure. Isopropanol evaporation will concentrate the reaction solution which will lead to reduction of the e.e.. Therefore, hindering the solvent loss can keep concentration constant and improve reaction performance. Using nitrogen bubbled in isopropanol prevents the solvent loss. In this series of experiments, dry nitrogen, nitrogen bubbled in isopropanol at 21°C and at 30°C were used as sweeping gas. The

temperature of isopropanol was controlled by a waterbath and the connecting tube was at room temperature. The results are summarized in Figure 7-27.

Conversion as function of time is plotted in Figure 7-27a. It can be seen that the conversion obtained with different IPA concentration in nitrogen are almost the same. The possible reason is the following. The residence time in Figure 7-27 is calculated as reactor volume divided by liquid inlet flowrate. In the experiment with dry N_2, some isopropanol was consumed to saturate the dry N_2, which results in longer real residence time in the reactor. Longer residence time results in higher conversion. The loss of isopropanol concentrated the reaction solution which results in higher products concentration. Higher products concentration favours backwards reaction and thus results in lower conversion. In the experiments with N_2 enriched with IPA, the reaction mixture volume remains constant and lower acetone concentration decreases the backwards reaction rate and thus increases conversion. Hence, these effects may compensate each other.

Figure 7-27b shows acetone concentration against conversion. Higher acetone concentration was obtained with dry nitrogen as sweeping gas. In the experiments using nitrogen bubbled with isopropanol, acetone concentration increased to a maximum, then decreased. Acetone concentration kept increasing in the experiments using dry nitrogen, which may result from the fact that isopropanol loss concentrated the reaction solution.

Different final e.e. was obtained with different IPA concentration in nitrogen (Figure 7-27c). The lowest e.e. was obtained by using dry nitrogen and the highest e.e. was obtained by using nitrogen bubbled in 30°C isopropanol. This can be explained by the final reaction solution concentration. Using dry nitrogen, nitrogen bubbled in 21°C isopropanol and nitrogen bubbled in 30°C isopropanol, although the initial concentrations are 0.14M which is same for all the cases, the final reaction solution concentrations (acetophenone+phenylethanol) are 0.25M, 0.20M and 0.14M, respectively. Because high product concentration favoured backwards reaction, e.e. dropped fast at high concentrations.
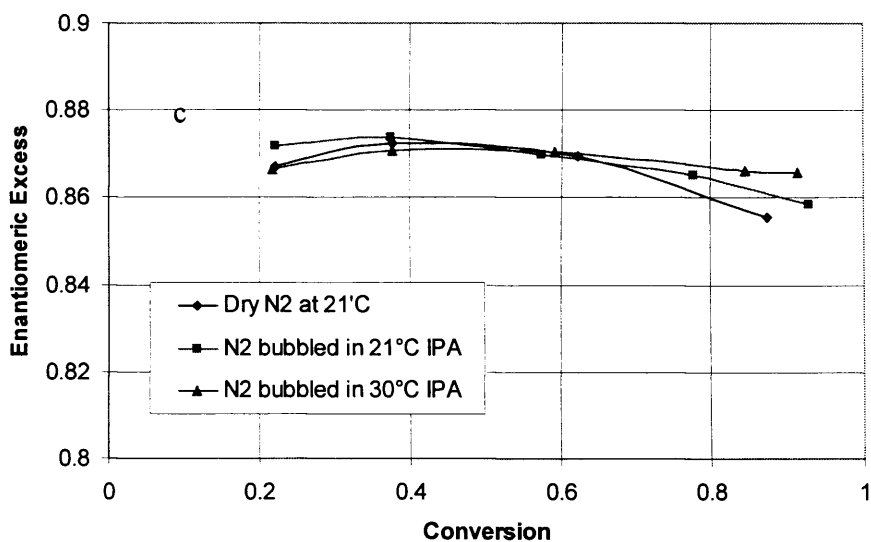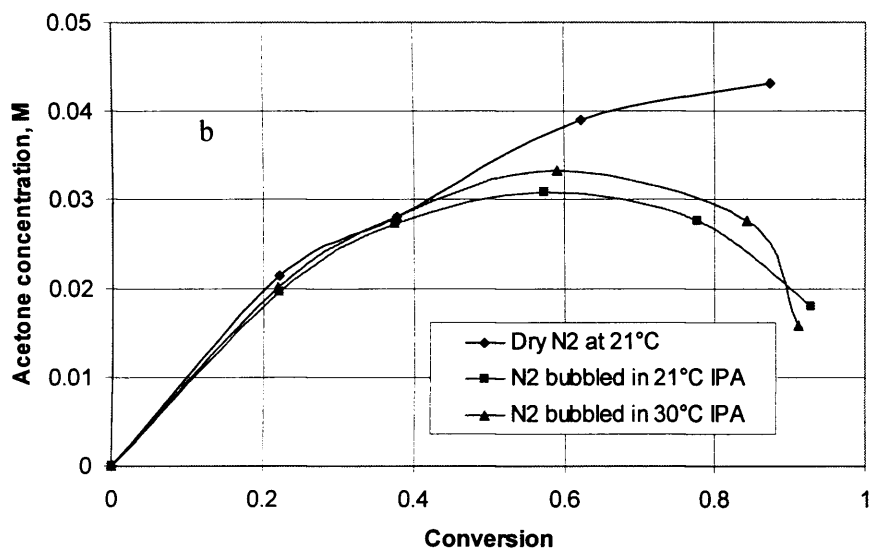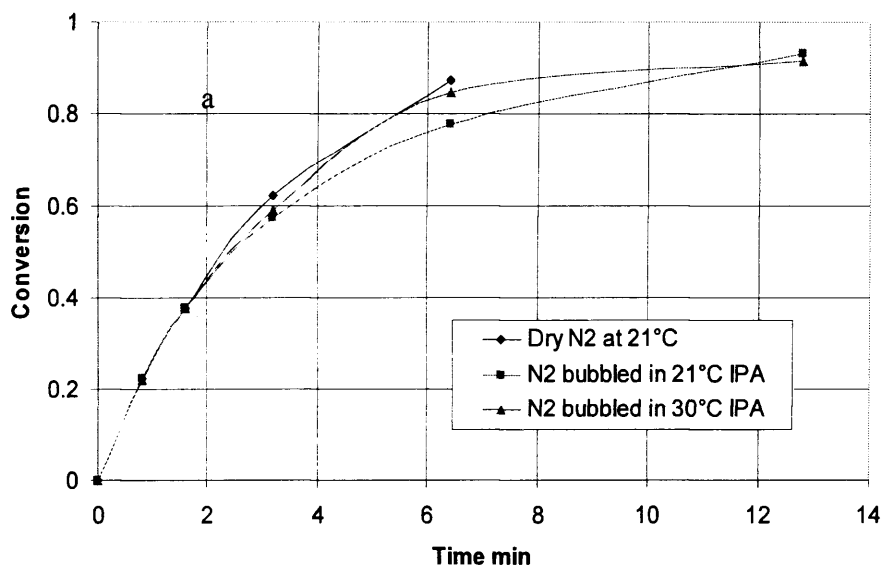
Figure 7-27 Effect of IPA content in nitrogen used as sweeping gas for asymmetric transfer hydrogeantion. a: Conversion as function of time; b: Acetone concentration as function of conversion; c: e.e. as function of conversion. (Reaction temperature: 30°C, N_2 flowrate: 70ml/min, [Substrate]: 0.14M; [Substrate]/[Catalyst]=1000)

7.5 Preliminary investigation of scale out and scale up of the micro-mesh reactor

7.5.1 Preliminary investigation of scale out

Current batch reactor technology is based on the scale-up of successful lab-scale reactions. However, at each stage of the scale-up, the use of larger reactors results in changes to the surface-to-volume ratios, which in turn can affect the thermal and mass-transport properties of the system. As a result of these variations it is often necessary to re-optimise the process at each stage of the scale-up process, a route both costly and time consuming. When using micro-fluidic systems, conversely, a reaction is first optimised using a single microreactor. To increase production volume, the number of reactors is simply increased using an approach referred to as scale-out or numbering up. Consequently, a reaction is only optimised once and all subsequent reactors are controlled using the same operating conditions. This approach is therefore cost-effective, time-efficient, and flexible, enabling changes in production volume by simply increasing or decreasing the number of reactors employed (Appleyard 2005).

In this work, scale out of the micro-mesh reactor was investigated. A pile-up micro-mesh reactor with five meshes was integrated. Figure 7-28 shows a pile-up micro-mesh reactor with two meshes for simplification.
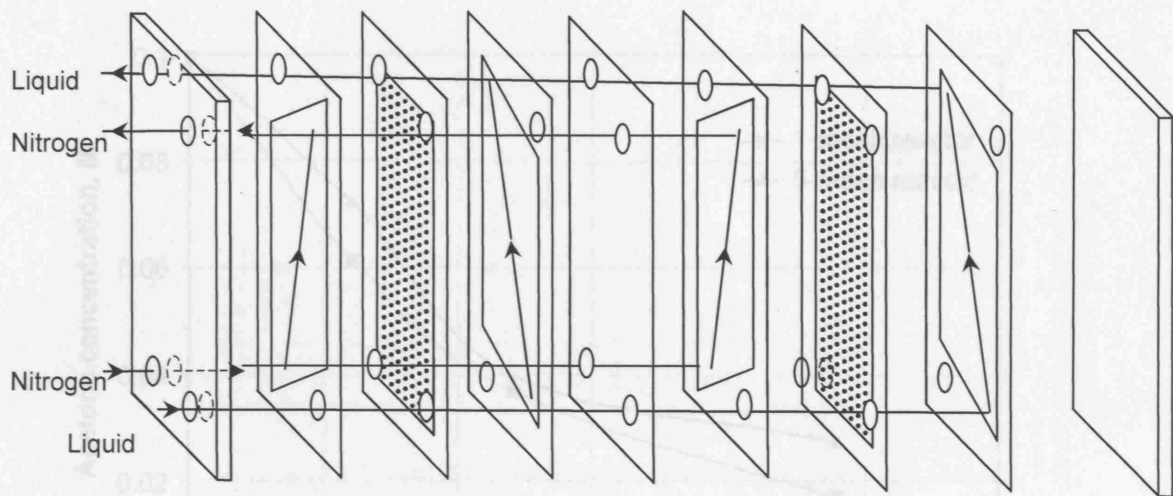
(a)
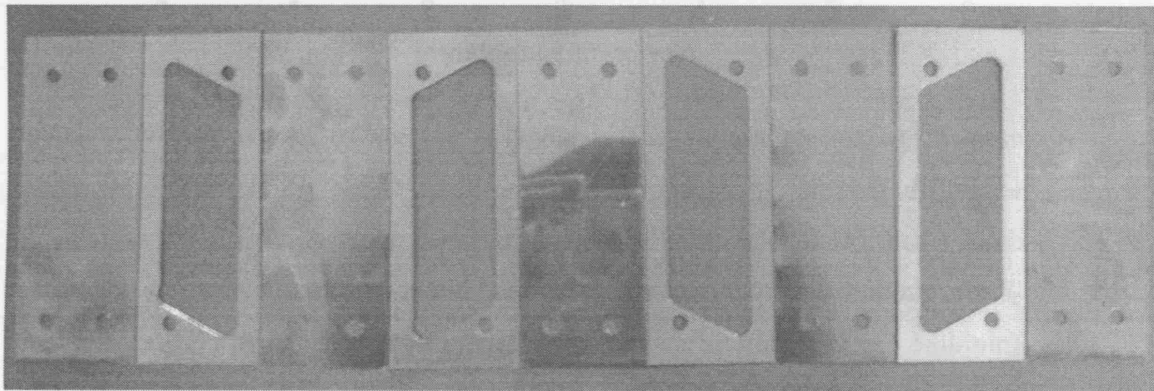
(b)

Figure 7-28 Configuration of the pile-up micro-mesh reactor (a) Schematic, (b) Picture

Acetone stripping was conducted in the five-layered pile-up micro-mesh reactor. The experimental set up was the same as shown in Figure 7-3. Acetone initial concentration was set at 0.1M. The pressure difference was kept at 30mmH$_2$O. Nitrogen flowrate was 280ml/min (gas breakthrough to liquid phase took place when the gas flow rate was set at 350ml/min). Temperature was controlled at 30°C. Liquid flowrate varied from 0.15ml/min to 1.5ml/min based on five times larger flowrate of the single mesh unit. The comparison of the acetone stripping results in the 1-mesh reactor and 5-mesh reactor are summarized in Figure 7-29.
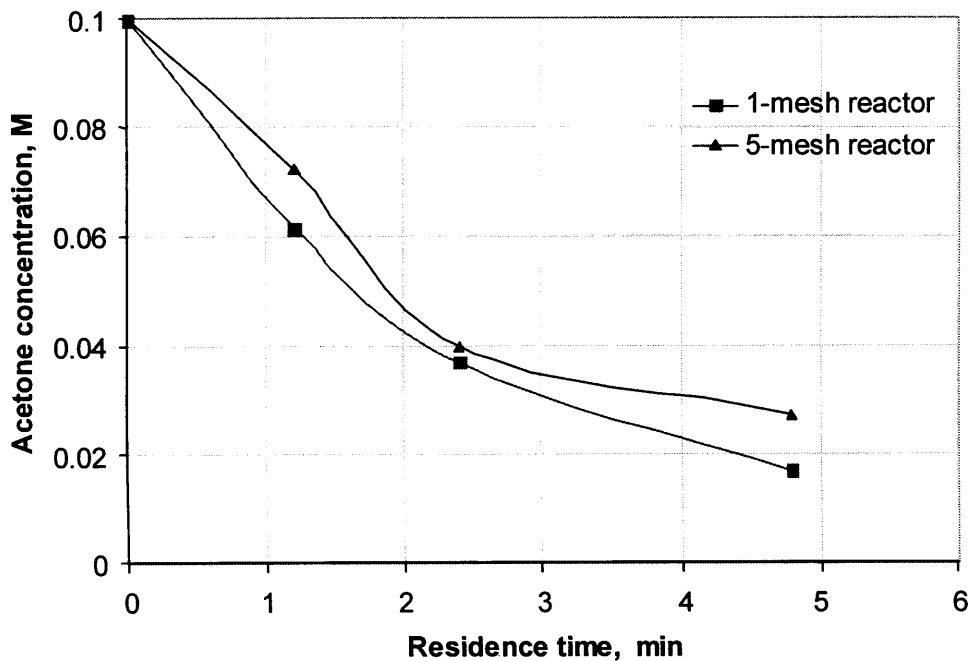
Figure 7-29 Comparison of acetone stripping in the 1-mesh reactor and 5-mesh reactor (Internetmesh; dry N_2; T=30°C; solvent: isopropanol; ΔP: pressure difference (P_{gas}-P_{liquid})=30mmH$_2$O; Acetone concentration in the liquid inlet=0.1M, For 1-mesh reactor: N_2 flowrate =70ml/min, liquid flowrate varies from 0.05 to 0.3ml/min; for 5-mesh reactor: N_2 flowrate =280ml/min, liquid flowrate varies from 0.15 to 1.5ml/min)

The second experiment conducted in the 5-mesh reactor was the asymmetric transfer hydrogenation. The experimental set up was the same as shown in Figure 7-17. The experiments were conducted twice to check the reproducibility. The comparison of the experimental results in the 1-mesh reactor and 5-mesh reactor are summarized in Figure 7-30.
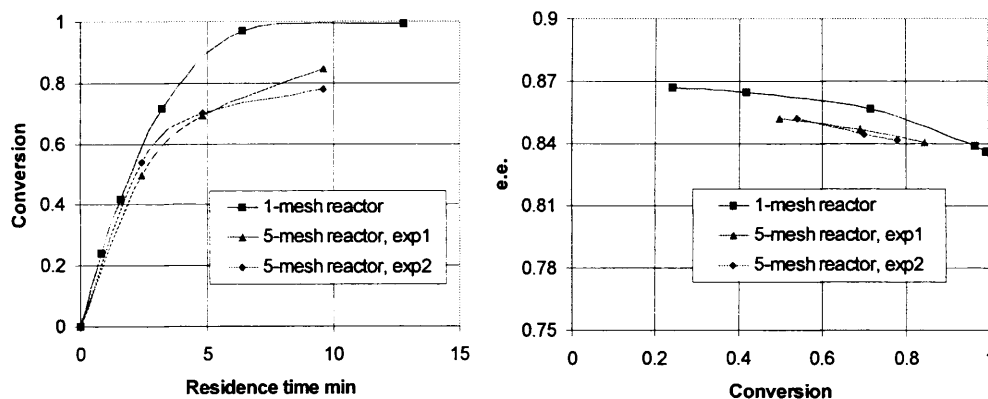
Figure 7-30 Comparison asymmetric transfer hydrogenation in 1-mesh reactor and 5-mesh reactor (Temperature=30°C, Nitrogen flowrate=280ml/min, bubbled in IPA, [Substrate]=0.33M, [Substrate]/[Catalyst]=1000)

It can be seen from Figure 7-29 that acetone concentration is higher in the 5-mesh reactor than that in the 1-mesh reactor. This is probably due to the fact that higher ratio of gas flowrate to liquid volume was utilised in the 1-mesh reactor than in the 5-mesh reactor. Figure 7-30 shows that conversion and enantiomeric excess are lower in the 5- mesh reactor. The reproducibility experiments show that conversion is reproducible within 7.1% and e.e. is reproducible within 0.23%. Therefore, the scale out version of the micro-mesh reactor was performed to a lower efficiency than the single reactor. The possible reason is that distribution of the flow to each layer is not uniform. In the 5-mesh reactor, flow channels in different layers were at different distances from the micromixer and pressure differences existed among them. Moreover, the flow distribution to each layer is different. Therefore, the residence time inside the reactor is different which will have effect on the reactor performance. Detailed calculation of the pressure difference in each layer and distribution channel is worth carrying out to investigate the flow distribution in each layer.

7.5.2 Preliminary investigation of scale up

Equal distribution of reagents to each reactor unit is the most significant technical problem in numbering up. The maximum number of reactor units is limited by the flow distribution problem (Kikutani et al 2002). Therefore, it is necessary to make the single reactor unit large to reduce the number of the single unit for 'achieving the

required productivity. In the following work, scale up of the mesh reactor was attempted.

Supporting posts

Supporting bars

Gasket area

Alignment pin hole

Feed through holes

(a)

Feed through holes

Mesh pores

Non-pore area

(b)

226

(c)

Figure 7-31 AutoCAD drawings and dimensions of the (a) channel plate and (b) mesh, (c) Assembled reactor

In the scale up micro-mesh reactor design, the plate is made of stainless steel and mesh is made of nickel by Tecan, a company based in UK. The dimensions of the plate and mesh are shown in Figure 7-31 and the units are in mm. The outside dimensions of the plate and mesh are 150mm×65mm. The gas liquid contact area is 42.6×90mm. The flow channels of the gas and liquid are etched in both sides of the patterned plate with 0.2mm depth. The pore size of the mesh is 35μm and the thickness is 25μm. The smaller pore size can cope with larger pressure difference between gas and liquid phase to prevent phase breakthrough. A thinner mesh can reduce the mass transfer resistance across the mesh. Because the mesh is very thin and large, it is necessary to design supports in the patterned plate to prevent the mesh bending. The supporting bars were designed in the patterned plate with 0.5mm width and with 7.5mm distance between each other. Corresponding to this, 1mm wide bar (no pores) with 7.1mm distance between each other were designed in the mesh area. The width of the bar in the mesh is bigger than that in the patterned plate to ensure the bar in the patterned plate does not touch the pores in the mesh to prevent the edge effect. 22 posts are designed in each side of the patterned plate to support the mesh. These posts may also help flow distribution. Alignment pin holes were designed in both plates and mesh to ensure the plate and mesh are in the right position. The sealing of the reactor is achieved by using 0.2mm PTFE gaskets. Two top and bottom plates were utilised to assemble the reactor units together and were made of 10mm thick stainless steel.

227

The gas liquid contact area for the scale up mesh reactor is $38.34cm^2$ and for the small mesh reactor is $12cm^2$. Therefore, the area scale up factor for the scale up mesh reactor is 3.195. The liquid volume for the scale up mesh reactor is $4.26*11.9*0.02=1.01cm^3$ and for the small mesh reactor is $2*6*0.02=0.24cm^3$. Therefore, the liquid volume scale up factor for the scale up mesh reactor is 4.2.

Acetone stripping was conducted in the scale-up mesh reactor. The experimental set-up was the same as shown in Figure 7-3. Acetone initial concentration was set at 0.1M. The pressure difference was kept at $30mmH_2O$. Nitrogen flowrate was kept at 70ml/min. Temperature was controlled at 30°C. Liquid flowrate varied from 0.2ml/min to 1.2ml/min. The comparison of the acetone stripping results in the single micro-mesh reactor and scale-up micro-mesh reactor is shown in Figure 7-32.
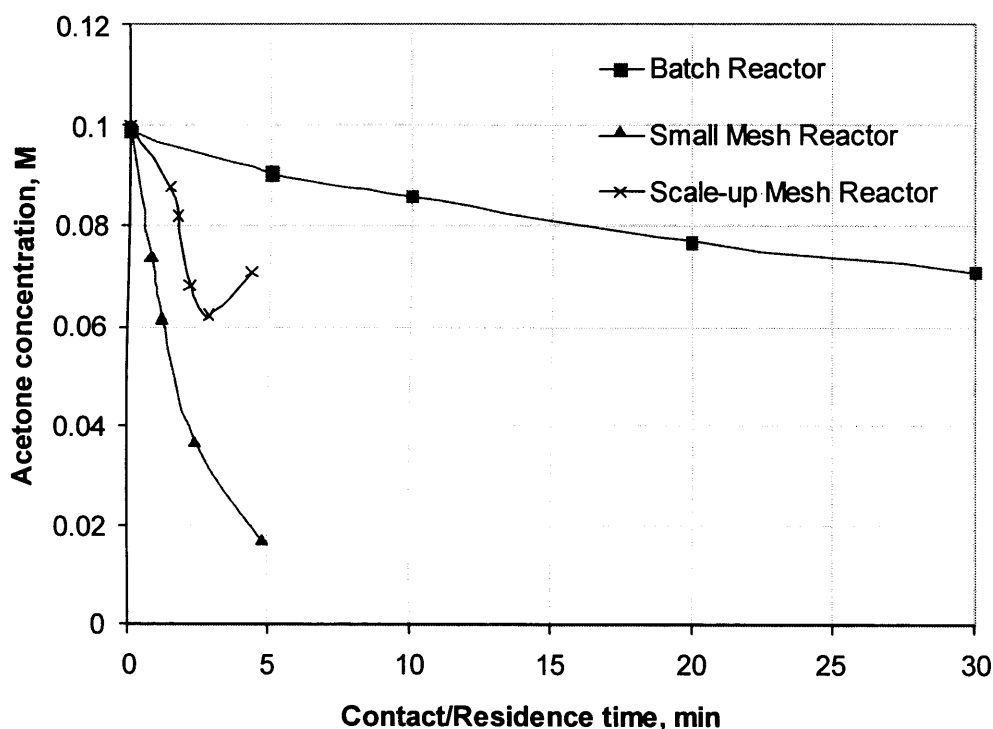
Figure 7-32 Comparison of acetone stripping in the small-mesh reactor, scale up mesh reactor and batch reactor (for small-mesh reactor and scale up mesh reactor, dry N_2; T=30°C; solvent: isopropanol; ΔP: pressure difference $(P_{gas}-P_{liquid})=30mmH_2O$; Acetone concentration in the liquid inlet=0.1M, N_2 flowrate =70ml/min, For small-mesh reactor: liquid flowrate varies from 0.05 to 0.3ml/min; for scale up of the reactor: liquid flowrate varies from 0.2 to 1.2ml/min; for batch reactor, N_2 flowrate=800ml/min)

It can be seen from Figure 7-32 that acetone concentration in the scale up mesh reactor is higher than the small mesh reactor. This is probably due to the fact that a lower ratio of gas flowrate to liquid volume was utilised in the scale up mesh reactor (The ratio of the gas flowrate/liquid flowrate in the small mesh reactor is from 233 to 1400 and in the scale up reactor is from 58 to 350). Moreover, there was no acetone removal in the area in the scale up mesh reactor where there are no pores (posts were used to support mesh) which might contribute to the smaller acetone removal. The last data point is surprisingly high because leakage of the liquid was observed in the scale-up mesh reactor. Although the scale up mesh reactor is less efficient than the small one, it still much better than the batch reactor. Therefore, it is still worth carrying on the improvement in the scale up mesh reactor.

7.6 Conclusions

The mesh reactor is an efficient contactor for stripping acetone from IPA. Due to the membrane being wetted by IPA, the pressure difference between gas and liquid phase should be precisely controlled to stabilise the gas-liquid interface and prevent breakthrough of one phase into the other. The membrane pores are filled with IPA spontaneously. The breakthrough of the gas into liquid phase occurs at the same time when the membrane pores are filled with gas phase. The operation range for the pressure difference is $0 \leq P_G - P_L \leq \dfrac{2\gamma}{r}$. In the operational pressure difference range, the gas-liquid interface is at the gas phase side of the membrane.

Acetone stripping experiments were conducted in the membrane contactor with Internetmesh, Laser mesh, PTFE membrane and Mott membranes which have different characteristics. With all membranes used and experimental conditions applied, the mass transfer resistance exists in the membrane side. The membrane contactor with Internetmesh offers lowest mass transfer resistance, and thus the best acetone stripping performance. Separation efficiency increased with gas flowrate. Using N_2 bubbled in IPA is a convenient method to avoid solvent evaporation from the reaction mixture.

Comparison of acetone removal performance in the mesh reactor and batch reactor is summarized in the Table 7-20. In 5 minutes, 83% of acetone was removed in the

229

mesh reactor while only 10% of acetone in the batch reactor. N_2 flowrate to liquid volume ratio, which is a very important parameter affecting acetone removal, was $292min^{-1}$ in the mesh reactor while only $3.2min^{-1}$ in the batch reactor.

Table 7-20: Acetone removal in 1-mesh small reactor and batch reactor

	Initial acetone concentration M	Acetone concentration at 5minutes M	Acetone removed in 5 minutes (%)	N_2 flowrate to liquid volume ratio (min^{-1})
Mesh reactor	0.10	0.017	83	292
Batch Reactor	0.10	0.09	10	3.2

(Mesh reactor: Dry N_2 flowrate: 70ml/min; ΔP=50mmH$_2$O; Temperature=30°C; Batch reactor: Dry N_2 flowrate: 800ml/min; Liquid volume:250ml; temperature=30°C)

Comparison of the asymmetric transfer hydrogenation of acetophenone in the mesh reactor and batch reactor are summarized in Table 7-21. It can be seen that it takes only 13 min to reach 100% conversion in the mesh reactor while 180 min are needed in the batch reactor. Although the same initial e.e. is obtained in both reactors, 83% final e.e. is obtained in the mesh reactor while only 79% e.e. is obtained in the batch reactor. The peak acetone concentration is significantly reduced from 0.23M in the batch reactor to 0.1M in the mesh reactor.

Table 7-21: Asymmetric transfer hydrogenation in mesh reactor and batch reactor

	Time reaching 100% conversion (min)	Initial e.e.	Final e.e.	Peak Acetone concentration (M)
Mesh Reactor	13	86.5%	83.0%	0.23
Batch Reactor	180	86.5%	79.0%	0.1

(Temperature: 30°C, [Substrate]: 0.33M, N_2 bubbled in IPA in mesh reactor.
N_2 flowrate(ml/min): Batch reactor=800, Mesh reactor=70)

Preliminary investigation of the scale out and scale up of the micromesh reactor was carried out. It was found that the scale out mesh reactor is less efficient for acetone stripping and asymmetric transfer hydrogenation which is probably due the flow distribution being non-uniform in each layer of the reactor and lower ratio of the gas flowrate to liquid volume ratio was utilized. Leakage was detected in the scale up

mesh reactor which is due to an inappropriate gasket used for sealing the plate and mesh.

In conclusion, the mesh reactor offers more efficient acetone removal than the batch reactor. Efficient acetone removal leads to higher reaction rate and shifts the reaction equilibrium which results in higher conversion for the asymmetric transfer hydrogenation of acetophenone. Lower level of acetone concentration in the reaction solution prevents backward reaction.

Chapter 8

Conclusions and Future Work

8.1 Conclusions

The main objective of this thesis was to design reactors for asymmetric transfer hydrogenation of acetophenone catalyzed by pentamethylcyclopentadienylrhodium chloride dimmer/ 1R,2S-aminoindanol. The reaction is reversible and the backwards reaction (acetone plus phenylethanol gives isopropanol and acetophenone) limits the reaction conversion and enantioselectivity. The by-product, acetone, is the most volatile compound in the system. Therefore, the reactor design aimed to remove acetone to shift the reaction equilibrium, thus increase the reaction conversion and enantioselectivity. A simple model for acetone stripping in batch reactor was formulated to study the limiting factors. The model showed that the mass transfer in the liquid phase and gas phase, gas/liquid interfacial area, gas/liquid equilibrium constant and gas flowrate to the liquid volume ratio are the factors which affect the acetone stripping. However, the limiting factor was found to be the gas flowrate to the liquid volume ratio. Therefore, the reactor design focused on how to improve the gas flowrate to the liquid volume ratio. Four reactors were studied for this purpose: gas-liquid batch reactor, tubular reactor, rotating disc reactor and micro-mesh reactor.

In Chapter 3 the asymmetric transfer hydrogenation of acetophenone in the batch reactor was studied. The experimental results showed that the catalyst deactivated when the reaction temperature was over 30°C and in the presence of air in the system. The addition sequence of reactants and catalyst solution had a significant effect on the reaction conversion. Mixing the catalyst solution and acetophenone before adding sodium isopropoxide to activate the catalyst gave the highest conversion. Increasing the amount of catalyst and temperature could increase the reaction rate; however, it had detrimental effects on enantioselectivity. The enantioselectivity decreased faster at higher substrate concentration. Reaction conditions for keeping high e.e. and reaction rate were: substrate concentration 0.1M; substrate and catalyst concentration ratio 1000; sodium isopropoxide and catalyst concentration ratio 8; temperature 30°C; under nitrogen atmosphere.

In Chapter 4 kinetic models for the asymmetric transfer hydrogenation of acetophenone were formulated and reaction rate constants were estimated. Two kinetic models (namely equilibrium model and non-equilibrium model) were established based on the metal-ligand bifunctional catalysis mechanism. The reaction

rate constants were estimated based on the non-equilibrium model because the equilibrium model can not capture the independence of the initial reaction rate on the initial substrate concentration while the non-equilibrium model can. The model was successful in predicting experimental results for reaction conditions outside the range of the experimental conditions used for the parameter estimation even though the confidence of the kinetic parameters, as expressed by the 95% t-value, was large. Experiments at 0°C, 15°C and 30°C were performed to calculate activation energies and pre-exponential factors. A ten-reaction model with acetone stripping was attempted to reduce the 95% t-value for the parameters estimated, but it showed no improvement.

In Chapter 5 the asymmetric transfer hydrogenation of acetophenone was investigated in single phase and gas-liquid tubular reactors. Similar to the batch reactor experimental findings, the different mixing sequence of reactant, catalyst and cocatalyst (sodium isopropoxide) had significant effect on the reaction conversion. The mixing sequence in which substrate and sodium isopropoxide were premixed before mixing with catalyst gave the best conversion. Other parameters were also investigated in the single phase tubular reactor such as the mixing by micromixer and union tee, tube size, sodium isopropoxide amount and catalyst age etc. It was found that micromixer performed better than union tee especially at low residence time. Tube size did not have any effect on reaction conversion and e.e.. Sodium isopropoxide amount had no effect on the reaction when the ratio to catalyst amount was in the range of 4-24. Catalyst deactivated with time, therefore, it is suggested to use fresh catalyst for each experiments. Slightly lower conversion and enantioselectivity were obtained in the single phase tubular reactor compared with batch reactor which is due to the fact that there was no acetone removal in the single phase tubular reactor. Slight lower enanatioselectivity was also observed in the two-phase tubular reactor compared with the batch reactor which is due to the fact that lower gas/liquid flowrate ratio was used in the two-phase tubular reactor. Moreover, a much longer tube was needed to achieve higher conversion in the tubular reactor.

In Chapter 6 a rotating disc reactor (RDR) for acetone removal and asymmetric transfer hydrogenation of acetophenone was studied. The RDR can offer other advantages such as wide range of the gas flowrate to liquid volume ratio and potential

scale out, although acetone stripping performance was found to be the same as the batch reactor with the same ratio of the gas flowrate/liquid volume. Acetone stripping performance can be improved by increasing the rotating speed and by bubbling nitrogen into the liquid phase instead of flowing it above. Higher conversion and higher e.e. of the asymmetric transfer hydrogenation of acetophenone were obtained in the RDR than in the batch reactor due to more efficient removal of acetone from RDR. The enantioslectivity can also be improved by topping up with the pure solvent, isopropanol to keep the reaction solution concentration constant.

In Chapter 7 a micro-mesh reactor for acetone stripping and asymmetric transfer hydrogenation of acetophenone was studied. The key parameter for the micro-mesh reactor is stabilising the gas-liquid interface inside the pores. Therefore, the pressure difference between gas and liquid phase should be precisely controlled to prevent breakthrough of one phase into the other. The operation range of the pressure difference is $0 \leq P_G - P_L \leq \dfrac{2\gamma}{r}$. In the operational pressure difference range, the gas-liquid interface was at the gas phase side of the membrane. Acetone stripping was first investigated in the micromesh reactor. Among the four membranes (Internetmesh, Laser mesh, PTFE membrane and Mott membrane) used in the reactor, internetmesh offered the lowest mass transfer resistance and therefore the best acetone stripping performance. A mathematical model was utilised to simulate acetone stripping. Calculations showed that the mass transfer resistance of the membrane was significant for the membrane used and experimental conditions employed. Acetone stripping efficiency was improved by increasing the gas flowrate/liquid flowrate ratio. Acetone stripping rate was much faster in the micro-mesh reactor rather than in the batch reactor. It improved the conversion and enantioselectivity of the asymmetric transfer hydrogenation of acetophenone. It takes only 13 min to reach 100% conversion in the mesh reactor while 180 min are needed in the batch reactor. Although the same initial e.e. is obtained in both reactors, 83% final e.e. is obtained in the mesh reactor while only 79% e.e. is obtained in the batch reactor. The enantioselectivity could be further improved by topping up isopropanol through nitrogen. Preliminary investigation of the scale out and scale up of the micromesh reactor was carried out. In the scale out mesh reactor, five meshes were used. It was found that the scale out mesh reactor is less efficient for acetone stripping and asymmetric transfer hydrogenation which is

probably due non-uniform flow distribution in each layer of the reactor and lower ratio of the gas flowrate to liquid volume ratio was utilized. In the scale up mesh reactor the gas/liquid contact area was scaled up by factor of the 3.195 and liquid volume was scaled up by factor of the 4.2. Leakage was detected in the scale up mesh reactor which is due to inappropriate gasket material used for sealing the plate and mesh. The experimental results showed that both scale out and scale up of the mesh reactor were less efficient than single mesh reactor unit.

In conclusion, the mesh reactor provides the best performance for the acetone stripping and asymmetric transfer hydrogenation of acetophenone among the batch reactor, tubular reactor and rotating disc reactor. The reaction rate, conversion and enantioselectivity are significantly increased in the mesh reactor. Moreover, the scale out/up is easy to achieve in the mesh reactor. Therefore, the process efficiency will be significantly improved with using of the mesh reactor.

8.2 Future Work

The future work will mostly focus on further development and optimisation of the rotating disc reactor and micro mesh reactor due to the fact that they are easy to scale out and they offered better performance on the acetone stripping and asymmetric transfer hydrogenation. However, accurate kinetic is the very important for reactor design. Therefore, more detailed kinetic study should be carried out as well. Optimal experimental design and reparameterization is suggested in the further investigation of the kinetic model for asymmetric transfer hydrogenation.

In the future work for the rotating disc reactor, vacuum pump with high vacuum capacity, such as rotary vacuum pump is suggested to replace the water vacuum pump and appropriate design of the sealing of the reactor is also suggested to prevent the reactor leaking. More efficient acetone removal will be expected after the improvement.

For the micromesh reactor, the following work is suggested in the future work:

- Counter-current operation needs to be investigated because it provides an opportunity of reducing the gas flowrate while keeping stripping efficiency acceptable. The disadvantage of counter-current operation regards to the

237

breakthrough as discussed in Chapter 2 maybe compensated by suitable inclination of the reactor.

- Another issue to be investigated is the potential effect of the gas flowrate on the breakthrough conditions.

- Experimental set up improvement: the pressure difference between gas phase and liquid phase should be measured instead of the measuring gas phase pressure using manometer.

- Nonwetting membranes need to be investigated in order to minimize the mass transfer resistance across the membrane by filling the pore with gas phase. However, one needs to bear in mind that such organic membranes may have very poor chemical resistance.

- Leakage is the problem for the scale up of the mesh reactor. A thin and soft gasket is suggested to use to seal the reactor instead of the hard PTFE gasket.

- Flow distribution is a key aspect for the mesh reactor scale out and scale up. Therefore, flow distribution needs to be further investigated. Commercial software Femlab is suggested to be used for this study.

References:

Abdallah R., Meille V., Shaw J., Wenn D. and de Bellefon C., "Gas-liquid and gas-liquid-solid catalysis in a mesh microreactor". Chem. Commun., 2004, 372-373

Adam N.K., "Principles of Penetration of Liquids into Solids", Discuss. Faraday Soc., 1948, 3, 5-11

Adamson A.W. and Gast A.P., "Physical Chemistry of Surfaces", Chapter II – Capillarity, Sixth Edition, John Wiley & Sons, Inc. (1997).

Anderson, N.G. "Practical process research & development" San Diego ; London : Academic Press, 2000.

Anderson N. G.. "Practical Use of Continuous Processing in Developing and Scaling Up Laboratory Processes". Organic Process Research & Development 2001, 5, 613-621

Aparício, J.J.C.; Jerónimo M.A.S.; Martins F.G.; Coelho M.A.N.; Martins C.; Braga A.S.; Costa C.A.C. "Two different approaches for RDC modelling when simulating a solvent deasphalting plant", Computers and Chemical Engineering, 2002, 26, 1369-1377

Appleyard D. "Micro-players edge microreactors into the mainstream" The Chemical Engineer, 2005, March, 42-43

Ardanuy A., Del Rio J., Menéndez M.D., Perez C., Suarez L. and Verde J.M., Análisisy Probabilidad C.O.U, ICE, Universidad de Salamanca (1986).

Ashby M. T. and Halpern J.. "Kinetics and Mechanism of Catalysis of the asymmetric Hydrogenation of α,β-Unsaturated Carboxylic Acids by Bis(carboxylato) {2,2'-bis(diphenylphosphino)-1,1'-binaphthyl}-ruthenium(II),[Ru^{II}(BINAP)(O$_2$CR)$_2$]" J. Am. Chem. Soc. 1991, 113,589-594

Atikinson A.C., Bogacka B., Bogacki M.B.. "D- and T-optimum designs for the kinetics of a reversible chemical reaction", Chemometrics and Intelligent Laboratory Systems", 1998, 43, 185-198

Bandini S., Gostoli C. and Sarti G. C., "Separation efficiency in vacuum membrane distillation", Journal of Membrane Science, 1992, 73, 217-229

Banat F. and Simandl J., "Removal of benzene traces from contaminated water by vacuum membrane distillation", Chemical Engineering Science 1996, 51, 1257-1265

Banerjee, G. "Hydraulics of bench-scale rotating biological contactor", Wat. Res., 1997, 31, 2500-2510.

Bayston D. J., Travers C. B. and Polywka M. E. C.. "Synthesis and evaluation of a chiral heterogeneous transfer hydrogenation catalyst". Tetrahedron: Asymmetry 9, 1998, 2015-2018

de Bellefon C., Tanchoux N., Caravieilhes S., "New reactors and methods for the investigation of homogeneous catalyst", Journal of Organometallic Chemistry. 1998, 567, 143-150

de Bellefon C. and Tanchoux N.. "Effect of non-linear kinetics on the enantioselectivity in the H-transfer asymmetric homogeneous reduction of arylketones with a Rhodium diamine catalyst" Tetrahdron: Asymmetry 9 (1998) 3677-3686

de Bellefon C. , Abdallah R., Lamouille T., Pestre N., Caravieilhes S., Grenouillet P., "High-through screening of molecular catalysts using automated liquid handling, injection, and microdevices", Chimia, 2002, 56, 621-626

de Bellefon C., Pestre N., Lamouille T., Grenouillet P., Hessel V., "High throughput kinetic investigations of asymmetric hydrogenations with microdevices", Adv. Synth. Catal., 2003, 345, 190-193

Bemard M., Guiral V., Delbecq F., Fache F., Sautet P., Lemarie M.. " Structure of the diamine-Rh(I) precursor in the asymmetric hydrid transfer reduction of ketones: A theoretical and experimental approach" J. Am. Chem. Soc. 1998, 120, 1441-1446

Bengtsson E., traardh G., Hallstrom B., "Concentration polarization during the enrichment of aroma compounds from a water solution by pervaporation", J. Food Eng., 1993, 19,399.

Berger R.J., Stitt E. H., Marin G.B., Kapteijn F., Moulijn J. A.. "Chemical reaction kinetics in practice", Cat. Tech. 2001, 5, 30-60

Bellara, S.R., Cui, Z.F., Pepper, D.S.. "Fractionation of BSA and lysozyme using gas sparged ultra6ltration in hollow fibre membrane modules. Biotech Progress 1997, 13, 869–872

Berčič G. and Pintar A.. "The role of gas bubbles and liquid slug lengths on mass transport in the Taylor flow through capillaries" Chemical Engineering Science, 1997, 52, 3709-3719

Bessarabov D.G., Jacobs E.P., Sanderson R.D., Beckman I.N., "Use of nonporous polymeric flat sheet gas-separation membranes in a membrane-liquid contactor: experimental studies". Journal of Membrane Science 1996, 113, 275-284

Bessoth, F.G., de Mello, A.J., Manz, A.. "Microstructure for efficient continuous flow mixing" Analytical Communications, 1999, 36, 213–215

Bintanja, H.H.J., van der Erve, J.J.V.M.; Boelhouwer, C. "Oxygen transfer in a rotating disc treatment plant", Water Res, 1975, 9, 1147-1153.

Blacker J. and Mellor B.. Patent WO9842643 26/03/97

Blacker J. "Development of some large scale catalytic asymmetric reactions" in "The scale-up of chemical processes", Jersey; 1998, P74-P81, ISBN 0953399400.

Blacker J. and Martin J., "Scale-up studies in asymmetric transfer hydrogenation" in "Asymmetric catalysis on industrial scale"; Editor: Blaser H.U. and Schmidt E. 2004, P201-216; ISBN:3-527-30631-5

Blackmond D. G.. "Kinetic Aspects of Nonlinear Effects in Asymmetric Catalysis" Acc. Chem. Res. 2000, 33, 402-411

Boodhoo, K.V.K.; Jachuck, R.J. "Process intensification: spinning disk reactor for styrene polymerisation", Appl. Thermal Eng., 2000, 20, 1127-1146

Brechtelsbauer, C.; Lewis, N.; Oxley, P.; Ricard, F. "Evaluation of a spinning disc reactor for continuous processing", Org. Proc. Res. Dev., 2001, 5, 65-68.

Butt J. B.. "Reaction kinetics and reactor design", 2nd edition, Marcel Dekker, Inc., New York, 2000, ISBN:0-8247-7722-0

Buzzi-Ferraris G.. "Planning of experiments and kinetic analysis", Catalysis Today, 1999, 52, 125-132

Caravieilhes S., Bellefon C. de., Tanchoux N., "Dynamic methods and new reactors for liquid phase molecular catalysis". Catalyst Today 2001, 66, 145-155

Cardew P. T. and Le M.S., "Membrane Processes: A technical Guide". RS.C, Cambridge, 1998, P2-15.

Cassie A.B.D., S. Baxter, Trans. Faraday Soc., 1944, 40, 546

Chambers R. D., Fox M.A., Holling D., nakano T., Okazoe T., Sandford G., "Versatile gas/liquid microreactors for industry" Chem. Eng. Technol. 2005, 28, 344-352

Cheng T. and Lin T.. "Characteristics of gas-liquid two phase flow in small diameter inclined tubes" Chemical Engineering Science, 2001, 56, 6393-6398

Chen M. Cong D. and Fang T.. "Principle of Chemical Engineering", Chemical Engineering Industry, Beijing, 1989, pp1-55

Corey E. J., Bakshi R. K., and Shibata S.. "Highly Enantioselective Borane Reduction of Ketones Catalyzed by Chiral Oxazaborolidines. Mechanism and Synthetic Implications" J. Am. Chem. Soc. 1987, 109, 5551-5553

Corey E. J., Bakshi R. K., Shibata S., Chen C. and Singh V. K.. "A stable and Easily Prepared Catalyst for the Enantioselective Reduction of Ketones. Applications to Multistep Syntheses" J. Am. Chem. Soc. 1987, 109, 7925-7926

Corey E. J., and Helal C. J. "Reduction of Carbonyl Compounds with Chrial Oxazaborolidines Catalyst: A New Paradigm for Enantioselective Catalysis and a Powerful New Synthetic Method." Angew. Chem. Int. Ed. 1998, 37, 1986-2012

Crabtree R. H., Felkin H. and Morris G. E.. "Cationic iridium diolefin complexes as alkene hydrogenation catalysts and the isolation of some related hydrido complexes" journal of Organometallic Chemistry. 1977, 141, 205-215

Crépy K. V. L. and Imamoto T.. "recent Developments in Catalytic Asymmetric hydrogenation Employing P-Chirogenic Diphosphine Ligands" Adv. Synth. Cata. 2003, 345, No.1+2, 79-101

Cunha L. M. and Oliveira A.R.. "Optimal experimental design for estimating the kinetic parameters of process described by the first-order Arrhenius model under linearly increasing temperature profiles", Journal of Food Engineering, 2000, 46, 53-60

Cussler E.L., "Hollow fiber contactors" in: J.G. Crespo, K.W. Böddeker (Eds) "Membrane process in separation and purification", Kluwer Academic Publishers, Netherlands, 1994, P375-394.

Cussler E.L., Reed B.W., Semmens M.J., Membrane contactors, in: R.D. Noble, S.A. Stern (Eds), Membrane Separation Technology: Principles and Applications, Elesvier, Amsterdam, 1995, 467-490.

Cypes S.H. and Engstrom J.R., "Construction, analysis and evaluation of a microfabricated stripping column", IMRET 7, Lausanne, Switzerland (2003).

Dabir, B.; Riazi, M. R.; Davoudirad, H. R. "Modelling of falling film reactors", Chem. Eng. Sci. 1996, 51, 2553-2558.

Davis, E. J.; van Ouwerkerk M.; Venkatesh, S. "An analysis of the falling film gas-liquid reactor", Chem. Eng. Sci. 1979, 34, 539-550.

Di Palma, L.; Merli, C.; Paris, M.; Petrucci, E. "A steady-state model for the evaluation of disk rotational speed influence on RBC kinetic: model presentation", Bioresource Tech., 2003, 86, 193-200.

Dindore V.Y., Brilman D.W.F., Geuzebroek F.H., Versteeg G.F.," Membrane-solvent selection for CO_2 removal using membrane gas-liquid contactors", Separation and Purification Technology, 2004, 40, 133-145

Ding H.B., Carr P.W., Cussler E.L., "Racemic leucine separation by hollow fiber extraction". AICHE J. 1992, 38(10), 1493-1498

Dirix, C.A.M.C. and van der Wiele, K. "Mass transfer in jet loop reactors", Chem. Eng. Sci., 1990, 45, 2333-2340

Dionysiou, D.D.; Khodadoust, A.P.; Kern, A.M.; Suidan, M.T.; Baudin, I., Laîne, J.M. "Continous-mode photocatalytic degradation of chlorinated phenols and pesticides in water using a bench-scale TiO_2 rotating disk reactor", Appl. Cat. B Env., 2000, 24, 139-135.

Dionysiou, D.D.; Suidan, M.T.; Baudin, I.; Laîne, J.M. "Oxidation of organic contaminans in a rotaing disk photocatalytic reactor: reactor kinetics in the liquid phase and the role of mass transfer based on the dimensionless Damköhler number", Appl. Cat. B Env., 2002, 38, 1-16.

Doraiswamy L.K., "Organic Synthesis Engineering" Oxford University Press. New York. 2001, P496

Drese, K.. "Optimization of interdigital micromixers via analytical modelling-exemplified with the SuperFocus mixer" Chemical Engineering Journal, 2003, 101, 403–407

Ehlers, S.; Elgeti K.; Menzel T.; WieBmeier G.. "Mixing in the offstream of a microchannel system" Chemical Engineering and Processing, 2000, 39, 291–298

Ehrfeld, W., Golbig K.; Hessel V.; Lowe H.; Richter T.. " Characterization of mixing in micromixers by a test reaction: single mixing units and mixer arrays" Industrial & Engineering Chemistry Research, 1999, 38, 1075–1082

Éll A. H., Johnson J. B. and Bäckvall J.. "Mechanism of Ruthenium-catalyzed hydrogen transfer reactions. Evidence for a stepwise transfer of CH and NH hydrogens from an amine to a (cyclopentadienone)ruthenium complex" Chem. Commun. 2003, 1652-1653

Elperin T. and Fominykh A.. "Liquid phase controlled mass transfer in gas-liquid slug flow at low Reynolds numbers" Int. Comm. Heat Mass Transfer, 1995, 22, 741-750

Everaere K., Mortreux A. and Carpentier J.. "Ruthenium (II)-Catalyzed Asymmetric Hydrogenation of Carbonyl Compounds with 2-Propanol and Ephedrine-type Ligands" Adv. Synth. Cata. 2003, 345, No. 1+2, 67-77

Everaere K., Mortreux A., Bulliard M., Brussee J., Gen A., Nowogrocki G. and carpentier J.. "(β-Amino alcohol)(arene)ruthenium(II)-catalyzed Asymmetric Transfer Hydrogenation of Functionalized Ketones-Scope, Isolation of the Catalytic Intermediates, and Deactivation Process" Eur. J. Org. Chem. 2001,275-291

Fache F., Schulz E., Tommasino M. L., and Lemaire M.. "Nitrogen-containing ligands for asymmetric homogeneous and heterogeneous catalysis". Chem. Rev. 2000, 100, 2159-2231

Fei, W.Y.; Wang, Y.D.; Wan, Y.K. "Physical modelling and numerical simulation of velocity fields in rotating disc contactor via CFD simulation and LDV measurement", Chem. Eng.J., 2000, 78, 131-139.

Fogler H. S.. "Elements of chemical reaction engineering", Third Edition, Prentice-Hall Inc., New Jersey, 1999, ISBN: 0-13-973785-5

Fonseca M. H. and König B.. "Chrial Tetraaza Ligands in Asymmetric Catalysis: Recent Progress" Adv. Synth. Catal. 2003, 345, 1173-1185

Fox, W. W., and Zisman, W. A., J. Colloid Sci. 1952, 7, 428

Franken A.C.M., Nolten J.A.M., Mulder M.H.V., Bargeman D., Smolders C.A., "Wetting criteria for the application of membrane distillation". Journal of Membrane Science, 1987, 33, 315-328

Friedman, A.A., Robbins, L.E., Woods, R.C., Wauford, J.R. "Effect of disk rotational spped on biological contactors efficiency", J. Water Pollut. Control Fed., 1979, 51, 2678-2690

Gabelman A. and Sub-Tak Hwang., "Hollow fiber membrane contactors" Journal of Membrane Sicence. 159, 1999, 61-106

Gamez P., Fache F., and Lemaire M.. "Asymmetric catalitic reduction of carbonyl compounds using C₂ symmetric diamines as chiral ligands" Tetrahedron: Asymmetry Vol. 6, No. 3, 705-716, 1995

Gamez P., Dunjic B., Pinel C. and Lemaire M. "Molecular Imprinting Effect" in the Synthesis of Immobilized Rhodium Complex Catalyst (IRC cat) Tetrahedron Letters, Vol. 36, No. 48, 8779-8782, 1995

García-Payo M. C., Izquierdo-Gil and Fernández-Pineda C., "Air gap membrane distillation of aqueous alcohol solutions", Journal of Membrane Science 2000, 169, 61-80

García-Payo M. C., Rivier C. A., Marison I. W., Stockar U. von., "Separation of binary mixtures by thermostatic sweeping gas membrane distillation II. Experimental results with aqueous formic acid solutions". Journal of Membrane Science 2002, 198, 197-210

Garcia Villaluenga J.P. and Tabe-Mohammadi A., "A review on the separation of benzene/cyclohexane mixtures by pervaporation process", Journal of Membrane Science, 2000, 169, 159-174.

Gao J., Xu P., yi X., Yang C., Zhang H., Cheng S., Wan H., Tsai K. and Ikariya T.. "Asymmetric transfer hydrogenation of prochrial ketones catalysed by chrial ruthenium complexes with aminophosphine ligands" Journal of Molecular Catalysis A: Chemical 147 (1999) 105-111

Ghosh R. and Cui Z.F.. "Mass transfer in gas-sparged ultrfiltation: upward slug flow in tubular membranes" Journal of Membrane Science, 1999, 162, 91-102

Gladiali S., Pinna L., Delogu G., Martin S., Zassinovich G. and Mestroni G.. "Optically active phenanthrolines in asymmetric catalysis.III. Highly efficient enantioselective transfer hydrogenation of acetophenone by chiral rhodium/3-alkyl phenanthroline catalysts." Tetrahedron: Asymmetry 1990, 1, 621-634.

Glasgow I.; Aubry N.. "Enhancement of microfluidic mixing using time pulsing" Lab on a Chip, 2003, 3, 114-120

Glatzer, H.J.; Desikan, S.; Doraiswamy, L.K. Triphase catalysis: a new rotating disk contactor for measuring mass transfer coefficients, Chem. Eng. Sci., 1998, 53, 2431-2449.

Glatzer, H.J.; Doraiswamy, L.K. Triphase catalysis: a correlation for Sherwood number using the rotating disk contactor (RDC) developed earlier, Chem.Eng. Sci. , 2001, 56, 3815-3827.

Godino P., Peña L., Mengual J. I. "Membrane distillation: Theory and experiments" Journal of the Membrane Science 1996, 121, 83-93

Gryta M., Tomaszewska M. and Morawski A. W., "Membrane distillation with laminar flow", Separation and Purification Technology, 1997, 11, 93-101

Hacck K., Hashiguchi S., Fujii A., Ikariya T. and Noyori R.. "The Catalyst Precusor, Catalyst, and Intermediate in the Ru^{II}-Promoted Asymmetric Hydrogenation Transfer between Alcohols and Ketones". Angew. Chem. Int. Ed. Engl. 1997, 36, 285-288

Halpern J.. "Mechanism and Stereoselectivity of Asymmetric Hydrogenation". Science, Volume 217, Issue 4558 (July. 30, 1982), 401-407

Hamill, N.A.; Weatherley, L.R.; Hardacre, C. Use of a batch rotating photocatalytic contactor for the degradation of organic pollutants in wastewater, App.Cat B Env., 2001, 30, 49-60.

Hardt, S.; Schönfeld, F.. "Laminar mixing in different interdigital micromixers—part 2: numerical simulations" A.I.Ch.E. Journal, 2003, 49, 578–584

Hashiguchi S., Fujii A., Tukehara J., Ikariya T. and Noyori R.. " Asymmetric Transfer hydrogenation of Aromatic Ketones Catalyzed by Chiral Ruthenium(II) Complexes." J. Am. Chem. Soc. 1995, 117, 7562-7563

Heiszwolf J.J; Kreutzer M.T.; Eijinden M.G.; Kapteijn F.; Moulijn J.A.. "Gas-liquid mass transfer of aqueous Taylor flow in monoliths" Catalysis Today, 2001, 69, 51-55

He J., Arnold R. G., Sáez A. E., Betterton E. A., Ela W. P., "Removal of aqueous phase trichloroethylene using membrane air stripping contactors" Journal of Environmental Engineering, 2004, 1232-1241.

Hessel V.; Löwe, H.. "Micro chemical engineering: components—plant concepts—user acceptance" Chemical Engineering and Technology, 2003, 26, 13–24

Hessel, V., Hardt, S.; Lowe H.; Schönfeld, F.. "Laminar mixing in different interdigital micromixers—part I: experimental characterization" A.I.Ch.E. Journal 2003, 49, 566–577

Hessel V.; Löwe H.; Schönfeld F.. "Micromixers-a review on passive and active mixing priciples" Chemical Engineering Science, 2005, 60, 2479-2501

Hessel V.; Löwe H.; Müller A.; Kolb G.. "Chemical Micro Process Engineering" Wiley-VCH Verlag GambH & Co. KGaA, Weinheim, 2005, ISBN-13 978-3-527-30988-6

Horvath, C., Solomon, B.A., Engasser, J.M.. "Measurement of radial transport in slug flow using enzyme tubes" Industrial and Engineering Chemistry Fundamentals, 1973, 12, 431–439.

Issanchou S., Cognet P., Cabassud M.. "Precise parameter estimation for chemical batch reactions in heterogeneous medium", Chemical Engineering Science, 2003, 58, 1805-1813

Iversen S.B., Bhatia V.K., Dam-Johansen K., Jonsson G.. "Characterization of microporous membranes for use in membrane contactors", Journal of Membrane Science, 1997, 130, 205-217

Jähnisch K., Baerns M., Hessel V., Ehrfeld W., Haverkamp V., Löwe H., Will C., Guber A., J. Fluorine Chem. 2000, 105, 117

James B. A., Andrew S. J. E., Godfery H. R. G., Mark S. A. and Iain S. R.. "Method and apparatus for diffusive transfer between immiscible fluids" Patent, US5961832

Jen, C.-P.; Wu C.; Lin Y.; Wu C.. "Design and simulation of the micromixer with chaotic advection in twisted microchannels" Lab on a Chip, 2003, 3, 77–81

Jiang, F; Drese K.S.; Hardt S.; Küpper M.; Schönfeld, F.. "Helical flows and chaotic mixing in curved micro channels" A.I.Ch.E. Journal, 2004, 50, 2297–2305

Johnson J. B. and Bäckvall J.. "Mechanism of Ruthenium-Catalyzed Hydroge Transfer Reactions. Concerted Transfer of OH and CH Hydrogens from Alcohol to a (Cyclopentadienone)ruthenium Complex" J. Org. Chem. 2003, 68, 7681-7684

Jonquières A., CléR. Lochon P., Néel J., dresch M. and Chrétien B., "Industry state-of-the-art of pervaporation and vapour permeation in the western countries", Journal of membrane Science 2002, 206, 87-117

Juang Ruey-Shin, Lin Su-Hsia, Yang Min-Chih, "Mass transfer analysis on air stripping of VOCs from waterin microporous hollow fibers" Journal of Membrane Science,2005, 25, 79-87

Katalin Balázsik, Béla Török, Károly Felföldi, Mihály Bartók. "Homogeneous and heterogeneous asymmetric reactions: Part II Sonochemical enantioselective hydrogenation of trifluoromethyl ketones over platinum catalysts" Ultrasonics Sonochemistry 5, 1999, 149-155

Kertész K, Schlosser Š and Šimo M.. "Mass-transfer characteristics of a spiral-channel SLM module in pertraction of phenylalanine" Desalination, 2004, 163, 103-117

Kharyet M., Godino P. and Mengual J. I., "Theory and experiments on sweeping gas membrane distillation", Journal of Membrane Science 2000, 165, 261-272

Kharyet M., Godino P. and Mengual J. I.. "Nature of flow on sweeping gas membrane distillation", Journal of Membrane Science 2000, 170, 243-255

Kharyet M., Godino M. P. and Mengual J. I.. "Theoretical and experimental studies on desalination using the sweeping gas membrane distillation method". Desalination 2003, 157, 297-305

Knowles W. S.. "Asymmetric hydrogenations(Nobel lecture)" Angew. Chem. Int. Ed. 2002, 41, 1998-2007

Kreith F., Black W.Z., Basic Heat Transfer, Harper and Row, New York, NY, USA, 1980.

Kreulen H., Smolders C.A., Versteeg G.F., Van Swaaij W.P.M, "Determination of mass transfer rates in wetted and non-wetted microporous membranes", Chem. Eng. Sci. 1993, 48 (11), 2093–2102.

Kreulen H., Smolers C.A., Versteeg G.F. and van Swaaij W.P.M., "Microporous hollow fibre membrane modules as gas – liquid contactors. Part 1. Physical mass transfer processes". Journal of Membrane Science, 1993, 78, 197 – 216.

Kubsad, V., Chaudhari, S.; Gupta, S.K. Model for oxygen transfer in rotating biological contactor, Wat. Res., 2004, 38, 4297-4304.

Kukula P. and Červený L.. " Effects of reaction variables on enantioselectivity of modified Raney nickel catalyst". Journal of Molecular Catalyst A: Chemical. 185, 2002, 195-202

LaGrega, M.D., Buchinghamm P.L. and Evans, J.C. (1994). Hazardous waste management, McGraw-Hill, New York.

Landis C. L. and Halpern J.. "Asymmetric Hydrogenation of Methyl-(Z)-α-acetamidocinnamate Catalyzed by {1,2-Bis((phenyl-o-anisoyl)phosphino)ethane} rhodium(I): Kinetics, Mechanism, and Origin of Enantioselection". J. Am. Chem. Soc. 1987, 109, 1746-1754

Laue S., Greiner L., Wöltinger J. and Liese A.. "Continuous application of chemzymes in a membrane Reactor: asymmetric transfer hydrogenation of acetophenone" Adv. Synth. Catal., 2001, 343, 711-720

Lawson K. W. and Lloyd D. R.. "Membrane distillation", Journal of Membrane Science 1997, 124, 1-25

Lee C. H. and hong W. H.. "Effect of operating variables on the flux and selectivity in sweep gas membrane distillation for dilute aqueous isopropanol", Journal of Membrane Science, 2001, 188, 79-86

Lévéque J.A., Les lois de la transmission de chaleur par convection, Annales de Mines 12 (13/14) (1928) 201–299

Lighthill, M.J.. "Pressure-forcing of tightlypellets along fluid-filled elastic tubes" Journal of Fluid Mechanics, 1968, 34, 113–143.

Lindermann, J.; Wiesmann, U. Single-disc investigation on nitrogen removal of higher loads in sequencing batch and continuously operated RDR systems, Wat.Sci.Tech., 2000, 41, 77-84.

Lipnizki F., Field R. W. and Ten P. K., "Pervaporation-based hybrid process: a review of process design, applications and economics", Journal of Membrane Science, 1999, 153, 183-210

Liu r. H.; Lenigk R.; Druyor-Sanchez R.L.; Yang J.; Grodzinski P.. "Hybridization enhancement using cavitation microstreaming" Anal. Chem. 2003, 75, 1911-1917

Liu r. H.; Yang J.; Pindera M. Z.; Athavale M.; Grodzinski P.. "Bubble-induced acoustic micromixing" Lab on a Chip, 2002, 2, 151-157

Löb, P.; Drese K.S.; Hessel V.; Hardt S.; Hofmann C.; Lowe H.; Schenk R.; Schonfeld F.; Werner B.. "Steering of liquid mixing speed in interdigital micromixers-from very fast to deliberately slow mixing" Chemical Engineering and Technology, 2004, 27, 340–345

Lu, C.; Li, H.C., Lee, L.Y. Effects of disc rotational speed and submergence on the performance of an anaerobic rotating biological contactor, Environmental International, 1997, 23, 253-263

Mahmud H., Kumar A., Narbaitz R.M. and Matsuura T., "Membrane air stripping: a process for removal of organics from aqueous solutions", Separation Science and Technology, 1998, 33, 2241-2255

Mahmud H., Kumar A., Narbaitz R.M., Matsuura T., "A study of mass transfer in the membrane air-stripping process using microporous polypropylene hollow fibers", Journal of Membrane Science, 2000, 179, 29–41

Mahmud H., Removal of Organics from Water/Wastewater by Membrane Air Stripping, Ph.D. Thesis, Department of Chemical Engineering, the University of Ottawa, Ottawa, ON, Canada, 2001

Mahmud H., Kumar A., Narbaitz R. M., Matsuura T,. "Mass transport in the membrane air-stripping process using microporous polypropylene hollow fibers: effect of toluene in aqueous feed". Journal of Membrane Science 2002, 209, 207-219

Moore J.W. and Pearson R.G.. "Kinetics and Mechanism", Third Edition, John Wiley & Sons, Inc. USA, 1981, ISBN: 0-471-03558

Mulder M, "Basic Principles of Membrane Technology",ISBN:0-7923-4247-X(HB), Kluwer Academic Publishers, Dordrecht, The Netherlands, 1996, Chapter VIII, P465-472

Murata K., Ikariya T. and Noyori R.. " New Chiral Rhodium and Irdium Complexes with Chiral Diamnie Ligands for Asymmetric Transfer Hydrogenation of Aromatic Ketones" J. Org. Chem. 1999, 64, 2186-2187

Niu X.; Lee Y.. "Efficient spatial-temporal chaotic mixing in microchannels" Journal of Micromechanics and Microengineering, 2003, 13, 454-462

Novakovic, K.; Morris, J.; Martin, E. Mathematical analysis of the formation of molecule sizes on a spinning disc reactor, Macromolecular Symposia, 2004, 216, 195-208

Noyori R., Hashiguchi S.. " Asymmetric Transfer Hydrogenation Catalyzed by Chiral Ruthenium Complexes" Acc. Chem. Res. 1997, 30, 97-102

Noyori R., Yamakawa M. and Hashiquchi S.. "Metal-Ligands Bifunctional Catalysis: A Nonclassical Mechanism for Asymmetric Hydrogen Transfer Between Alcohols and Carbonyl Compounds. " J. Org. Chem. 2001, 66, 7931-7944

Noyori R.. "Asymmetric catalysis: Science and Opportunities (Nobel Lecture) " Angew. Chem. Int. Ed. 2002, 41, 2008-2022

Oddy M.H.; Santoago J.G.; Mikkelsen J.C.. "Electrokintic instability micromixing" Anal. Chem. 2001, 73, 5822-5832

Oliver, D.R., Wright, S.J.. "Pressure drop and heat transfer in gas–liquid slug flow in horizontal tubes. Chemical Engineering 1964, 9, 590–596.

Oliver, D.R., Young Hoon, A.. "Two-phase non-Newtonian flow-II. Heat transfer. " Transactions of the Institution of Chemical Engineers 1968, 46, 116–122.

Palmer M. J., Walsgrove T. and Wills M.. "(1R,2S)-(+)-cis-1-Amino-2-indanol: An Effective Ligand for Asymmetric Catalysis of Transfer Hydrogenation of Ketones". J. Org. Chem. 1997, 62, 5226-5228.

Palmer M. and Wills M.. "Asymmetric transfer hydrogenation of C=O and C=N bonds". Tetrahedron:Asymmetry 10, (1999) 2045-2061

Pamies O., Backvall J.. "Studies on the Mechanism of Metal-Catalyzed Hydrogen Transfer from Alcohols to Ketones" Chem. Eur. J. 2001, 7, 5052-5058

Paik P.; Pamula V. K.; Fair R. B.. "Rapid droplet mixers for digital microfluidic systems" Lab on a Chip, 2003, 3, 253-259

Pastor I., Västilä P. and Adolfsson H.. " Novel simple and highly modular ligands for efficient asymmetric transfer-hydrogenation of ketones" Chem. Commun. 2002, 2046-2-47

Petra D. G. I., Reek J. N.H., Handyraaf J., Meijer E. J., Dierkes P., Kamer P. C.J., Brussee J., Schoemaker H. E., Van Leeuwen P. W.N.M.. "Chiral Induction Effects in Ruthenium(II) Amino Alcohol Catalysed Asymmetric Transfer Hydrogenation of Ketones: An Experimental and Theoretical Approach." Chem. Eur. J. 2000, 6, 2818-2829

Prasad, R. and Sirkar K.K., "Dispersion-free solvent extraction with microporous hollow-fiber modules" AIChE J. 1988, 34, 177 – 188

Prasad R., and Sirkar K.K., "Hollow fiber solvent extraction of pharmaceutical products: a case study", Journal of Membrane Science, 1989, 47, 235-259

Prasad R. and Sirkar K.K., "Hollow fiber solvent extraction: performances and design", Journal of Membrane Science, 1990, 50, 153 – 175.

Prasad R, Sirkar KK. 1992. Membrane-based solvent extraction. In: Winston WS, Sirkar KK, editors. Membrane handbook. New York: Chapman & Hall. p. 727–763

Prothero, J., Burton, A.C.. "The physics of blood flow in capillaries—I. The nature of the motion" Biophysical Journal, 1961, 1, 565–575.

Qi Z., Cussler E.L., "Microporous hollow fibers for gas absorption. Part I. Mass transfer in the liquid", Journal of Membrane Science, 1985, 23, 321–332.

Qi Z,. Cussler E.L, "Microporous Hollow Fibers for Gas Absorption. Part II. Mass transfer across the membrane", Journal of Membrane Science, 1985, 23, 333–345.

Qian S.; Bau H.H.. "A chaotic Electroosmotic Stirrer" Anal. Chem. 2002, 74, 3616-3625

Rautenstrauch V., Hoang-Cong X., Churlaud R., Abdur-Rashid K. and Morris R. H.. "Hydrogenation versus transfer hydrogenation of ketones: two established ruthenium systems catalyze both". Chem. Eur. J. 2003, 9, 4954-4967

Reddy D., Reineke C.E., "Dehydration with perfluorosulfonic acid ionomer membranes", AICHE Symp. Ser. 1998, 84, 84

Reed, B.W., Semmens, M.J., Cussler, E.L., Membrane contactors, in : R.D. Noble, S.A.Stern (Eds.), Membrane separation technology. Principles and application, Elsevier, Amsterdam, 1995, P474.

Richardson J. F. and Peacock D.G.. "Chemical Engineering", Volume 3, Third edition, 1994, Elsevier Science Ltd, Oxford, ISBN 0-08-041002-2,

Rivier C. A., García-Payo M. C., Marison I. W., Stockar U. von.. "Separation of binary mixtures by thermostatic sweeping gas membrane distillation I. Theory and simulations". Journal of Membrane Science 2002, 201, 1-16

Sakurai, A.; Imai, H.; Takenaka, Y.; Sakakibara, M. Simulation of citric acid production by rotating disc contactor, Biotech. and Bioeng., 1997, 56, 689-696.

Salmi, T.; Lehtonen, J.; Kaplin, J.; Vuori, A.; Tirronen, E. Haario, H. A homogeneous-heterogeneous catalysed reaction system in a loop reactor, Cat. Today, 1999, 48, 139-145.

Saluzzo C. and Lemaire M. "Homogeneous-supported catalysts for enantioselective hydrogenation and hydrogen transfer reduction". Adv. Synth. Catal. 2002, 344, No. 10, 915-928

Sandee A. J., Petra D. G. I., Reek J. N. H., Kamer P. C. J. and van Leeuwen P. W. N. M.. "Solid-phase synthesis of homogenuous ruthenium catalyst on silica for the continuous asymmetric transfer hydrogenation reaction" Chem. Eur. J. 2001, 7, 1202-1208

Schönfeld, F., Hardt, S.. "Simulation of helical flows in microchannels" A.I.Ch.E. Journal, 2003, 50, 771-778

Schultz W.G., Schultz T.H., Carlson R.A., Hudson J.S., "Pilot-plant extraction with liquid CO_2", Food Technol. 1974, 28(6), 32- 88

Schwesinger, N.; Frank, T.; Wurmus, H.. "A modular microfluidic system with an integrated micromixer" Journal of Micromechanics and Microengineering, 1996, 6, 99–102

Seibert A.F., and Fair J.R., "Scale-up of hollow fiber extractors", Sep. Sci. Technol. 1997, 32(1 - 4), 573 - 583

Semmens, M. J., R. Qin, et al., "Using a microporous hollow-fiber membrane to separate VOCs from water." J. Am. Water works Assoc., 1989, 81(4), 162-167

Shemer L.. "Hydrodynamics and statistical parameters of slug flow" International Journal of Heat and Fluid Flow, 2003, 24, 334-344

Sieder E.N., Tate G.E., "Heat transfer and pressure drop of liquids in tubes", Ind. Eng. Chem. 1936, 28 (12), 1429–1435.

Sims M.J., Robinson J.R., and Dennis A.J., Porocritical fluid extraction: a new technique for continuous extraction of liquids with near-critical fluids, in: P.R. von Rohr, C. Trepp (Eds.), High Pressure Chemical Engineering, Elsevier, Amsterdam, 1996, pp. 205 - 209

Skelland A.H.P. "Diffusion mass transfer", John Wiley & Sons, Inc,· USA, 1974, ISBN:0-471-79374-4, P177

Smet K. D., Aerts S., Gevers L., Vankelecom I. F. J. and Jacobs P.. "Nafion based catalytic membranes for the partial oxidation of light alkanes in a multiphase reaction system" 13th International Congress on Catalysis, 2004, Paris, P3-043

Smith S.R. and Cui Z. F.. "Analysis of developing laminar pipe flow-an application to gas slug enhanced hollow fibre ultrafiltration", Chemical Engineering Science, 2004, 59, 5975-5986

Smitha B., Suhanya D., Sridhar S., Ramakrishna M., "'Separation of organic-organic mixtures by pervaporation-a review", Journal of Membrane Science, 2004, 241, 1-21

Sokal, R. R., and F. J. Rohlf. Biometry. Third edition. W. H. Freeman and Company, New York. 1995, pp. 139-151

Solomon, T.N.; Mezic, I.. "Uniform resonant chaotic mixing in fluid flows" Nature, 2003, 425, 376–380

Steiner L. and Hartland S., A new type of agitated liquid/liquid extraction column with enhanced coalescence plates. Sep. Sci. Technol. 1980, 15, 907

Stroock, A.D.; Dertinger S.K.; Whitesides G.M.; Ajdari A.. "Patterning flows using grooved surfaces" Analytical Chemistry, 2002, 74, 5306–5312

Suga, K.; Boongorsrang, A. A new model of mass transfer in a rotating disc contactor, Chem.Eng. Sci., 1984, 39, 767-773.

Sun X., Manos G., Blacker J., Martin J., Gavriilidis A., "Asymmetric transfer hydrogenation of acetophenone with 1R,2S-aminoindanol/pentamethylcyclopentadienylrhodium catalyst" Organic Process research and Development, 2004, 8, 909-914.

Sutter T.A.; Morrison G.L., Tatterson G.B.. "Sound spectra in an aerated agitated tank", AICHE Journal, 1987, 33, 668-671

Taha T. and Cui Z.F.. "Hydrodynamics of slug flow inside capillaries" Chemical Engineering Science, 2004, 59, 1181-1190

Takeuchi T., Horikawa R., and Tanimura T., "Resolution of dl-valine by countercurrent solvent extraction with continous sample feeding", Sep. Sci. Technol. 1990, 25(7 - 8), 941

Tales-Alesson, F. I. The modelling of falling film chemical reactors, Chem. Eng. Sci. 1999, 54, 1871-1881.

Tatterson G.B. and Morrison G.L.. "Effect of tank to impeller diameter ratio on flooding transition for disc turbines", AICHE Journal, 1987, 33, 1751-1753

Te Grotenhuis W. E., Cameron R. J., Butcher M. G., Martin P. M. and Wegeng R. S.. "Microchannel devices for efficient contacting of liquids in solvent extraction" IMRET, New Orleans, 1998, 329-334

Teixeira, P. and Oliveira, R. Denitrification in a closed rotating biological contactor: effect of disk submergence, Proc. Biochemistry., 2001, 37, 345-349.

ter Halle R. Schulz E. and Lemaire M. "Heterogeneous Enantioselective Catalytic Reduction of Ketones" Synlett. 1997, 1257

Treybal R.E., Mass Transfer Operations, 3rd ed., McGraw-Hill, New York, 1980

Thakur R.K.; Vial Ch.; Nigam K.D.P.; Nauman E.B.; Djelveh G.. "Static mixers in the process industries-a review" Trans IchemE, 2003, 81, 787-826

Touchard F., Bernard M., Fache F, Delbecq F., Guiral V., Sautet P., Lemaire M. "Optically active nitrogen ligands in asymmetric catalysis. Effect of nitrogen substitution on the enatioselective hydride transfer reduction of acetophenone." J. Org. Chem. 1998, 567, 133-136

Triplett K.A.; Ghiaasiaan Abdel-Khalik S.I.; Sadowski D.L.. "Gas-liquid two-phase flow in microchannels Part I: Two-phase flow patterns" International journal of Multiphase Flow, 1999, 25, 377-394

Vaidya A.M., Bell G., Halling P.J., "Aqueous-organic membrane bioreactors. Part I. A guide to membrane selection", Journal of Membrane Science, 1992, 71, 139-149

Vaidya A.M., Bell G., Halling P.J., "Aqueous-organic membrane bioreactors. Part II. Breakthrough pressure measurement", Journal of Membrane Science, 1994, 97, 13-26

Velan, M. and Ramanujam, T.K. Gas-liquid mass transfer in a down flow jet loop reactor, Chem. Eng. Sci., 1992, 47, 2871-2876.

Volpe C.D., Maniglio D., Morra M. and Siboni S., "The Determination of a 'Stable Equilibrium' Contact Angle on Heterogeneous and Rough Surfaces" Colloids and Surfaces A, 2002, 206, 47-67

Wang K.L. and Cussler E.L., "Baffled membrane modules made with hollow fiber fabric". Journal of Membrane Science, 1993, 85, 265 – 278

Wang, Y.D.; Fei, W.Y.; Sun, J.H., Wan, Y.K. Hydrodynamics and mass transfer performance of a modified rotating disc contactor, Trans IChemE, 2002, 80, 392-400.

Wenn D. A., Shaw J. E. A., Mackenzie B.. "A mesh microcontactor for 2-phase reactions". Lab Chip, 2003, 3, 180-186.

West J.; Karamata B.; Lillis B.; Gleeson J.P.; Alderman J.; Collins J.K.; Lane W.; Mathewsona A.; Berneya H.. "Application of magnetohydrodynamic actuation to continuous flow chemistry" Lab on a Chip 2002, 2, 224-230

Wills M., Gamble M., Palmer M., Smith A., Studley J. and Kenny J.. "Novel catalyst for asymmetric reduction of carbonyl groups" Journal of Molecular Catalysis A: Chemical 146 (1999) 139-148

Wolfgang Ehrfeld, Klaus Golbig, Volker Hessel, Holger Lolwe, and Thomas Richter. "Characterization of Mixing in Micromixers by a Test Reaction: Single Mixing Units and Mixer Arrays". Ind. Eng. Chem. Res. 1999, 38, 1075-1082

Woo, B.G.; Choi, K.Y.; Song, K.H. Melt Polycondensation of bisphenol a polycarbonate by forced gas seeping process II. Continuous rotating disc reactor, Ind. Eng. Chem. Res., 2001, 40, i3459-3466.

Xu Q., Liang Y., Fang K.. "The effects of different experimental design on parameter estimation in the kinetics of a reversible chemical reaction", Chemometrics and Intelligent Laboratory Systems", 2000, 52, 155-166

Yamakawa M., Ito H. and Noyori R.. " The Metal-ligands bifunctional catalysis: A theoretical study on the ruthenium(II)-catalyzed hydrogen transfer between alcohols and carbonyl compounds." J. Am. Chem. Soc. 2000, 122, 1466-1478

Yang M.C. and Cussler E.L., "Designing hollow-fiber contactors", AICHE J. 32, 1986, 1910-1915

Yang Z.; Matsumoto S.; Goto H.; Matsumoto M.; Maeda R.. "Ultrasonic micromixer for microfluidic systems" Sensors and Actuators A, 2001, 93, 266-272

Yeong K. K., Gavriilidis A., Zapf R. and Hessel V.. "Experimental studies of nitrobenzene hydrogenation in a microstructured falling film reactor" Chemical Engineering Science, 2004, 59, 3491-3494

Zander A.K., Semmens M.J., Narbaitz R.M., "Removing VOCs by membrane stripping", J. Am. Water Works Assoc. 1989, 81 (11), 76-81

Zeevalkink, J.A.; Kelderman, P.; Visser, D.C.; Boelhouwer, C Liquid film thickness in a rotating disc gas-liquid contactor, Water Res, 1978, 12, 577-581.

Zeevalkink, J.A.; Kelderman, P.; Visser, D.C.; Boelhouwer, C. Physical mass transfer in a rotating disc gas-liquid contactor, Water Res, 1979, 13, 913-919.

Zhang Q. and Cussler E.L., "Microporous hollow fibers for gas absorption", Journal of Membrane Science, 1985, 23, 321-345

Appendix A

Modelling of Gas-Liquid Mass Transfer in the Batch Reactor

(Collaboration with Dr. Monica Zanfir)

Stripping of a chemical species from a binary liquid mixture using an inert gas was modelled according to two-resistance film theory in order to understand the limiting factors of acetone removal from acetone-isopropanol mixtures. The model assumptions are as follows:

- gas and liquid phases are considered isothermal and perfectly mixed;
- liquid phase is in unsteady state;
- gas phase is at steady state;
- equilibrium composition is achieved at gas-liquid interface instantaneously.

The model consists of molar balances in gas and liquid phase, having as boundary conditions at the gas-liquid interface the condition for the thermodynamic equilibrium and the assumption that the molar flux across the interface is continuous.
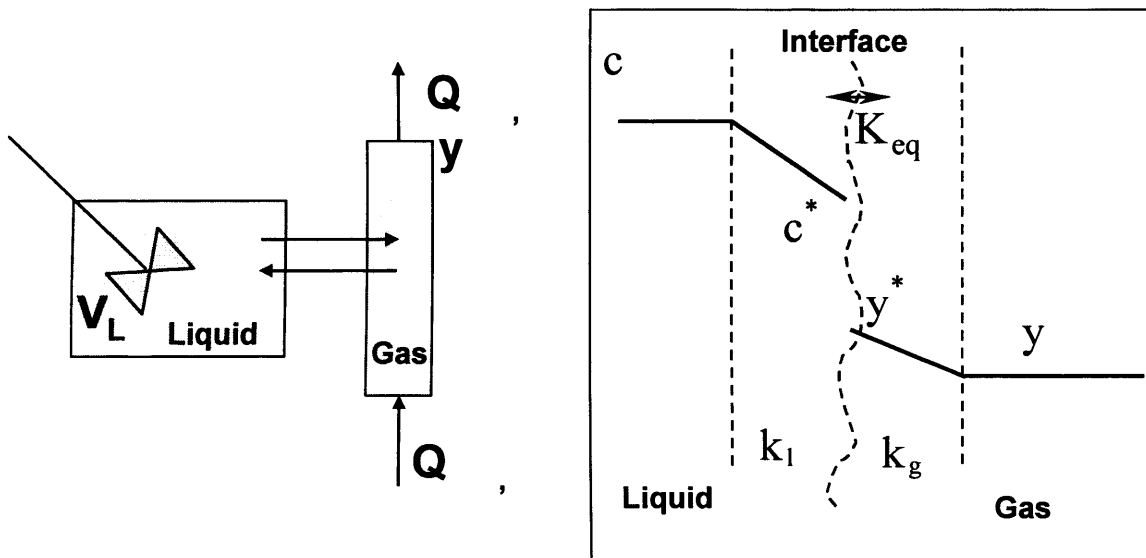
Figure 1. Main parameters and variables involved in modelling of mass transfer in gas-liquid systems

Liquid phase

$$\frac{dc}{dt} = -k_l \cdot a \cdot (c - c^*) \ ; \quad c(0) = c_0$$

Gas phase

$$k_g \cdot a \cdot V_L (y^* - y) = Q \cdot y$$

$$y = \frac{k_g \cdot a \cdot V_L}{Q + k_g \cdot a \cdot V_L} \cdot y*$$

Interface:

- continuity of the molar flux

$$k_g(y*-y) = k_l(c - c*)$$

- equilibrium

$$y* = K_{eq}^{'} \cdot c*$$

$$k_g(y* - \frac{k_g \cdot a \cdot V_L}{Q + k_g \cdot a \cdot V_L} \cdot y*) = k_l(c - c*)$$

$$k_g(1 - \frac{k_g \cdot a \cdot V_L}{Q + k_g \cdot a \cdot V_L})y* = k_l(c - c*)$$

$$\frac{k_g \cdot Q}{Q + k_g \cdot a \cdot V_L} \cdot y* = k_l(c - c*)$$

$$\frac{k_g \cdot Q}{Q + k_g \cdot a \cdot V_L} \cdot K_{eq}^{'} \cdot c* = k_l(c - c*)$$

$$c* = \frac{1}{1 + \dfrac{k_g \cdot Q \cdot K_{eq}^{'}}{k_l \cdot Q + k_l \cdot k_g \cdot a \cdot V_L}} \cdot c$$

$$\frac{dc}{dt} = -k_l \cdot a \cdot (c - \frac{1}{1 + \dfrac{k_g \cdot Q \cdot K_{eq}^{'}}{k_l \cdot Q + k_l \cdot k_g \cdot a \cdot V_L}} \cdot c)$$

$$\frac{dc}{dt} = \frac{-k_l \cdot a}{1 + \dfrac{k_l}{k_g} \cdot \dfrac{1}{K_{eq}^{'}}\left(1 + \dfrac{k_g \cdot a \cdot V_L}{Q}\right)} \cdot c$$

$$\frac{c(t)}{c_0} = \exp\left[-\frac{k_l \cdot a \cdot t}{1 + \dfrac{k_l}{k_g} \cdot \dfrac{1}{K_{eq}^{'}}\left(1 + \dfrac{k_g \cdot a \cdot V_L}{Q_{gas}}\right)}\right] = \exp\left[-\frac{t}{\dfrac{1}{k_l \cdot a} + \dfrac{1}{k_g \cdot a \cdot K_{eq}^{'}} + \dfrac{V_l}{Q_{gas} \cdot K_{eq}^{'}}}\right]$$

If $K_{eq} = \dfrac{1}{K_{eq}^{'}}$, then

$$\frac{c(t)}{c_0} = \exp\left[-\frac{t}{\dfrac{1}{k_l \cdot a} + \dfrac{K_{eq}}{k_g \cdot a} + \dfrac{K_{eq} \cdot V_l}{Q_{gas}}} \right]$$

Parameter Estimation

Calderbank (1959) underlined that the small diffusion path in the small bubbles together with the high diffusion coefficients as compared with those obtained in the liquid phase coupled with the effect of turbulence in the gas bubble combine to make the bubbled gas phase mass transfer resistance negligible compared with the liquid phase resistance. Assuming that the gas bubbles behave as rigid spheres without internal circulation, which is the condition for a minimum mass-transfer rate in the gas phase, the mass transfer coefficient in the gas phase can be estimated as:

$$k_g' = \frac{2\pi^2}{3} \cdot \frac{D_g}{d_b}$$

At low gas flowrates bubble size is a function of the orifice size, d_o, liquid surface tension and gas and liquid densities (Miller 1974):

$$d_b = 1.817 \cdot \left[\frac{\sigma \cdot d_o}{g(\rho_l - \rho_g)} \right]^{1/3},$$

The gas hold-up can be estimated as:

$$\varepsilon = \frac{u_g}{u_t + u_g}$$

where u_g is the gas superficial velocity, while the terminal velocity of the bubble rise u_t can be predicted by Mendelson's wave equation (Mendelson, 1967):

$$u_t = \sqrt{\frac{2 \cdot \sigma}{\rho_L \cdot d_b} + \frac{g \cdot d_b}{2}}$$

Interfacial area can be calculated based on gas hold-up as:

$$a = 6 \cdot \frac{\varepsilon}{d_b}$$

Mass transfer coefficient in the liquid side, k_L, can be estimated using the equations proposed by Calderbank and Moo-Young (1961):

$$k_L = A \cdot \left(\frac{g \cdot \mu_L}{\rho_L}\right)^{1/3} \left(\frac{D_L \rho_L}{\mu_L}\right)^n$$

where   A=0.31 and n=2/3 for small bubbles, d_b<2.5 mm

     A=0.42 and n=1/2 for large bubbles, d_b>2.5 mm

Therefore, for the batch reactor with 250ml liquid volume and 800ml/min nitrogen flowrate the parameters above can be calculated as,

$$d_b = 1.817 \cdot \left[\frac{\sigma \cdot d_o}{g(\rho_l - \rho_g)}\right]^{1/3} = 1.817 \times \left[\frac{0.021 \times 1.65 \times 10^{-3}}{9.81 \times (786 - 1.209)}\right]^{1/3} = 2.99 \times 10^{-3} m = 2.99 mm$$

$$k_g^{'} = \frac{2\pi^2}{3} \cdot \frac{D_g}{d_b} = \frac{2 \times 3.14^2 \times 1.136 \times 10^{-5}}{3 \times 2.99 \times 10^{-3}} = 2.98 \times 10^{-2} m/s$$

$$k_g = k_g^{'} \cdot \frac{P}{RT} = 2.98 \times 10^{-2} \cdot \frac{101325}{8.314 \times 303} = 1.19 mol/(m^2 \cdot s)$$

$$u_t = \sqrt{\frac{2 \cdot \sigma}{\rho_L \cdot d_b} + \frac{g \cdot d_b}{2}} = \sqrt{\frac{2 \times 0.021}{786 \times 2.99 \times 10^{-3}} + \frac{9.81 \times 2.99 \times 10^{-3}}{2}} = 0.18 m/s$$

$$u_g = \frac{F_g}{\pi \cdot r^2} = \frac{800 \times 10^{-6}/60}{3.14 \times (5 \times 10^{-2})^2} = 0.0017 m/s$$

$$\varepsilon = \frac{u_g}{u_t + u_g} = \frac{0.0017}{0.18 + 0.0017} = 0.0094$$

$$\alpha = 6 \cdot \frac{\varepsilon}{d_b} = 6 \times \frac{0.0094}{2.99 \times 10^{-3}} = 18.8 m^{-1}$$

$$\alpha_{surface} = \frac{\pi \cdot r^2}{V_l} = \frac{3.14 \times (5 \times 10^{-2})^2}{250 \times 10^{-6}} = 31.4 m^{-1}$$

$$\alpha = 18.8 + 31.4 = 50.2 m^{-1}$$

$$k_L = A \cdot \left(\frac{g \cdot \mu_L}{\rho_L}\right)^{1/3} \left(\frac{D_L \rho_L}{\mu_L}\right)^n = 0.42 \times \left(\frac{9.8 \times 1.73 \times 10^{-3}}{786}\right)^{1/3} \times \left(\frac{0.81 \times 10^{-9} \times 786}{1.73 \times 10^{-3}}\right)^{1/2} = 2.38 \times 10^{-4} m/s$$

$$\frac{1}{k_l \cdot \alpha} = \frac{1}{2.38 \times 10^{-4} \times 50.2} = 83.7$$

$$\frac{K_{eq}}{k_g \cdot \alpha} = \frac{1.174 \times 10^4}{1.19 \times 50.2} = 196.5$$

$$\frac{K_{eq} \cdot \frac{RT}{P} \cdot V_1}{Q} = \frac{1.174 \times 10^4 \cdot \frac{8.314 \times 303}{101325} \cdot 250 \times 10^{-6}}{800 \times 10^{-6}/60} = 5473$$

Appendix B

Gas-Liquid Equilibrium for Acetone-Isopropanol System

(Collaboration with Dr. Monica Zanfir)

Gas-liquid equilibrium is achieved if the fugacities, which are function of composition, pressure and temperature, of the two phases are equal as given by equation

$$f^L(x_i, P, T) = f^G(x_i, P, T)$$

which can be expressed as:

$$\gamma_i \cdot x_i \cdot P_i^{vap} = \Phi_i \cdot y_i \cdot P_{total}$$

For low pressure, the gas phase can be considered ideal, having a fugacity coefficient $\Phi_i = 1$, thus at equilibrium the relation between composition of the gas and liquid phase can be written as:

$$y_i = x_i \cdot \frac{P_i^{Vap}}{P^{total}} \cdot \gamma_i$$

For the acetone-IPA system,

$$x_i = \frac{C_{Acetone}}{C_{Acetone} + C_{IPA}} = \frac{C_{Acetone}}{C_{total}}$$

Therefore,

$$C_{Acetone} = y_i \cdot \frac{P_i^{total}}{P^{Vap} \cdot \gamma_i} \cdot C_{total}$$

Thus the equilibrium constant can be expressed as:

$$K_{eq} = \frac{P_i^{total}}{P^{Vap} \cdot \gamma_i} \cdot C_{total}$$

For the convenience of the calculation, we also define:

$$K'_{eq} = \frac{1}{K_{eq}} = \frac{P_i^{Vap}}{P^{total} \cdot C_{total}} \cdot \gamma_i$$

and

$$m = \frac{P_i^{Vap}}{P^{total}} \cdot \gamma_i$$

Appendix C

Activity Coefficient Estimation

(Collaboration with Dr. Monica Zanfir)

Experimental equilibrium data for isothermal conditions give, for a range of gas composition, y_i^{exp} and liquid composition, x_i^{exp} the vapour pressure of the mixture, P_{mix}^{vap}. Using such data, experimental activity coefficients can be calculated as:

$$\gamma_i^{exp} = \frac{y_i^{exp}}{x_i^{exp}} \cdot \frac{P_{mix}^{vap}}{P_i^{vap}} \qquad (C-1)$$

Further, Gibbs excess free energy can be calculated as given by equation

$$G^{ex} = RT\left(x_1 \ln\gamma_1 + x_2 \ln\gamma_2\right) \qquad (C-2)$$

and fitted using different thermodynamic methods, for example a Redlich-Kirster type expansion (C-3), or Wilson equation (C-4).

$$\frac{G^{ex}}{RT} = x_1 \cdot x_2\left[a + b\left(x_1 - x_2\right) + c\left(x_1 - x_2\right)^2\right] \qquad (C-3)$$

where a, b, c are parameter to be estimated.

$$\frac{G^{ex}}{RT} = -x_1 \cdot \ln\left(x_1 + \Lambda_{12} \cdot x_2\right) - x_2 \cdot \ln\left(x_2 + \Lambda_{21} \cdot x_1\right) \qquad (C-4)$$

where Λ_{12}, and Λ_{21} are parameter to be estimated.

Thermodynamic equilibrium data from *Detherm* database was utilised to calculate the excess Gibbs free energies for the system acetone-isopropanol. Fitting of these data allows estimation of the parameters of the thermodynamic models as given in Table C-1. The fitting for excess Gibbs free energies together with their estimated values from experimental data are given in Figure C-1.

Table C-1. Estimated parameters of the thermodynamic models.

Thermodynamic Model	Parameters Value
Redlich-Kirster	a=1.1204
	b=0.2668
	c=0.3837
Wilson	Λ_{12}= 0.8427
	Λ_{21}=0.2178
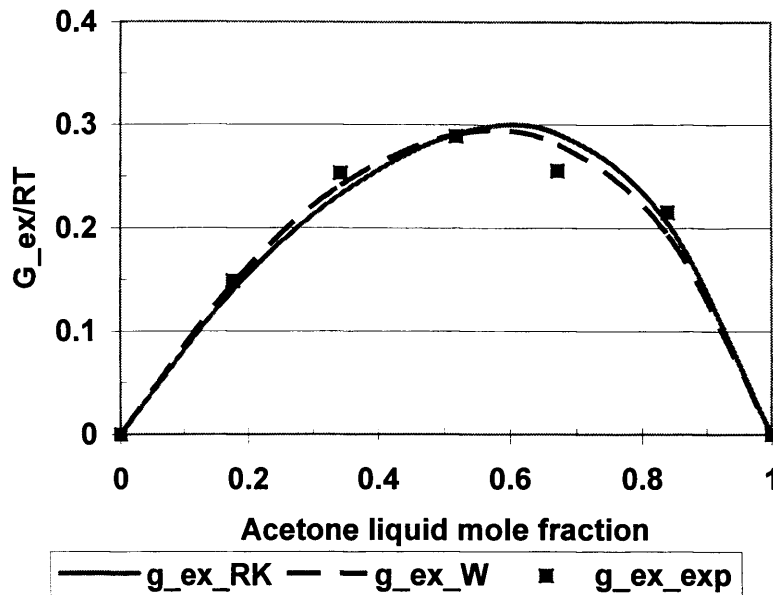
Figure C-1 Fitting of excess Gibbs free energy for acetone-isopropanol mixtures

After the parameters of the thermodynamic model were estimated, the activity coefficient can be calculated from its definition as:

$$\ln \gamma_1 = \frac{1}{RT} \cdot \left(\frac{\partial G^{ex}}{\partial RT} \right)_{T,P,N_2}$$ (C-5)

Thus the expression for the activity coefficient using a Redlich-Kirster type expansion is

$$\ln \gamma_1 = x_2^2 \left[a + b(x_1 - x_2) + c(x_1 - x_2)^2 \right] + 2x_1 x_2^2 \left[b + 2c(x_1 - x_2) \right]$$ (C-6)

and for Wilson equation is:

$$\ln \gamma_1 = -x_1 \cdot \ln(x_1 + \Lambda_{12} \cdot x_2) + x_2 \cdot \left[\frac{\Lambda_{12}}{x_1 + \Lambda_{12} \cdot x_2} - \frac{\Lambda_{21}}{x_2 + \Lambda_{21} \cdot x_1} \right]$$ (C-7)

The activity coefficient can be calaulated from Equation C-6 and C-7 which is shown in Figure C-2. It can be seen that when $x_{acetone} \rightarrow 0$, the values of the activity coefficient are in the range [1.5-3.5].
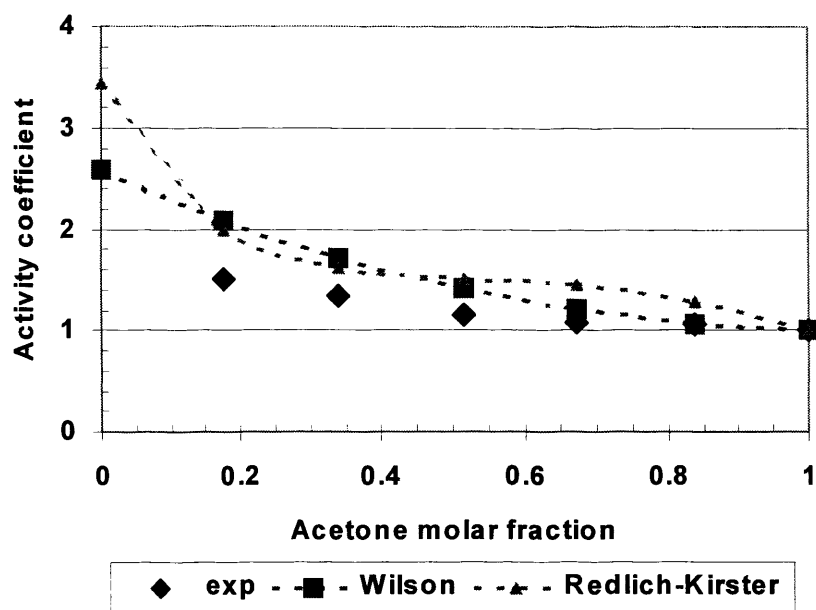
Figure C-2 Calculated and predicted values for acetone activity coefficient in acetone-isopropanol mixtures

Appendix D

Design Equations for Co-current

Flow Mesh Contactor

A semi-quantitative-analysis model is presented for the system as represented in Figure A-1 and is based on the following assumptions (Seader and Henley 1998):

- Gas flowrate and liquid flowrate are constant
- Isothermal process
- Mass transfer coefficients are constant during operation
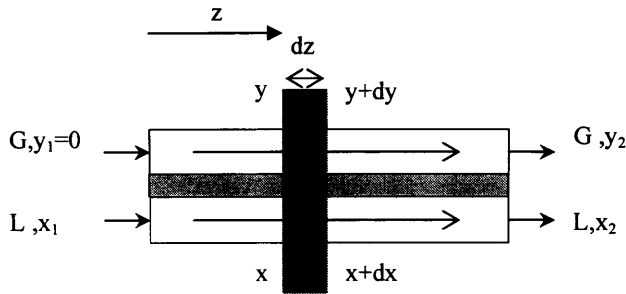
Figure A-1 Co-current flow in micro-mesh gas-liquid contactor

The flux from liquid to gas phase is defined as:

$$N_A = K_y \cdot (m \cdot x - y) \qquad \text{(A-1)}$$

The solubility of the acetone is defined as:

$$y = m \cdot x \qquad \text{(A-2)}$$

$$G \cdot dy = N_A \cdot a \cdot dz \qquad \text{(A-3)}$$

$$G \cdot dy = K_y \cdot a \cdot (m \cdot x - y) \cdot dz \qquad \text{(A-4)}$$

$$dz = \frac{G}{K_y \cdot a} \cdot \frac{dy}{mx - y} \qquad \text{(A-5)}$$

$$\int_0^L dz = \frac{G}{K_y \cdot a} \cdot \int_0^{y_2} \frac{dy}{mx - y} \qquad \text{(A-6)}$$

$$H = \frac{G}{K_y \cdot a} \cdot \int_0^{y_2} \frac{dy}{mx - y} \qquad \text{(A-7)}$$

$$H = HTU \bullet NTU \qquad \text{(A-8)}$$

Based on the gas phase driving force, HTU_G can be written as:

$$\boxed{HTU_G = \frac{G}{K_y a}}$$ (A-9)

Where G is gas flowrate, K_y is overall mass transfer coefficient based on vapor side driving force and α is gas/liquid interfacial area.

NTU_G can be written as

$$NTU_G = \int_{y_1=0}^{y_2} \frac{dy}{mx - y}$$ (A-10)

From a mole balance between z=0 and z,

$$G \cdot (y - 0) = L \cdot (x_1 - x)$$ (A-11)

$$x = -\frac{G}{L} \cdot y + x_1$$ (A-12)

$$NTU_G = \int_0^{y_2} \frac{dy}{m \cdot (-\frac{G}{L} \cdot y + x_1) - y}$$ (A-13)

$$NTU_G = \int_0^{y_2} \frac{dy}{m \cdot x_1 - (1 + \frac{mG}{L})y}$$ (A-14)

Defining

$$A = \frac{mG}{L}$$ (A-15)

then,

$$NTU_G = \int_0^{y_2} \frac{dy}{m \cdot x_1 - (1 + A)y}$$ (A-16)

$$NTU_G = -\frac{1}{1+A} \cdot \int_0^{y_2} \frac{d(1+A)y}{(1+A)y - mx_1}$$ (A-17)

$$NTU_G = -\frac{1}{1+A} \cdot \ln(\frac{(1+A) \cdot y_2 - mx_1}{0 - mx_1})$$ (A-18)

$$NTU_G = -\frac{1}{1+A} \cdot \ln(\frac{mx_1 - (1 + \frac{mG}{L}) \cdot y_2}{mx_1})$$ (A-19)

Using the mole balance between z=0 and z=H,

$$NTU_G = -\frac{1}{1+A} \cdot \ln(\frac{mx_1 - y_2 - m(\frac{G}{L} \cdot y_2)}{mx_1})$$ (A-20)

$$NTU_G = -\frac{1}{1+A} \cdot \ln(\frac{mx_1 - y_2 - m(x_1 - x_2)}{mx_1})$$ (A-21)

$$\boxed{NTU_G = -\frac{1}{1+A} \cdot \ln(\frac{mx_2 - y_2}{mx_1})}$$ (A-22)

Where, y_2 is outlet gas phase concentration, x_1 and x_2 are liquid phase inlet and outlet concentration, m is the solubility of the acetone in isopropanol.

Alternatively,

$$N_A = K_x \cdot (x - \frac{y}{m})$$ (A-23)

$$-L \cdot dx = N_A \cdot a \cdot dz$$ (A-24)

$$-L \cdot dx = K_x \cdot a \cdot (x - \frac{y}{m}) \cdot dz$$ (A-25)

$$dz = \frac{L}{K_x \cdot a} \cdot \frac{dy}{\frac{y}{m} - x}$$ (A-26)

$$\int_0^L dz = \frac{L}{K_x \cdot a} \cdot \int_{x_1}^{x_2} \frac{dx}{\frac{y}{m} - x}$$ (A-27)

$$H = \frac{L}{K_x \cdot a} \cdot \int_{x_1}^{x_2} \frac{dx}{\frac{y}{m} - x}$$ (A-28)

Based on the a liquid side driving force, HTU_L can be written as:

$$\boxed{HTU_L = \frac{L}{K_x a}}$$ (A-29)

Where L is liquid flowrate, K_x is overall mass transfer coefficient based on liquid side driving force and a is gas/liquid interfacial area.

NTU_L can be written as

$$NTU_L = \int_{x_1}^{x_2} \frac{dx}{\frac{y}{m} - x} \tag{A-30}$$

$$G \cdot (y - 0) = L \cdot (x_1 - x) \tag{A-31}$$

$$y = \frac{L}{G} \cdot x_1 - \frac{L}{G} \cdot x \tag{A-32}$$

$$NTU_L = \int_{x_1}^{x_2} \frac{dx}{\frac{1}{m}(\frac{L}{G}x_1 - \frac{L}{G} \cdot x) - x} \tag{A-33}$$

$$NTU_L = \int_{x_1}^{x_2} \frac{dx}{\frac{L}{mG}x_1 - (1 + \frac{L}{mG}) \cdot x} \tag{A-34}$$

$$B = \frac{L}{mG} \tag{A-35}$$

$$NTU_L = \int_{x_1}^{x_2} \frac{dx}{Bx_1 - (1 + B) \cdot x} \tag{A-36}$$

$$NTU_L = -\frac{1}{1 + B} \int_{x_1}^{x_2} \frac{d(1 + B)x}{(1 + B) \cdot x - Bx_1} \tag{A-37}$$

$$NTU_L = -\frac{1}{1 + B} \cdot \ln(\frac{(1 + B)x_2 - Bx_1}{(1 + B)x_1 - Bx_1}) \tag{A-38}$$

$$NTU_L = -\frac{1}{1 + B} \cdot \ln(\frac{x_2 + B \cdot x_2 - Bx_1}{x_1}) \tag{A-39}$$

$$NTU_L = -\frac{1}{1 + \frac{L}{mG}} \cdot \ln(\frac{x_2 + \frac{L}{mG} \cdot x_2 - \frac{L}{mG}x_1}{x_1}) \tag{A-40}$$

$$NTU_L = -\frac{1}{1 + \frac{1}{\frac{mG}{L}}} \cdot \ln(\frac{x_2 + \frac{1}{m} \cdot \frac{L}{G} \cdot (x_2 - x_1)}{x_1}) \tag{A-41}$$

$$NTU_L = -\frac{1}{1 + \frac{1}{A}} \cdot \ln(\frac{x_2 - \frac{y_2}{m}}{x_1}) \tag{A-42}$$

$$\boxed{NTU_L = -\frac{1}{1 + \frac{1}{A}} \cdot \ln(\frac{mx_2 - y_2}{mx_1})} \tag{A-43}$$

So the overall reactor length can be given by:

$$H = \frac{G}{K_y a} \cdot \left\{ -\frac{1}{1+A} \cdot \ln(\frac{mx_2 - y_2}{mx_1}) \right\} = \frac{L}{K_x \cdot a} \cdot \left\{ -\frac{1}{1+\dfrac{1}{A}} \cdot \ln(\frac{mx_2 - y_2}{mx_1}) \right\} \qquad \text{(A-44)}$$

To find exit concentration, one can start from equation A-40:

$$H = \frac{L}{K_x \cdot a} \cdot \left\{ -\frac{1}{1+B} \cdot \ln(\frac{x_2 + B \cdot x_2 - Bx_1}{x_1}) \right\} \qquad \text{(A-45)}$$

$$H = \frac{L}{K_x \cdot a} \cdot \left\{ -\frac{1}{1+B} \cdot \ln((1+B) \cdot \frac{x_2}{x_1} - B) \right\} \qquad \text{(A-46)}$$

$$\frac{x_2}{x_1} = \frac{1}{1+B} \cdot \exp\left(-\frac{K_x \cdot a \cdot H}{L} \cdot (1+B) \right) + \frac{B}{1+B} \qquad \text{(A-47)}$$

$$\frac{x_2}{x_1} = \frac{1}{1+\dfrac{L}{mG}} \cdot \exp\left(-\frac{K_x \cdot a \cdot H}{L} \cdot (1+\frac{L}{mG}) \right) + \frac{\dfrac{L}{mG}}{1+\dfrac{L}{mG}} \qquad \text{(A-48)}$$

$$\frac{x_2}{x_1} = \frac{1}{1+\dfrac{mG}{L}} \cdot \left(1 + \frac{mG}{L} \cdot \exp\left(-\frac{K_x \cdot a \cdot H}{L} \cdot (1+\frac{L}{mG}) \right) \right) \qquad \text{(A-49)}$$

Utilizing

$$L = \frac{F_l \cdot \rho}{M \cdot A_F} \qquad \text{(A-50)}$$

$$A_F = H_L \cdot w \qquad \text{(A-51)}$$

$$G = \frac{F_g \cdot P}{R \cdot T \cdot A_F} \qquad \text{(A-52)}$$

$$m = \frac{C_{total}}{K_{eq}} \qquad \text{(A-53)}$$

$$C_{total} = \frac{\rho}{M} \qquad \text{(A-54)}$$

Equation A-15 gives:

$$\frac{mG}{L} = \frac{\dfrac{C_{total}}{K_{eq}} \cdot \dfrac{F_g \cdot P}{R \cdot T \cdot A_F}}{\dfrac{F_l \cdot \rho}{M \cdot A_F}} = \frac{F_g}{F_l} \cdot \frac{P}{R \cdot T} \cdot \frac{1}{K_{eq}} = \Omega \qquad \text{(A-55)}$$

Using

$$K_x = C_{total} \cdot K_T \qquad\qquad\qquad (A\text{-}56)$$

$$\alpha = \frac{A_m}{V} \qquad\qquad\qquad (A\text{-}57)$$

$$A_m = l \cdot w \qquad\qquad\qquad (A\text{-}58)$$

The term $\dfrac{K_x \cdot \alpha}{L}$ becomes

$$\frac{K_x \cdot \alpha}{L} = \frac{C_{total} \cdot K_T \cdot \dfrac{l \cdot w}{l \cdot w \cdot h}}{\dfrac{F_l \cdot \rho}{M \cdot w \cdot h}} = \frac{1}{F_l} \cdot w \cdot K_T = \frac{K_T}{h_l \cdot u_l} = \frac{K_T \cdot \tau_l}{h_l \cdot H} = \beta \qquad (A\text{-}59)$$

Then, the equation can be written:

$$\boxed{\frac{x_2}{x_1} = \frac{C_{out}}{C_{in}} = \frac{1}{1+\Omega}\left\{1 + \Omega \cdot \exp\left[-\beta \cdot \left(1 + \frac{1}{\Omega}\right)H\right]\right\}} \qquad (A\text{-}60)$$

where, H is reactor length,

$$\Omega = \frac{F_g}{F_l} \cdot \frac{P}{R_g T} \cdot \frac{1}{K_{eq}}, \qquad\qquad\qquad (A\text{-}61)$$

$$\beta = \frac{K_T \cdot \tau_l}{h_l \cdot H} \qquad\qquad\qquad (A\text{-}62)$$

273

Appendix E

Mass Transfer Coefficient

Calculations

The mass transfer in a membrane contactor mainly involved three steps: mass transfer in the liquid phase, mass transfer across the membrane and mass transfer in the gas phase. The following assumptions have been made to calculate the mass transfer coefficient:

1. The pore membrane are straight and filled with liquid, and the concentration and partial pressure profiles of the volatile component (acetone) in liquid, membrane and gas phase are as shown in Figure 8

2. At gas-membrane interface the vapour-liquid is achieved instantaneously, and the equilibrium conditions is written as $C^{GM} = K_{eq} \cdot p^{GM}$

3. The solvent (isopropanol) does not evaporate
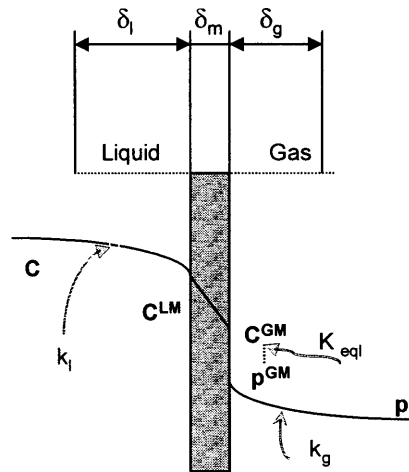
Figure 1. Domains of the model with its dimensions, concentration profile and mass transfer coefficients.

The individual and overall mass transfer coefficient can be calculated as:

The overall mass transfer coefficient is calculated as:

$$\frac{1}{K_T} = \frac{1}{k_l} + \frac{1}{k_m} + \frac{K_{eq}}{k_g}$$

The individual mass transfer coefficient, for liquid and gas phase are estimated based on the empirical correlation for laminar flow between flat plates, (Perry's page 5-63)

$$Sh = \frac{k(2h)}{D} = 8.23$$

The mass transfer coefficient in the membrane was calculated as:

$$k_m = \frac{D_{Acetone-isopropanol} \cdot \varepsilon}{\delta_m \cdot \tau}$$

Appendix F

Gas Chromatograph Calibration

The analysis system

An Agilent 6890N Network GC system was used to quantitatively analyse the reactants. First of all, the GC was calibrated by normalising the measurement with respect to acetophenone. The relative response factor $K_{R/AP}$ for R-phenylethanol and $K_{S/AP}$ for S-phenylethanol could be calculated.

GC analysis conditions

The inlet temperature was 250°C, the inlet pressure 20psi, split ratio 200:1. An injection volume of 0.2μl was used in the autoinjector. A CYCLODEX-B capillary column (30.0m×250μm×0.25μm) was employed for the separation of the acetophenone, (R)-1-phenylethanol and (S)-1-phenylethanol, in order to estimate conversion and enantiomeric excess, along with a flame ionisation detector at 250°C. The oven temperature was kept at 110°C. The internal normalisation method (with acetophenone) (Rouessac and Rouessac 2000) was used for quantification. Acetone concentration was determined using a DB-624 capillary column (30.0m×530μm×3.00μm) and a thermal conductivity detector at 250°C, with an oven temperature program: 60°C to 100°C at 10°C/min; 100°C for 4mins; 100°C to 200°C at 40°C/min; 200°C for 2min. Figure 1 shows a typical GC chromatogram by using these analysis conditions.
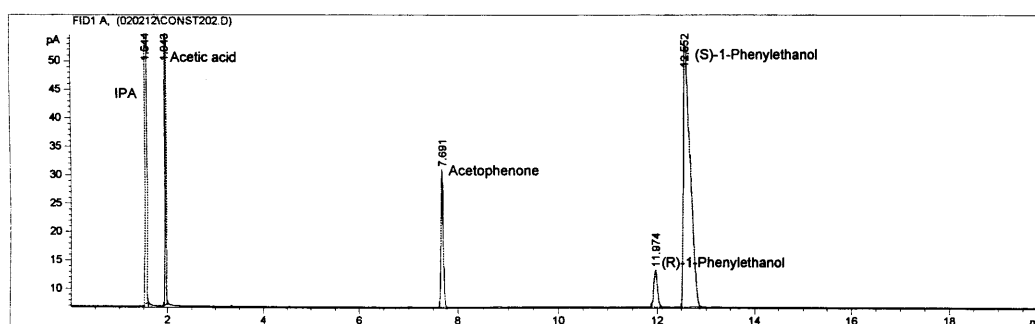
Figure 1 A typical GC chromatogram

Calibration of R-phenylethanol

Standard samples with different concentrations of R-phenylehanol and acetophenone in 1ml 2-propanol were prepared and then analysed by GC. The results are shown in Table 1. Figure 2 shows a linear relation between the GC peak ratio of area and the mole ratio.

Table 1 Preparation of R-phenylethanol calibration sample

Ap	R	Peak Area		Area Ratio	Mole Ratio	Factor
mmol	mmol	AP	R	R/AP	R/AP	$K_{R/AP}$
0.05194	0.006511	174.1871	30.66908	0.17607	0.125357	0.711974
0.020776	0.009763	71.3589	33.21389	0.465448	0.469929	1.009625
0.008904	0.01116	41.21793	44.50358	1.079714	1.253333	1.160801
0.01484	0.010017	57.56084	36.51737	0.634413	0.675	1.063975
0.067522	0.005055	230.8778	28.44292	0.123195	0.074863	0.607677
0.017849	0.0497	67.14558	178.6117	2.660067	2.78447	1.046767
0.017849	0.08284	71.7222	291.0351	4.057811	4.641156	1.143759

(Ap=Acetophenone; R=R-phenylethanol)
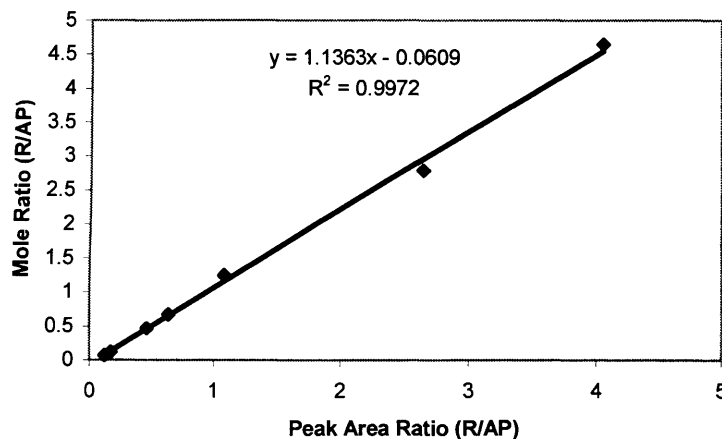
Figure 2 Calibration curve of R-Phenylethanol

Calibration of S-phenylethanol

Standard samples with different concentrations of S-phenylehanol and acetophenone in 1ml 2-propanol were prepared and then analysed by GC. The results are shown in Table 2. Figure 3 shows a linear relation between the GC peak ratio and the mole ratio.

Table 2 Preparation of S-phenylethanol calibration sample

AP	S	Peak Area		Peak ratio	Mole ratio	Factor
mmol	mmol	AP	S	S/AP	S/AP	$K_{S/AP}$
0.05194	0.089949	167.994	300.9357	1.791348	1.731786	0.96675
0.020776	0.117861	74.89846	392.8902	5.245639	5.672929	1.081456
0.084588	0.059664	248.8952	201.1598	0.808211	0.705351	0.872731
0.067522	0.075823	219.9289	257.3115	1.169976	1.12294	0.959797
0.116097	0.028992	368.5204	92.28184	0.250412	0.249726	0.997259
0.02679	0.074552	93.80685	258.5741	2.756453	2.782829	1.009569
0.022311	0.082835	82.6371	282.953	3.424043	3.712743	1.084315

(Ap=Acetophenone; S=S-phenylethanol)
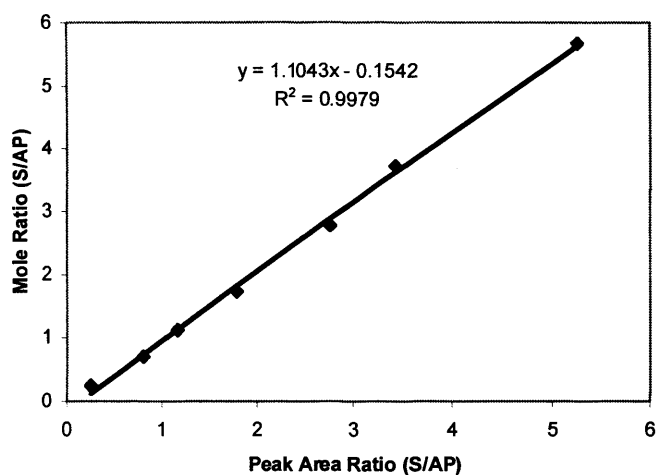
Figure 3 Calibration curve of S-Phenylethanol

Relative response factor $K_{R/AP}$ and $K_{S/AP}$

According to the flame ionization detector (FID) principle, the relative response factor of R and S should be the same because they have the same formula. Therefore, putting the calibration results of both R and S samples together, we could obtain the linear line between peak area ratio and mole ratio as shown in Figure 4. From Figure 4, the value of both $K_{R/AP}$ and $K_{S/AP}$ can be taken as 1.1.
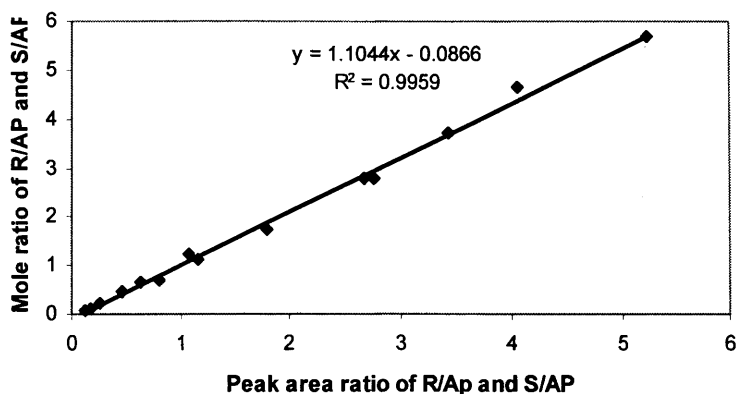
Figure 4 The standard curve of R and S-Phenylethanol

Calibration of reactant conversion and enantioselectivity

From peak area obtained from the chromatography with relative response factor $K_{R/AP}$

and $K_{S/AP}$, the reaction conversion of acetophenone was calculated as:

$$conversion = \frac{[Ap]_0 - [Ap]}{[Ap]_0} = \frac{[R]+[S]}{[Ap]+[R]+[S]} = \frac{1}{1+\dfrac{1}{\dfrac{[R]}{[Ap]}+\dfrac{[S]}{[Ap]}}} = \frac{1}{1+\dfrac{1}{K_{R/Ap} \times \dfrac{A_R}{A_{Ap}} + K_{s/Ap} \times \dfrac{A_s}{A_{Ap}}}}$$

the product enantioselectivity was characterised using enantiomeric excess (e.e.):

$$ee = \frac{[S]-[R]}{[S]+[R]} = \frac{A_S - A_R}{A_S + A_R}$$

where,

[Ap] $_0$ is the initial acetophenone concentration,

[Ap]   is the acetophenone concentration,

[S]   is the (S)-1-phenylethanol concentration and

[R]   is the (R)-1-phenylethanol concentration.

Appendix G

gPROMS Code for Kinetic Models

Variable Types

Name	Lower bound	Default value	Upper bound	Units
Acetone	-1000000.0	0.0	1000000.0	mol/l
CONSTANT	-1.0E30	1.0	1.0E30	
Conversion	-1000000.0	0.0	1000000.0	
Eq const	-1.0E20	0.07	1.0E20	
IPA	0.0	12.79	50.0	mol/l
Mole fraction	-1000000.0	0.01	1000000.0	
NAcetone stripped	-1000000.0	5.391E-5	1000000.0	mol/s l^3
NIPA stripped	-1000000.0	5.391E-5	1000000.0	mol/s l^3
R Acetone	-1000000.0	0.0	1000000.0	mol/(lxs)
R Im	-1000000.0	0.0	1000000.0	mol/l
R IPA	-1000000.0	0.00116	1000000.0	mol/(lxs)
R Prod	-1000000.0	0.0	1000000.0	mol/l
R R Im	-1000000.0	0.0	1000000.0	mol/(lxs)
R R Prod	-1000000.0	0.0	1000000.0	mol/(lxs)
R RhL	-1000000.0	0.0	1000000.0	mol/(lxs)
R RhL H2	-1000000.0	0.0	1000000.0	mol/(lxs)
R S Im	-1000000.0	0.0	1000000.0	mol/(lxs)
R S Prod	-1000000.0	0.0	1000000.0	mol/(lxs)
R Sub	-1000000.0	0.0	1000000.0	mol/(lxs)
R1	-1000000.0	0.00116	1000000.0	mol/(lxs)
R10	-1000000.0	0.0	1000000.0	mol/(lxs)
R11	-1000000.0	0.0	1000000.0	mol/(lxs)
R2	-1000000.0	0.0	1000000.0	mol/(lxs)
R3	-1000000.0	0.0	1000000.0	mol/(lxs)
R4	-1000000.0	0.0	1000000.0	mol/(lxs)
R5	-1000000.0	0.0	1000000.0	mol/(lxs)
R6	-1000000.0	0.0	1000000.0	mol/(lxs)
R7	-1000000.0	0.0	1000000.0	mol/(lxs)
R8	-1000000.0	0.0	1000000.0	mol/(lxs)
R9	-1000000.0	0.0	1000000.0	mol/(lxs)
RhL	-1000000.0	0.0	1000000.0	mol/l
RhL H2	-1000000.0	0.0	1000000.0	mol/l
S Im	-1000000.0	0.0	1000000.0	mol/l
S Prod	-1000000.0	0.0	1000000.0	mol/l
Selectivity	-1000000.0	0.0	1000000.0	
Sub	0.0	0.145	1.0	mol/l
Vap press	-1.0E20	0.01	1.0E20	
Vg	-1.0E20	0.0010	1.0E20	

1

Volume   0.0   0.2574   1.0E10   litres

MODEL: Gas

#=====================================

PARAMETER

kg, F_N2, GAS_holdup, K_eq, y_IPA_eq, A
AS REAL

VARIABLE

Molfr_g_Acetone   AS
Mole_fraction

Molfr_g_Acetone_eq   AS   Mole_fraction

Molfr_g_IPA_eq   AS
Mole_fraction

NIPA_stripped   AS
NIPA_stripped

NAcetone_stripped   AS
NAcetone_stripped

Vg   AS
Vg

V   AS
Volume

EQUATION

$0.0402*Vg*\$Molfr\_g\_Acetone$ =NAcetone_stripped-
F_N2*Molfr_g_Acetone/(1-Molfr_g_IPA_eq-Molfr_g_Acetone);

NAcetone_stripped =kg*A*V*0.001*
(Molfr_g_Acetone_eq-Molfr_g_Acetone);

NIPA_stripped =F_N2*Molfr_g_IPA_eq/
(1-Molfr_g_IPA_eq-Molfr_g_Acetone) ;

Molfr_g_IPA_eq =y_IPA_eq ;

MODEL: INTERFACE

#===================================

UNIT

           L   AS Liquid

           G   AS Gas

EQUATION

G.GAS_holdup=G.Vg/(G.Vg+L.V);

#EQUALITY OF IPA AND ACETONE RATE STRIPPING;

L.NAcetone_stripped=G.NAcetone_stripped;

L.NIPA_stripped=G.NIPA_stripped;

#Equilibrium conditions, molar fraction at equilibrium

G.Molfr_g_Acetone_eq=L.Kc*L.Acetone_eq;

L.Kc=L.Activity_coeff*G.K_eq/L.Tot_con_eq;

G.V=L.V;

MODEL: Liquid

#Declare

#=================================

PARAMETER

#rate constants for each reaction step
k1, k2, k3, k4, k5, k6, k7, k8, k9, k10   AS REAL

#mass trasfer parameters

#mass transfer coefficient in the liquid phase, m/s

kL AS REAL

#interfacial area, a, m^-1

A   AS REAL

#nitrogen flowrate, mol/s

F_N2 AS REAL

#Saturated mole fraction of IPA

y   AS REAL

VARIABLE

k1, k2, k3, k4, k5, k6, k7, k8, k9, k10   AS CONSTANT
#reaction mixture volume; liters

V

Volume   AS

moles/s   # rate of IPA and Acetone stripped from the liquid phase;

NIPA_stripped   AS   NIPA_stripped
NAcetone_stripped AS   NAcetone_stripped

#species concentration mol/l

IPA   AS   IPA
Sub   AS   Sub
Acetone   AS   Acetone
S_Prod   AS   S_Prod
R_Prod   AS   R_Prod
RhL   AS   RhL
RhL_H2   AS   RhL_H2
S_Im   AS   S_Im
R_Im   AS   R_Im

#Equilibrium concentrations

#IPA_eq   AS   IPA

Acetone_eq   AS   Acetone

4

```
                Acetone_eq           AS            Acetone

        #Total concentration

        Tot_con                              AS              IPA

        Tot_con_eq              AS          IPA


        # reaction rates

        R1                                               AS
R1
        R2                                               AS
R2
        R3                                               AS
R3
        R4                                               AS
R4
        R5                                               AS
R5
        R6                                               AS
R6
        R7                                               AS
R7
        R8                                               AS
R8
        R9                                               AS
R9
        R10                                              AS
R10
```

```
        #reaction rates per chemical specie


                R_IPA                    AS            R_IPA
                R_Sub                    AS            R_Sub
                R_Acetone                    AS
R_Acetone

                R_S_Prod                 AS            R_S_Prod
                R_R_Prod                 AS            R_R_Prod
                R_RhL                AS            R_RhL
                R_RhL_H2                 AS            R_RhL_H2
                R_S_Im                   AS            R_S_Im
                R_R_Im                   AS            R_R_Im

        #conversion and selectivity

        Conversion          AS
        Selectivity         AS            Conversion
                                          Selectivity

        #equilibrium constant, 1/mol

        Kc
Eq_const                                          AS


        Activity_coeff
Eq_const                                          AS
```

EQUATION

#reaction rates


```
R1=k1*RhL*IPA
R2=k2*RhL_H2*Acetone                        ;
R3=k3*RhL_H2*Sub                    ;
R4=k4*S_Im                              ;
R5=k5*RhL_H2*Sub              ;
R6=k6*R_Im                          ;
R7=k7*S_Im                          ;
R8=k8*RhL*S_Prod              ;
R9=k9*R_Im                      ;
R10=k10*RhL*R_Prod          ;
```


#Reaction rate per species


```
R_IPA             =-R1+R2 ;
R_Sub             =-R3+R4-R5+R6
R_Acetone = R1-R2                      ;
R_S_Prod= R7-R8                              ;
R_R_Prod= R9-R10                              ;
R_RhL             =-R1+R2+R7-R8+R9-R10          ;

R_RhL_H2= R1-R2-R3+R4-R5+R6 ;
R_S_Im             = R3-R4-R7+R8

R_R_Im             = R5-R6-R9+R10
```

#volume variation

```
$V=-(NIPA_stripped*60.1/782+NAcetone_stripped*58.08/786);
```

#SPECIES VARIATION


```
V*$IPA+IPA*$V=V*R_IPA-NIPA_stripped

V*$Sub+Sub*$V=V*R_Sub

V*$Acetone+Acetone*$V=V*R_Acetone-NAcetone_stripped

V*$S_Prod+S_Prod*$V=V*R_S_Prod                ;
V*$R_Prod+R_Prod*$V=V*R_R_Prod                ;
V*$RhL+RhL*$V=V*R_RhL

V*$RhL_H2+RhL_H2*$V=V*R_RhL_H2                ;
V*$S_Im+S_Im*$V=V*R_S_Im

V*$R_Im+R_Im*$V=V*R_R_Im
```

6

```
# Total concentration
Tot_con=(IPA+Sub+Acetone+S_Prod+R_Prod+RhL+RhL_H2+S_IM+R_Im) ;

#Total concentration at interface

Tot_con_eq=Tot_con-(Acetone)+Acetone_eq;
```

equilibrium;

```
(#Corelation between liquid mole fraction and concentrations at
```

```
#IPA_eq=Molfr_1_IPA_eq*Tot_con_eq;

Acetone_eq=Molfr_1_Acetone_eq*Tot_con_eq;)
```

fraction and

```
#Correlation between the equilibrium constant based on mol

#equilibrium constat based on concentration
```

```
#Rate of stripping for IPA and Acetone, mol/s
```

```
NAcetone_stripped=kL*A*V*(Acetone-Acetone_eq);
```

```
#NRTL method, with coefficients determined by myself
```

```
LOG(Activity_coeff)=(IPA/Tot_con)^2*(0.9050*(0.447/
(Acetone/Tot_con+0.447*IPA/Tot_con))^2+
```

```
*0.144/(IPA/Tot_con+0.144*Acetone/Tot_con)^2);
```
2.18

```
Conversion=1-V*Sub/0.2574/0.14569;

Selectivity=(S_Prod-R_Prod)/(S_Prod+R_Prod+1e-10) ;
```

```
#==========================================

         UNIT RB AS Interface


     SET
                WITHIN RB DO
                  WITHIN L DO

             {                    k1:=0.877;
                                  k2:=179.7;
                                  k3:=308.2;
                                  k4:=0.0033;
                                  k5:=112.1;
                                  k6:=9.5;
                                  k7:=11.3;
                                  k8:=2176.3;
                                  k9:=2.39;
                                  k10:=2.88;
                                  #K:=0.01/60;}

                                  kL:=1.4E-4;  #sec^-1

                                  A:=118 ;  #m^-1



                                  y:=0.08;
                                  F_N2:=5.5085E-6*80;
```

```
                WITHIN #Within

                WITHIN G DO
                               kg:=1.5                    ;#mol/(l s)

                               A:=118 ;  #m^-1

                               F_N2:= 5.5085E-6*80   ;#mol/s

                               Gas_holdup:=0.05     ;

                               K_eq:=37720/101325;      #3.423


                               y_IPA_eq:=0.0798 ;
                END #Within
              END#Within

     ASSIGN

         WITHIN RB DO
                    WITHIN L DO

                                  k1:=37.5/60;
                                  k2:=3677.5/60;
                                  k3:=15162.7/60;
                                  k4:=27.7/60;
                                  k5:=5478/60;
                                  k6:=511.5/60;
                                  k7:=655.9/60;
                                  k8:=80390.8/60;
```

```
                              k9:=114.4/60;
                              k10:=3430.9/60;
                              #K:=0.01/60;



                    END #Within
     END

          INITIAL

               WITHIN RB DO
                    WITHIN L DO
                                   IPA              =12.79                    ;# mol/l
                                   Sub              =0.14569                  ;
                                   Acetone=0;
                                   S_Prod=0;
                                   R_Prod=0;
                                   RhL= 1.457E-4;
                                   RhL_H2=0 ;
                                   S_Im=0;
                                   R_Im=0;
                                   V=0.2574; #liters
                    END #WITHIN L

                    WITHIN G DO
                                   Molfr_g_Acetone=0                    ;


               END #Within


               END #Within

     {SOLUTIONPARAMETERS
                    AbsoluteAccuracy            :=1.0E-10;
                    InitAccuracy                         :=1.0E-10;
                    RelativeAccuracy            :=1.0E-10;
                    OutputLevel                          :=1;
                    MaxinitIterations            :=50;}

          SCHEDULE

                    CONTINUE FOR 3600
```

ESTIMATION: Mass_trasnf

ESTIMATE
RB.L.K1
0.625 0 1e6

ESTIMATE
RB.L.K2
610 0 1e6

ESTIMATE
RB.L.K3
252 0 1e6

ESTIMATE
RB.L.K4
0.5 0 1e6

ESTIMATE
RB.L.K5
91 0 1e6

ESTIMATE
RB.L.K6
8.5 0 1e6

ESTIMATE
RB.L.K7
10.9 0 1e6

ESTIMATE
RB.L.K8
1339 0 1e6

ESTIMATE
RB.L.K9
2 0 1e6

ESTIMATE
RB.L.K10
77 0 1e6

MEASURE
RB.L.ACETONE
HETEROSCEDASTIC MEASURED_VALUES
(0.001:0.000001:10;0.5:0:1)

MEASURE
RB.L.SUB
HETEROSCEDASTIC MEASURED_VALUES
(0.001:0.000001:10;0.5:0:1)

MEASURE
RB.L.R_Prod
HETEROSCEDASTIC MEASURED_VALUES
(0.0001:0.000001:10;0.5:0:1)

MEASURE
RB.L.S_Prod
HETEROSCEDASTIC MEASURED_VALUES

(0.001:0.000001:10;0.5:0:1)


```
RUNS
REACTION2 1
REACTION3 1
REACTION4 1
REACTION7 1
REACTION8 1
{REACTION1 1
REACTION5 1
REACTION6 1}
REACTION9 1
REACTION11 1
```